Reconstructing Holocene climatic and environmental change using molecular and isotopic proxies from lake sedimentary records

Inaugural-Dissertation

zur

Erlangung des Doktorgrades

der Mathematisch-Naturwissenschaftlichen Fakultät

der Universität zu Köln

vorgelegt von

Matthias Thienemann
aus Düsseldorf

Köln, 2017

Berichterstatter:	Prof. Dr. Janet Rethemeyer
(Gutachter)	Prof. Dr. Hans-Rudolf Bork

Tag der mündlichen Prüfung: 29.06.2017

*“Die Lebewelt des Sees ist in ihrer Entwicklung
nicht nur abhängig von ihrer Umwelt, sie verändert
auch ihrerseits ihren Lebensraum; Lebewelt
und Umwelt stehen in Wechselwirkung zueinander.“*

Thienemann, August (1941)

Abstract

Greater understanding of Holocene climatic and environmental variability and processes, as well as about feedback and forcing mechanisms of the climate system is crucial for the assessment of both natural and anthropogenic future climate and environmental changes. Compared to prior epochs in earth's history, the climate of the Holocene is traditionally regarded as relatively stable. However, Holocene climate also showed significant fluctuations although perturbation were smaller in magnitude compared to Pleistocene. These fluctuations can be assessed by organic geochemical molecular and isotope analyses of lake sedimentary organic matter (OM) that have the potential to reveal a variety of information regarding physical, chemical and biological changes and processes of the lake, its environment, and the climate. Therefore, within the scope of this thesis, sedimentary archives from selected lakes from the Sub-Artic (Lake Torneträsk), the Mediterranean (Lake Dojran), and the African tropics (Lake Dendi) were analyzed using various analytical methods including the analysis of lipid biomarker and compound specific leaf wax stable isotopes, as well as palynological, microcharcoal, and inorganic sedimentological analyses. All three lakes are situated in key regions for the understanding of northern hemispheric Holocene climate variability and natural/anthropogenic forcing and feedback mechanisms:

To constrain changes in atmospheric circulation patterns and their effects on the environment in the Fennoscandian sub-arctic, lipid biomarker, inorganic proxies, and compound specific δD analysis are applied to a Holocene sedimentary record from Lake Torneträsk (NW Sweden). Owing to its climate being influenced by both the North Atlantic and the polar frontal zone, northern Fennoscandia can be regarded as a key region to better understand the regional expression and potential threshold effects of insolation-forced migrations of atmospheric circulation systems. The results indicate a non-linear reorganization of the atmospheric circulation expressed as a change from zonal towards more meridional flow starting at ~4,000 and intensifying ~2,000 cal yrs BP.

For the reconstruction of the climatic, environmental, and human impact on the southern Balkan Peninsula lipid biomarker, microcharcoal, and pollen analyses are applied to a Holocene sedimentary record from Lake Dojran (Macedonia/Greece). The southern Balkan region played a key role in the early migration of the Neolithic lifestyle to Central Europe and is thus very suitable for studies of human-environment forcing and feedback mechanisms. The results suggest a relationship between anthropogenic activity and centennial to millennial scale environmental/climatic changes, since increased human impact corresponds to phases of higher humidity and high lake levels at Lake Dojran.

To detect changes in atmospheric circulation, hydrology, and vegetation in East Africa, associated with the African Humid Period (AHP), lipid biomarker and compound specific δD and $\delta^{13}C$ analysis are applied to sedimentary OM from Lake Dendi (Ethiopia). Due to its location in proximity of the Congo Air Boundary (CAB) and the Intertropical Convergence Zone (ITCZ), the Dendi region can play a crucial role in the understanding of past changes in atmospheric circulation pattern of the tropical regions. The results indicate a rapid re-strengthening of the monsoonal circulation in the Early Holocene followed by Peak AHP conditions between ~9,800 yrs cal BP and ~8,000 yrs cal BP. Subsequently a moderate decrease in

precipitation and a shift in moisture sources due to weakening monsoonal systems and associated shifts of the ITCZ and the CAB have been detected.
Together, the lakes datasets suggest a thermal maximum and a northernmost position of the atmospheric circulation systems in the Early Holocene followed by a long-term trend of decreasing temperatures and environmental changes in accordance with decreasing NH summer insolation. Despite some differences in nature and timing, all tree records further indicate a southwards migration and weakening of NH atmospheric circulation systems over the course of the Holocene with significant phases of climatic/environmental changes around 4,500 yrs cal BP and 2,000 yrs.

Zusammenfassung

Für die Beurteilung künftiger, sowohl natürlicher als auch anthropogener Klima- und Umweltveränderungen ist ein umfangreiches Verständnis der holozänen Klimavariabilität sowie von Feedback und Forcing Mechanismen des Klimasystems entscheidend. Im Vergleich zu früheren Epochen in der Erdgeschichte gilt das Klima des Holozäns traditionell als relativ stabil. Allerdings weist das holozäne Klima auch signifikante Schwankungen auf, auch wenn diese ein kleineres Ausmaß annehmen, als im Pleistozän. Diese Schwankungen können durch organisch-geochemische, sowie durch Isotopen Analysen an organischem Material aus Seesedimenten erforscht werden. Seesedimente haben das Potenzial eine Vielzahl von Informationen über physikalische, chemische und biologische Veränderungen und Prozesse des Sees, der Umgebung und des Klimas zu speichern. So wurden im Rahmen dieser Arbeit Sedimentarchive aus ausgewählten Seen aus der Sub-Arktis (Lake Torneträsk), dem Mittelmeerraum (Lake Dojran) und den afrikanischen Tropen (Dendi-See) mit verschiedenen analytischen Methoden untersucht. Dazu zählen die Analyse von Lipid-Biomarkern und komponentenspezifischen stabilen Isotopen von Blattwachsen, sowie die Untersuchung von Pollen und Mikro-Holzkohle, als auch anorganische sedimentologische Analysen. Alle drei Seen liegen in Schlüsselregionen, die für das Verständnis von nordhemispherischer, holozänen Klimavariabilität, sowie von natürlichen und anthropogenen Forcing und Feedback Mechanismen von großer Bedeutung sind:

Um Veränderungen in der atmosphärischen Zirkulation und ihre Auswirkungen auf die Umwelt in der skandinavischen Sub-Arktis festzustellen werden Lipid Biomarker, komponentenspezifische D-Isotopenverhältnisse und anorganische Proxies in einem holozänen Sedimentkern aus dem Torneträsk See (NW Schweden) untersucht. Aufgrund der geographischen Lage der Region, deren Klima vom Nordatlantik als auch von der polaren Frontalzone beeinflusst wird, spielt das nördliche Skandinavien eine Schlüsselrolle bei der Erforschung von potenziellen Schwelleneffekten und von insolationsbedingten Migrationen der atmosphärischen Zirkulationssysteme. Die Ergebnisse deuten auf eine nichtlineare Reorganisation der atmosphärischen Zirkulation hin, ausgedrückt durch eine Veränderung von einer dominant zonalen zu einer verstärkt meridionalen atmosphärischen Strömung um ~ 4.000 cal BP und ~ 2.000 cal BP.

Für die Rekonstruktion von Klima, Umwelt und anthropogenem Einfluss auf der südlichen Balkan-Halbinsel werden Lipid-Biomarker, Pollen sowie Mikro-Holzkohlen aus einem holozänen Sedimentkern aus dem Dojran See (Mazedonien/Griechenland) analysiert. Da die südliche Balkanhalbinsel eine wichtige Route für die Migration des neolithischen Lebensstils nach Mitteleuropa darstellte, eignet sich diese Region besonders gut für die Erforschung von frühen Mensch-Umwelt Verflechtungen. Die Ergebnisse deuten auf eine Beziehung zwischen anthropogener Aktivität und Klima-/Umweltveränderungen hin, da Phasen erhöhter menschlicher Aktivität mit Phasen höherer Feuchtigkeit und hohem Seespiegel des Dojran Sees zusammenfallen.

Um Veränderungen in der atmosphärischen Zirkulation, der Hydrologie und der Vegetation in Ost Afrika, assoziiert mit der African Humid Period (AHP), zu rekonstruieren, werden Lipid-Biomarker und komponentenspezifische δD- und δ^{13}C-Analysen an sedimentärem, organischem Material aus dem Dendi

See (Äthiopien) durchgeführt. Aufgrund der Nähe zur Congo Air Boundary (CAB) und der Intertropischen Konvergenzzone (ITCZ) spielt die Dendi-Region eine entscheidende Rolle für das Verständnis holozäner Veränderungen in der atmosphärischen Zirkulation in tropischen Regionen. Die Ergebnisse deuten auf eine rapide Reorganisation der Monsun-Zirkulation im frühen Holozän, gefolgt von Peak-AHP Bedingungen zwischen ~ 9.800 cal BP und ~ 8.000 cal BP, hin. Anschließend werden eine mäßige Abnahme des Niederschlags und eine Verschiebung der Feuchtequellen aufgrund abgeschwächter Monsunsysteme und eine damit verbundene Verschiebungen der ITCZ und der CAB festgestellt.

Gemeinsam deuten die See-Datensätze auf ein thermisches Maximum und eine nördliche Position der atmosphärischen Zirkulationssysteme im frühen Holozän hin. Es folgt ein langfristiger Trend abnehmender Temperaturen und Umweltveränderungen in Übereinstimmung mit einer abnehmenden NH-Sommer-Insolation. Trotz einiger zeitlicher Unterschiede weisen alle Datensätze auf eine südwärtige Verlagerung und Abschwächung der atmosphärischen Zirkulationssysteme im Verlauf des Holozäns hin. Phasen von signifikanten Klima-/Umweltveränderungen lassen sich dabei um 4.500 cal BP und 2.000 cal BP feststellen.

Table of content

Abstract IV
Zusammenfassung VI
Table of content VIII
List of figures X
List of tables XII
List of abbreviations XIII

1. Introduction 1

1.1 Holocene climate variability – Forcing and Feedbacks 1
1.2 Holocene climate evolution 4
1.3 Thesis outline 5

2. Biomarker from lake sediments as proxies for climate and environmental variability 7

2.1 n-Alkanes and fatty acids 8
2.1.1 Compound specific stable isotope analysis of plant leaf wax hydrocarbons 10
2.2 Glycerol dialkyl glycerol tetraether lipids 15
2.3 Biomarker in Geo-archeology 18
2.3.1 Sterols 18
2.3.2 Polycyclic aromatic hydrocarbons 18
2.4 Analytical Methods 19

3. Neoglacial changes in atmospheric circulation patterns over the North Atlantic and Fennoscandia recorded in Lake Torneträsk sediments 22

3.1 Site description 24
3.2 Material and Methods 25
3.3 Results and Discussion 27
3.3.1 Hydrological source signatures 30
3.3.2 Reconstruction of the Holocene hydrological and environmental history 32
3.4 Summary and Conclusions 36

4. Organic geochemical and palynological evidence for Holocene natural and anthropogenic environmental change at Lake Dojran (Macedonia/Greece) 37

4.1 Site description 38
4.2 Material and Methods 40
4.3 Results 41
4.3.1 Plant wax *n*-alkanes 41
4.3.2 Steroids 42
4.3.3 PAHs 42

4.3.4 GDGT based indices 43
4.3.5 Pollen 43
4.3.6 Microcharcoals 44
4.3.7 Catchment 46

4.4 Discussion 46
4.4.1 Early Holocene (11,700 – 8,200 yrs cal BP) 48
4.4.2 Middle Holocene (8,200 – 4,200 yrs cal BP) 51
4.4.3 Late Holocene (4,200 yrs cal BP - present) 52
4.5 Summary and Conclusions 56

5. Holocene hydrological and atmospheric changes in East Africa inferred from lipid biomarker and leaf wax *n*-alkane δD of Lake Dendi (Ethiopia) sediments 57

5.1 Site description 58
5.2 Material and Methods 59
5.3 Results 60
5.3.1 Plant wax *n*-alkanes 60
5.3.2 Plant wax *n*-alkane hydrogen isotopes 61
5.3.3 Plant wax *n*-alkane carbon isotopes 61
5.3.4 GDGT-based indices 62
5.4 Discussion 64
5.4.1 Hydrological source signatures 64
5.4.2 Younger Dryas and Early Holocene - Peak AHP 65
5.4.3 Middle Holocene - Transition out of the AHP 69
5.4.4 Late Holocene climatic fluctuations and return to wetter conditions 72
5.5 Summary and Conclusions 72

6. Synthesis and outlook 74
6.1 Biomarker from lacustrine sediments in different environments 74
6.2 Holocene climate variability 75
6.3 Future outlook 80

Acknowledgements 81

References 82

Appendix 101

Erklärung (Explanation in German) 110

List of figures

Figure 1. Holocene orbital climate forcing. 2

Figure 2. Schematic map of NH atmospheric and oceanic circulation pattern including positions of lake sedimentary records analyzed for this thesis: 1) Lake Torneträsk, Sweden (see chapter 3); 2) Lake Dojran, Macedonia/Greece (see chapter 4); 3) Lake Dendi, Ethiopia (see chapter 5). Blue, purple, and red zones indicate the position of the polar front, subtropical high, and the intertropical convergence zone respectively. Blue arrows indicate major wind directions. Red/blue arrow indicates the position of the AMOC. 3

Figure 3. Molecular structure of *n*-alkanes and fatty acids (alkanoic acids). 8

Figure 4. *n*-Alkane distributions from two lacustrine sediment samples displaying an odd over even predominance. 9

Figure 5. Hydrogen and oxygen fractionation processes during evaporation and change in isotopic signature of precipitation due to the rainout effect (SAHRA, 2014). 13

Figure 6. Fractionations during lipid biosynthesis (modified after Yang and Leng, 2009). 14

Figure 7. Molecular structure of branched and isoprenoid GDGTs after Schouten et al. (2013) and De Jonge et al. (2014). 16

Figure 8. Molecular structure of the fecal stanols 5ß-coprostanol and 5ß-stigmastanol. 18

Figure 9. Molecular structure of three different combustion derived polycyclic aromatic hydrocarbon. 19

Figure 10. Schematic diagram of analytical methods for lipid analyses. 20

Figure 11. Map of Fennoscandia and the North Atlantic region with schematic positions of the polar frontal zone at (a) positive NAO/AO index and (b) negative NAO/AO. Asterisk marks the position of Lake Torneträsk. 23

Figure 12. a) Lake Torneträsk satellite image. b) Coring location of core Co1280. Yellow line indicates track lines of hydroacoustic profiles. c) Seismic profile (blue line) crosscutting Abiskojåkka delta from NW to SE including location of core Co1280. For details on hydroacoustic data acquisition see Vogel et al. (2013). 25

Figure 13. Biomarker and inorganic data of core Co1280 plotted against age. (a) δD_{wax}, (b) flood frequency, (c) *n*-alkane ACL, (d) BIT index, (e) summer MAT. Also shown are (f) pollen-inferred mean annual precipitation at Lake Tibetanus (Barnekow 1999), (g) Scandinavian glacier and tree line advance (Karlén and Kuylenstierna, 1996), (h) GISP2 potassium (K^+; ppb) ion (Mayewski et al., 1997) and (h) July insolation at 65°N calculated after Berger and Loutre (1991). 30

Figure 14. Lake Torneträsk, Core Co1280: Diagram of biomarker and inorganic data plotted against age. a) δD_{C28} (blue), δD_{C26} (red), b) $\delta^{13}C_{C28}$ (green), $\delta^{13}C_{C26}$ (brown), c) mean flood layer thickness, d) concentration of HMW *n*-fatty acids, e) concentration of HMW *n*-alkanes, f) MBT'/CBT derived MAT calibrated after Peterse et al. (2012), g) MBT'/CBT-derived MAT calibrated after De Jonge et al. (2014). 32

Figure 15. Elemental data of core Co1280 showing a) Titanium (Ti), b) Iron (Fe), and c) Calcium (Ca). Also shown is d) North Atlantic drift ice stack (in percentage variations in petrologic tracers; Bond et al., 2001). 33

Figure 16. Map of the study area including Lake Dojran and adjacent paleorecords. 39

Figure 17. Map of topsoil (red, 1-5) and bird feces (blue, A-B) samples from the Dojran catchment. 46

Figure 18. Lake Dojran, core Co1260: diagram of biomarker and pollen data plotted against age. (a) Δ annual MAT, (f) BIT index, (g) HMW *n*-alkanes, (h) PAHs, (i) microcharcoal (asterisks mark the presence of largest microcharcoal particles (>250 µm)), (j) β-stanols, (k) total pollen of terrestrial plants, (l) cultivated/cultivable, (m) ACL, (n) deciduous and conifer trees, and (o) AP (pollen of arboreal plants), NAP (pollen of nonarboreal plants) comprehending grasses and other herbs (for taxonomic affiliation see section 4.5). Also shown are previously published data including (b) $\delta^{18}O_{carb}$, (c) $\delta^{13}C_{org}$, (d) potassium and iron counts, and (e) TOC and TOC/TS (Francke et al., 2013). 49

Figure 19. Schematic modern positions of the ITCZ (dark blue) and the CAB (light blue) over Africa during NH summer and winter. Also shown are paleorecords including: 1. Lake Dendi (this study); 2. Lake Tana (Costa et al., 2014); 3. Lake Chew Bahir (Foerster et al., 2012); 4. Lake Victoria (Berke et al., 2012); 5. Lake Challa (Tierney et al., 2011b); 6. Lake Tanganyika (Tierney et al., 2008; 2010b); 7. Lake Yoa (Kröpelin et al., 2008); 8. Qunf cave (Fleitmann et al., 2007); 9. Northwest African margin (deMenocal et al., 2000; Tierney et al., 2017); 10 Gulf of Aden (Tierney and deMenocal, 2013); 11 Congo River outflow (Schefusz et al., 2005); 12 Nile river fan (Castañeda et al., 2016). 59

Figure 20. Concentrations of Crenarchaeol (blue line) and brGDGTs (brown line) in Lake Dendi sediment cores DEN1 and DEN2. Red shading marks strongly fluctuating Crenarchaeol concentrations. 62

Figure 21. Comparison of African plant leaf wax δD records including: a) Lake Dendi, b) Gulf of Aden (Tierney and deMenocal, 2013), c) Lake Victoria (Berke et al., 2012), d) Lake Tana (Costa et al., 2014), e) Lake Challa (Tierny et al., 2011b), f) Lake Tanganyka (Tierny et al., 2010b), g) Congo Basin (Schefuß et al., 2005). Also shown is h) the mean July insolation at 15°N after Berger and Loutre (1991). 66

Figure 22. Comparison of b) Lake Dendi plant leaf wax δD data and pace of the a) Indian Ocean Monsoon (Fleitmann et al., 2003) and c) West African Monsoon (Weldeab et al., 2007). 67

Figure 23. Comparison of African molecular temperature records including: a) Lake Dendi, b) Lake Malawi (Powers et al., 2005), c) Lake Tanganyka (Tierny et al., 2008), d) Congo Basin (Weijers et al., 2007c), e) Lake Victoria (Berke et al., 2012). 70

Figure 24. Lake Dendi plant leaf wax a) $\delta^{13}C$, b) $\%C_4$ vegetation estimates, c) $\delta^{13}C_{C29}$-$\delta^{13}C_{C31}$ isotope spread, d) HMW *n*-alkane ACL (C_{27}-C_{33}), e) BIT index. Also shown: f) Mean insolation August-September-October at 10°N after Berger and Loutre (1991). 71

Figure 25. Selected molecular records of Holocene climate change from Lake Torneträsk, Lake Dojran, and Lake Dendi. Blue box marks the onset of the monsoonal circulation and re-strengthening of the AMOC. Red shading marks the Holocene thermal optimum period. Green shading mark periods of Holocene climatic and environmental changes. 76

List of tables

Table 1. Range of $\delta^{13}C$*n*-alkane values for different plant types of subtropical (Bi et al., 2005) and tropical African (Castañeda et al., 2009) vegetation. 11

Table 2. Average fractionation factors (ε_{water}) between environmental water and *n*-alkanes of plants from Japan and Thailand detected by (Chikaraishi and Naraoka, 2003). 15

Table 3. AMS ^{14}C ages of terrestrial plant macrofossils and bulk sediment samples from Core Co1280. 26

Table 4. Molecular and isotopic data of Core Co1280. 29

Table 5. Lake Dojran, core Co1260: Biomarker concentrations and molecular proxy data. 45

Table 6. MBT'/CBT proxy-derived annual MAT of topsoil samples and β-stanols of bird feces from the Dojran catchment. 46

Table 7. Biomarker-based indices, temperatures, and stable carbon and hydrogen isotopic data of Lake Dendi sediment cores DEN1 and DEN2.Molecular and isotopic data of cores DEN1 and DEN2. 63-64

List of abbreviations

ACL average chain length
$AgNO_3$ silver nitrate
AHP African Humid Period
AMS accelerator mass spectrometry
AMOC Atlantic Meridional Overturning Circulation
AO Arctic Oscillation
AP arboreal pollen
ASE Accelerated Solvent Extraction
a.s.l. above sea level
BC before Christ
BIT branched vs. isoprenoidal tetraether index
BP before present (present = 1950)
br branched
C carbon
Ca calcium
CAB Congo air boundary
cal calibrated
CAM crassulacean acid metabolism
carb carbonate
CBT cyclisation ratio of branched tetraether
CH_4N_2O urea
CO_2 carbon dioxide
conc concentrated
CPI carbon preference index
cts counts
D deuterium
DCM dichloromethane
DOXP 1-deoxy-D-xylulose-5-phosphate
E east
Et evapotranspiration
EQ equator
FA fatty acid
FAME fatty acid methyl ester
Fe iron
FID flame ionization detector
g gram
GC gas chromatography
GDGT glycerol dialkyl glycerol tetraether
GMWL global meteoric water line
H_2O_{MQ} ultrapure water
ha hectar
HCl hydrochloric acid
HCO_3 bicarbonate
Hex hexane
HMW high molecular weight
IRD ice rafted debris
IRMS isotope ratio mass spectrometry
ITCZ Intertropical Convergence Zone
Iso isoprenoid
K potassium
ka kiloannum (thousand years)
KCl potassium chloride
KOH potassium hydroxide
kV kilovolt
LIA Little Ice Age
LMW low molecular weight
LMWL local meteoric water line
LST lake surface temperature
m meter
M molar
mA milliampere
MAT mean air temperature
MBT methylation index of branched tetraethers
MeOH methanol
MEP 2-methylerythroyl-4-phosphate
MHW medium molecular weight
MRT mean residence time
MVA mevalonic acid
MWP medieval warm period
n normal
N_2 nitrogen
NADPH nicotinamide adenine dinucleotide phosphate
NAO North Atlantic Oscillation
NAP non arboreal pollen
NH Northern hemisphere
N north
OM organic matter
PAH polycyclic aromatic hydrocarbon
Ppb part per billion
R ratio
R^2 coefficient of determination
rH relative humidity
S south
SiO_2 Siliciumdioxid
SST Sea Surface Temperature
TEX_{86} tetraether index of 86 carbons
Ti titanium
TLE total lipid extract
TOC total organic carbon
TS total Sulphur
UHPLC ultrahigh performance liquid chromatograph
V volume
VPDB Vienna Pee Dee Belemnite
VSMOW Vienna Standard Mean Ocean Water
W west
XRF X-ray fluorescence
YD Younger Dryas
yr year
yrs years
µg microgram
µm micrometer
µS micro Siemens

1. Introduction

Since the mid-20th century, global ocean and atmospheric temperatures have been rising most likely due to an anthropogenic derived increase in the atmospheric concentration of greenhouse gases (Oreskes, 2004; Stocker, 2014). For the future, climate models predict an ongoing global warming trend inevitably leading to major climatic and environmental changes all over the globe (Diffenbaugh and Field, 2013; Stocker, 2014). Anticipated effects, apart from rising temperatures, include changing precipitation patterns, melting of glaciers and sea ice, a rising sea level, changing seasonality, ocean acidification, and an increase in extreme weather events (Walther et al., 2002; Meehl et al., 2005; Rosenzweig et al., 2008). However, climate model predictions exhibit significant uncertainties and differences in the magnitude of change due to insufficient knowledge about natural climate variability, processes and feedback mechanisms (Lashof and et al., 1997; Liepert and Previdi, 2009). Thus, more detailed insights into climatic processes and mechanisms are essential for the prediction of future climate and environmental change. Of particular importance is the climate of the Holocene (11.7 ka BP until present; Walker et al., 2012), due to its analogues to the modern day climate. Furthermore, Holocene climate dynamics occur on scales significant to humans and ecosystems (Mayewski et al., 2004). In this context, multiple studies suggest societal collapse of ancient civilizations connected to Holocene rapid climate changes (Hodell et al., 1995; Weiss and Bradley, 2001; deMenocal, 2001; White, 2011; Dalfes et al., 2013). Thus, knowledge about Holocene climatic processes is crucial for the assessment of both natural and anthropogenic future climate and environmental change.

1.1 Holocene climate variability – Forcing and Feedbacks

Compared to prior epochs in earth’s history, the climate of the Holocene is traditionally regarded as relatively stable (Dansgaard et al., 1993; Johnsen et al., 1997). However, Holocene climate also showed significant fluctuations although perturbation occurred on a smaller magnitude compared to Pleistocene (Bond et al., 1997; Bianchi and McCave, 1999; Mayewski et al., 2004). The extrinsic forcing of Holocene climate is mainly controlled by the precession and the changing angle of the earth’s axial (obliquity; Milankovitch, 1941; Hays et al., 1976). Changes in these orbital parameters (Fig. 1) resulted in a decrease in the solar radiation (insolation) of ~0.2 % (~40 W/m^2) in Northern Hemispheric (NH) summer since the Early Holocene until present (Berger and Loutre, 1991). Furthermore, solar activity exhibits periodical fluctuations on different time-scales (solar variation). The most prominent examples include the 11 year Schwabe cycle (Eddy, 1976), the 88 year Gleißberg cycle (Peristykh and Damon, 2003) and the 205 year de Vries cycle (Wagner et al., 2001).

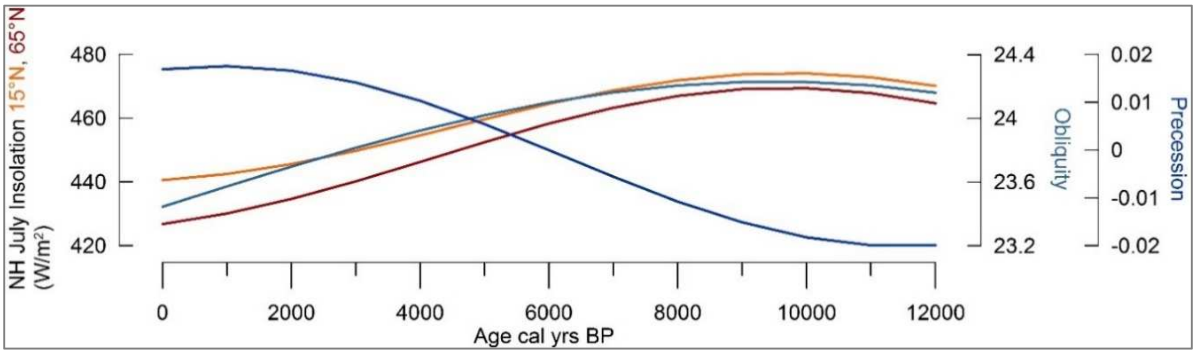

Figure 1. Holocene orbital climate forcing.

Internal variabilities in large-scale atmospheric and oceanic circulation systems (Fig. 2) exhibit the intrinsic forcing of Northern Hemisphere climate: The Atlantic Meridional Overturning Circulation (AMOC), for example, is a large-scale ocean circulation system driven by density variations of the Atlantic Ocean water (Rahmstorf, 2003a) that plays a major role for decadal/multidecadal variability in the climate system (Polyakov et al., 2010; Mahajan et al., 2011). The AMOC is part of the global thermohaline circulation and functions as a heat and energy conveyor to the northern latitudes (Trenberth and Caron, 2001). Therefore, variabilities in the strength of the AMOC can lead to changes in mean annual temperatures of up to 10 °C in the circum-North Atlantic region even on a very short time scale (Ganopolski and Rahmstorf, 2001; Knight et al., 2005). Furthermore, fluctuations in the North Atlantic sea surface temperature (SST), commonly referred to as the Atlantic Multidecadal Oscillation (AMO; Kerr, 2000) exhibit widespread climatic influence on precipitation pattern/distribution in the Sahel (Rowell et al., 1995), in Northeast Brazil (Folland et al., 2001) and in North America (Sutton and Hodson, 2005). Global circulation models suggest a strong linkage between the AMOC and AMO (Wang and Zhang, 2013; Marini and Frankignoul, 2014).

The North Atlantic/Arctic Oscillations (NAO/AO) describe the atmospheric pressure gradient between the Arctic and the lower latitudes and control the position and sinuosity of the polar front, the polar Jetstream and the westerlies (Visbeck et al., 2001; Hurrell et al., 2013). Fluctuations in the NAO/AO index are associated with large-scale changes in temperature, precipitation and atmospheric circulation pattern from northern Africa (Moulin et al., 1997), the Middle East (Felis et al., 2000), and Europe (Rodwell et al., 1999; Trigo et al., 2002), up to the high latitudes (Dickson et al., 2000). It has also been suggested that AMOC and NAO/AO are linked by strong bilateral teleconnections (Ottera et al., 2010; Frankignoul et al., 2013; Wen et al., 2016). The climate in the lower latitudes is mainly controlled by the seasonal shift of the Intertropical Convergence Zone (ITCZ), a zenithal controlled latitudinal belt of wind convergence and precipitation, and associated monsoonal flow (Shangcheng, 1988; Okajima et al., 2003; Fleitmann et al., 2007). Major monsoonal systems, exhibiting seasonal reversing wind circulations, of the NH include the West African (Weldeab et al., 2007), East African (Weldeab et al., 2014) and Indian Ocean (Fleitmann et al., 2003; Fleitmann et al., 2007) monsoons. In addition to these natural factors, early anthropogenic land-use also exhibited/induced a forcing of Holocene climates and environments. Especially since the Neolithic revolution and the introduction of agriculture roughly 8,000 years ago, humans have altered a significant part of the earth's terrestrial and aquatic ecosystems (Ellis, 2011; Goudie, 2013). Land use practices such as "slash-and-burn" or extensive livestock grazing have often resulted in vegetation shifts, destabilization of soils or water quality degradation (Dubois and Jacob, 2016). By altering the earth's albedo and surface heat balance through widespread deforestation, humans might have even affected regional patterns of hydrology and temperature (Strandberg et al., 2014).

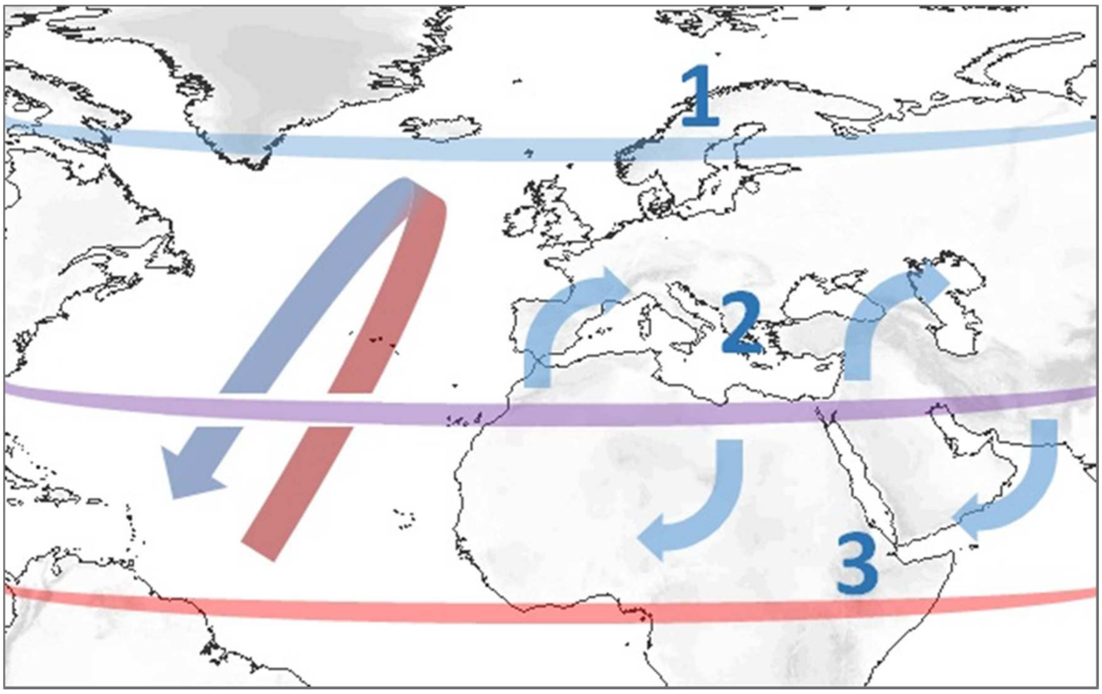

Figure 2. Schematic map of NH atmospheric and oceanic circulation pattern including positions of lake sedimentary records analyzed for this thesis: 1) Lake Torneträsk, Sweden (see chapter 3); 2) Lake Dojran, Macedonia/Greece (see chapter 4); 3) Lake Dendi, Ethiopia (see chapter 5). Blue, purple, and red zones indicate the position of the polar front, subtropical high, and the intertropical convergence zone respectively. Blue arrows indicate major wind directions. Red/blue arrow indicates the position of the AMOC.

Holocene climate forcing lead to a long-term cooling trend in the Northern Hemisphere (Davis et al., 2003; Liu et al., 2014; Sejrup et al., 2016) and to migrations of the earths atmospheric and oceanic circulation systems since the Early Holocene (Haug et al., 2001). As of today, the nature, timing and regional environmental impacts of these shifts are still relatively uncharted (deMenocal et al., 2000; Haug et al., 2001; Anderson et al., 2005; Tierney et al., 2017; Kröpelin et al., 2008; Junginger et al., 2014). Furthermore, this long-term climatic trend is thought to be superimposed by centennial to millennial scale climate oscillations with a proposed frequency of ~ 2,800–2,000 years and ~1,500 years (Stuiver and Braziunas, 1989; Bond et al., 1997; Mayewski et al., 1997; Bond et al., 2001; Wanner et al., 2008; Nederbragt and Thurow, 2005). Evidence of these events is most prominent by ice-rafted debris found in North Atlantic sediment cores (Bond et al., 1997; Bond et al., 2001). The cyclicity of Holocene millennial scale climate fluctuations, however, is highly debated and forcing mechanisms, whether solar or oceanic/atmospheric are still insufficiently unraveled (Rahmstorf, 2003b; Turney et al., 2005; Braun et al., 2005; Nederbragt and Thurow, 2005; Debret et al., 2007).

1.2 Holocene climate evolution

The Holocene started with a transitional warming after the cold Younger Dryas period (12.9 - 11.7 ka; Broecker et al., 2010; Carlson, 2010) at the end of the last glacial at about 11,700 yrs cal BP. The end of the YD, led to a reinvigoration of the AMOC and an associated enhancement of northward heat transport (Clark et al., 2002), as well as to a re-strengthening of the Northern Hemisphere monsoon circulations (Weldeab et al., 2014; Fleitmann et al., 2003). After the deglaciation, Holocene peak warming occurred during the so-called Holocene Thermal Maximum period (HTM; Renssen et al., 2012; Marcott et al., 2013) between approximately 9,500 to 5,000 yrs BP. Warmer conditions during the HTM period were interrupted by a short cold and dry spell around 8.200 cal yrs BP, globally known as the 8.2 ka event (Alley and Ágústsdóttir, 2005; Kobashi et al., 2007). This rapid climatic change was most likely initiated by a meltwater pulse to the North Atlantic due to the collapse of the Laurentide ice sheet and resulted in a slowdown of the AMOC and the associated heat transport (Barber et al., 1999; Ellison et al., 2006). After ~5,000 yrs cal BP global mean temperatures declined, following a linear decrease in NH summer insolation. The decreasing temperature trend culminated during the Little Ice Age period (LIA ~ AD 1,300 and 1,900 Bradley and Jonest, 1993; Matthews and Briffa, 2005). Furthermore, an associated southward migration and weakening of global circulation systems over the course of the

Holocene as well as long-term changes in NAO/AO like atmospheric circulation resulted in significant climatic and environmental changes all over the globe: Examples of these changes are drying in the Mediterranean (Wick et al., 2003), drying in northern Africa and the Sahel, known as the termination of the African humid period (AHP; deMenocal et al., 2000; Tierney et al., 2017; Kröpelin et al., 2008), and rebirth/growth of Northern-Hemispheric mountain- (Ryder and Thomson, 1986; Herren et al., 2013) and high latitude glaciers (Nesje et al., 2001) as well as ice sheets (neoglaciation; Kumar, 2011).

1.3 Thesis outline

The aim of this thesis is to assess the variability and natural/anthropogenic forcing and feedback mechanisms of the Holocene climate and environment. Therefore, molecular, isotopic, and inorganic sedimentological analyses are applied to three different sedimentary records from the Arctic, the middle latitudes and the Tropics (Fig. 2):

Chapter 2: Lipid Biomarker from lake sediments as proxies for climate and environmental variability.

This chapter describes and assesses the proxies and methodology used for this thesis.

Chapter 3: Neoglacial changes in atmospheric circulation patterns over the North Atlantic and Fennoscandia recorded in Lake Torneträsk sediments.

To constrain changes in Holocene atmospheric circulation pattern in response to orbital forcing and their effects on the environment in Fennoscandian we use lipid biomarker, inorganic proxies, and compound specific δD analysis of sedimentary organic matter from a sedimentary record from Lake Torneträsk (Sweden). Owing to its climate being influenced by both the North Atlantic and the polar frontal zone, northern Fennoscandia can be regarded as a key region to better understand the regional expression and potential threshold effects of insolation-forced migrations of atmospheric circulation systems.

Chapter 4: Organic geochemical and palynological evidence for Holocene natural and anthropogenic environmental change at Lake Dojran (Macedonia/Greece).

In this chapter we apply biomarker, microcharcoal and pollen analyses to a sedimentary record from Lake Dojran (Macedonia/Greece) to reconstruct climatic, environmental, and human impact on the southern Balkan.

The southern Balkan region played a key role in the migration of the Neolithic lifestyle to Central Europe and is thus very suitable for studies of human-environment forcing and feedback mechanisms. This chapter refers to Thienemann et al., (2017) doi: 10.1177/0959683616683261.

Chapter 5: Holocene hydrological and atmospheric changes in East Africa inferred from lipid biomarker and leaf wax *n*-alkane δD of Lake Dendi (Ethiopia) sediments.

Here, we use compound specific δD and $\delta^{13}C$ analysis of sedimentary organic matter from Lake Dendi (Ethiopia) to detect changes in atmospheric circulation pattern, hydrology, and vegetation associated with the African Humid Period. Due to its location in proximity of the Congo Air Boundary and the ITCZ, the Dendi region can play a crucial role in the understanding of past changes in atmospheric circulation pattern of the tropical regions.

2. Biomarker from lake sediments as proxies for climate and environmental variability

Studies of past climatic and environmental changes can be obtained from multiple diverse types of archives such as ice cores (Mayewski et al., 1997; Abram et al., 2013), stalagmites (Bar-Matthews et al., 1999; Fleitmann et al., 2003; Fairchild and Baker, 2012), tree rings (McCarroll and Loader, 2004; Wilson et al., 2016), peat bogs (Blackford, 2000; Poto et al., 2013), and marine (Schilman et al., 2001; Rothwell and Croudace, 2015), and lacustrine (Meyers and Ishiwatari, 1993; Leng and Marshall, 2004) sediments. For the investigation of paleo-environmental and -climatic changes, especially on shorter time-scales, lacustrine sediments are particularly suitable as archives for several reasons: The lakes small water body leads to relatively high sedimentation rates and thus allows high temporal resolutions compared to ocean archives. Usually, only small amounts of sediments are lost through discharges, which leads to a high continuity of lacustrine archives. Furthermore the relatively small water body of a lake reacts/responds very quickly to external forcing, thus being able to record rapid centennial to millennial scale climate changes (Talbot and Allen, 1996; Cohen, 2003; Elias, 2006).

Sedimentary organic matter (OM) from lacustrine archives can reveal a variety of information regarding physical, chemical and biological changes and processes of the lake and its environment (Meyers and Ishiwatari, 1993). The main sources of sedimentary organic matter are terrestrial higher plants, phytoplankton, bacteria and algae. The deposited OM can be divided into two main groups: material with a terrestrial origin produced outside the lake is designated allochthonous, while aquatic material which is produced in the lake itself, is referred to as autochthonous (Cohen, 2003; Elias, 2006). However, in most lakes, the overwhelming majority (> 99%) of organic matter is recycled while sinking through the water column and in the surface sediment layer (Hedges and Keil, 1995). Only a small fraction of the organic matter, such as certain lipid molecules, is recalcitrant against remineralization and is accumulated in the sediment (Tegelaar et al., 1989). These type of molecules have the potential to be used as so-called biomarkers in paleo-environmental and –climatic studies.

These Biomarker molecules are stable over geological timescales and can be traced to a specific biosynthetic origin or process (Eglinton et al., 1964; Killops et al., 2004b; Eglinton and Pancost, 2004). The majority of biomarker belong to the group of lipids (Brocks and Pearson, 2005), a compound class in organic geochemistry which is insoluble in water but soluble in organic solvents (Killops et al., 2004b). The occurrence, structure, ratio, and isotopic composition of lipid biomarker molecules from lake sediments can help to unravel paleo-environmental and -climatic questions, e.g., about element cycling, oxidation-reduction conditions, sediment and water chemistry, vegetation, and temperature histories (Peters et al., 2005). Different transport mechanism of biomarker molecules, however, can result in leads and lags of certain proxies (Eglinton and Eglinton, 2008). Thus, for example branched Glycerol dialkyl glycerol tetraether produced in soils are transported into the lake via fluvial/riverine input (Schouten et al., 2013). Soil turnover rates and storage of organic matter, however, can vary in different latitudes and climates (Chen et al., 2013) leading to different setbacks of biomarker produced/stored in soils. Other biomarker molecules such as *n*-alkanes can also be transported via an aeolian mode through for example wind-abrasion from plant leaf surfaces (Schefuß et al., 2003). Apart from leads and lags, different transport modes can further lead to proxy signals representing more proximal (fluvial) or more distant (aeolian) source areas (e.g. Thienemann et al., 2017). Dilution effects by lithogenic and aquatic-produced Material can be accounted for by the normalization to the total organic carbon (TOC) content of the sediment.

2.1 *n*-Alkanes and fatty acids

Normal- or *n*-alkanes and fatty (alkanoic) acids belong to the group of acyclic hydrocarbons and consist of hydrogen and carbon with the formula C_nH_{2n+2} (Fig. 3). Fatty acids also contain of a carboxyl group (Killops et al., 2004b).

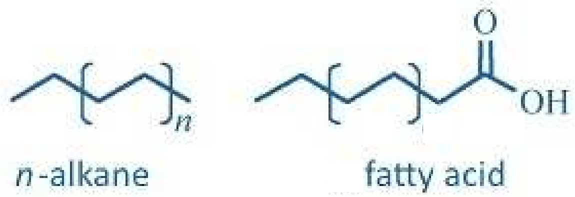

Figure 3. Molecular structure of *n*-alkanes and fatty acids (alkanoic acids).

In nature, *n*-alkanes and fatty acids are produced by various types of organisms such as bacteria, archaea, fungi, plants, and animals (Peters et al., 2005). The chain length (number of carbon atoms) of *n*-alkanes and fatty acids can be diagnostic for the respective biosynthetic origin (Cranwell, 1973). In this context, high molecular weight (HMW) fatty acids (C_{26}-C_{32}) and *n*-alkanes (C_{27}-C_{33}) mainly derive from the epicuticular leaf waxes of higher land plants, protecting the plant against water loss, bacteria, fungi, and leaching of minerals (Meyers and Ishiwatari, 1993; Bianchi and Canuel, 2011). In contrast, algae and aquatic plants, are dominated by low molecular weight (LMW) fatty acids such as C_{16} and C_{18} and the LMW *n*-alkanes C_{17} and C_{19}. Due to this fact, changing concentrations of HMW/LMW *n*-alkanes and fatty acids can indicate a change in terrestrial input versus aquatic production respectively.

Medium molecular weight (MMW) *n*-alkanes (mainly C_{21} - C_{25}) are dominant in emerged and submerged macrophytes. The average chain length (ACL) of HMW *n*-alkanes can be further diagnostic for specific terrestrial plant types, such as woody or herbaceous/grass vegetation (Maffei, 1996; D'Anjou et al., 2012).

(1) $$ACL = \frac{(C27*27+C29*29+C31*31+C33*33)}{(C27+C29+C31+C33)}$$

Despite the vegetation type, the *n*-alkane chain length distribution is controlled by environmental factors such as temperature and humidity (Gagosian and Peltzer, 1986; Poynter et al., 1989), potentially complicating the use of the ACL proxy. While fatty acids show an even-number over odd-number predominance in higher plants, *n*-alkanes usually occur with an odd over even dominance (Fig. 4).

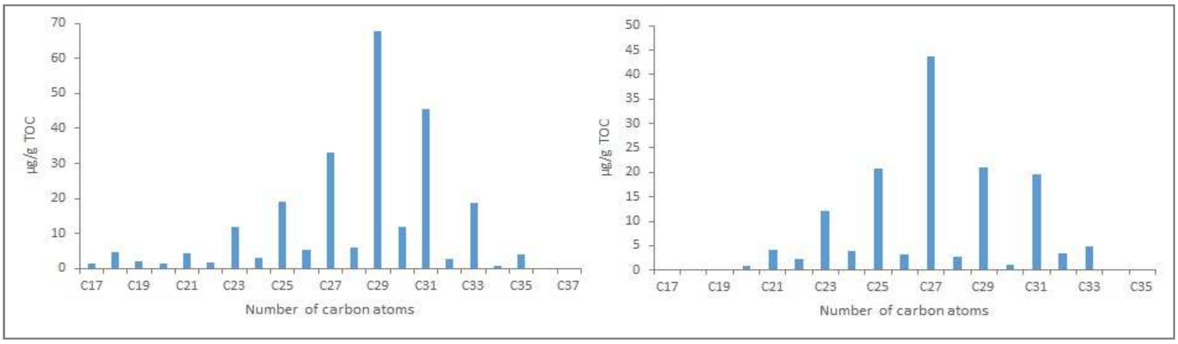

Figure 4. *n*-Alkane distributions from two lacustrine sediment samples displaying an odd over even predominance.

The inverse proportion results from the loss of a carbon atom during decarboxylation from the precursor even-numbered fatty acid (Eglinton and Eglinton, 2008). Furthermore, odd numbered *n*-alkanes can get degraded to even numbered in the processes of diagenesis and catagenesis (Meyers and Ishiwatari, 1993). The relative abundances of odd and even numbered compounds in a sample is estimated by the carbon preference index (CPI; Bray and Evans, 1961).

(2) $$CPI = 0.5 * \left[\frac{(C27+C29+C31*C33)}{(C26+C28+C30+C32)} + \frac{(C27+C29+C31+C33)}{(C28+C30+C32+C34)}\right]$$

In this context, the CPI can be used as an indicator for the maturity of a sediment sample and for the degree of fossil fuel contribution, which is crucial for the analyses of compound specific stable isotopes. Natural vegetation waxes typically show CPI values above 5 (Eglinton and Hamilton, 1963).

2.1.1 Compound specific stable isotope analysis of plant leaf wax hydrocarbons

Studies of stable carbon, oxygen and hydrogen isotopes in lake sediments exhibit a powerful tool for resolving paleo-environmental and –climatic questions. However, organic matter in lacustrine deposits consists of a very wide variety of different organic compounds that each differ significantly in their isotopic composition (Schimmelmann et al., 2006; Chikaraishi and Naraoka, 2007). The analysis of individual compounds, especially lipids, can circumvent this problem (Sachse et al., 2012).
Isotopic values are expressed with the help of the Delta (δ) notation, which describes the relative deviation of the Ratio (R) of the heavy isotope to the light isotope in a sample over the isotope ratio of a standard in per mil (‰).

(3) $$\delta R = \left[\frac{(R\ sample - R\ sample)}{R\ standard}\right] * 1000\ ‰$$

International reference standards for carbon (Vienna Pee Dee Belemnit; VPDB) and for hydrogen (Vienna Standard Mean Ocean Water; VSMOW) are issued by the International Atomic Energy Agency (IAEA). Isotopic ratios are affected by a multitude of isotopic fractionation effects during various physical and biochemical processes. The magnitude of fractionation is expressed as the fractionation factor α, while the fractionation between source and product can also be expressed with the enrichment factor ε (Cohen, 2007; Hoefs, 2008; Michener and Lajtha, 2008).

Compound specific carbon isotopes

Carbon is the major compound of all living organisms on earth and exhibits two stable isotopes of which the light ^{12}C occurs with a percentage of ~98.9 % and the heavy ^{13}C with a percentage of ~1.1 % (Killops et al., 2004a). A multitude of studies from various environmental settings (Bird et al., 1995; Schefuß et al., 2003; Liu et al., 2005; Castañeda et al., 2009; Berke et al., 2012; Tierney and deMenocal, 2013; Aichner et al., 2015) have proven that analysis of compound specific leaf wax carbon isotopes reliably mirror past changes in vegetation type and cover. During plant photosynthesis, the fixation of carbon from atmospheric CO_2 can happen via three different biosynthetic pathways, that each involve different carbon isotopic fractionations. The largest group of plants (C_3), consisting of ~95% of the earth's terrestrial biomass (including trees and shrubs), use the Calvin-Benson cycle for carbon fixation. In contrast, C_4 plants including mostly grasses (*poaceae*) and sedges (*cyperaceae*), mainly grow in tropical and sub-tropical regions and use the Hatch-Slack cycle for carbon fixation. An additional mechanism is the Crassulacean acid metabolism (CAM), involving uptake and CO_2 fixation during the night and only used by a relatively small group of aridity adapted plants (O'Leary, 1988; Meyers and Ishiwatari, 1993). The different carbon isotopic fractionation factors inherent in these pathways are incorporated in the carbon isotopic signature of plant wax lipids such as *n*-alkanes or *n*-fatty acids. Hence, plant leaf waxes of C_3 plants are generally depleted in ^{13}C with respect to waxes produced by C_4 vegetation (Tab. 1). Leaf waxes derived from plant utilizing the CAM typically show intermediate $\delta^{13}C$values (Chikaraishi and Naraoka, 2003; Bi et al., 2005; Eglinton and Eglinton, 2008). *n*-Alkanes and Fatty acids exhibit very similar fractionation factors during photosynthesis (C_3, C_4, CAM), leading to similar carbon isotopic signatures. Fatty acids only show a slight ^{13}C-depletion (averaging 1.4 ‰ ± 1.1 ‰) compared to *n*-alkanes from the same plant species (Chikaraishi et al., 2004; Chikaraishi and Naraoka, 2007;). Furthermore, various environmental factors can influence the $\delta^{13}C$ values of plant wax lipids: Hence, during periods of higher aridity, plants tend to narrow their leaf stomata to account for enhanced loss of water, which in turn can lead to a ^{13}C-enrichment of plant lipids (Diefendorf et al., 2010). Decreasing light intensity (canopy effect) can lead to ^{13}C depleted isotopic values due to variations in in-leaf processes in response to increased shade (van der Merwe and Medina, 1991; Bonafini et al., 2013). The uptake of respirated CO_2 from soils, usually depleted in ^{13}C compared to atmospheric CO_2, can lead to a further ^{13}C depletion of plants (Bowling et al., 2008). Since atmospheric carbon is the source for plant photosynthesis, variations in atmospheric CO^2 can also alter the plants' carbon isotopic composition (Fontugne and Calvert, 1992; Feng and Epstein, 1995). A similar phenomenon, the so-called "Suess effect", caused by the anthropogenic release of fossil-fuel derived ^{13}C depleted CO_2 leads to a lowering of modern ^{13}C values in plants (Keeling, 1979).

Table 1. Range of $\delta^{13}C$*n*-alkane values for different plant types of subtropical (Bi et al., 2005) and tropical African (Castañeda et al., 2009) vegetation.

Subtropical plants		Tropical African plants	
plant type	$\delta^{13}C_{n\text{-alkanes}}$	plant type	$\delta^{13}C_{n\text{-alkanes}}$
C_3	-38.9‰ to - 29.1‰	C_3	-41.8‰ to -28‰
C_4	-26.4‰ to -14.1‰	C_4	-25.5‰ to -15.3‰
CAM	-29.5‰ to -21.5‰		

Compound specific hydrogen isotopes

With an abundance of 75 %, Hydrogen is the most common element in the universe. Hydrogen exhibits two stable isotopes of which the light ^{1}H protium (H) occurs with a proportion of >99.98 %, while the heavy ^{2}H deuterium (D) appears with a percentage of <0.002 (Schimmelmann et al., 2006). Compound specific hydrogen isotopes from lake sediments have been shown to reliably record past changes in the hydrological cycle (Schefuß et al., 2005; Tierney et al., 2008; Tipple and Pagani, 2010; Berke et al., 2012; Costa et al., 2014; Zhuang et al., 2014; Aichner et al., 2015). This is due to the fact that plant wax lipids incorporate, by interference, the D-isotopic composition of the plants source water (Sachse et al., 2012). Furthermore, compound specific isotope analysis of leaf wax hydrogen can have several advantages over the use of the classic $\delta^{18}O_{carbonate}$ proxy (Leng and Marshall, 2004) that in some cases might be biased by changing in-lake processes such as lake hydrology and temperature, seasonality of precipitation, or changes in taxa/species assemblages. In addition, suitable carbonate or silica producers are not ubiquitous in every lake (Sachse et al., 2012; Sauer et al., 2001). The relationship between ^{18}O and D in natural waters is described by the global meteoric water line (GMWL) defined after Craig (1961) as:

(4) $$\delta D = 8 * \delta 18O + 10‰$$

Site-specific environmental factors such as differences in humidity/aridity can lead to local deviations from the GMWL, resulting in local meteoric water lines (LMWL; Rozanski et al., 1993). The D isotopic composition of water vapor in the atmosphere shows additionally substantial variations over space and time. This can be attributed to Rayleigh type fractionation processes during evaporation and condensation of water (seawater δD = 0‰), with the evaporate being depleted in the heavy isotope D and the condensate being enriched in D (Fig. 5) (Kendall and Caldwell, 1998). These processes can be categorized into several environmental effects:

Continental/rainout effect: As precipitation is enriched in D relative to its source vapor, air masses that progress further inland onto the continent get progressively more D-depleted (Dansgaard, 1964; Rozanski et al., 1993). A similar effect occurs with increasing altitude (altitude effect), which leads to water vapor/precipitation being more D-depleted by -1 to -4‰ per 100 m (Holdsworth et al., 1991).

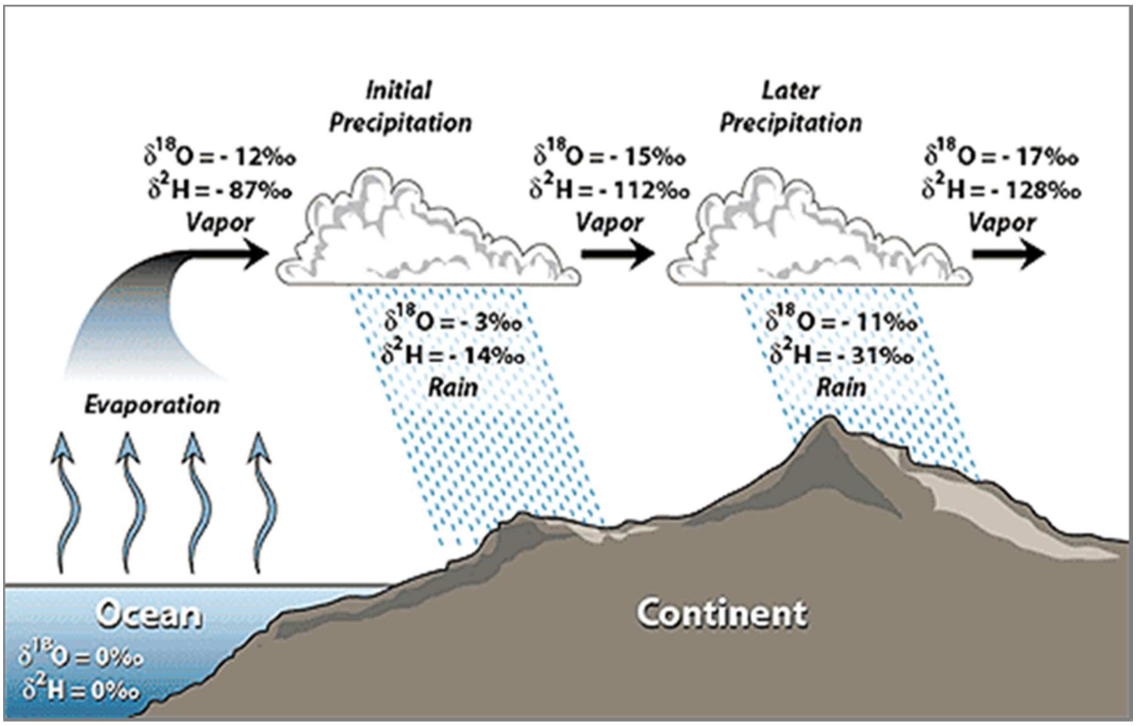

Figure 5. Hydrogen and oxygen fractionation processes during evaporation and change in isotopic signature of precipitation due to the rainout effect (SAHRA, 2014).

Temperature effect: The magnitude of isotopic fractionation between vapor and condensate increases with temperature. Thus, at 25°C, liquid water is enriched in $^{1}HD^{16}O$ by approximately 74 ‰ relative to the source vapor, whereas the fractionation becomes stronger at colder temperature (101‰ at 0°C) (Sachse et al., 2012). Dansgaard (1964) suggest a temperature-isotope relation based on measurements of North Atlantic coastal station of 0.69‰/°C for $\delta^{18}O$ and 5.6‰/°C for δD respectively. The temperature effect is most prominent in regions with a high magnitude of temperature variability, e.g. the high latitudes and regions with a strong continental climate (Bowen, 2008).

Amount effect: The amount effect describes the relationship between precipitation amounts and δD. Due to evaporation from falling raindrops and associated D-enrichment, small amounts of rainfall exhibit an isotopically heavier signature compared to higher amounts of rainfall (Dansgaard, 1964; Rozanski et al., 1993). This effect is further enhanced by high evaporation in arid climates leading to a further enrichment of environmental waters in D. Some studies suggest a threshold for the effect of evapotranspiration from soils and leafs (Hou et al., 2008; Pedentchouk et al., 2008; Feakins and Sessions, 2010;) at a relative humidity (rH) < 0.7 and

evapotranspiration (Et) < 1,000 mm/yr. The amount effect exhibits a strong control on δD in regions with insignificant temperature fluctuations such as the tropical regions (Bowen, 2008).
In addition to Rayleigh type environmental fractionation effects, the D-isotopic composition of lipids is further influenced by fractionation processes during biosynthesis (Fig. 6).

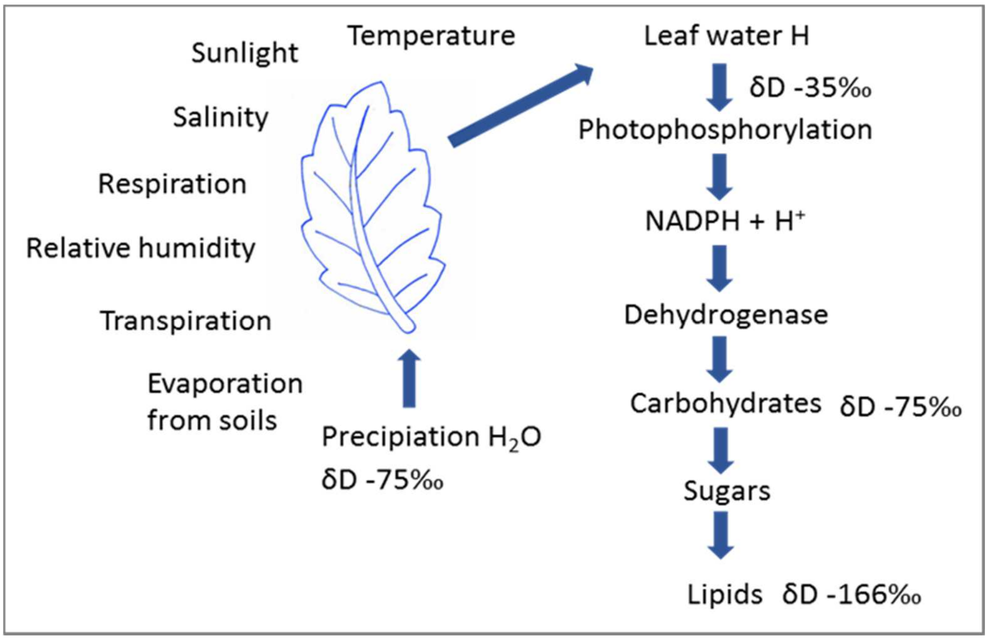

Figure 6. Fractionations during lipid biosynthesis (modified after Yang and Leng, 2009).

Fractionations during biosynthesis: The plant´s uptake and assimilation of hydrogen involves multiple different biochemical process and enzymatic reactions in which hydrogen is either removed, added, or exchanged. These reactions are associated with a variety of different isotopic fractionation effects leading to a wide range of δD values between −400‰ and +200‰ for lipids commonly employed as biomarkers (Sauer et al., 2001; Chikaraishi and Naraoka, 2003; Chikaraishi and Naraoka, 2007; Zhang and Sachs, 2007). The differences in isotopic compositions can be explained by 3 major biosynthetic effects (Sachse et al., 2012 and references therein):
1. Different biosynthetic pathways for lipid biomarker molecules. Steroids and terpenoids are produced via the mevalonic acid (MVA) pathway. The 1-deoxy-D-xylulose-5-phosphate (DOXP)/2-methylerythroyl-4-phosphate (MEP) pathway produces isoprenoid lipids. *n*-Alkyls are produced by the acetogenic pathway (Sachse et al., 2012).

2. Secondary hydrogen exchange reactions, hydrogenations, and dehydrogenations. For example decarboxylation leads to *n*-alkanes commonly being depleted in δD (25‰ ±16‰) compared to the corresponding fatty acid (Chikaraishi 2007).
3. Differences in the isotopic composition of H derived from nicotinamide adenine dinucleotide phosphate (NADPH; Sachse et al., 2012).

Influence of photosynthetic pathway and life form: According to Sachse (2012), *n*-alkanes from C_4 monocots are systematically ~15‰ more D-enriched than *n*-alkanes from C_3 monocots. These differences in fractionation have been attributed to, both, differences in leaf architecture (Helliker and Ehleringer, 2000) and pathways for NADPH formation (McInerney et al., 2011). Furthermore, variations in physiognomy and lipid biosynthesis lead to dicots (shrubs, trees, and forbs) being more D-enriched compared to monocots (grasses; Sachse et al., 2012). In paleo-environmental δD studies vegetational changes have thus to be accounted for. In comprehensive studies (Sachse et al., 2004) found a mean fractionation factor between *n*-alkanes and environmental water of -128 ‰ obtained from a N-S European transect and (Chikaraishi and Naraoka, 2003) reported a fractionation factor of -117 ‰ for long-chain *n*-alkanes from several C3 plants (Tab. 2).

Table 2. Average fractionation factors (ε_{water}) between environmental water and *n*-alkanes of plants from Japan and Thailand detected by (Chikaraishi and Naraoka, 2003).

Plant type	ε_{water} *n*-alkanes	
C4 plants	-132‰	±12‰
C3 angiosperms	-117‰	±27‰
C3 gymnosperms	-116‰	±13‰
CAM plants	-147‰	±10‰
freshwater plants	-135‰	±17‰

2.2 Glycerol dialkyl glycerol tetraether lipids

Glycerol dialkyl glycerol tetraether (GDGTs) are membrane lipids synthesized by archaea and bacteria (Schouten et al., 2013), that can be found in a very wide variety of natural environments such as marine (Sinninghe Damsté et al., 2002; Wuchter et al., 2005), lacustrine (Powers et al., 2004; Blaga et al., 2009), and terrestrial realms (Weijers et al., 2006; Huguet et al., 2010). GDGTs can be divided into branched (brGDGTs) and isoprenoid (isoGDGTs) forms (Fig. 7). While isoGDGTs mainly derive from archaea from the aquatic realm, the inversely structured brGDGTs are produced by bacteria with a mostly terrestrial origin (Schouten et al., 2013).

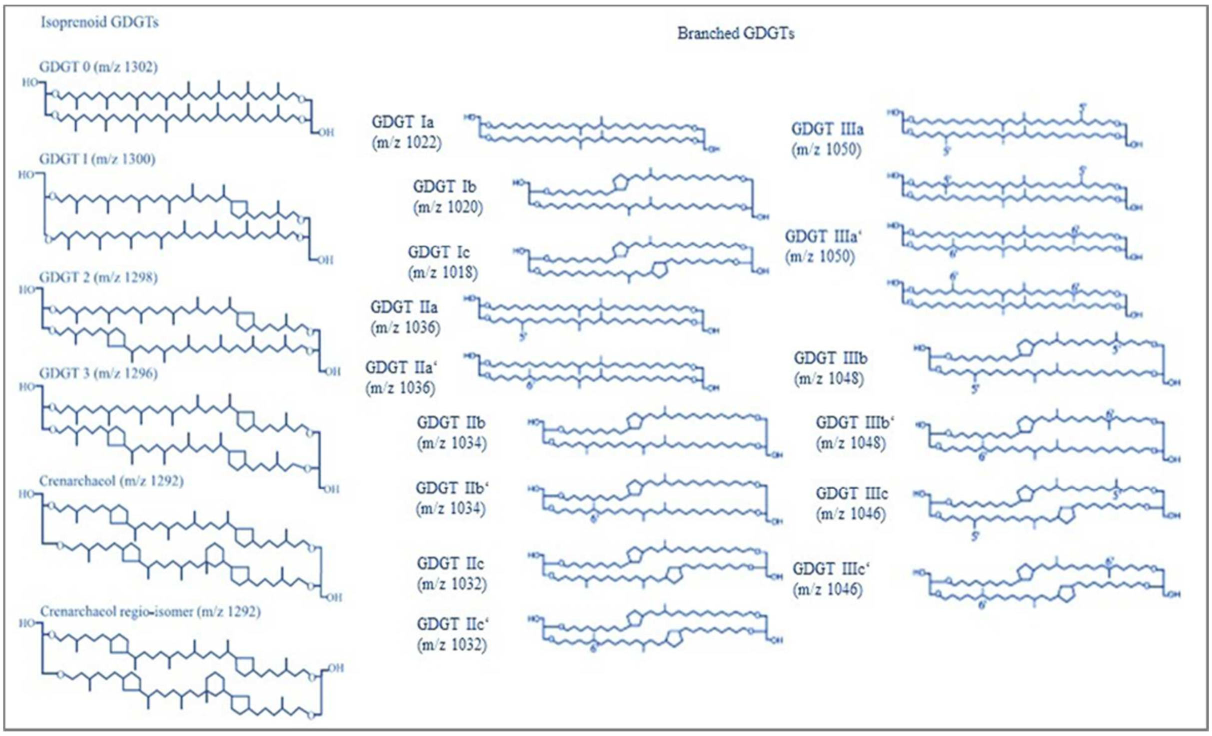

Figure 7. Molecular structure of branched and isoprenoid GDGTs after Schouten et al. (2013) and De Jonge et al. (2014).

Several paleo-environmental proxies are based on the relative abundance of different GDGTs as well as on their structural characteristics which are influenced by environmental factors such as temperature, pH or salinity (Hopmans et al., 2004; Powers et al., 2010; Peterse et al., 2012). For example, the branched vs. isoprenoidal tetraether index (BIT) is based on the distribution of brGDGTs and isoGDGTs and serves as a proxy for soil OM input (Schouten et al., 2013).

(5) $$BIT = \frac{(Ia+IIa+IIIa)}{(Crenarcheol+Ia+IIa*IIIa)}$$

It can be utilized to reconstruct soil erosion/runoff processes in lacustrine settings or near-shore environments (Verschuren et al., 2009; Sinninghe Damsté et al., 2011). However, in some cases the BIT index is biased by the aquatic endmember isoGDGT (Crenarchaeol). Hence, Fietz et al. (2011) suggest the use of brGDGT concentrations instead of the BIT index as indicator for terrestrial input.

The tetraether index of tetraethers consisting of 86 carbons (TEX_{86}) is based on the distributions of isoGDGTs which have been shown to correlate with annual mean sea surface temperatures (SST) (Schouten et al., 2002; Kim et al., 2008). In this context, the application of TEX_{86} as paleothermometer has been widely applied in both lacustrine (Berke et al., 2012; Blaga et al., 2013; Morrissey et al., 2017) and marine (Schouten et al., 2003; Huguet et al., 2007; Xing et al., 2013) settings. However, it has been suggested that isoGDGT Crenarchaeol also occurs in soil organic matter (Weijers et al., 2006). Thus, in some environments (BIT > 0.3), high contributions of terrestrial derived Crenarchaeol preclude the use of the TEX_{86} proxy as paleothermometer. Furthermore, production of isoGDGTs (mainly GDGT-2, see Fig. 7) by sedimentary Euryarchaeota involved in anaerobic oxidation might render TEX_{86} values inappropriate. Therefore, (Weijers et al., 2011) introduced the GDGT-2/Crenarchaeol ratio as a control value for anaerobic oxidation.
Furthermore, extensive studies (Weijers et al., 2007b) reported a strong relationship between mean annual air temperature (MAT), soil pH, and the methylation and cyclisation of branched tetraethers (MBT/CBT) in soils, allowing the application of the MBT/CBT as paleothermometer. More recent studies (Peterse et al., 2012), however suggest the use of MBT', which is based on the seven most common brGDGTs in soils, over MBT.

(6) $$MBT' = \frac{(Ia+Ib+Ic)}{(Ia+Ib+Ic+IIa+IIb+IIc+IIIa)}$$

(7) $$CBT = -\log\left[\frac{(Ib+IIb)}{(Ia+IIa)}\right]$$

A global relationship of MBT' and CBT to MAT is reported by (Peterse et al., 2012) as follows:

(8) $$MAT = 0.81 - 5.67 * CBT + 31 * MBT'$$

However, there are significant differences in the correlations of MBT/CBT with soil pH and MAT at different locations and environmental settings (Sinninghe Damsté et al., 2008; Tierney and Russell, 2009; Shanahan et al., 2013; Coffinet et al., 2017) emphasizes the importance of appropriate local calibrations for the calculation of annual mean air temperature.

2.3 Biomarker in Geo-archeology

Recent studies (D'Anjou et al., 2012; Thienemann et al., 2017) apply proxies that have been traditionally used in environmental pollution studies (Readman et al., 1987; Grimalt et al., 1990; Leeming et al., 1996; Carreira et al., 2004) to unravel the interrelations between human, climate and environment. For an extensive review of molecular biomarker of anthropic impacts see (Dubois and Jacob, 2016). Only the biomarkers utilized for the thesis are outlined here:

2.3.1 Sterols

Sterols are lipids that belong to the group of triterpenoids and exist in a wide variety of organisms such as plants (Campesterol, Sitosterol, and Stigmasterol), animals (Cholesterol) and fungi (Ergosterol; Peters et al., 2005). After the ingestion of organic matter by humans or mammals, sterols are reduced to stanols (e.g. cholesterol → coprostanol) by intestinal microbial hydrogenation (Bull et al., 2002). 5β-coprostanol is the main stanol present in human feces, while feces of grazing, herbivorous mammals such as cattle are dominated by 5β-stigmastanol (Leeming et al., 1996; Shah et al., 2007; Fig. 8).

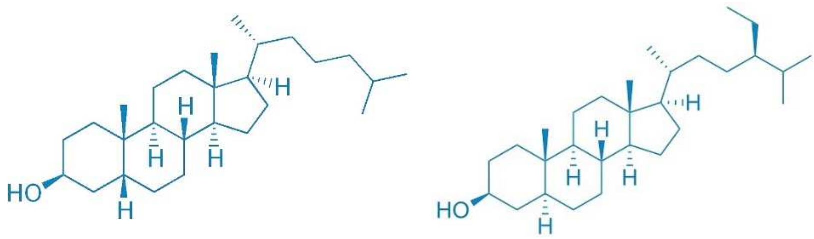

Figure 8. Molecular structure of the fecal stanols 5ß-coprostanol and 5ß-stigmastanol.

5ß-stanols are preserved in sedimentary records and thus can be used as biomarkers for the presence of human/mammalian fecal matter (Bull et al., 2002; D'Anjou et al., 2012). However, other possible sources of 5β-Stanols, such as avian- or even in-situ bacterial distribution have to be further evaluated (Holtvoeth et al., 2010; Devane et al., 2015; Cheng et al., 2016).

2.3.2 Polycyclic aromatic hydrocarbons

Polycyclic aromatic hydrocarbons (PAHs) are organic compounds that comprise multiple aromatic hydrocarbon rings (Fig. 9; Boehm, 2005) and are commonly regarded as environmental contaminants (Baek et al., 1991). PAHs are produced through a variety of natural processes including diagenesis, and biosynthesis (Boehm, 2005). As a result, hundreds of different PAH compounds are present in nature (Bjørseth, 1983; Sander and Wise, 1997). Some of them (Pyrolytic PAHs) are produced from organic matter during combustion processes and thus can be used as a proxy for natural and anthropogenic fire activity (D'Anjou et al., 2012; Thienemann et al., 2017). Due to the fact, that PAHs can be supplied from the atmosphere via dry and wet deposition they can represent signals from proximal as well as distant sources (Lima et al., 2005).

Figure 9. Molecular structure of three different combustion derived polycyclic aromatic hydrocarbon.

2.4 Analytical methods

In the following, a general overview and description of the methods for lipid analysis is given (Fig. 10). Details are provided in the respective chapters.

For lipid analyses, the sediment samples have to be ground and freeze-dried. Subsequently, the lipid extraction can be performed by different extraction techniques depending on, for example, sample size, -quantity, and designated compounds:

1. Accelerated solvent extraction (ASE); The ASE exhibits an automated extraction method at elevated pressure and temperature (e.g. 150 bar, 100°C).
2. Ultrasonic extraction; During the ultrasonic extraction, the sediment samples are sequentially extracted in an ultrasonic bath using solvents of decreasing polarity.
3. Soxhlet extraction; Soxhlet extraction exhibits a distillation-condensation extraction method with a mixture of solvents over a longer time period (e.g. 48 h).

After lipid extraction and solvent evaporation, the total lipid extract (TLE) is saponified with 0.5 molar potassium hydroxide (KOH) and Methanol (MeOH) : ultrapure water (H^2O_{MQ}) to release bound fatty acids by the cleavage of ester bonds. Subsequently, the neutral lipids are extracted from the TLE with potassium chloride (KCl) and an organic solvent. The neutral lipids, still containing a multitude of different compounds, can be further separated into fractions of different polarity by column chromatography. The chromatographic separation is based on the different adsorption of the eluted (mobile phase) analyte compounds to a silica gel (SiO_2) column (stationary phase). Compound classes usually include: 1. Aliphatic hydrocarbons, 2. Aromatic Hydrocarbons, 3. Ethers.

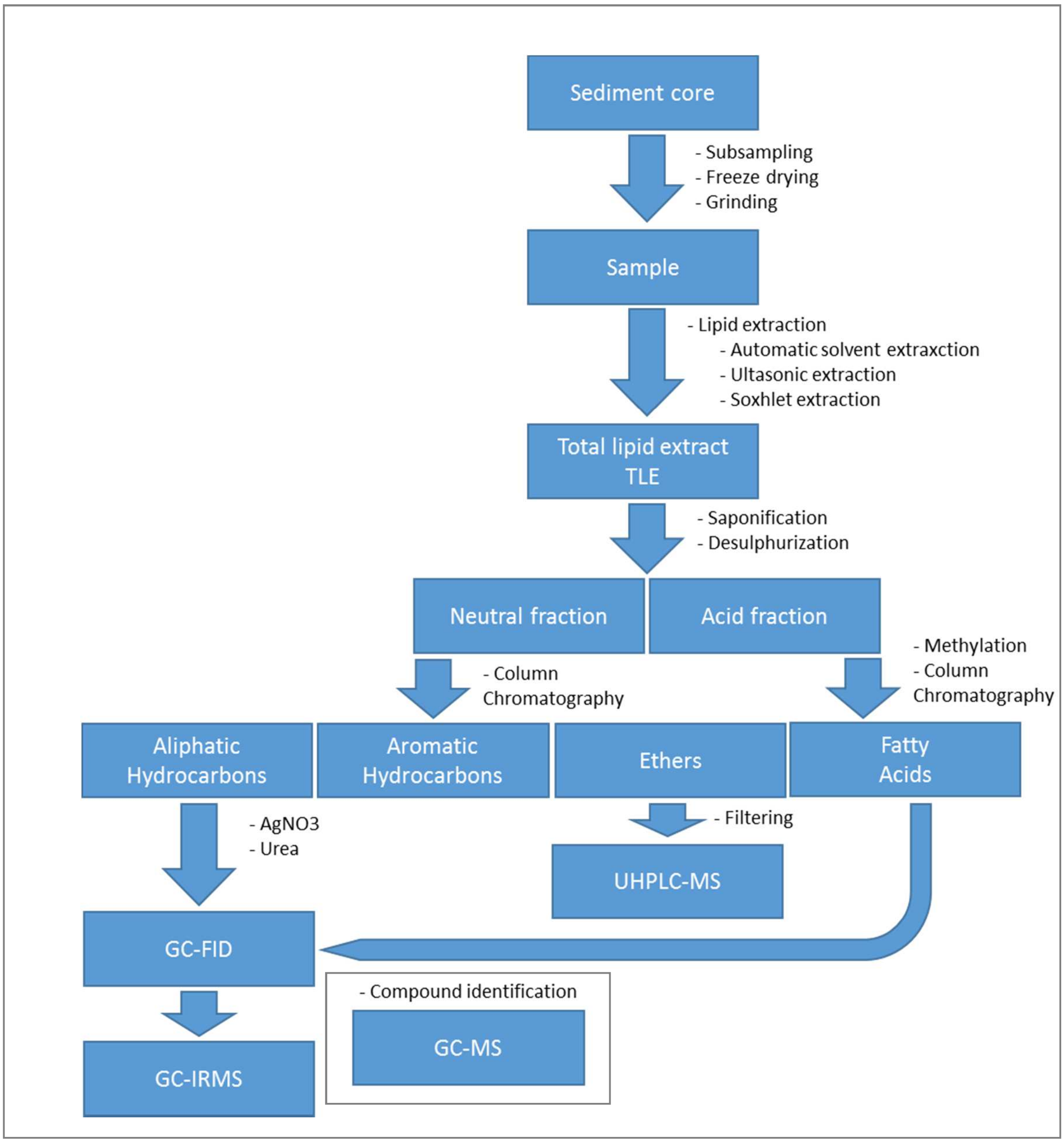

Figure 10. Schematic diagram of analytical methods for lipid analyses.

The aliphatic hydrocarbon fraction can be further treated with silver nitrate ($AgNO_3$) and/or urea (CH_4N_2O) for a separation of unsaturated and branched compounds. The remaining saturated aliphatic hydrocarbon fraction (*n*-alkanes) is analyzed on a gas chromatograph equipped with a flame ionization detector (GC-FID). Compound identification can be obtained by mass-spectrometry (GC-MS) and the addition of external standards to the samples. For the analysis of GDGTs, the ether fractions has to be filtered with a 0.45 µm Polytetrafluoroethylene (PTFE) filter using Hexane (hex) : Isopropanol (IPA). GDGTs are analyzed on an ultrahigh performance liquid chromatograph equipped with a mass spectrometer (UHPLC-MS).

The residual lipid fraction of the TLE is treated with concentrated Hydrochloric acid (HCl_{conc}). Subsequently, fatty acids are extracted with dichloromethane (DCM) and then methylated with a mixture of MeOH : HCl_{conc} at 80 °C for a minimum of 10 hours. In cases of subsequent isotopic analyses, the MeOH has to be of a known isotopic composition due to the transferring of a methyl group in the process of methylation. Subsequently, non-methylated compounds are removed by column chromatography using DCM : hexane (2:1). Remaining fatty acids (*n*-alkanoic acids) are analyzed on a GC-FID. Compound specific stable isotope analysis of hydrogen and carbon of the *n*-alkanes and fatty acids are carried out on a gas chromatograph equipped with an isotope ratio mass spectrometer (GC-IRMS).

3. Neoglacial changes in atmospheric circulation patterns over the North Atlantic and Fennoscandia recorded in Lake Torneträsk sediments

Earth's northern hemisphere high latitude regions are much more sensitive to climatic change than low latitude regions due to their susceptibility to external climatic forcing and substantial internal amplification through positive feedback mechanisms. Positive feedbacks, working in both temperature directions, involve primarily ice-albedo, ice-insulation, vegetation, and permafrost feedbacks (Bigelow et al., 2003; ACIA, 2005; Miller et al., 2010a; Miller et al., 2010b; Stocker, 2014). Understanding the behavior and modulation of intrinsic factors and thresholds in response to extrinsic and intrinsic forcing is therefore critical to determine the response of high latitude regions to climatic change.

The European high latitudes are located downwind of the North Atlantic, which exerts the dominant influence on atmospheric pressure and circulation patterns, primarily as a result of northward heat advection by the Atlantic Meridional Overturning Circulation (AMOC; Marshall et al., 2001; Slonosky et al., 2001) and its ability to alter the sinuosity and amplitude of the jet streams via the North Atlantic/Arctic oscillation (NAO/AO; Frankignoul et al., 2013; Wen et al., 2016). Variabilites intrinsic to the AMOC and complex interactions between the North Atlantic and the atmosphere are complicating the identification of the impact of external climate forcing and regional responses during the Holocene. Gradually decreasing temperatures in the Northern Hemisphere high latitudes (Wanner et al., 2008; Sejrup et al., 2016) have been linked to the orbitally forced decline in boreal summer insolation throughout the Holocene (Berger and Loutre, 1991; Miller et al., 2010b). Moreover, as of to date it is suggested that insolation changes also resulted in a long-term southward shift of the Northern Hemisphere atmospheric circulation systems over the course of the Holocene (Seppä and Poska, 2004; Knudsen et al., 2011; Wirth et al., 2013; Benito et al., 2015), similarly to a long-term weakening of the North Atlantic/Arctic Oscillation (NAO/AO) index (Rimbu et al., 2003; Andersen et al., 2004; de Vernal et al., 2005). In turn, this long-term Holocene trend of southward migrating atmospheric circulation systems in combination with an inferred stronger sinuosity of the polar frontal jet is thought to have led to a decrease in westerly zonal airflow and to an increase in meridional circulation (Shemesh et al., 2001; Hammarlund et al., 2002; Rosqvist et al., 2007; Jonsson et al., 2010; Jessen et al., 2011). Reduction of westerly airflow is consequently thought to have led to a decreased supply of warm and moist air from the North Atlantic relative to cold and dry air from the Arctic and Baltic Sea

(Rosqvist et al., 2004; Jonsson et al., 2010). Despite the wealth of information concerning the general long-term Holocene trend of changes in the pattern and style of atmospheric circulation in the North Atlantic realm, relatively little is known about potential climatic and environmental thresholds associated with the transitional pattern.

Owing to its climate being influenced by both the North Atlantic and the polar frontal zone (Fig. 11), northern Fennoscandia can be regarded as a key region to better understand the regional expression and potential threshold effects of the insolation-forced migration of atmospheric circulation systems.

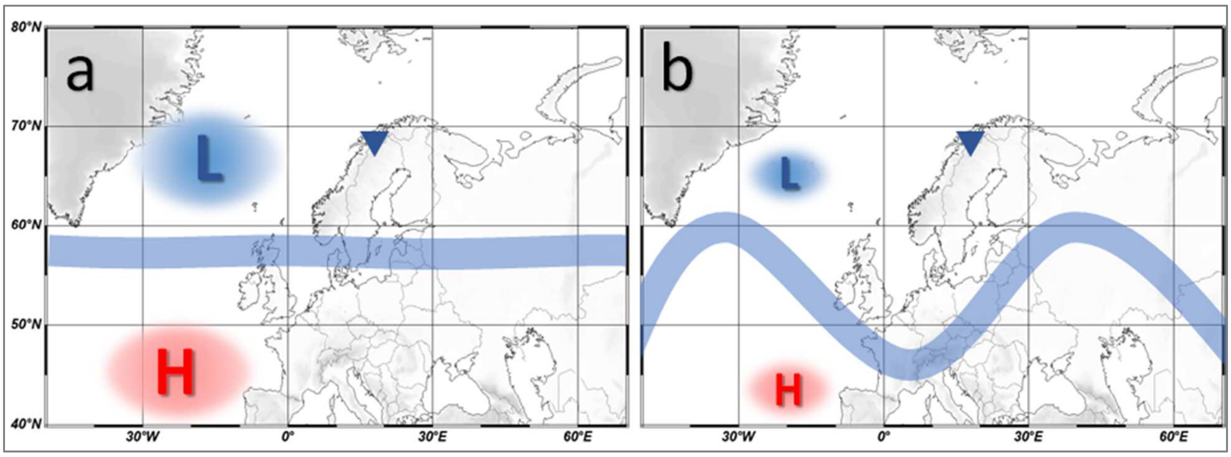

Figure 11. Map of Fennoscandia and the North Atlantic region with schematic positions of the polar frontal zone (blue line) at (a) positive NAO/AO index and (b) negative NAO/AO. Asterisk marks the location of Lake Torneträsk.

Previous reconstructions (Shemesh et al., 2001; Hammarlund et al., 2002; Rosqvist et al., 2007; Andersson et al., 2010) of changes in atmospheric circulation patterns in this region are based on the stable oxygen isotope composition of endogenic carbonates/microfossils ($\delta^{18}O_{carbonate}$). Changing in-lake factors such as lake hydrology and temperature, seasonality of precipitation, or changes in taxa/species assemblages may, however, bias the paleoclimatic information obtained from $\delta^{18}O$ analyses. To overcome these limitations and to provide a more comprehensive understanding of Holocene climate-environment interactions, we applied sedimentological and geochemical tools to a lacustrine sedimentary sequence from the representative subarctic catchment of Lake Torneträsk (northernmost Sweden). We used compound-specific δD analysis of long chain fatty acids (vascular plant leaf wax lipids) and utilized sediment imprints of heavy precipitation events to deduce changes in precipitation sourcing, amount, and intensity. Variations in δD of fatty acids provide a signal of the changing rainfall isotopic compositions (Sachse et al., 2012) depending on moisture sources and, thus, allow reconstructing atmospheric circulation changes. In addition, we analyzed branched and isoprenoidal glycerol dialkyl glycerol tetraethers (GDGTs) to reconstruct soil erosion processes (BIT index) and to determine changes in mean air temperatures (MAT) that we also use for the evaluation of the temperature fractionation effect. Plant wax lipid proxies (concentrations and chain-length distribution of *n*-alkanes and fatty acids) offer additional insights into local environmental/vegetational feedbacks owing to Lake Torneträsk's sensitivity to experience large biotic shifts (MacDonald et al., 1993; Körner 1998; Barnekow, 1999) due to its location at the present-day tree line.

3.1 Site description

Lake Torneträsk (68°29′–68°11′ N, 20°01′–18°36′ E; 341 m.a.s.l.; 70 km long, 10 km wide; 330 km^2 surface area; 3350 km^2 catchment; maximum water depth 168 m) is located in the subarctic landscape of NW Sweden, about 50 km east of the Atlantic coast (Fig. 11). The catchment reaches up to 1,800 m.a.s.l. and is drained by several small streams and rivers. The Abiskojåkka River (Fig. 12) entering to the West of the Abisko village is the largest inlet with a discharge of 14 $m^3 \cdot s^{-1}$. The climate of the Torneträsk region is characterized by a strong oceanity/continentality gradient from West to East intensified by the orographic effect of the Scandes Mountains (Barnekow, 1999), which results in mean annual precipitation between ~300 and 850 mm (1961–1990; Alexandersson and Eggertsson Karlström, 2001). Precipitation seasonality shows opposite patterns with elevated precipitation in the western compared to the eastern catchment of Lake Torneträsk during winter months and vice versa during summer months. Annual precipitation amount is, however, equally distributed throughout the year. Temperatures (-0.8°C MAT at Abisko station; 388 m.a.s.l., 1971-1990; Alexandersson and Eggertsson Karlström, 2001) show a strong seasonal contrast of extended winters (October-April) with average temperatures of approximately -7°C and short summers (May-September) with average temperatures of on average +7.5°C. The lake is (ultra-) oligotrophic and streams carry only low amounts of dissolved and suspended loads (Jonasson and Nyberg 1999; Andrén et al. 2002) resulting in low sedimentation rates in the distal parts of the lake (Vogel et al., 2013) and minor authochthonous sedimentation (Meyer-Jacob et al., in review). The amount of suspended loads can, however, increase substantially during rare albeit heavy precipitation events occurring during summer months (Jonasson and Nyberg 1999). The present day vegetation in the catchment consists mainly of open subarctic/-alpine birch forest (< 700 m.a.s.l.; *Barnekow, 1999)* with sporadic stands of pine (< 450 m.a.s.l.) in the SE part of the catchment. Above the present-day tree line dwarf-shrubs, grasses, sedges, and herbs prevail.

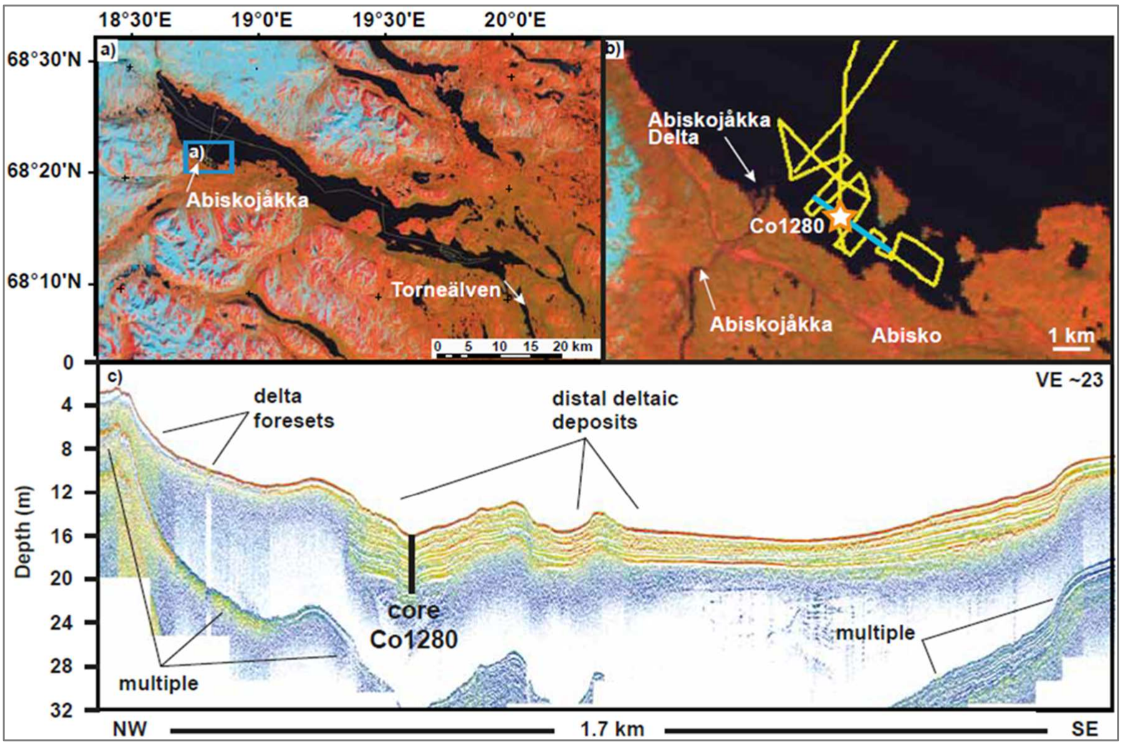

Figure 12. a) Lake Torneträsk satellite image. b) Coring location of core Co1280. Yellow line indicates track lines of hydroacoustic profiles. c) Seismic profile (blue line) crosscutting Abiskojakka delta from NW to SE including location of core Co1280. For details on hydroacoustic data acquisition see Vogel et al. (2013).

3.2 Material and Methods

The Co1280 composite sequence (600 cm) was recovered from a small embayment in the north-western part of Lake Torneträsk that receiving fluvial sediment supply from the Abiskojåkka River (Fig. 12) in spring 2012. The coring location was chosen based on hydro-acoustic sub-bottom data showing an acoustically stratified and undisturbed sediment package (Fig. 12; Vogel et al. 2013). Sediments in our composite core comprise glacio-fluvial deposits between 600 cm and 410 cm followed by distal deltaic-lacustrine sediments deposited below base level between 410 cm and the core top (Tab. 3). The chronology of Co1280 is based on AMS ^{14}C ages of seven terrestrial plant macrofossils sampled between 51 cm and 319 cm depth and two bulk sediment samples from 338 cm and 389 cm depth. Conventional radiocarbon ages were calibrated using the IntCal09 calibration curve (Reimer et al. 2009). The age-depth model was fitted using the Bayesian age-depth modelling software Bacon 2.2. (Blaauw & Christensen 2011).

Table 3. AMS ^{14}C ages of terrestrial plant macrofossils and bulk sediment samples from Core Co1280.

Origin	Location	Core	Depth [cm]	14C yr BP error	2 sigma cal yr BP age range	Probability distribution
Terrestrial	Torneträsk Lake - Abisko Bay, NW Sweden	Co_1280-6	51.00	671 ±47	**619-684**	**50.9**
					553-613	43.9
Terrestrial	Torneträsk Lake - Abisko Bay, NW Sweden	Co_1280-5-II	83.80	2371 ±19	**2345-2439**	**93.1**
					2449-2455	1.8
Terrestrial	Torneträsk Lake - Abisko Bay, NW Sweden	Co_1280-3-I	132.80	3374 ±20	**3572-3643**	**83.4**
					3664-3685	11.5
Terrestrial	Torneträsk Lake - Abisko Bay, NW Sweden	Co_1280-5-III	177.80	4002 ±20	**4462-4520**	**64.6**
					4422-4453	30.1
Terrestrial	Torneträsk Lake - Abisko Bay, NW Sweden	Co_1280-5-III	210.60	4789 ±23	**5474-5549**	**80.2**
					5573-5589	14.7
Terrestrial	Torneträsk Lake - Abisko Bay, NW Sweden	Co_1280-3-II	244.60	5619 ±25	**6316-6448**	**95**
Terrestrial	Torneträsk Lake - Abisko Bay, NW Sweden	Co_1280-3-3	319.00	7412 ±62	**8154-8374**	**88.7**
					8052-8093	4.6
					8108-8119	1.1
					8133-8139	0.6
Lake	Torneträsk Lake - Abisko Bay, NW Sweden	Co_1280-3-III	338.40	7496 ±25	**8298-8381**	**79.6**
					8211-8259	15.4
Lake	Torneträsk Lake - Abisko Bay, NW Sweden	Co_1280-4-1	389.00	9333 ±69	**10369-10710**	**89.9**
					10298-10334	3.3
					10336-10357	1.7

The molecular analyses were performed on 28 freeze-dried and homogenized samples, which were Soxhlet-extracted using a mixture of dichloromethane and methanol (9:1 v:v). The lipid extract was saponified and further separated into polarity fractions using SiO_2 column chromatography (Höfle et al., 2013). *n*-Alkanes and fatty acids were analyzed on an Agilent 7890 series II GC-FID following the method described by Höfle et al. (2013) and quantified against authentic external standards including normalization to total organic carbon (TOC) content. GDGTs were analyzed using an Agilent 1290 UHPLC coupled to an Agilent 6460 QQQ equipped with an APCI ion source operated in SIM mode according to Hopmans et al. (2016). MBT'/CBT values were calibrated to annual MAT using the calibration of De Jonge et al. (2014) and Peterse et al. (2012). Compound-specific stable isotope analysis ($\delta^{13}C$ and δD) were conducted on the most abundant C_{28} and C_{26} fatty acids. $\delta^{13}C$ compositions were measured using a Thermo Trace GC coupled to a Finnigan MAT 252 isotope-ratio monitoring-mass spectrometer (irm-MS) via a modified Finnigan GC/C III combustion interface operated at 1000 °C. δD was measured with a Thermo Trace GC coupled to a Thermo Fischer Scientific MAT 253 irm-MS via a pyrolysis reactor operated at 1420 °C. Methods were following Häggi et al. (2016). The isotope values were measured at least twice against calibrated reference gas using H_2 for δD and CO_2 for $\delta^{13}C$ and are reported in ‰ versus VSMOW and VPDB, respectively. The long-term precision monitored by external standard analyses is 0.3‰ for $\delta^{13}C$ and 2.8‰ for δD. Flood layer identification is based on macroscopic core descriptions and aided by characteristic elemental distributions and density variations in the sediment core. For this purpose, scanning-XRF elemental analyses (2mm) and radiographic imaging (200µm) were conducted using an ITRAX XRF core scanner (Cox Ltd.) equipped with a Mo X-ray tube set to 30 kV and 30 mA and 50 kV and 50 mA, respectively. Grey-value calculations for flood layer identification were performed using ImageJ (National Institute of Health, USA, ImageJ 1.45s) and BMPix according to Weber et al. (2010). Flood frequency and flood layer thickness are calculated as a 100 yr moving average and a 100 yr mean, respectively (Wirth et al., 2013).

3.3 Results and Discussion

3.3.1 Hydrological source signatures

The Torneträsk catchment receives moisture from three different sources. Moisture advected over the North Atlantic is the predominant source for precipitation, especially for the westernmost parts of the catchment. During periods of a decreased pressure gradient between the North Atlantic and the European continent, the polar frontal zone and the polar jet migrate southwards (Rosqvist et al., 2007) and the Torneträsk catchment receives moisture from the Arctic Ocean and the Baltic Sea (Jonsson et al., 2009). These three different moisture sources are characterized by different D/H isotopic compositions as Arctic and Baltic surface seawaters are both D-depleted relative to the North Atlantic surface waters (Bigg and Rohling, 2000; LeGrande and Schmidt, 2006). In addition, the lower temperatures during evaporation and higher continentality of moisture originating from the Arctic and the Baltic Sea lead to enhanced D-depletion of precipitation from these sources (Rosqvist et al., 2007; Jonsson et al., 2009). Since cuticular leaf wax lipids from vascular plants incorporate the D/H isotopic composition of precipitation (Sachse et al., 2012), changes in the relative contributions of these moisture sources and, by inference, atmospheric circulation patterns across northern Sweden during the Holocene can be traced using compound-specific δD analysis. The Torneträsk compound-specific δD values of the n-C_{28} and n-C_{26} fatty acid (Fig. 13, Tab. 4) agree well (r^2 = 0.6) and range from -204.1‰ to -185.9‰ (n-C_{28}) and -202.3‰ and -184.7‰ (n-C_{26}). In the following, we are referring to δD_{C28} as δD_{wax}. At Lake Torneträsk, δD_{wax} values mainly reflect the summer precipitation δD between May and September due to temperature and light limitations of plant growth in the high latitudes during the rest of the year. However, during snowmelt in May/June, meltwater and associated soil moisture might also contribute to a limited amount to the plants' source water. To confirm summer precipitation as the major water source for plants, the fractionation factor between the plant wax lipid and the environmental water ($\varepsilon_{wax/water}$) can be calculated using the equation:

(9) $$\varepsilon_{wax/water} = 1000 * [(\delta D_{wax}+1000) / (\delta D_{precipitation}+1000)-1]$$

Thus, the Torneträsk (core-top δD_{wax} -204.1‰) kinetic isotope fractionation factor for C_{28} metabolized using summer season precipitation, (calculated with isotopic data from Namikaa, Abisko, and Kiruna stations 1975–1980; IAEA/WMO), amounts to $\varepsilon_{wax/water}$= -127.8‰. Winter season precipitation exhibits more D-depleted values resulting in a kinetic fractionation factor of $\varepsilon_{wax/water}$= -95.3‰. Mean fractionations between precipitation and fatty acids ($\varepsilon_{wax/water}$) of -117‰ (trees) and -171‰ (grasses) were found by Hou et al. (2007). Data obtained by Wilkie et al. (2013) for Lake El'Gygygtgyn show a mean fractionation between modern day vegetation *n*-C_{28} and source water of -125‰ (streams) and -116‰ (precipitation) respectively. Despite large interspecies variations in $\varepsilon_{wax/water}$ (Hou et al., 2007), these values lie much more closely to the Torneträsk summer season $\varepsilon_{wax/water}$. Hence, we assume summer precipitation to be the major source of water utilized by plants at our study site, with minor seasonality effects of the source water δD signature during the Holocene. Furthermore, isotopic fractionation effects caused by evaporation can also largely be excluded in the Torneträsk catchment due to the high relative humidity (~0.7) throughout the year and resulting low evaporation rates (~100-150 mm), (Hammarlund et al., 2002). These data argue against an evaporative loss of soil water and transpiration of leaf water (Sachse et al., 2012) and are confirmed by the good agreement (r^2 = 0.84) of the slope of the local meteoric water line after Jonsson et al. (2009)

(10) $$\delta D = 7.2 * \delta 18O + 0.3‰$$

and the global meteoric water line (Rozanski et al., 1993) in the Torneträsk region. Accordingly, changes of the molecular D/H isotopic composition throughout the Holocene are interpreted to be largely driven by changes of the atmospheric moisture source. Changes in local condensation temperatures affecting δD_{wax} values (Dansgaard, 1964; Bowen, 2008) are accounted for by measurements of MBT'/CBT-derived mean summer air temperatures (Fig. 13, Tab. 4). Reliability of the temperature reconstruction is confirmed by the good agreement of the MBT'/CBT core-top value of 5.2°C with instrumental measurements of the Abisko meteorological station during the summer season (6.3°C during May-October) implying limited bacterial metabolism and brGDGT production during winter when soils are frozen (Weijers et al., 2007a; Rueda et al., 2009).

Table 4. Molecular and isotopic data of Core Co1280.

Age (cal yrs BP)	Depth (cm.)	[a] Σ HMW n-alkanes (µg/g TOC)	[b] Σ HMW fatty acids (µg/g TOC)	[c] ACL *n*-alkanes	[d] BIT	[e] MAT (°C)	[f] MAT (°C)	[g] δD_{C26} (‰)	[g] δD_{C28} (‰)	[h] $\delta^{13}C_{C26}$ (‰)	[h] $\delta^{13}C_{C28}$ (‰)
-60	0	185	1453	29.0	0.95	5.2	-2.6	-202.3	-204.1	-32.7	-33.0
300	29	175	1372	29.1	0.94	4.8	0.0	-200.3	-200.0	-31.7	-32.4
600	50	188	1410	29.1	0.95	5.0	-0.2	-198.3	-197.1	-31.8	-32.1
910	68	132	1003	29.2	0.94	4.9	-0.1	-198.0	-192.5	-31.8	-32.1
1,200	83	190	1166	29.2	0.90	5.7	0.3	-196.2	-192.5	-31.4	-32.0
1,500	97	282	1584	29.2	0.92	5.9	0.8	-198.1	-191.8	-31.9	-32.2
1,800	110	239	1517	28.0	0.82	5.6	1.8	-189.0	-188.9	-32.5	-32.2
2,090	122	133	767	29.0	0.91	5.2	0.2	-194.8	-189.3	-31.9	-32.3
2,400	134	140	884	29.0	0.88	5.6	0.5	-196.0	-193.6	-31.5	-32.0
2,690	145	114	1160	28.9	0.89	5.2	0.8	-197.1	-192.4	-31.7	-32.2
3,000	156	180	1017	29.1	0.88	5.2	0.8	-197.3	-191.9	-31.8	-32.1
3,490	173	142	1045	29.2	0.89	5.9	0.7	-197.2	-194.6	-31.7	-32.2
4,000	190	92	626	28.9	0.85	5.4	0.9	-193.6	-187.9	-31.8	-32.4
4,500	206	92	664	28.8	0.85	5.8	0.3	-191.8	-186.3	-31.8	-32.1
4,970	221	132	682	28.5	0.79	5.7	1.0	-189.1	-185.9	-32.1	-32.1
5,500	237	94	735	28.5	0.77	5.6	1.4	-191.0	-187.2	-31.8	-32.1
5,790	246	89	587	28.7	0.79	6.1	1.2	-191.8	-186.4	-31.9	-32.1
6,090	255	108		28.6	0.76	4.9	0.8	-	-	-	-
6,390	264	80	606	28.3	0.75	5.7	1.6	-192.9	-188.4	-32.1	-32.3
6,690	273	22	395	27.8	0.73	5.1	1.2	-189.9	-186.4	-32.0	-32.3
7,000	282	193	651	28.2	0.76	6.0	1.5	-190.3	-186.3	-31.9	-32.1
7,500	297	107	789	27.9	0.77	5.6	1.3	-190.3	-187.1	-31.7	-32.2
8,000	312	118	888	28.2	0.79	6.6	2.2	-192.4	-188.0	-32.1	-32.4
8,500	327	131	830	28.2	0.80	5.9	2.2	-192.1	-188.1	-32.4	-32.4
8,990	342	197	1073	28.2	0.80	5.6	2.2	-197.5	-189.3	-32.0	-32.4
9,490	357	108	488	29.1	0.90	6.2	0.4	-196.7	-187.9	-31.5	-31.9
9,980	372	147	1077	28.2	0.82	5.9	1.1	-186.3	-189.3	-32.2	-32.5
10,500	388	90	579	28.3	0.86	6.2	1.0	-184.7	-187.2	-31.6	-31.9

[a] $(C_{27}+C_{29}+C_{31}+C_{33})$
[b] $(C_{26}+C_{28}+C_{30}+C_{32})$
[c] $(C_{27}*27+C_{29}*29+C_{31}*31+C_{33}*33) / (C_{27}+C_{29}+C_{31}+C_{33})$
[d] According to De Jonge et al. (2014)
[e] According to De Jonge et al. (2014)
[f] According to Peterse et al. (2012)
[g] calculated vs VSMOW
[h] calculated vs VPDB

3.3.2 Reconstruction of the Holocene hydrological and environmental history

Throughout the Early and Mid Holocene, until ~4,000 cal yrs BP, the δD_{wax} record shows little variability with D-enriched values between -189.3‰ and -185.9‰ implying stable moisture sourcing primarily from the North Atlantic through predominantly westerly/zonal atmospheric circulation.

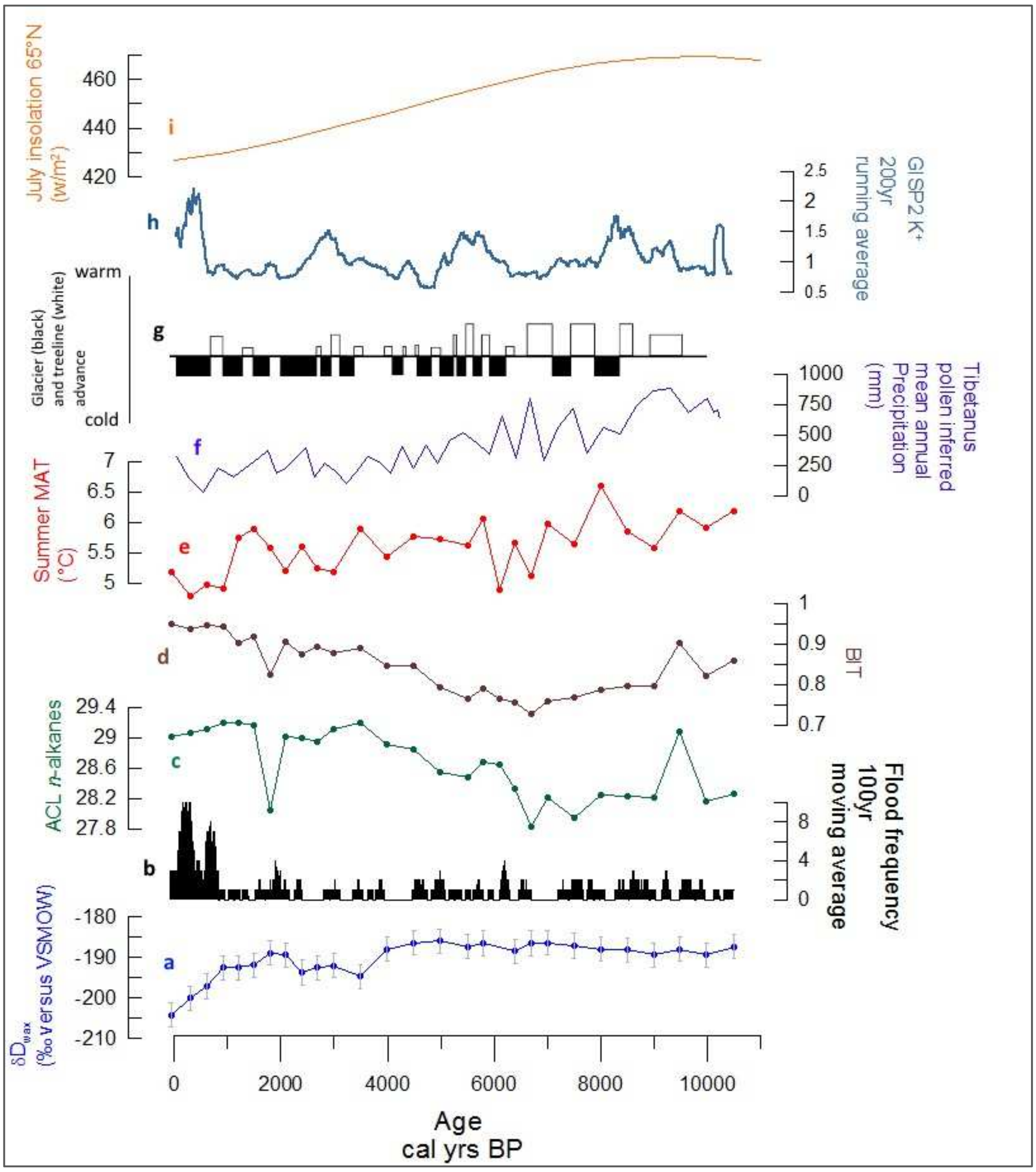

Figure 13. Biomarker and inorganic data of core Co1280 plotted against age. (a) δD_{wax}, (b) flood frequency, (c) *n*-alkane ACL, (d) BIT index, (e) summer MAT. Also shown are (f) pollen-inferred mean annual precipitation at Lake Tibetanus (Barnekow 1999), (g) Scandinavian glacier and tree line advance (Karlén and Kuylenstierna, 1996), (h) GISP2 potassium (K^+; ppb) ion (Mayewski et al., 1997) and (h) July insolation at 65°N calculated after Berger and Loutre (1991).

This is also suggested by studies of sea ice cover variability (de Vernal et al., 2005) and North Atlantic SSTs (Rimbu et al., 2003; Andersen et al., 2004), which suggest an early Holocene atmospheric state similar to a positive AO/NAO situation, commonly associated with an increase in westerly winds. Furthermore, modeling atmospheric circulation patterns indicate that the Icelandic Low and the polar frontal jet were located further north during the early Holocene compared to today due to increased summer insolation resulting in an increased westerly flow (Harrison et al., 1992). In addition, Fennoscandian pollen data suggest an enhanced oceanic climate during the Early Holocene compared to today (Giesecke et al., 2008). The Torneträsk δD_{wax} record in combination with the other regional reconstructions, thus, suggests a predominance of moisture sourcing from the North Atlantic as a result of a prevailing positive NAO/AO index and/or a northward position of the polar front. MBT'/CBT-derived mean summer air temperatures amount to ~6°C in the Early Holocene. Deglaciation of the Torneträsk area, including the drainage of the ice-dammed precursor lake and the establishment of the present day shoreline and catchment morphology of Lake Torneträsk around ~9,500 cal yrs BP (Shemesh et al., 2001; Stroeven et al., 2002; Bigler et al., 2003). During the deglaciation, strong fluctuations of high molecular weight (HMW) *n*-alkanes (C_{27}-C_{33}) and fatty acids (C_{26}-C_{32}) concentrations (Fig. 14, Tab. 4), in the branched and isoprenoid tetraether (BIT) index (up to 0.9 at ~9,500 cal yrs BP; Fig. 13, Tab. 4), and high Ti, Fe, and Ca counts all indicate a strong susceptibility of minerogenic and organic substrates to erosion (Fig. 15, appendix). Furthermore, flood frequency and mean flood layer thickness show relatively high variability but low recurrence rates of significant flood events until about 8,000 cal yrs BP (Fig. 13, 14). At ~8,000 cal yrs BP we observe a temperature maximum (6.6°C) consistent with the Holocene thermal maximum (HTM) in the North Atlantic region (Davis et al., 2003; Andersen et al., 2004; Sejrup et al., 2016) and high boreal summer insolation (Berger and Loutre, 1991). During the HTM between about 8,500 cal yrs BP and 6,000 cal yrs BP, Ti, Fe, and Ca counts decrease and the BIT index declines to as low as 0.75 at 6,700 cal yrs BP suggesting vegetation-driven soil stabilization and reduced catchment erosion. In conjunction with the flood record, indicating lowest recurrence rates between 8,000 and 6,500 cal yrs BP, this suggests reduced occurrence of heavy precipitation events and soil erosion. The increase of the proportion of woody vegetation during the HTM in the Torneträsk catchment, as documented in local vegetation reconstructions (Barnekow, 1999; 2000), is also clearly reflected by low values of the average chain length (ACL) of the odd-numbered HMW *n*-alkanes (27.8 at 6,700 cal yrs BP; Fig. 13, Tab. 4). These combined datasets suggest that soil stabilization by a denser and more extensive vegetation cover is the main factor reducing soil erosion during the HTM.

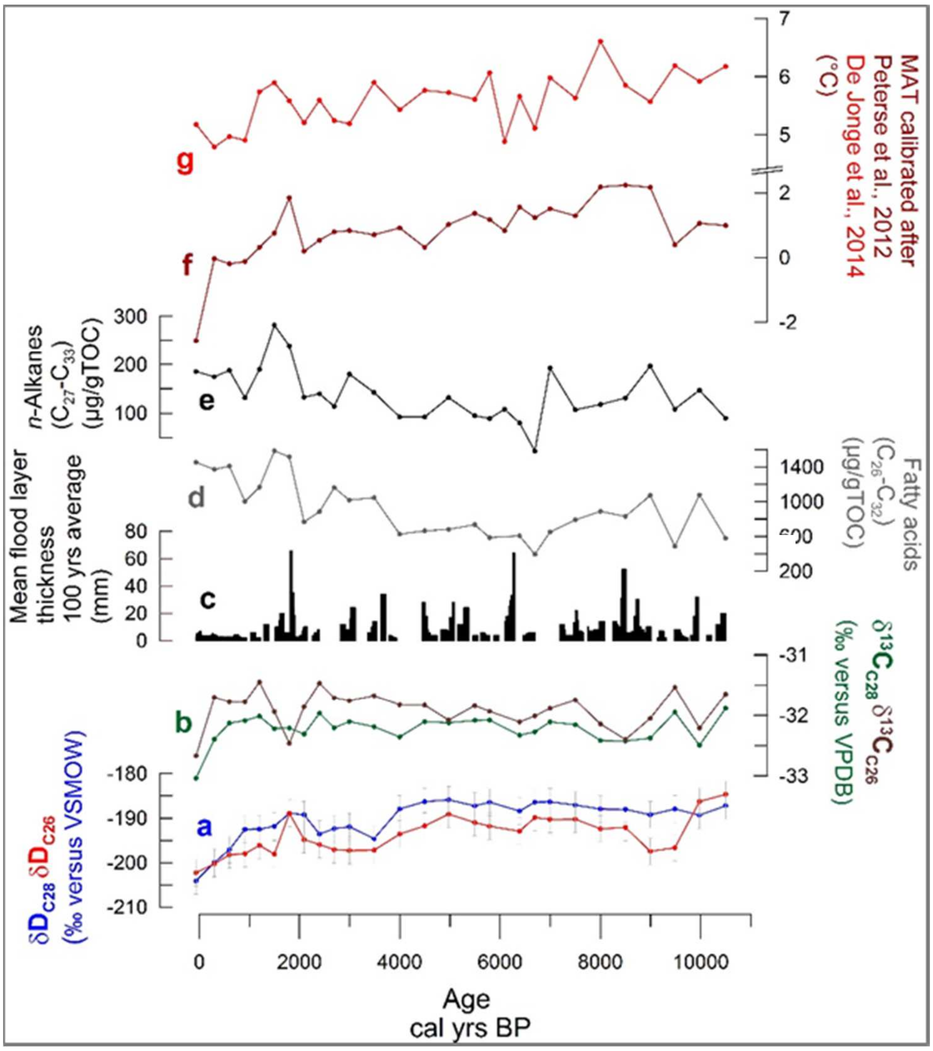

Figure 14. Lake Torneträsk, Core Co1280: Diagram of biomarker and inorganic data plotted against age. a) δD_{C28} (blue), δD_{C26} (red), b) $\delta^{13}C_{C28}$ (green), $\delta^{13}C_{C26}$ (brown), c) mean flood layer thickness, d) concentration of HMW fatty acids, e) concentration of HMW *n*-alkanes, f) MBT'/CBT derived MAT calibrated after Peterse et al. (2012), g) MBT'/CBT-derived MAT calibrated after De Jonge et al. (2014).

From the temperature maximum at 8.000 yrs cal BP until present, MATs show a cooling trend of ~1.8°C until present as a result of glacio-isostatic uplift of Fennoscandia and a decrease of Northern Hemisphere summer insolation. Considering a glacio-isostatic uplift of about 100 m since 9,000 cal yrs BP and a general lapse rate for Fennoscandia of 0.57 °C/ 100 m (Laaksonen, 1976), the cooling effect due to the uplift is about 0.6 °C. Palynological data imply subsequent vegetational changes after the HTM from a boreal forest to todays' open subalpine woodland and the retreat of the tree-line due to decreasing temperatures and increasing continentality in the Torneträsk catchment (Barnekow, 1999; 2000). These changes are also mirrored by an increasing trend in the ACL from the HTM (27.8 at 6,700 cal yrs BP) until the modern period (29.2 at 900 cal yrs BP), indicating decreasing contributions from woody and herbaceous vegetation (Cranwell, 1973; D'Anjou et al., 2012). Likewise, the BIT index shows a long-term increasing trend after 6,700 cal yrs BP until present (to 0.95) in tandem with rising ACL values (r^2=0.6) suggesting a strong coupling of decreasing vegetation cover and enhanced catchment erosion. Furthermore, concentrations of HMW *n*-alkanes and fatty acids increase between 6,700 cal yrs BP and the present by factors of eight and four, respectively. This increase is paralleled by higher elemental counts confirming a trend towards enhanced detrital silici-clastic input. This long-term trend in the XRF-derived terrigenous elemental data is superimposed by centennial to millennial fluctuations, which are in good temporal agreement with maxima of ice rafted debris (IRD) supply from the North Atlantic (Bond et al., 1997; 2001), indicating a strong coupling to the North Atlantic circulation pattern (Fig. 15).

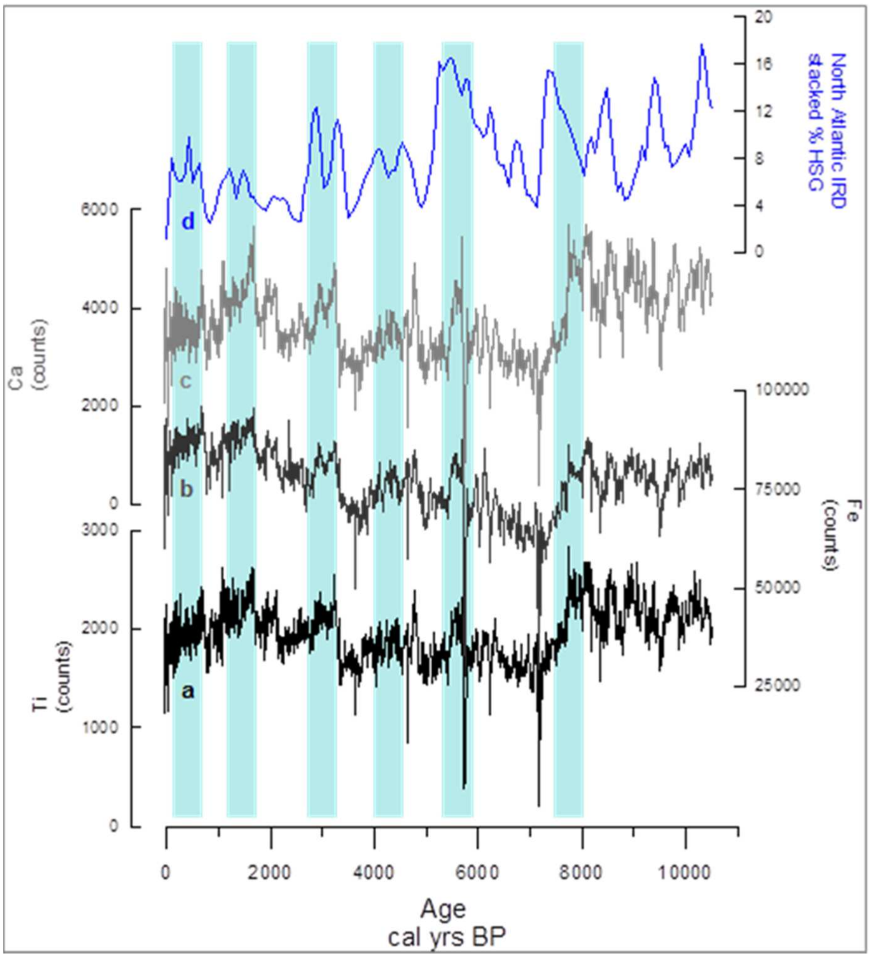

Figure 15. Elemental data of core Co1280 showing a) Titanium (Ti), b) Iron (Fe), and c) Calcium (Ca). Also shown is d) North Atlantic drift ice stack (in percentage variations in petrologic tracers; Bond et al., 2001).

These events are commonly associated with colder conditions and northerly/northeasterly winds due to a short-term southward shift of the polar frontal zone (Bond et al., 2001; Rosqvist et al., 2004). The cold conditions most likely enhanced catchment erosion through a decreasing vegetation cover and promoted export of minerogenic substrates in the Torneträsk catchment. The rapid climatic fluctuations are, however, indiscernible in the biomarker records, most probably due to the coarse sample resolution (~350 yrs) and sedimentary integration (~110 yrs) and, thus, a lack of sensitivity for these short-term changes. Thus, the suggested link between catchment erosion and climatically driven reduction in vegetation cover and the retreating tree line after the HTM is further invigorated.

Between ~4,000 and ~3,500 cal yrs BP, the δD_{wax} values decrease by -6.7 ‰ to as low as -194.6‰. Similar substantial shifts towards a more depleted isotopic composition are also displayed by $\delta^{18}O$ studies from the region (Shemesh et al., 2001; Hammarlund et al., 2003; Jonsson et al., 2010). The overall increasing trends of BIT index, the elemental data, and in the plant-derived lipid biomarker records since 6,700 yrs cal BP continue implying sustained and enhanced mobilization and transport of soil organic matter in response to the negative temperature evolution. The Torneträsk biomarker signals are matched by similar and contemporaneous signals of catchment erosion in sedimentary records from Lake Tibetanus (Barnekow, 1999) and Lake Njulla (Bigler et al., 2003). After ~2,000 cal yrs BP the δD_{wax} values show a rapid further decrease of -15.2‰ to as low as -204.1‰ at the modern core-top coinciding with a dramatic increase in flood frequency and a drop in summer MAT of ~1°C. A peak in δD_{wax} and the biomarker proxies at 1,800 cal yrs BP results from sampling of reworked/-deposited sediments from a thick flood deposit in the core. The overall decrease in δD_{wax} of ~18.2‰ cannot be explained by the amount effect (Dansgaard, 1964; Rozanski et al., 1993). Both, pollen and diatom-inferred precipitation reconstructions in the region suggest a decreasing trend in precipitation since the Mid Holocene (Fig. 13) (Barnekow, 1999; Seppä and Birks, 2001), which would result in D-enrichment. The drop in δD_{wax} can also not be explained by the temperature of condensation effect (Dansgaard, 1964). Changes in the MBT'/CBT-derived MAT suggest that only -4.1‰ change in δD_{wax} can be explained by temperature considering a local temperature dependency of 2.3‰ per °C (calculated from isotopic precipitation data of Namikaa, Abisko, and Kiruna 1975–1980; IAEA/WMO). When using the δD-temperature dependency for North Atlantic coastal stations (Dansgaard, 1964), the temperature effect would similarly only amount to 10.1‰. Likewise, the vegetation changes described above are thought to have only minor impact on the δD_{wax} trend since palynological data (Barnekow, 1999; 2000) reveal a simultaneous advance of both grass (D-depleted) and shrubs (D-enriched;

Hou et al., 2007) over the Mid and Late Holocene. Changes in C_3/C_4 vegetation can be excluded, since $\delta^{13}C_{wax}$ values of -33.0 to -31.5‰ (+-0.3‰) (Fig. 14, Tab. 4) reflect predominantly C_3 vegetation (Chikaraishi et al., 2004; Bi et al., 2005) throughout the Holocene. A slight decreasing trend in modern $\delta^{13}C$ values might mirror the anthropogenic Suess effect (Keeling, 1979). Therefore, we assume the remaining overall decrease in δD_{wax} of about -14.1% (-8.1‰) to be the result of relative changes in moisture sources of the Torneträsk region starting at about 4,000 cal yrs BP and intensifying after 2,000 cal yrs BP. Considering the isotopic signatures of the different moisture sources, the decreasing δD_{wax} trend implies a declining influence of westerly airflow and moisture sourcing from the North Atlantic. Instead, influence of northern/north-easterly and south-easterly airflow and moisture sourcing from the Arctic Ocean and Baltic Sea increases. This relative change in moisture sourcing suggests a shift in atmospheric circulation patterns from a dominant zonal to increasingly meridional air-flow. We attribute this re-organization to a southward migration and/or stronger meandering of the polar front/jet due to a decreased sea-level air-pressure gradient between the Arctic and the Eurasian continent (Visbeck et al., 2001). Similarly, alkenone derived sea surface temperature data as wells an atmospheric circulation model suggest an overall weakening of the NAO/AO and a southward shift of the Icelandic low from the Early to the Late Holocene (Harrison et al., 1992; Rimbu et al., 2003; Bendle and Rosell-Melé, 2007). The rapid change in atmospheric circulation is furthermore supported by the simultaneous and substantial increase in flood frequency starting at ~2,000 cal yrs BP and intensifying after 1,200 cal yrs BP. Contrary to other Scandinavian lakes (Stroeven et al., 2002) and similar to most other settings such as the European Alps (e.g. Glur et al. 2013), the occurrence of flood layers in the Torneträsk record is not linked to snow melt, but primarily to heavy precipitation events during summer and fall (Jonasson and Nyberg, 1999). These events are commonly favored by weather patterns with a distinct meridional component, northward low-pressure system trajectories, and primarily associated with a decrease in the westerly airflow (Hellström, 2005). Furthermore, in Sweden such events mostly occur under cyclonic weather conditions, which are more frequent under zonal conditions, but more vigorous and persistent with a higher probability to promoting major floods during a meridional atmospheric flow (Hellström, 2005; Gustafsson et al., 2010;). Interestingly, both our δD_{wax} and flood records show a relatively abrupt and nonlinear response to extrinsic and intrinsic forcings starting at ~2,000 yrs cal BP, unmatched in the remainder of the Holocene record at our site. Additional regional records are, however, required to discern whether this could represent a true regional pattern and possibly tipping point of the climate system in the Fennoscandian subarctic with consequences for the vulnerable ecosystems.

3.4 Summary and Conclusions

This study underlines that compound-specific leaf wax stable isotopes are able to constrain changes in atmospheric circulation pattern and moisture sourcing throughout the Holocene. Furthermore, lipid biomarker analyses proofs to be a valuable tool for the reconstruction of climate-induced soil erosion processes.

Our data reveal a Holocene thermal maximum in the Torneträsk region at ~8,000 cal yrs BP followed by a long-term cooling trend of ~1.8 °C until present due to glacio-isostatic uplift and a decrease in northern hemisphere summer insolation. The resulting retreat of the tree-line and the development from a boreal forest to an open subalpine woodland vegetation most probably led to a stronger exposure and destabilization of soil. This long-term trend is superimposed by centennial to millennial scale climatic changes, which co-vary with ice rafted debris maxima from the North-Atlantic and thus indicate a strong coupling to North Atlantic climate variability. The δD_{wax} record indicates a stable atmospheric circulation system with a dominant westerly airflow and moisture sourcing from the North Atlantic Ocean until about 4,000 cal yrs BP. Subsequently, δD-depleted values suggest a decreasing role of North Atlantic moisture sourcing being balanced by a stronger influence of air masses from the Arctic and Baltic Sea. Abruptly decreasing δD_{wax} values matched by a contemporaneous increase in flood recurrence rates suggest a further intensification of meridional relative to the zonal atmospheric flow after 2,000 cal yrs BP. This points to a reorganization/change of the atmospheric circulation system in the North Atlantic region in form of a southward migration of the polar front and/or long-term changes in the AO/NAO index towards more negative mode causing a decreasing influence of westerly winds, and a stronger influence of meridional airflow for moisture transport to our site. Both our δD_{wax} and flood records show a relatively abrupt and nonlinear response to forcing extrinsic and intrinsic to Earth's climate system starting at ~2,000 yrs cal BP.

4. Organic geochemical and palynological evidence for Holocene natural and anthropogenic environmental change at Lake Dojran (Macedonia/Greece)

The Holocene climate promoted the rise and development of early human civilizations all over the globe. Especially the Neolithic revolution, i.e., the spread of agriculture and the transition from a Mesolithic hunter-gatherer to a sedentary lifestyle during the Early Holocene (Willis and Bennett, 1994; Connor et al., 2013), might have been influenced or even triggered by climatic change (Richerson et al., 2001; Feynman and Ruzmaikin, 2007). However, the climate of the Holocene), showed also significant fluctuations (Bond et al., 1997; Bianchi and McCave, 1999; Casford et al., 2001), which supposedly led to relocation, downfall, and even societal collapse of ancient civilizations (deMenocal, 2001; Dalfes et al., 2013; Cullen et al., 2000). In reverse, with the beginning of the Holocene, humans also started to leave significant imprints on landscape and vegetation (Dubois and Jacob, 2016). While earlier Mesolithic hunter-gatherers had only little influence on their environment (Behre, 1988), the Neolithic lifestyle and agricultural land-use has been able to transform landscapes profoundly and on a bigger scale than ever before (Goudie, 2013). Thus, during the Holocene and especially with the beginning of the Neolithic, humans, climate, and the environment became strongly connected. These interrelations may be identified and even explained by the analyses of sediments, which yield valuable climatic as well as anthropogenic paleo-environmental information. For example, D'Anjou et al. (2012) revealed a relationship between human occupation and agricultural activities and summer temperature using lipid biomarkers in lake sediments from northern Norway. The authors showed that humans had a profound impact on the nearby environment including deforestation and increased wildfires. However, human-environment forcing and feedback mechanisms are highly debated and still insufficiently unraveled (Dearing, 2006).

Whilst emerging from the Fertile Crescent in the Middle East, Neolithic lifestyle expanded to central Europe with the Balkan Peninsula acting as an important bridge (Fouache and Pavlopoulos, 2011). Especially the Macedonian region, lying strategically between the Aegean and the Danube river basin, operated as a cultural mediator. Hence, its history can be relevant not only for the Balkan but for the whole of central Europe (Gimbutas, 1974; Kokkinidou and Trantalidou, 1991; Fouache and Pavlopoulos, 2011). Of particular importance for human migration were rivers and lakes as natural pathways and habitats (van Andel and Runnels, 1995). In Macedonia, the Vardar and Struma rivers acted as such pathways for the early Neolithic cultures (Andreou et al., 1996) migrating from Anatolia and Greece in the 7th millennium BC (Bocquet-Appel et al., 2009; Kaiser and Voytek, 1983). Lake Dojran is located within this natural corridor (Fig. 16) and its sediments have been shown to accurately and sensitively record the regional Holocene climatic change. Using sedimentological and geochemical (Francke et al., 2013), and micropaleontological (Zhang et al., 2014) tools, previous studies of Lake Dojran showed that following a cold and dry Younger Dryas, temperatures and humidity increased during the Early Holocene culminating in relatively stable climatic conditions (warm but changing humidity) throughout the Middle Holocene. During the Late Holocene (since about 3,000 yrs cal BP), the sedimentary record suggests increased anthropogenic activities in concert with varying climatic conditions including the Medieval Warm Period and the Little Ice Age. Accordingly, Lake Dojran provides the opportunity to investigate a record of both environmental change and human impact, which spans the entire Holocene.

Here, we present a multi-proxy biomarker and palynological approach to trace changes of both past anthropogenic impact and climate in the Dojran area throughout the Holocene. We use aliphatic hydrocarbons (*n*-alkanes) and the glycerol dialkyl glycerol tetraethers (GDGTs) based branched and isoprenoid tetraether (BIT) index to reconstruct vegetation type and soil erosion, respectively, as well as annual mean air temperature (MAT) based on the methylation and cyclisation of branched tetraethers (MBT/CBT) indices. Furthermore, we use fecal steroids to investigate human/livestock presence and polycyclic aromatic hydrocarbons (PAHs) to trace biomass burning, both being traditionally used in environmental pollution studies but fairly new in geo-archaeological approaches (D'Anjou et al., 2012; Dubois & Jacob, 2016). We also align biomarker curves to those of selected pollen groups and microcharcoal concentrations normalized to sedimentation rate (influx curves) as well as previously published sedimentological, geochemical, and micropaleontological data from the same core (Francke et al., 2013; Zhang et al., 2014). Our results trace previously observed climate change during the Early and Middle Holocene and indicate a relationship between human impact and environmental/climatic change during the Late Holocene (particularly during Late to Mid Holocene transition, the Medieval and the modern period).

4.1 Site description

Lake Dojran is located on the southern Balkan Peninsula in a karstic basin directly at the border of Greece and the Former Yugoslavian Republic of Macedonia (Stojanov and Micevski, 1989). It lies at an altitude of 144 m.a.s.l., has a water surface area of about 40 km^2, and a water depth of

6-7 m, however, seasonal and decadal lake level fluctuations are common. The lake catchment covers 274 km^2 and ranges from the Belasitsa Mountain crest (1874 m.a.s.l.) in the North to the Krusa Mountain crest in the Southeast (Sotiria and Petkovski, 2004). Lake Dojran drains into the Aegean via the Doirantis and Vardar rivers, but has been endorheic since the 1950s due to increased irrigation and the canalization of the Doiranitis River (Zhang et al., 2014). During winter and spring the lake is fed by small rivers, creeks, and groundwater while during summer a net loss of water is due to evaporation and possible groundwater outflow (Francke et al., 2013). Today, Lake Dojran is dimictic and eutrophic to hyper-eutrophic due to fertilizer input resulting in moderate oxygen depletion (Zacharias et al., 2002).

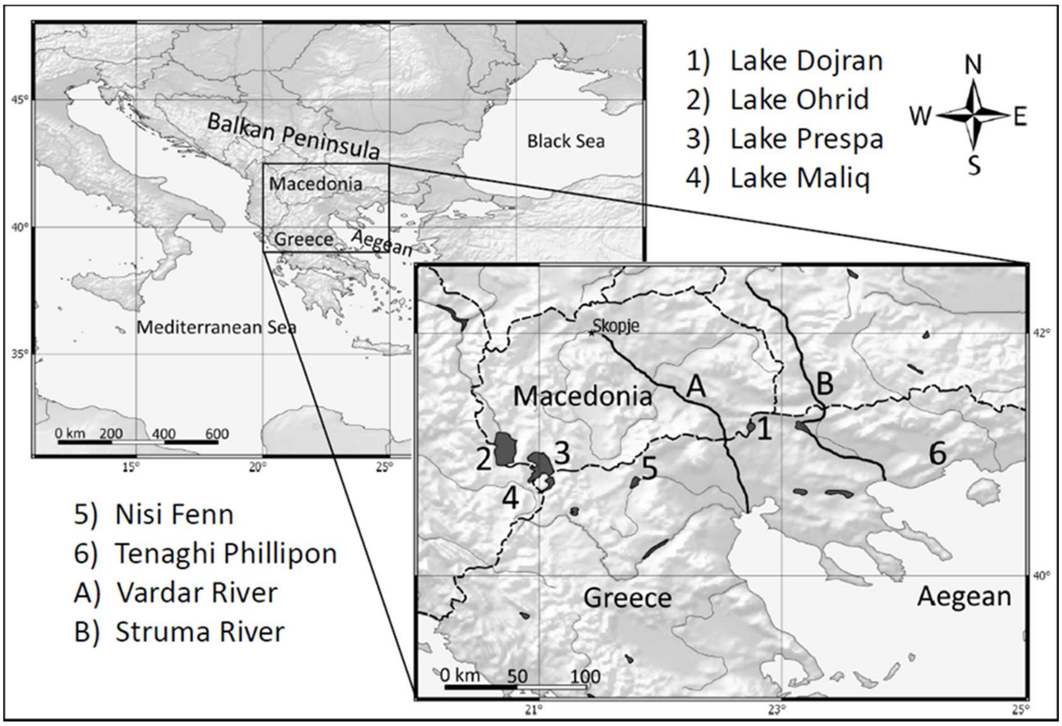

Figure 16. Map of the study area including Lake Dojran and adjacent paleorecords.

The climate of the Dojran area is characterized by a mixture of Mediterranean and continental influences resulting in hot, dry summers and mild, wet winters. Mean annual air temperature averages 14.3°C and mean annual precipitation is ~600 mm (Sotiria and Petkovski, 2004). The vegetation of the Dojran catchment is characterized by a typical Submediterranean biome. The lowlands (<400 m.a.s.l.) are mainly covered by sclerophyllous evergreen vegetation and *Quercetalia pubescentis* forest (Athanasiadis et al., 2000). At higher altitudes above 1,000 m.a.s.l. beech forests prevail. In some parts sporadic stands of fir can be found. The direct fringe of the lake is covered by up to 30 m wide reed bed areas and submerged plants (Athanasiadis et al., 2000). This present-day vegetation is the product of intensive anthropogenic overprinting, especially in the lowland areas. The former natural ecosystem consisted of mesophilous, periodically-flooded, forest (Mattfeld, 1927).

4.2 Material and Methods

Core Co1260 was drilled in the southern central part of Lake Dojran (41°11.703’ N, 22°44.573’ E) at a water depth of about 6.6 m in June 2011. A total of 7 m sediment were recovered, spanning approximately 12,500 years back to the Younger Dryas. The age model of the core was developed by Francke et al. (2013). The sedimentation rate decreases from 0.14 cm/yr at the base of the core to as low as 0.02 cm/yr (6,320 yrs cal BP) and than inceases again until the modern core top to as high as 0.14 cm/yr. For this study, 34 sub-samples at a resolution of approximately 500 to 1,000 year intervals in the lower part of the core and at 200 year intervals in the upper part were selected for lipid biomarker analyses omitting the lowermost core section (Younger Dryas), which consists of reworked sediment (Francke et al., 2013). The samples were freeze-dried, ground, and extracted by ultrasonication using 25 ml of each methanol, methanol: dichloromethane (1:1,v:v) and dichloromethane: hexane (1:1, v:v). Afterwards, the total lipid extract was saponified with 0.5 M potassium hydroxide in methanol: water (9:1, v:v) at 80°C for 2 h. Neutral lipids were liquid-liquid extracted with dichloromethane and further separated into four polarity fractions using silica gel column chromatography. Sequential elution was performed using hexane (aliphatic hydrocarbons), dichloromethane: hexane (7:1, v:v) (aromatic hydrocarbons), chloroform (sterols), and methanol (ethers). Subsequently, the aliphatic hydrocarbon fraction was desulfurized using activated copper and the sterol fraction was derivatized with N,O-bis(trimethylsilyl)trifluoroacetamide at 80°C for 2 h. The ether fraction was filtered over 0.45 µm PTFE filters using hexane: isopropanol (95:5, v:v).

n-Alkanes, and sterols were analyzed on a Hewlett Packard 5890 series II gas chromatograph with a flame ionization detector (GC-FID) equipped with an Agilent DB-5MS column (50 m x 0.2 mm, film thickness 0.33 µm). For aliphatic hydrocarbons, the oven temperature was held at 40°C for 2 min, increased to 140°C with a rate of 10°C min^{-1} and then to 320°C min^{-1} at 3°C min^{-1}. For the analysis of the sterol fraction, oven temperature was programmed to be held at 40°C for 2 min and increase to 290°C with 5°C min^{-1} and then to 320°C with 0.5°C min^{-1}. PAHs were analyzed using a Hewlett Packard 6890N GC coupled to a 5975C MSD and equipped with an Agilent HP-5 column (30 m x 0.32 mm, film thickness 0.25 µm). The oven temperature was programmed from

40°C held for 2 min increased to 140°C with a rate of 10°C min^{-1} and to 320°C with a rate of 5°C min^{-1}. GDGTs were analyzed using an Agilent 1290 UHPLC coupled to a 6460 QQQ-MS equipped with an APCI ion source following the methods of Hopmans et al. (2004) and Peterse et al. (2012) and were calibrated using the calibration of Peterse et al. (2012). Compounds were identified based on their GC-MS or LC-MS spectra and by comparison with external standards. Compound concentrations were quantified using authentic external standards and are normalized to total organic carbon (TOC) content to exclude effects governed by organic matter delivery or preservation.

Pollen and microcharcoals were extracted from 132 sediment samples with a resolution of about 90 years using hydrochloric acid (37%), hydrofluoric acid (40%) and hot sodium hydroxide (10%). A known amount of *Lycopodium* spores was added to the dry weighted sediment in order to estimate pollen concentrations (number of pollen grains/g of sediment; Stockmarr, 1971). Identification and quantification of pollen grains and charcoals was carried out using a transmitted light microscope (magnification 400x and 630x) with the support of atlases and the reference collection of the University of Rome “La Sapienza”. Pollen data are presented either as total (trees plus herbs) pollen influx (pollen grains incorporated annually per gram of sediment; grains*cm/g*yr derived from pollen concentration (grains/g) or percentage curves of plant groups. Microcharcoal particles were counted in pollen slides and sorted in three dimensional classes (10-50 µm, 50-125 µm, and >125 µm) measuring their shortest axis (Sadori and Giardini, 2008). Similarly to those of pollen, results are reported as influx values (particles incorporated annually per gram of sediment; particles*cm/g*yr).

4.3 Results

4.3.1 Plant wax *n*-alkanes

The odd-numbered high molecular weight (HMW) vascular plant *n*-alkane concentrations (C_{27}, C_{29}, C_{31}, C_{33}) decrease in the lowermost part of the record (Fig. 18, Tab. 5) from 34.5 µg/g TOC (total organic carbon) at 11,510 yrs cal BP to 9.3 µg/g TOC at 10,480 yrs cal BP, then increase to 34.3 µg/g TOC at 9,540 yrs cal BP and decrease again to 17.4 µg/g TOC at 8,530 yrs cal BP. Afterwards, HMW *n*-alkane concentrations show an increasing trend to 30 µg/g TOC at 6,190 yrs cal BP followed by slightly lower values until 5,220 yrs cal BP (23.5 µg/g TOC) and a peak at 4,490 yrs cal BP (43.4 µg/g TOC). Between 4,490 yrs cal BP and the top of the core, HMW *n*-alkane concentrations decrease to a slightly lower level with four distinct peaks at 3,290 yrs cal BP (32.6

µg/g TOC), 1,710 yrs cal BP (29.2 µg/g TOC), 780 yrs cal BP (30.9 µg/g TOC), and 370 yrs cal BP (40 µg/g TOC). The average chain length (ACL) of the odd-numbered HMW *n*-alkanes (C_{25}, C_{27}, C_{29}, C_{31}, C_{33}) varies strongly particularly in the upper half of the core (Fig. 18, Tab. 5). In the lower half of the record, we observe an overall trend of decreasing values from 29.3 at 11,510 yrs cal BP to 28.8 at 5,680 yrs cal BP. Between 5,680 and 3,290 yrs cal BP the ACL increase to 29.5 followed by a period of relatively high but strongly fluctuating values with peaks at 2,800 yrs cal BP (29.5), 2,140 yrs cal BP (29.9), and 1,710 yrs cal BP (29.4). From 1,710 yrs cal BP to 1.170 yrs cal BP the ACL decreases to values as low as 28.9 (1,170 yrs cal BP) followed by an overall increase to the core-top (as high as 29.4 at 120 yrs cal BP).

4.3.2 Steroids

In the lower part of the record, the fecal stanol (5β-cholestan-3β-ol, 5β-cholestan-3α-ol) concentrations show an overall increasing trend from 10 µg/g TOC (11,510 yrs cal BP) to 36.1 µg/g TOC (4,490 yrs cal BP) with minor peaks at 9,540 yrs cal BP (23.4 µg/g TOC), 7,180 yrs cal BP (25.3 µg/g TOC) (Fig. 18, Tab. 5). After 4,490 yrs cal BP the β-stanol concentrations show greater fluctuations with lower values (18.4 µg/g TOC) from 3,930 yrs cal BP to 3,670 yrs cal BP, higher values from 3,480 yrs cal BP to 2,800 yrs cal BP peaking at 3,110 yrs cal BP (51 µg/g TOC), and a period of lower values from 2,510 yrs cal BP to 1,520 yrs cal BP (17.1 µg/g TOC). At 1,520 yrs cal BP β-stanol concentrations start to increase to a maximum at 780 yrs cal BP (60.3 µg/g TOC) followed by a short decrease until 640 yrs cal BP (32.8 µg/g TOC). Subsequently, β-stanol concentrations increase again and peak at the core-top (48 µg/g TOC).

4.3.3 PAHs

Combustion-derived polycyclic aromatic hydrocarbons (PAHs) (fluoranthene, pyrene, benzo[ghi]fluoranthene, benzo[bj]fluoranthene, benzo[k]fluoranthene, benzo[a]fluoranthene, benzo[e]pyrene, benzo[a]pyrene, and benzo[ghi]perylene) decrease between 11,510 yrs cal BP (560 ng/g TOC) and 10,480 yrs cal BP (280 ng/g TOC) (Fig. 18, Tab. 5). Subsequently, the PAH concentrations increase to 720 ng/g TOC at 9,540 yrs cal BP and then remain fairly stable until 4,490 yrs cal BP (650 ng/g TOC). After 4,490 yrs cal BP, the PAH concentration show a minor peak at 3,930 yrs cal BP (860 ng/g TOC) and a major peak at 3,290 yrs cal BP (1,200 ng/g TOC) followed by an overall decrease until 930 yrs cal BP (40 ng/g TOC). Subsequently, the PAH concentrations increase rapidly to 710 ng/g TOC at 780 yrs cal BP. Following a decrease to 350 ng/g TOC at 570 yrs cal BP, the uppermost part of the core (120 yrs cal BP to modern) is characterized by a strong increase in PAH concentrations reaching the highest values of the entire record with 5,200 ng/g TOC at 120 yrs cal BP.

4.3.4 GDGT-based indices

The BIT index shows relatively high values between 0.75 and 1.00 throughout the entire record (Fig. 18, Tab. 5). The BIT index decreases from 0.85 at 11,510 yrs cal BP to a minimum of 0.75 at 10,480 yrs cal BP. Afterwards, the values steadily increase to 0.98 at 4,490 yrs cal BP. Subsequently, the BIT index decreases to 0.86 at 3,930 yrs cal BP followed by an increase to 0.96 at 3,480 yrs and another decrease to 0.84 at 3,110 yrs cal BP. After 3,110 yrs cal BP the BIT index generally increases until 780 yrs cal BP (0.99). Following slightly lower values at 370 yrs cal BP (0.92), the BIT index increases to 1.00 at the core-top.

MBT'/CBT proxy-inferred annual MATs show the lowest value at 11,510 yrs cal BP (7.6°C) (Fig. 18, Tab. 5). Subsequently, temperatures rise to 10.7°C at 9,540 yrs cal BP followed by an overall decline of about 2.5°C until present (8.3°C). The proxy-derived annual MATs of the core-top sediment (8.3°C) apparently mismatch the instrumental MAT data of 14.3°C (Sotiria and Petkovski, 2004). However, the MBT'/CBT based annual MATs of recent topsoil samples (Fig. 17, Tab. 6) show a similar mismatch with instrumental annual MATs. Accordingly, in the following we will interpret the relative ΔMAT changes throughout the sedimentary record rather than absolute annual MAT values.

4.3.5 Pollen

Percentage and influx curves of selected taxa and groups are shown in Fig. 18 and have to be taken as general changes in the environment and in the vegetal landscape (see appendix). The total (trees plus herbs) pollen influx curve shows low/medium values (roughly between 3,000 and 6,000 grains*cm/g*yr) from the base of the diagram until around 2,500 years BP. In this time frame, there are three intervals, from between 9,500 and 8,600 yrs cal BP, between 5,600 and 4,600 yrs cal BP, and between 3,200 and 2,800 yrs cal BP with increased influx values (max 13,500 grains*cm/g*yr). Subsequently, the total pollen influx shows a strong increase to a maximum of 26,000 grains*cm/g*yr at 2,200 yrs cal BP. After a strong decrease to as low as 2,800 grains*cm/g*yr at 1,610 yrs cal BP, the pollen influx increases to another relative maximum at

780 yrs cal BP (25,000 grains*cm/g*yr) followed by a decrease until 120 yrs cal BP (7,500 grains*cm/g*yr).

In general, pollen assemblages of core Co1260 are dominated by arboreal pollen (AP). %AP increases from a minimum of 14% at 11,620 yrs cal BP to 93% at 8,260 yrs cal BP driven mainly by the abundance of deciduous taxa (*Acer*, *Betula*, *Carpinus betulus*, *Fagus*, *Fraxinus*, *Ostrya*/*Carpinus orientalis*, deciduous *Quercus*, *Quercus* cf. *cerris*, *Tilia*, *Ulmus*), which increase from 5% to 70% while coniferous taxa (*Abies*, *Juniperus*, *Picea*, *Pinus*) vary between 5% and 18%. Then AP varies between 82% and 95% displaying a relatively stable pattern. However, among "stable" AP the relative abundance of coniferous taxa increase to up 45% from 4,000 to 2,030 yrs cal BP, while deciduous taxa slowly decrease to about 38%. Thereafter, conifers rapidly drop to 6-15% until about 1,090 yrs cal BP causing the concurrent decrease of AP. After a recovery around 1,000 yrs cal BP, AP and deciduous pollen decrease to 68% and 22%, respectively, while conifer relative abundances remain somewhat stable (20-28%) until about 240 yrs cal BP, followed by a decrease to as low as 13% at the core-top. The bulk of non arboreal pollen (NAP) is mirrored by Poaceae, which vary between 1% and 25% while ruderal plant taxa (*Centaurea* cf. *cyanus*, *Plantago lanceolata* type, *Rumex, Trifolium*) generally account for < 2% throughout the record with lowest abundances (0-1%) between 9,500 yrs and 2,800 yrs cal BP.

Relative abundances of pollen grouped as cultivated/cultivable plant taxa (*Castanea*, *Juglans*, *Olea*, *Vitis*, *Hordeum* type, *Secale*, *Avena*/*Triticum*) vary little until about 2,800 yrs cal BP accounting for < 2%. Subsequently, the relative abundance of these taxa increases while showing stronger fluctuations with values to up to 8%.

4.3.6 Microcharcoals

The influx of small (10-50 µm) microcharcoals varies between 0 and 1,100 particles *cm/g*yr in the interval between 11,620 yrs cal BP and 6,580 yrs cal BP with only minor fluctuations except for a peak at 9,950 yrs cal BP (1,300 particles*cm/g*yr) (Fig. 18, appendix). Lower values (maximum 500 particles*cm/g*yr) between 6,580 yrs cal BP and 4,920 yrs cal BP are followed by increased values (1,500 particles*cm/g*yr at 3,870 yrs cal BP). Subsequently, the influx shows stronger fluctuations with many peaks of up to 5,000 particles*cm/g*yr). The influx of medium size (50-125 µm) microcharcoal particles varies between 0 and 700 particles*cm/g*yr throughout the core showing its maximum at 1,010 yrs cal BP and at the core-top (300 particles*cm/g*yr). Microcharcoal particles >125 µm mainly occur in the lower part of the record until 7,870 yrs cal BP, at 2,580 yrs cal BP, and at the core-top.

Table 5. Lake Dojran, core Co1260: Biomarker concentrations and molecular proxy data.

Depth (cm.)	[a] Age (yrs. BP)	[b] β-stanols (μg/g TOC)	[c] PAHs (ng/g TOC)	[d] ACL	[e] Σ HMW *n*-alkanes (μg/g TOC)	[f] BIT	[g] Δ annual MAT (°C)	[g] MBT'	[g] CBT
1	0	48.0	5,010	29.3	26.8	1.00	0	0.28	0.20
25	120	38.3	5,190	29.4	27.8	0.94	0.5	0.28	0.12
57	370	44.0	400	29.3	40.0	0.92	0.4	0.28	0.16
81	570	34.0	340	29.3	20.3	0.93	0.4	0.29	0.16
89	640	32.8	580	29.0	22.7	0.98	0	0.28	0.20
105	780	60.3	710	29.0	30.9	0.99	0.1	0.29	0.22
113	850	46.6	210	29.1	18.5	0.97	0	0.28	0.23
121	930	55.1	40	29.0	16.8	0.96	0.2	0.28	0.19
145	1,170	27.9	110	28.9	22.7	0.94	1.3	0.31	0.13
161	1,340	20.3	310	28.9	16.6	0.91	1	0.30	0.15
177	1,520	17.1	340	28.9	16.9	0.93	1.2	0.30	0.12
193	1,710	22.6	340	29.4	29.2	0.93	0.8	0.30	0.17
209	1,920	26.9	540	29.2	24.5	0.92	1.4	0.31	0.11
225	2,140	27.1	530	29.9	12.9	0.93	1.1	0.30	0.12
241	2,380	25.7	690	29.1	18.3	0.93	1.2	0.30	0.11
249	2,510	17.7	540	29.4	21.7	0.88	1.7	0.30	0.05
265	2,800	37.0	780	29.5	21.3	0.86	1.5	0.30	0.06
273	2,950	35.1	540	29.3	24.6	0.87	1.1	0.29	0.06
281	3,110	51.0	780	29.2	19.6	0.84	1.6	0.30	0.03
289	3,290	29.8	1,200	29.5	32.6	0.91	1.6	0.30	0.05
297	3,480	31.4	560	29.4	29.2	0.96	0.9	0.29	0.11
305	3,690	18.4	580	29.4	17.8	0.93	0.9	0.28	0.07
313	3,930	18.4	860	29.4	27.2	0.86	1.7	0.31	0.04
329	4,490	36.1	650	29.0	43.4	0.98	1.4	0.31	0.11
345	5,220	23.3	560	28.9	23.5	0.95	1.6	0.30	0.05
353	5,680	20.3	530	28.8	25.7	0.95	1.4	0.30	0.10
361	6,190	16.3	700	29.0	30.0	0.95	1.3	0.29	0.07
369	6,710	17.5	580	29.2	24.2	0.95	1.4	0.31	0.11
377	7,180	25.3	690	29.0	23.2	0.94	1.6	0.31	0.08
385	7,600	15.4	570	29.2	17.9	0.89	1.9	0.31	0.07
409	8,530	11.2	620	29.1	17.4	0.89	2.2	0.33	0.11
449	9,540	23.4	720	29.3	34.3	0.81	2.4	0.33	0.07
505	10,480	10.0	280	29.2	9.3	0.75	1.8	0.31	0.07
593	11,510	10.0	560	29.3	34.5	0.85	-0.7	0.27	0.27

[a] According to Francke et al. (2013)
[b] 5β-cholestan-3β-ol, 5β-cholestan-3α-ol
[c] Fluoranthene, pyrene, benzo[ghi]fluoranthene, benzo[bj]fluoranthene, benzo[k]fluoranthene, benzo[a]fluoranthene, benzo[e]pyrene, benzo[a]pyrene, and benzo[ghi]perylene
[d] $(C_{25}*25+C_{27}*27+C_{29}*29+C_{31}*31+C_{33}*33) / (C_{25}+C_{27}+C_{29}+C_{31}+C_{33})$
[e] $(C_{27}+C_{29}+C_{31}+C_{33})$
[f] According to Hopmans et al. (2004)
[g] According to Peterse et al. (2012)

4.3.7 Catchment

For comparison of MBT'/CBT proxy-derived annual MATs and instrumental annual MAT data we analyzed five topsoil samples from the lake catchment (Fig. 17, Tab. 6). MBT'/CBT proxy-derived annual MATs are consistently lower than instrumental annual MATs (14.3°C; Sotiria and Petkovski, 2004) consistent with the observations of Peterse et al. (2012) who found significant underestimation of MBT'/CBT proxy-derived annual MATs in arid regions. The significant variability of MBT'-CBT proxy-derived annual MATs in the Dojran topsoil samples restrict their use for a Dojran catchment-specific MBT'/CBT calibration and highlight that relative changes of sedimentary MBT'/CBT proxy-derived annual MATs should be discussed rather than absolute MATs. Bird-feces sampled along the fringe of Lake Dojran (Fig. 17, Tab. 6) contains detectable amounts of the β-stanols coprostanol and epi-coprostanol (1.63 and 1.95 μg/g TOC) confirming that background β-stanol concentrations in Dojran sediments likely have an avian origin.

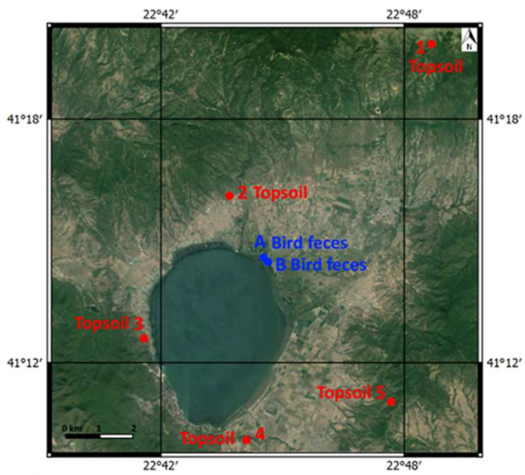

Figure 17. Map of topsoil (red, 1-5) and bird feces (blue, A-B) samples from the catchment.

Table 6. MBT'/CBT proxy-derived annual MAT of catchment topsoil samples and β-stanols of bird feces from the Dojran catchment.

Sample	[a] MAT °C	[b] β-stanols μg/g TOC
Topsoil 1	3.8	-
Topsoil2	9.7	-
Topsoil 3	10.6	-
Topsoil 4	4.2	-
Topsoil 5	7.5	-
Bird feces A	-	2.0
Bird feces B	-	1.6
[a] According to Peterse et al. (2012)		
[b] 5β-cholestan-3β-ol, 5β-cholestan-3α-ol		

4.4 Discussion

Lake Dojran sediments receive input from various sources including autochthonous production and allochthonous material supplied by different transport modes (aeolian and riverine). Accordingly, the proxies used here represent both broader regional signals as well as signals confined to the Dojran catchment (accordingly, leads and lags of the different proxy records may be caused by different transport modes) and are characteristic environmental and/or anthropogenic markers (for an extensive review see Dubois & Jacob, 2016).

We trace the input of terrestrial vascular plant organic carbon using high molecular weight (C_{27}, C_{29}, C_{31}, C_{33}) *n*-alkanes, which derive from the epicuticular wax cover of terrestrial vascular plant leaves (Eglinton & Hamilton, 1967). Their average chain length provides further information about the major vegetation type such as woody and herbaceous/grassy plants and, by inference, temperature and aridity (Castañeda & Schouten, 2011; Ficken et al., 2000; Cranwell, 1973; Meyers, 1997). The molecular information is directly comparable to relative abundances of trees (AP, arboreal pollen) and herbs (NAP, non arboreal pollen) indicating vegetation physiognomy. Likewise, the tree and herb pollen influx can be used as a proxy of plant biomass indicating the density of vegetation (cf. Panagiotopoulos et al., 2013; Sadori et al., 2016; Sadori et al., 2004). Since epicuticular waxes as well as pollen are transported via aeolian and fluvial transport mechanisms, they represent both a regional and catchment-derived signal of vegetation change. Furthermore, we use the BIT index, a ratio of soil-derived and aquatic GDGTs indicating fluvial soil organic matter input (Hopmans et al. , 2004; Schouten et al., 2013), to reconstruct soil erosion processes in the catchment. These should either be linked to anthropogenic deforestation and agricultural activities or natural variations in precipitation, runoff, and vegetation cover. For soil-derived biomarkers (*n*-alkanes and GDGTs), we assume relatively rapid turnover since Chen et al., (2013) show that the mean residence time (MRT) of soil organic carbon around 40°N is less than 60 yrs and the good agreement of *n*-alkane ACL and pollen imply no major leads or lags.

The reconstruction of human/livestock presence in the catchment is based on the input of feces-derived β-stanols, which are produced from cholesterol by microbes in the mammalian gut and persist in sedimentary records (Bull et al., 2002; D'Anjou et al., 2012). We assume allochthonous β-stanols are supplied solely via runoff of soil OC within the catchment and, thus, carry a local signal. Furthermore, we use pyrolytic PAHs, aromatic hydrocarbons produced from organic matter during combustion processes including natural and anthropogenic fire activities. PAHs are supplied from the atmosphere via dry and wet deposition from proximal as well as distant sources (Meyers and Ishiwatari, 1993; Lima et al., 2005). Microcharcoal size provides an additional level of information since charcoal fragments >125 µm are generally taken as an evidence of local fire, while charred fragments between 10 and 50 µm and between 50 and 125 µm indicate regional fire, together with background noise, and fire occurrence at the landscape/regional scale, respectively (Whitlock and Millspaugh, 1996; Sadori et al., 2015b). Besides tracing absolute concentrations of β-stanols, PAHs, and microcharcoal, pollen of cultivated and weed plants provide evidence of human presence and impact in the territory (Marinova et al., 2012).

This multi-proxy approach is particularly useful to disentangle natural and anthropogenic influences for those proxies, which may be influenced both ways. For example, deforestation and "slash-and-burn" agriculture have been used by humans since Neolithic times (Rius et al., 2009). Accordingly, an increase of the *n*-alkanes ACL due to deforestation (growing proportion of herbaceous vegetation) should correlate with an increase of NAP, PAHs and microcharcoals >125 µm, and β-stanol abundances in the record, while an increase of the latter is not expected during natural climatic variations. Likewise, some cultivated plants such as olive or vine are native to the region and both cereal and ruderal plant pollen also include pollen of other grasses or herbs, respectively. Accordingly, we interpret significant increases above the background of pollen as indicator for agricultural activities if they match other "anthropogenic" proxies such as β-stanols. For the following discussion, we use the stratigraphic classification of the Holocene suggested by Walker et al. (2012). The archeological periods are defined according to Marinova et al. (2012).

4.4.1 Early Holocene (11,700 – 8,200 yrs cal BP)

Following a cold and arid Younger Dryas (Bordon et al., 2009; Kotthoff et al., 2008; Kotthoff et al., 2011; Valsecchi et al., 2012; Kallel et al., 1997), the Late Glacial/Early Holocene transition on the Southern Balkan (Bordon et al., 2009; Aufgebauer et al., 2012; Panagiotopoulos et al., 2013), the Aegean (Kotthoff et al., 2008), and the Central Mediterranean region (Allen et al., 1999; Sadori et al., 2011) was marked by more humid conditions, rising temperatures, and increasing vegetation cover. The changing climate and landscape of the Early Holocene is also reflected in our data set. We observe an increase of annual MATs based on GDGTs of about 3°C during the Early Holocene to a relative thermal maximum at 9,540 yrs cal BP. This increase of temperature is accompanied by a significant increase of AP with a concomitant decrease of NAP (Fig. 18). The pollen trend is mirrored by gradually decreasing HMW *n*-alkane ACL (from 29.3 to 29.1), which tracks the input of grasses and/or conifers such as *Pinus* (pine) and fir (*Abies*) (dominance of C_{31} *n*-alkane) and deciduous trees such as *Fagus* (beech) (dominance of C_{27} *n*-alkane) and deciduous *Quercus* (oaks) (dominance of C_{29} *n*-alkane) (Maffei et al., 2004; Holtvoeth et al., 2016). In addition, the rising humidity could have contributed to the decrease in HMW *n*-alkane ACL (Schefuß et al., 2003). While the diatom-inferred rise in lake level might indicate higher runoff (Zhang et al., 2014), the denser vegetation cover and/or root system stabilizing the soils most likely led to reduced soil erosion processes as reflected by the BIT index, which shows the lowest value (0.75 at 10,480 yrs cal BP) of the entire record.

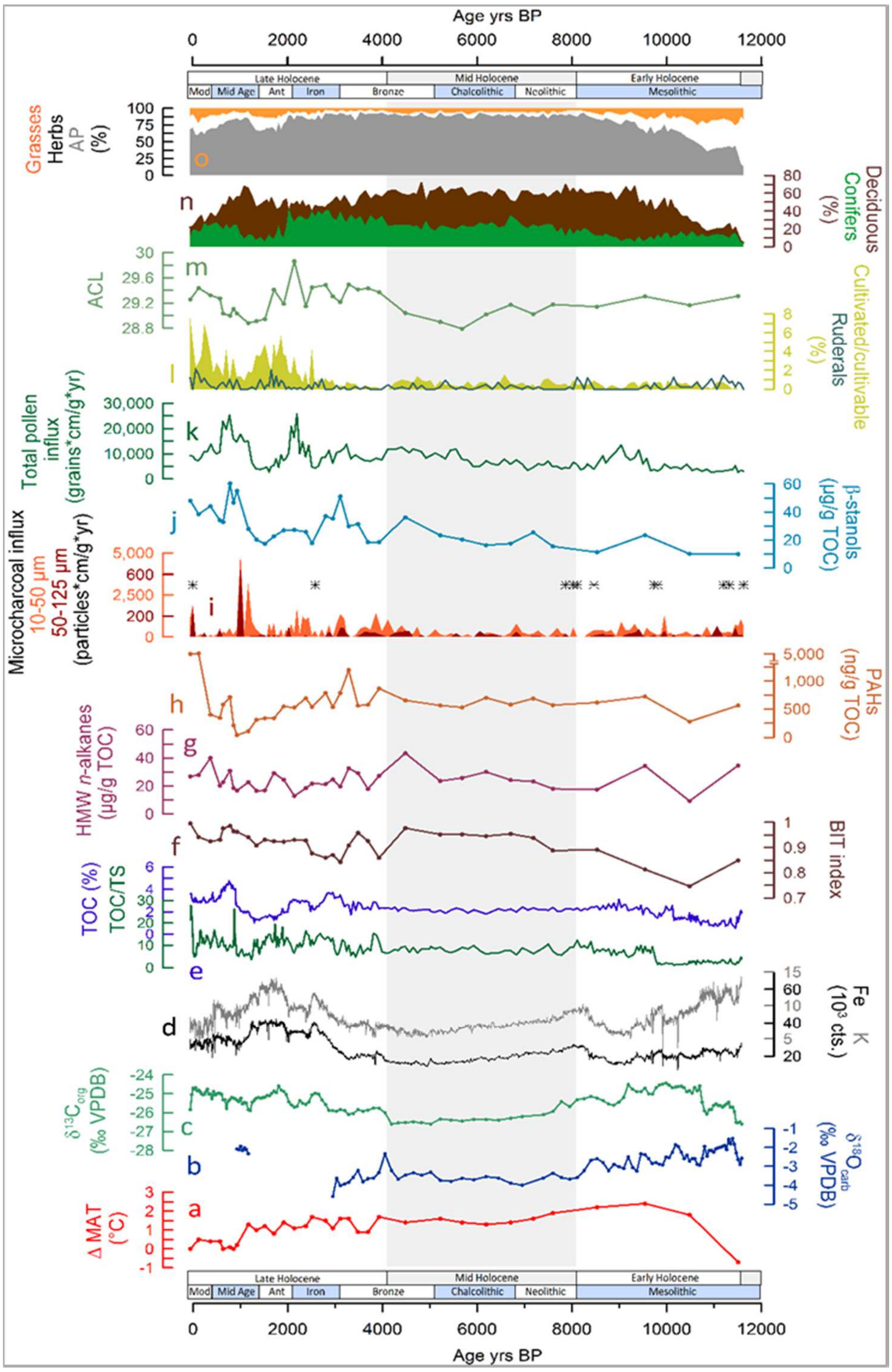

Figure 18. Lake Dojran, core Co1260: diagram of biomarker and pollen data plotted against age. (a) Δ annual MAT, (f) BIT index, (g) HMW *n*-alkanes, (h) PAHs, (i) microcharcoal (asterisks mark the presence of largest microcharcoal particles (>250 µm)), (j) β-stanols, (k) total pollen of terrestrial plants, (l) cultivated/cultivable, (m) ACL, (n) deciduous and conifer trees, and (o) AP (pollen of arboreal plants), NAP (pollen of nonarboreal plants) comprehending grasses and other herbs (for taxonomic affiliation see section 4.5). Also shown are previously published data including (b) $\delta^{18}O_{carb}$, (c) $\delta^{13}C_{org}$, (d) potassium and iron counts, and (e) TOC and TOC/TS (Francke et al., 2013).

Absolute pollen data confirm this reconstruction, showing increasing plant biomass (trees and herbs pollen influx). Decreasing erosion rates in the catchment are also implied by the lower input of potassium (K) and iron (Fe) and higher $\delta^{13}C_{org}$ values observed by Francke et al. (2013). PAH concentrations are relatively low at the beginning of the Early Holocene (280 to 560 ng/g TOC) implying low natural fire activity in concomitance with microcharcoal influx curves, which indicate low fire activity both locally and regionally. While higher temperatures and a higher proportion of forest vegetation as indicated by pollen and *n*-alkane ACL could promote wildfires (increased fuel; Doyen et al., 2015; Brown et al., 2005), the low PAH concentrations and microcharcoal influx indicate that the fire regime in the Dojran catchment might rather be driven by moisture than fuel availability. Wildfire activity has been correlated to phases of aridity in other humid and woody regions in the Mediterranean (Sadori and Giardini, 2007; Vannière et al., 2008). The discrepancy in the late Early Holocene (9,540 to 8,530 yrs cal BP) between BIT index indicating rising runoff/humidity and slightly increased PAH and microcharcoal concentrations (all size fractions roughly double) compared to 10,480 yrs cal BP might, thus, result from increased precipitation seasonality, since drier summer conditions favor the occurrence of wildfires (Vannière et al., 2008). Stronger seasonality of wet winters and dry summers were indeed proposed for Lake Dojran by Zhang et al. (2014) and the Aegean region by Dormoy et al. (2009) during the late Early Holocene.

Since we observe no indication for human settlement activities either in the ACL, BIT index, PAH, or pollen record and archeological evidence for agriculture and Neolithic lifestyle on the Balkan Peninsula is absent (Willis and Bennett, 1994; Bocquet-Appel et al., 2009), we consider the fairly low fecal stanol concentrations throughout the Early Holocene (10-23 µg/g TOC) to be derived from natural sources. Lake Dojran is known to be a major wintering area for waterbirds under today's conditions (Velevski et al., 2010), thus, the stanol background may derive from bird feces. While previously reported 5β-stanols profiles in bird feces are inconsistent (Leeming et al., 1996; Martin et al., 1973; Sugano, 1967; Cheng et al., 2016), two bird feces samples taken at the fringe of Lake Dojran in 2015 indeed confirm the presence of 5β-stanols. In addition, for neighboring Lake Ohrid Holtvoeth et al. (2016) suggest that 5β-coprostanol may be produced in-situ by anaerobic bacteria. Such anaerobic bacteria could also contribute to the observed background 5β-stanol concentrations. However, we exclude major contributions from anaerobic bacteria since TOC/TS ratios (Fig. 18) are >5 throughout the record after 9,770 yrs cal BP implying oxygen repletion of bottom waters and surface sediments. During the Early Holocene between 11,510 yrs cal BP and 9,770 yrs cal BP, however, TOC/TS ratios are lower (~2) indicative for more reducing conditions (Francke et al., 2013), which would have promoted anaerobic in-situ production of β-stanols.

4.4.2 Middle Holocene (8,200 – 4,200 yrs cal BP)

The Middle Holocene Mediterranean climate was characterized by an early humid phase associated with the deposition of sapropel 1b in the Mediterranean Sea (Ariztegui et al., 2000) followed by a shift to higher aridity (Wick et al., 2003; Roberts et al., 2008; Kotthoff et al., 2008; Joannin et al., 2012; Peyron et al., 2011; Abrantes et al., 2012). Temperature reconstructions for the Middle Holocene, however, are rather scarce and show a high variability with both increasing and decreasing temperature trends (e.g., Finné et al., 2011; Abrantes et al., 2012). Our MBT'/CBT proxy-derived annual MATs show an approximately 1°C cooling trend from the Early Holocene thermal maximum across the Middle Holocene (Fig. 18; Tab. 5). The climatic shift towards more arid conditions was only moderate at Lake Dojran, since seismic data as well as bulk organic carbon isotope ($\delta^{13}C_{org}$) and carbonate oxygen isotope ($\delta^{18}O_{carb}$) data indicate stable atmospheric and climatic conditions and a relatively high lake level between 7,900 and 4,300 yrs cal BP (Francke et al., 2013). Overall, our data suggest relatively stable conditions for the Middle Holocene in comparison to the Early and Late Holocene as implied by the rather low variability of the data, in particular annual MATs, PAH, and HMW *n*-alkane concentrations as well as stable AP and NAP abundances. More pronounced changes are shown by the BIT index (increasing to up to 0.95) indicating enhanced catchment runoff/soil erosion probably indicating enhanced precipitation. The continued decrease of the *n*-alkane ACL (to 28.8) during the early Middle Holocene coincides with the expansion of deciduous trees as seen in pollen records from neighboring lakes Ohrid (Wagner et al., 2009) and Prespa (Panagiotopoulos et al., 2013) although AP indicate relatively stable forest formations at Lake Dojran. PAH concentrations and microcharcoal influx indicate medium to low fire activity at the local and regional scale. The observed increase of the ACL starting at 5,680 yrs cal BP and continuing into the early Late Holocene matches a concurrent slight increase of pollen influx, which is characterized by increasing proportions of conifers. Since MATs are stable, but runoff and soil erosion are enhanced (increase of the BIT index, high lake level and enhanced nutrient supply inferred by diatoms, Zhang et al. 2014), the ACL trend may not indicate overall aridification but rather increasing seasonality.

Towards the end of the Middle Holocene, during the early Bronze Age, we observe increasing trends of fecal stanol concentrations, HMW *n*-alkane ACL, and the BIT index as well as a slight increase of pollen of cultivated plants possibly related to first human activities in the catchment. Lithological and sedimentological data including TOC/TS ratios indicate a stable depositional environment throughout the Middle and Late Holocene (Francke et al., 2013), thus, the increase of fecal stanol concentrations should not be driven by increased anaerobic bacterial activity. First small-scale human impact is consistent with archaeological evidence, which indicates that during the Middle Holocene early cultures such as Starčevo and Körös-Criș started to migrate into the Balkans. However, human influence on the environment was limited, since early settlements were very small (usually less than 1 ha) and had only temporal character due to a semi-sedentary lifestyle (Kaiser and Voytek, 1983). The continued increase of HMW *n*-alkane ACL during the early and middle Bronze Age supported by increasing PAH and microcharcoal concentrations might be the result of first “slash-and-burn” agriculture, and/or human wood exploitation although any landscape management was probably mainly related to pastoralism. Nonetheless, human impact probably led to further enhanced soil erosion processes as reflected by the high BIT index (0.98) and a substantial increase of HMW *n*-alkane concentrations. Furthermore, archaeological findings from the site of Vardaroftsa (Axiokhori), about 40 km away from the lake, suggest the beginning colonization of the greater Dojran area in the Bronze Age (Davies et al., 1926; Hammond, 1972).

4.4.3 Late Holocene (4,200 yrs cal BP - present)

The transition from the Middle to the Late Holocene is characterized by a significant climatic and environmental change attributed to the dry and cold 4.2 ka event evident throughout the Mediterranean (Magny et al., 2009; Wagner et al., 2009; Vogel et al., 2010; Sadori et al. 2015a) and the Near East (Bar-Matthews et al., 1999; Masi et al. 2013). Subsequently, in the early Late Holocene, findings from the western and central Mediterranean (Magny et al., 2009) show a restoration of the previous wetter conditions, with increased lake levels and recovery of forests. At Lake Dojran Francke et al. (2013) identify a phase of drier conditions and lower temperatures around 4,000 yrs cal BP (Fig. 18), and observe a general trend towards environmental instability in the early Late Holocene, which is in agreement with our proxy records showing significant changes during the Mid- to Late Holocene transition. BIT index (0.86 at 3,930 yrs cal BP) and HMW *n*-alkane concentrations (17.8 µg/g TOC at 3,670 yrs cal BP) decrease, indicating a period of lower runoff/soil erosion. The simultaneous slight decrease in total pollen influx probably indicates a reduction of overall plant biomass. As conifer pollen continues to increase, the landscape was more open and degraded and the climate most likely changed to more arid conditions accompanied by enhanced fire activity as implied by slightly increased PAH concentrations (860 ng/g TOC) at 3,930 yrs cal BP and an increased influx of microcharcoal. The fecal stanol concentrations (18.4 µg/g TOC) decrease between 3,930 yrs cal BP and 3,670 yrs cal BP possibly indicating reduced or changing anthropogenic activity. Since Francke et al. (2013) and Zhang et al. (2014) observe decreased autochthonous production and a peak in the TOC/TS ratio indicating oxygen repletion, anaerobic in-situ production of β-stanols can be excluded. Decreased anthropogenic land-use might also be indicated by minimum concentrations of cultivated taxa and the sharp decrease in the BIT index and the total HMW *n*-alkane concentrations due to less human-induced erosion. This decline might have been a response to the climatic perturbation (aridity), which occurred in the Dojran area around 4,000 yrs cal BP as observed by Francke et al. (2013). Site abandonment and resettlement of early Bronze Age cultures following the Mid Holocene-Late Holocene transition were previously reported for Greece and the Levante (Rosen, 1997), indicating a potential anthropogenic response to climatic change in the Mediterranean.

Furthermore, starting at the Middle to Late Holocene transition, major vegetational changes occur in the conifer/deciduous tree ratio of AP, which is also reflected by increasing HMW *n*-alkane ACL mirroring the conifer pollen abundances throughout the Late Holocene. The combined vegetational response and the degradation of deciduous forest taxa might be due to both water shortage and long-term effects of previous agricultural and/or pastoral activities.

Starting at 3,670 yrs cal BP, we observe a considerable increase of fecal stanol concentrations (to up to 51 µg/g TOC at 3,110 yrs cal BP) accompanied by a peak in PAH (1,200 ng/g TOC) and HMW *n*-alkane (32.6 µg/g TOC) concentrations at 3,290 yrs cal BP and increasing abundance of cultivated plant taxa. This together points to a stronger human impact/re-settlement consistent with the Late Bronze Age maximum in settlement activities in the nearby Struma River valley observed by Grebska-Kulowa and Kulow (2007) and the establishment of a permanent settlement at Vardarski Rid (Mitrevski, 2009) approximately 10 km west of Lake Dojran. Higher BIT values and HMW *n*-alkane concentrations as well as increasing input of clastic material (K, Fe) demonstrate reinvigorated soil erosion likely caused by both human agricultural activity and higher humidity/runoff.

Pollen data indicate a strong human impact since 2,600 yrs cal BP implied by increased cultivated and ruderal plant taxa. HMW *n*-alkane ACL also remains at high values, most likely indicating continued forest clearing activities of the deciduous forest in the lowlands of the catchment. However, fecal stanol input and PAH concentrations decrease after 2,510 yrs cal BP. TOC/TS ratios do not indicate changing bottom water oxygenation and lake productivity is already low at 3,000 yrs cal BP (Francke et al., 2013) indicating that the decrease of fecal stanol concentrations should not be driven by sedimentological changes affecting anaerobic bacteria. Based on the pollen evidence still implying intensive exploitation of the region and a peak in regional fire activity (microcharcoals 10-50 µm), this might be the result of a reorganization/relocation of the settlements or even a change in settlement type away from pile dwellings (palafittes). Palafittes dating back to the late Bronze/early Iron Age (1,500-700 BC) have been discovered in Lake Ohrid (Mitrevski, 2009a) and Lake Prespa. Even the Greek historian Herodotus described the life in a settlement on ancient Lake Prasiad in the nearby Strymon valley during the fifth century BC. Due to the relative shallowness of Lake Dojran, a lake level change and an expansion of shallow reed areas could have affected lakeside settlements and especially palafittes located on the lake or in the reed beds. Sedimentary (Francke et al., 2013) and microfossil (Zhang et al., 2014) data suggest a substantial lake level lowering between 2,800 and 1,200 yrs cal BP and other records from the Mediterranean region indicate more arid conditions during this period compared to the Mid Holocene (Schilman et al., 2001; Roberts et al., 2008; Sadori and Narcisi, 2001; Sadori et al., 2013, 2016). Temperature reconstructions from NE Italy (Frisia et al., 2005) and the Adriatic Sea (Piva et al., 2008) indicate warmer temperatures attributed to the Roman Warm Period (2,400 yrs cal BP to 1,600 yrs cal BP), albeit MBT'/CBT based annual MATs in our record are relatively stable. Thus, the lake level lowering might have led to settlement relocation further away from the shoreline (i.e. different settlement type) albeit Fouache et al. (2010) suggest that settlements were moving with the shoreline at Lake Maliq. While the input of anthropogenic biomarkers (5β-stanols) into the lake was reduced after 2,510 yrs cal BP, intensive agriculture and forestry might still have been practiced in the catchment. The sharp decrease of pollen influx and conifer pollen abundances in particular as well as the decrease of *n*-alkane ACL during the Roman Period at about 2,000 yrs cal BP may have been the result of lumbering of pines and firs, which have been used as an important construction material for Roman ships and were in fact exported from the Macedonian and Thracian region (Harris, 2013). Forestry might have not required permanent settlements.

In the uppermost core interval, during the Middle Ages and the early Modern Era, Francke et al. (2013) identified climatic fluctuations related to the Medieval Warm Period (MWP) and the subsequent Little Ice Age (LIA). Both climatic oscillations are also recorded in sedimentary records on the Balkan (Wagner et al., 2009; Aufgebauer et al., 2012; Vogel et al., 2010) and the SE Mediterranean Basin (Schilman et al., 2001). For Lake Dojran, Francke et al. (2013) linked more humid conditions and enhanced runoff with a warmer climate between 1,200 and 900 yrs cal BP (MWP), and subsequently colder temperatures and more arid conditions during the LIA. This is the period in which the AP, in particular *Pinus*, recovers from the previous drastic decline at 2000 yrs cal BP. Our lipid based annual MATs record an approximately 1°C cooling starting at 1,170 yrs cal BP, followed by relatively stable temperatures until present, implying either no or only rather small temperature fluctuations. However, the biomarker record suggests changes in anthropogenic activity that could be related to the hydrological rather than to temperature variations of the MWP and LIA. Thus, the increased fecal stanol input (to up to 60.3 µg/g TOC between 930 yrs cal BP and 780 yrs cal BP) and a peak in PAH and HMW *n*-alkane concentrations as well as in the BIT index at 780 yrs cal BP indicate increased human activity. Pollen data show a constant reduction of arboreal vegetation starting at about 1,010 yrs cal BP. In addition, cultivated and ruderal taxa percentages show high but fluctuating values during this time period. This core section (~1,250 to 850 yrs cal BP) is characterized by fine laminations, high autochthonous production and lower TOC/TS ratios (~5) indicating less oxygenated (but still aerobic) sedimentary conditions (Francke et al., 2013). Thus, β-stanol concentrations could be partly influenced by possible in-situ bacterial production during this period. Subsequently, decreased 5β-stanol concentrations from 640 to 570 yrs cal BP in combination with a low in PAH and HMW *n*-alkane concentrations at 570 yrs cal BP again indicate a decrease of human impact or changes in land-use/settlement pattern. This could imply that hydrological rather than temperature fluctuations during the last 1,000 yrs cal BP may have influenced human settlement history at Lake Dojran. Albeit PAH concentrations follow a similar pattern observed for the BIT index and 5β-stanol concentrations, they remain on a relatively low level during the middle Late Holocene (Antiquity and the Middle Ages) compared to the Middle Holocene and the Early Late Holocene indicating low fire activity. At the same time, the microcharcoal (10-50 µm and 50-125 µm) influx peaks at 1,010 yrs cal BP implying intensified regional fires after the biomass (pollen influx) recovered from the decline during the Roman period.

The uppermost part of the record, i.e. the last two centuries, represents the Modern Era. This is particularly emphasized by the highest PAH concentrations (up to 5,200 ng/g TOC) of the entire record as well as high microcharcoal influx, both reflecting fossil fuel combustion and industrial emissions caused by increasing traffic and tourism, the urbanization of the villages Star and Nov Dojran, and industrialization as shown by other studies (Sanders et al., 1995; Liu et al., 2013). High 5β-stanol concentrations, a maximum BIT value (1.00), and the high abundances of cultivated plant taxa also point to increased anthropogenic activity, respectively, soil erosion processes during the Modern Era. 5β-Stanol concentrations are high at the core top (48.0 µg/g TOC), but lower than at 2,950 yrs cal BP or 780 yrs cal BP. Based on our data, we cannot determine why absolute 5β-stanol concentrations are lower, but factors may include sewage treatment, different transport mode (sewage vs. soil erosion), reduced livestock presence or a yet unknown mechanism.

4.5 Summary and Conclusions

Our molecular and palynological data reveal strong humidity and increasing vegetation cover during the Early Holocene with annual MATs rising to a Holocene thermal maximum at 9,540 yrs cal BP and likely increased precipitation seasonality during the late Early Holocene. The Middle Holocene at Lake Dojran is characterized by relatively stable conditions with an only moderate trend towards higher aridity. The Late Holocene is characterized by climatic instability and strong anthropogenic overprint with first evidence for human impact towards the Mid- to Late Holocene transition (early Bronze Age). In the early Late Holocene, we observe a brief phase of decreased anthropogenic activity possibly triggered by climatic perturbation, e.g. aridity, around 4,000 yrs cal BP. Subsequently, we detect a reinvigoration of human impact after 3,670 yrs cal BP. From around 2,500 yrs cal BP until 1,170 yrs cal BP pollen indicate intensive land-use while fecal stanol and PAH concentrations are low, which could be explained by either ecosystem changes and/or settlement relocation/-organization. Forestry and/or agriculture most likely continued to be practiced inside the lake catchment accounting for increased erosion. Increased human activity during the Middle Ages and the Modern Era, with a relative high around 780 yrs cal BP and a relative low around 640 yrs cal BP, may have been linked to hydrological rather than to temperature variations during the Medieval Warm Period and the Little Ice Age since temperature variations are small during the last millennium. Overall, the observed pattern suggests a relationship between increased human activity and phases of humidity, i.e., high lake levels, at Lake Dojran.

5. Holocene hydrological and atmospheric changes in East Africa inferred from lipid biomarker and leaf wax *n*-alkane δD of Lake Dendi (Ethiopia) sediments

Tropical Africa and the Sahara region experienced extreme hydrological variations over the course of the Holocene with a prolonged period of strongly increased humidity controlled by the last precessional cycle (Tierney et al., 2010b; Berke et al., 2012; Foerster et al., 2012; Tierney and deMenocal, 2013; Junginger et al., 2014; Liu et al., 2017). The ca. six-fold increase in precipitation (Tierney et al., 2017) between 15 ka and 5 ka, known as the African Humid Period (AHP) (deMenocal et al., 2000), transformed the Saharan desert into an open grass savannah indicated by pollen data and climate simulations (Lézine et al., 1990; Claussen and Gayler, 1997; Kröpelin et al., 2008). Even in the present day hyper-arid core of the Sahara numerous lakes were present (COHMAP-Members, 1988; Tierney et al., 2011b).

While the causes of the AHP are widely understood, spatial and temporal patterns are still highly debated (deMenocal et al., 2000; Kröpelin et al., 2008; Shanahan et al., 2015; Tierney et al., 2017). Uncertainties in the reconstructions arise from the complex nature of the North and East African climate, which is controlled by the strength and interactions of different monsoonal systems (Weldeab et al., 2014), sea surface temperatures of the Atlantic and the Indian Ocean, and resulting shifts in the Intertropical Convergence Zone (ITCZ) and the Congo Air Boundary (CAB) (Tierney et al., 2011b; Tierney and de Menocal, 2013; Costa et al., 2014; Junginger et al., 2014; Castañeda et al., 2016). Therefore, changes in the location of the ITCZ and the CAB may affect the sedimentary archives differently depending on their location (Fig. 19). Further complications arise from the dynamics in Indian Ocean sea surface temperatures connected to the Indian Ocean dipole (IOD) or the El Nino-Southern Oscillation (ENSO) (Tierney and deMenocal, 2013), land surface feedbacks, the nonlinear behavior and different sensitivity of certain paleoclimate proxies (Castañeda et al., 2016). In addition, centennial- to millennial-scale climatic changes such as the Younger Dryas and the 8.2 ka event further complicate the interpretation of onset and termination of the AHP (Garcin et al., 2006; Revel et al., 2010; Costa et al., 2014).

Due to the location in proximity of the ITCZ and the CAB, paleoclimatic records from the central Ethiopian plateau in Northeast Africa can provide new insights into past shifts in the two major wind regimes in East Africa. The CAB reaches the plateau during northern hemispheric summer (July-August), delivering great amounts of moisture from the Atlantic Ocean. During the rest of the year, the Ethiopian plateau is dominated by precipitation originating from the Indian Ocean and transported via the ITCZ (Mitchell and Jones, 2005; Degefu and Schagerl, 2015; Wagner et al., in review). In this study, we analyze stable carbon and hydrogen isotopes of plant leaf wax *n*-alkanes in a sediment core from Lake Dendi covering a period of ~12,000 years. This allows us to reconstruct past hydrological and vegetation changes and thereby to identify major changes in moisture sources from the Indian Ocean (via the ITCZ) and the Atlantic Ocean (via CAB) to the Ethiopian highlands over the course of the AHP. In addition, we present Holocene temperature reconstructions based on the MBT/CBT proxy.

5.1 Site description

Lake Dendi is situated at 8° 50’ N; 38° 02’ E on the Ethiopian Plateau about 80 km to the west of Addis Ababa (Ethiopia; Fig. 19). The lake comprises two basins of ~2 km diameter connected via a shallow sill and has a maximum water depth of 60 m (Wagner et al., in review). Lake Dendi lies 2,836 meters above sea level (m a.s.l.) inside an 8 km wide caldera of the dormant volcano Mount Dendi. The crater rim rises to a maximum elevation of ~3,270 m a.s.l. Maximum water depth of Lake Dendi amounts to 60 m (Wagner et al., in review). The lake is oligotrophic and the water temperature ranges between 15°C and 17°C (Degefu et al., 2014). Lake Dendi has no permanent in- and outflow but is fed by rivers and streams during the rainy season, thereby charging rivers like the Huluka River in lower valley regions (Prabu et al., 2010). The Lake catchment can be associated with the Lower Dega region which is characterized by a sub-humid climate with mean temperatures of 15°C to 16°C during the winter months, the highest mean temperatures being around 18°C during March to May, and 16°C to 17°C from June to October. Annual rainfall of the Dendi region averages ~1,200 mm (Mitchell and Jones, 2005; Degefu et al., 2014). Three hydrological seasons result from the shifting positions of the ITCZ and CAB over the course of the year. As a result, the Dendi catchment experiences a main rainy season from May/June to September when the ITCZ reaches its northernmost position (Fig. 19). During July and August the Congo Air Boundary (CAB) reaches the area, bringing great amounts of moisture from the Atlantic Ocean. A relatively dry season between October and February is characterized by predominant northeasterly winds. February/March to May exhibit a spring rainy season when easterly and southeasterly winds from the Indian Ocean prevail (Wagner et al., in review). Lake Dendi can be assigned to the Afromontane forest region (Heslop-Harrison, 2011). The natural vegetation in the catchment of the lake is most likely a mixture of open forest with dominant conifers, African juniper trees, and African redwood, interspersed with high-mountain steppes, mosses and lichens

(Williams et al., 2004; Fritzsche et al., 2007), which today is largely replaced by a landscape characterized by cleared trees and intensive agricultural activity (Wagner et al., in review).

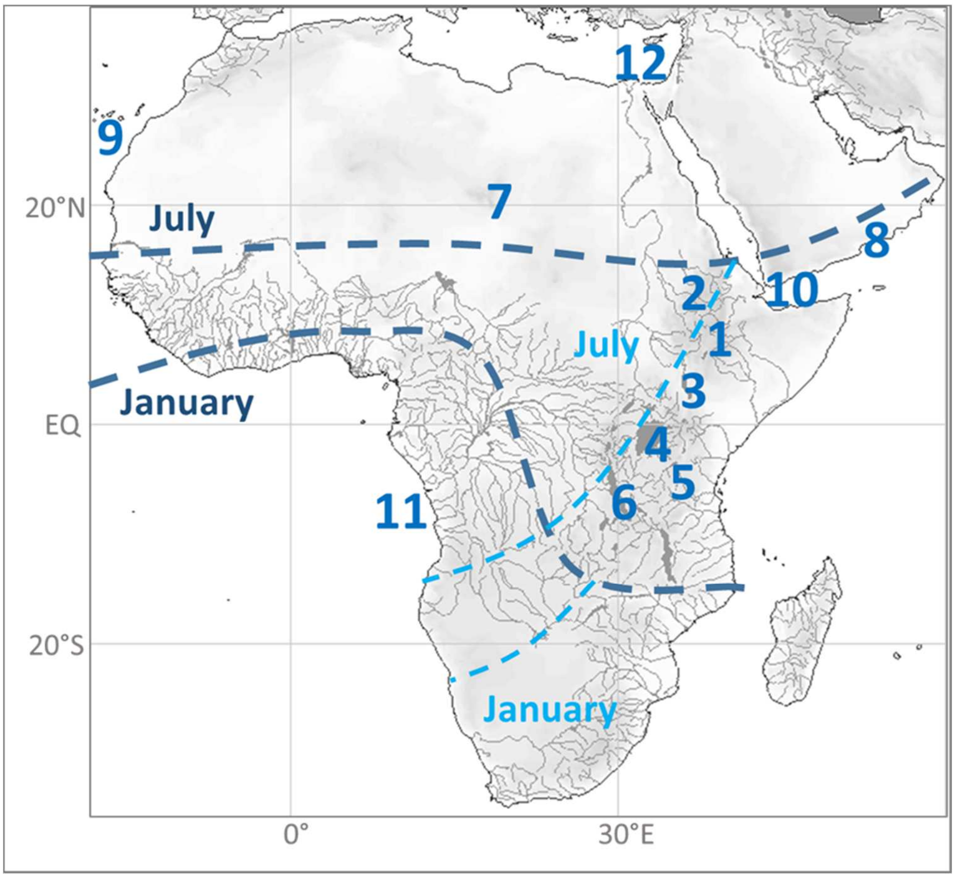

Figure 19. Schematic modern positions of the ITCZ (dark blue) and the CAB (light blue) over Africa during NH summer and winter. Also shown are paleorecords including: 1. Lake Dendi (this study); 2. Lake Tana (Costa et al., 2014); 3. Lake Chew Bahir (Foerster et al., 2012); 4. Lake Victoria (Berke et al., 2012); 5. Lake Challa (Tierney et al., 2011a); 6. Lake Tanganyika (Tierney et al., 2008; 2010b); 7. Lake Yoa (Kröpelin et al., 2008); 8. Qunf cave (Fleitmann et al., 2007); 9. Northwest African margin (deMenocal et al., 2000; Tierney et al., 2017); 10 Gulf of Aden (Tierney and deMenocal, 2013); 11 Congo River outflow (Schefuß et al., 2005); 12 Nile river fan (Castañeda et al., 2016).

5.2 Material and Methods

The Lake Dendi sediment cores DEN1 (08°50.178’N, 38°00.974’E) and DEN2 (08°50.153’N, 38°01.075’E) were obtained in March and April 2012 from the eastern twin-lake from a water depth of 50 m and 54 m, respectively (Wagner et al., in review). The cores were correlated based on optical and XRF analyses. Age-depth modelling was conducted using 24 radiocarbon (^{14}C) ages (Wagner et al., in review). The molecular analyses for this study were performed on 57 freeze-dried and ground samples with a resolution of ~200 yrs. Samples were 2 x ultrasonically extracted using 25ml mixtures of DCM:MeOH (9:1, v:v) and DCM:MeOH (1:1, v:v) respectively. The lipid extracts were saponified and further separated into polarity fractions using SiO_2 column chromatography using the method of Höfle et al. (2013). The aliphatic hydrocarbons were separated into saturated and unsaturated hydrocarbon fractions using $AgNO_3$-impregnated silica gel. The polar fractions, containing the tetraether lipids, were dissolved in HEX:IPA (95:5, v:v) and filtered through 0.45 µm PTFE syringe filters. *n*-Alkanes were analyzed on an Agilent 7890 series II GC-FID following the method described by Höfle et al. (2013) and quantified against authentic external standards including normalization to total organic carbon (TOC) content. GDGTs were analyzed using an Agilent 1290 UHPLC coupled to an Agilent 6460 QQQ equipped with an APCI ion source operated in SIM mode according to Schouten et al. (2007). MBT/CBT values were calibrated to annual mean air temperature (MAT) using the East African Lake calibration of Tierney et al. (2010a). Stable isotopes ($\delta^{13}C$ and δD) were measured of the most abundant *n*-alkane compounds (C_{29}, C_{31}). $\delta^{13}C$ were measured on a Thermo Trace GC coupled to a Finnigan MAT 252 isotope-ratio monitoring-mass spectrometer (irm-MS) via a modified Finnigan GC/C III combustion interface operated at 1000 °C. δD compositions were measured with a Thermo Trace GC coupled to a Thermo Fischer Scientific MAT 253 irm-MS via a pyrolysis reactor operated at 1420 °C. Methods were following Häggi et al. (2016). The isotope values were measured at least twice against calibrated reference gas using H_2 for δD and CO_2 for $\delta^{13}C$ and are reported in ‰ versus VSMOW and VPDB, respectively. The long-term precision monitored by external standard analyses is 0.3‰ for $\delta^{13}C$ and 2.8‰ for δD.

5.3 Results

5.3.1 Plant wax *n*-alkanes

The *n*-alkane distribution in all sediment samples shows a strong odd over even predominance with highest abundances of the C_{29} and C_{31} *n*-alkanes. The sum of the high molecular weight (HMW) *n*-alkanes, including C_{27}-C_{33}, varies between 47 µg/gr TOC and 263 µg/gr TOC, showing the highest fluctuations in the Early Holocene after 5,200 yrs cal BP (Tab. 7). The CPI values of the HMW *n*-alkanes generally amount to over 5, indicating no major contribution from fossil sources (Grice et al., 1968) that might bias compound specific δD and $\delta^{13}C$ values. Average chain length (ACL) values of the HMW *n*-alkanes (C_{27}-C_{33}) range between 29.3 and 30.5 (Fig. 24, Tab. 7) with highest values (as high as 30.4 at 650 yrs cal BP) in the older and the younger part of the record. The middle part of the record between about 7,200 yrs cal BP and 3,400 yrs cal BP is characterized by intermediate to low values (as low as 29.3 at 5,210 yrs cal BP). ACL values show a moderate correlation (r^2 = 0.5) with the *n*-alkane $\delta^{13}C$ isotopic values ($\Delta\ ^{13}C_{31}$-$^{13}C_{29}$) (Fig. 24, Tab. 7).

5.3.2 Plant wax *n*-alkane hydrogen isotopes

δD values of the most abundant C_{29} and C_{31} *n*-alkanes (δD_{wax}) show a strong correlation (r^2=0.9) and exhibit a wide range of almost 50‰, which is comparable to the record of Lake Tana (~60‰) (Costa et al., 2014), situated ~300 km to the northwest (Fig. 19, Fig. 21, Tab. 7). In comparison to other plant wax δD records from East Africa (Tierney et al., 2010b; Tierney et al., 2011b; Berke et al., 2012; Tierney and deMenocal, 2013), we observe relatively D-depleted values ranging between -130.1‰ and -178.8‰ (C_{29}) and between 131.7‰ and 178.9‰ (C_{31}) (Fig. 21, Tab. 7). The Late Glacial is characterized by relatively positive δD values (between -131.2‰ and -142‰) of the C_{29} and C_{31} *n*-alkanes. Two rapid decreases of about -20‰ at 11,700 yrs cal BP and 10,000 yrs cal BP, respectively, are followed by a brief plateau phase of about 2,000 yrs with δD_{wax} values around -175‰. Subsequently, starting at ~8,000 yrs cal BP δD_{wax} values exhibit a long-term gradual increase to ca -130‰ at about 2,000 yrs cal BP. δD_{wax} values then gradually decrease of about -10‰ to the present, with some distinct fluctuations.

5.3.3 Plant wax *n*-alkane carbon isotopes

$\delta^{13}C$ values of the HMW *n*-alkanes range between -26.8‰ and -21.6‰ (C_{29}) and between -28.8‰ and 25.6‰ (C_{31}) (Fig. 24, Tab. 7). $\delta^{13}C_{29}$ values generally show little variation but slightly ^{13}C-enriched values are observed during the Early Holocene until about 8,000 cal yrs cal BP and during the Late Holocene starting at about 2,000 yrs cal BP. $\delta^{13}C_{31}$ values are generally more ^{13}C enriched, especially from 9,000 yrs cal BP to 8,000 yrs cal BP and from 6,500 yrs cal BP to 5,000 yrs cal BP. This results in an isotopic spread between C_{29} and C_{31}, which shows a gradually increasing trend from the late glacial until 5,500 yrs cal BP, followed by a gradual decreasing trend until the present (Fig. 24). For an estimation of the major vegetation types, we applied a combined weighted two endmember mixing model assuming endmember values for C_3 and C_4 vegetation of -34.7‰ and -21.4‰ for C_{29} and -35.2‰ and -21.7‰ for C_{31} according to Berke et al. (2012) and Castañeda et al. (2009). The resulting percentages of C_3 and C_4 plants for C_{29} and C_{31} were weighted according to the specific compound concentrations (Fig. 24, Tab. 7). Uncertainties in the endmember values, however, may lead to an error in the percentage of C_4 vegetation of up to 20% (Castañeda et al., 2009).

5.3.4 GDGT-based indices

The BIT index varies in a wide range of 0.21 and 1 (Fig. 24, Tab. 7). In the older part of the record (~8,200 yrs cal BP), the BIT index shows relatively low values between 0.21 and 0.63, mainly driven by high abundances of the aquatic endmember Crenarchaeol (Fig.20). After 8,200 yrs cal BP, the BIT index rises abruptly to values as high as 1 between 7,800 yrs cal BP and 7,400 yrs cal BP, caused by an abrupt decline in Crenarchaeol concentrations. The strongly fluctuating concentrations of both Crenarchaeol and brGDGTs stabilize on a lower level after 7,400 yrs cal BP, complicating the interpretation of the BIT values before 7,400 yrs cal BP (Fig. 20). Therefore, as suggested by Fietz et al. (2011), the concentrations of brGDGTs could be a more reliable proxy for terrestrial input into Lake Dendi before 7,400 yrs cal BP than the BIT index. Furthermore, the high ratios of GDGT-2/crenarchaeol (>2) might indicate the presence of a sulfate-methane transition zone (SMTZ; Weijers et al., 2011). After 7,400 yrs cal BP, BIT values decline until 5,200 yrs cal BP to as low as 0.5, then rise again until 4,200 yrs cal BP (0.7) and then decline until 650 yrs cal BP. The core top (230 yrs cal BP) again shows a higher BIT value of 0.62. The high BIT values (BIT > 0.3) throughout most part of the record indicate substantial terrestrial input of soil OM and thus preclude the use of the TEX_{86} proxy as a reliable paleothermometer (Weijers et al., 2006). Therefore, we use temperature estimates based on the methylation and cyclisation indices of branched tetraethers (MBT/CBT; Weijers et al., 2007b). Applying the East-African lake calibration of Tierney et al. (2010a), MAT estimates range between 17.9°C (at 9,400 yrs cal BP) and 15.1 °C (8,600 yrs cal BP; Fig. 23, Tab. 7). Our core-top value of 15.7 °C is close to the measured instrumental values from the Dendi region (Degefu and Schagerl, 2015). MATs show strong fluctuations of about 2.8°C in the older part of the record until ~7,800 yrs cal BP (15.2 °C). Temperatures then gradually increase to 17.2 °C at 1,400 yrs cal BP followed by stronger fluctuations in the uppermost core interval.

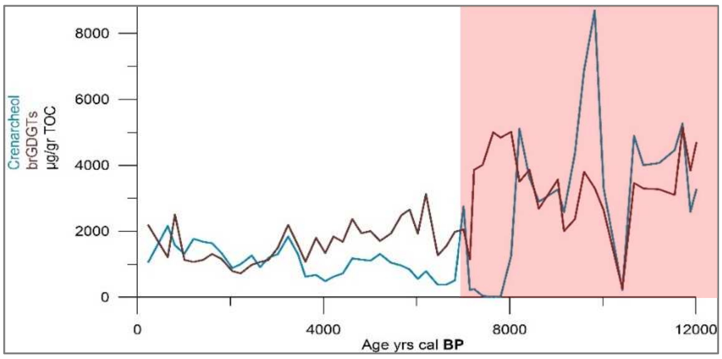

Figure 20. Concentrations of Crenarchaeol (blue line) and brGDGTs (brown line) in Lake Dendi sediment cores DEN1 and DEN2. Red shading marks strongly fluctuating Crenarchaeol concentrations.

Table 7. Biomarker-based indices, temperatures, and stable carbon and hydrogen isotopic data of Lake Dendi sediment cores DEN1 and DEN2.

[a] Age (yrs cal BP)	[b] BIT	[c] MAT (°C)	[d] HMW *n*-alkane ACL	δD_{C29} (‰ versus VSMOW)	δD_{C31}	$\delta^{13}C_{29}$ (‰ versus PDB)	$\delta^{13}C_{31}$	C_4 weighted (%)
240	0.62	15.7	30.2	-135.6	-141.2	-26.5	-24.6	71.3
650	0.31	16.7	30.4	-137.7	-143.3	-27.2	-25.9	63.9
810	0.33	16.2	30.3	-135.4	-143.0	-27.7	-26.3	60.6
1010	0.40	15.8	30.3	-133.0	-138.4	-28.2	-26.5	58.9
1210	0.32	16.6	30.4	-139.6	-146.4	-27.1	-25.4	66.2
1410	0.35	17.2	30.2	-139.0	-146.8	-27.3	-25.1	66.0
1600	0.38	17.2	30.3	-136.7	-143.9	-26.9	-25.3	67.5
1810	0.40	16.8	30.2	-132.8	-138.2	-27.3	-25.3	65.4
2040	0.41	16.8	29.8	-130.1	-131.7	-28.4	-25.4	58.5
2220	0.36	16.8	29.9	-	-	-	-	-
2450	0.38	16.8	30.1	-131.7	-136.5	-28.2	-25.3	61.3
2640	0.47	17.0	29.7	-	-	-	-	-
2810	0.43	16.6	29.8	-132.9	-134.6	-27.8	-25.2	62.5
3020	0.47	16.6	30.0	-134.7	-136.1	-27.9	-25.2	62.1
3240	0.48	17.0	29.7	-139.3	-139.5	-27.2	-24.4	68.5
3450	0.48	16.3	29.5	-141.2	-138.3	-27.8	-24.1	65.2
3610	0.57	16.9	29.5	-139.7	-135.0	-28.1	-24.9	60.9
3840	0.67	16.3	29.4	-138.8	-137.0	-28.3	-24.8	60.8
4040	0.68	16.6	29.4	-142.7	-140.1	-28.2	-25.1	59.7
4210	0.70	16.1	29.5	-140.9	-140.6	-28.2	-24.7	60.5
4410	0.64	16.4	29.5	-140.9	-140.6	-28.5	-25.0	58.4
4620	0.61	15.9	29.6	-146.6	-145.3	-28.1	-24.6	62.5
4810	0.57	16.3	29.6	-145.4	-145.9	-28.0	-24.3	63.7
5010	0.59	16.0	29.5	-148.2	-149.6	-27.8	-23.2	66.4
5210	0.50	16.1	29.3	-148.3	-152.4	-27.7	-23.9	67.1
5450	0.59	15.8	29.6	-148.6	-151.4	-27.7	-23.0	70.4
5670	0.67	16.1	29.5	-149.6	-152.8	-27.5	-23.2	70.2
5850	0.71	15.9	29.7	-155.2	-159.5	-27.7	-23.2	69.7
6030	0.73	15.9	29.5	-152.5	-156.7	-27.6	-23.1	70.8
6200	0.76	16.3	29.7	-154.0	-157.9	-27.5	-23.5	70.1
6450	0.73	16.4	29.8	-161.2	-166.1	-27.6	-23.2	71.6
6640	0.76	16.5	29.6	-157.5	-160.0	-27.7	-24.3	65.2
6820	0.75	16.2	29.5	-162.3	-166.9	-27.9	-24.4	64.8
7150	0.81	16.1	29.3	-	-	-	-	-
7240	0.92	15.9	29.5	-162.8	-164.1	-27.7	-24.8	64.0
7430	0.99	16.3	29.7	-167.8	-171.9	-27.6	-24.6	64.6
7650	1.00	15.6	29.8	-165.3	-169.8	-27.6	-24.4	66.1
7810	0.99	15.2	29.8	-168.1	-173.6	-27.2	-23.5	70.6
8040	0.76	16.1	29.9	-173.6	-179.2	-26.4	-22.1	79.4

[a] Age (yrs cal BP)	[b] BIT	[c] MAT (°C)	[d] HMW *n*-alkane ACL	δD_{C29} (‰ versus VSMOW)	δD_{C31}	$\delta^{13}C_{29}$ (‰ versus PDB)	$\delta^{13}C_{31}$	C_4 weighted (%)
8220	0.34	15.9	30.0	-169.5	-181.1	-25.8	-21.6	84.3
8430	0.45	15.8	29.8	-	-	-	-	-
8630	0.43	15.1	30.1	-168.4	-175.8	-26.7	-24.2	71.4
8840	0.63	15.6	29.6	-	-	-	-	-
9040	0.45	16.8	29.6	-178.8	-178.9	-26.8	-22.8	75.4
9170	0.37	17.6	29.8	-168.4	-177.9	-27.6	-25.6	60.3
9410	0.29	17.9	29.9	-170.7	-178.1	-26.8	-24.4	69.9
9600	0.30	17.1	30.1	-175.1	-178.2	-26.9	-24.6	69.1
9830	0.21	17.4	30.1	-176.5	-179.7	-26.3	-24.4	72.8
10020	0.37	16.8	29.8	-152.8	-156.6	-27.8	-26.8	57.3
10420	0.48	15.7	29.8	-	-	-	-	-
10680	0.34	17.8	29.8	-161.0	-163.1	-26.0	-24.5	72.5
10880	0.38	16.5	30.1	-161.4	-164.9	-25.6	-24.8	72.9
11210	0.37	16.1	30.0	-160.0	-162.8	-25.7	-25.5	70.1
11550	0.36	15.6	30.4	-154.0	-160.9	-25.6	-24.0	77.6
11720	0.42	17.2	30.5	-133.6	-142.0	-26.1	-24.5	74.1
11890	0.53	15.7	30.3	-132.7	-141.9	-26.4	-24.9	71.4
12010	0.52	15.9	30.4	-131.9	-140.5	-26.4	-24.8	71.8

[a] According to Wagner et al. (in review)
[b] According to Hopmans et al. (2004)
[c] According to Tierney et al. (2010a)
[d] $(C_{27}*27+C_{29}*29+C_{31}*31+C_{33}*33) / (C_{27}+C_{29}+C_{31}+C_{33})$

5.4 Discussion

5.4.1 Hydrological source signatures

Compound specific δD analyses of plant leaf waxes from Africa have been frequently used to reconstruct past changes in the hydrological cycle (Schefuß et al., 2005; Tierney and deMenocal, 2013; Castañeda et al., 2016; Tierney et al., 2017). In tropical regions with only minor temperature variations, the most prominent factor influencing δD values is the amount effect (Bowen, 2008; Sachse et al., 2012). Apart from precipitation amounts, shifting wind regimes and associated variations in moisture sources have a strong control on δD values in East Africa (Costa et al., 2014; Castañeda et al., 2016). At Lake Dendi, the main modern sources of precipitation are the Indian and Atlantic Ocean via the ITCZ and the CAB, respectively. The Atlantic Ocean moisture is being recycled through the West African Congo Basin before arriving in East Africa (Schefuß et al., 2003), resulting in unusually low δD values of precipitation (e.g. Levin et al., 2009). During July and

August, when the CAB reaches the Dendi area, isotopic precipitation data from Addis Ababa (IAEA/WMO, 2016) shows relatively D-depleted values, suggesting a D-depletion of moisture originating from the Atlantic ocean/Congo Basin compared to Indian Ocean derived moisture. This isotopic source effect could amount up to about -15‰ D-depletion (Tierney et al., 2011b; Costa et al., 2014). In addition, a modeling study by Herold and Lohmann (2009) suggests that stronger moisture advection from the Atlantic resulted in isotopically depleted rainfall in East Africa during the Eemian with strong analogues to present day conditions. Thus, relative changes in moisture sources (Indian Ocean vs Atlantic Ocean/Congo Basin) could also exhibit a strong impact on the δD_{wax} signature at Lake Dendi.

The $\delta^{13}C$ inferred vegetational changes (Fig. 22, Tab. 7) do not significantly bias Lake Dendi δD_{wax} values: Assuming endmembers for C_{29} of 34.7‰ (35.2‰ for C_{31}) for C_3 vegetation and 21.4‰ (21.7‰ for C_{31}) for C_4 vegetation, respectively (Castañeda et al., 2009; Berke et al., 2012), the vegetational changes at Lake Dendi mirrored by changes in $\delta^{13}C$ of 3.2‰ (C_{29}) and 5.2‰ (C_{31}) can account for only -5‰ or -8‰ variation in δD. Furthermore, recent results from the region have shown that fractionation differences of δD between C_3 trees and C_4 grasses may in fact be small, or even negligible (Tierney et al., 2010b).

MBT/CBT inferred temperature changes during the Holocene are rather small (~3°C; Fig. 21, Tab. 7), implying only a minor influence of the temperature effect (Dansgaard, 1964) on the δD_{wax} records. Compared to other East-African records, Lake Dendi exhibits strongly D-depleted values, most probably as a result of its high altitude position (~2,800 m) in the Ethiopian highlands, if assuming a D-depletion of about -1 to -4 ‰ per 100 m (Holdsworth et al., 1991; Rozanski et al., 1993). The large amplitude of δD_{wax} values observed at Lake Dendi (~50‰; Fig. 21, Tab. 7) points to significant changes in the amount of precipitation but also to a changing influence of the CAB, similar to Lake Tana (~60‰) (Costa et al., 2014).

5.4.2 Younger Dryas and Early Holocene - Peak AHP

Strongly D-enriched δD_{wax} values during the Younger Dryas period until 11,700 yrs cal BP coincide with an interruption of the AHP and dry conditions at many Northeast and East African sites (Tierney et al., 2011b; Foerster et al., 2012; Junginger et al., 2014). Relatively dry conditions at Lake Dendi during the YD are also suggested by XRF derived elemental distributions obtained by Wagner et al. (in review). The dry conditions in East Africa were most likely a result of a southwards positioned ITCZ, weakened monsoonal systems, and decreased moisture exchange between oceans and land (Talbot et al., 2007).

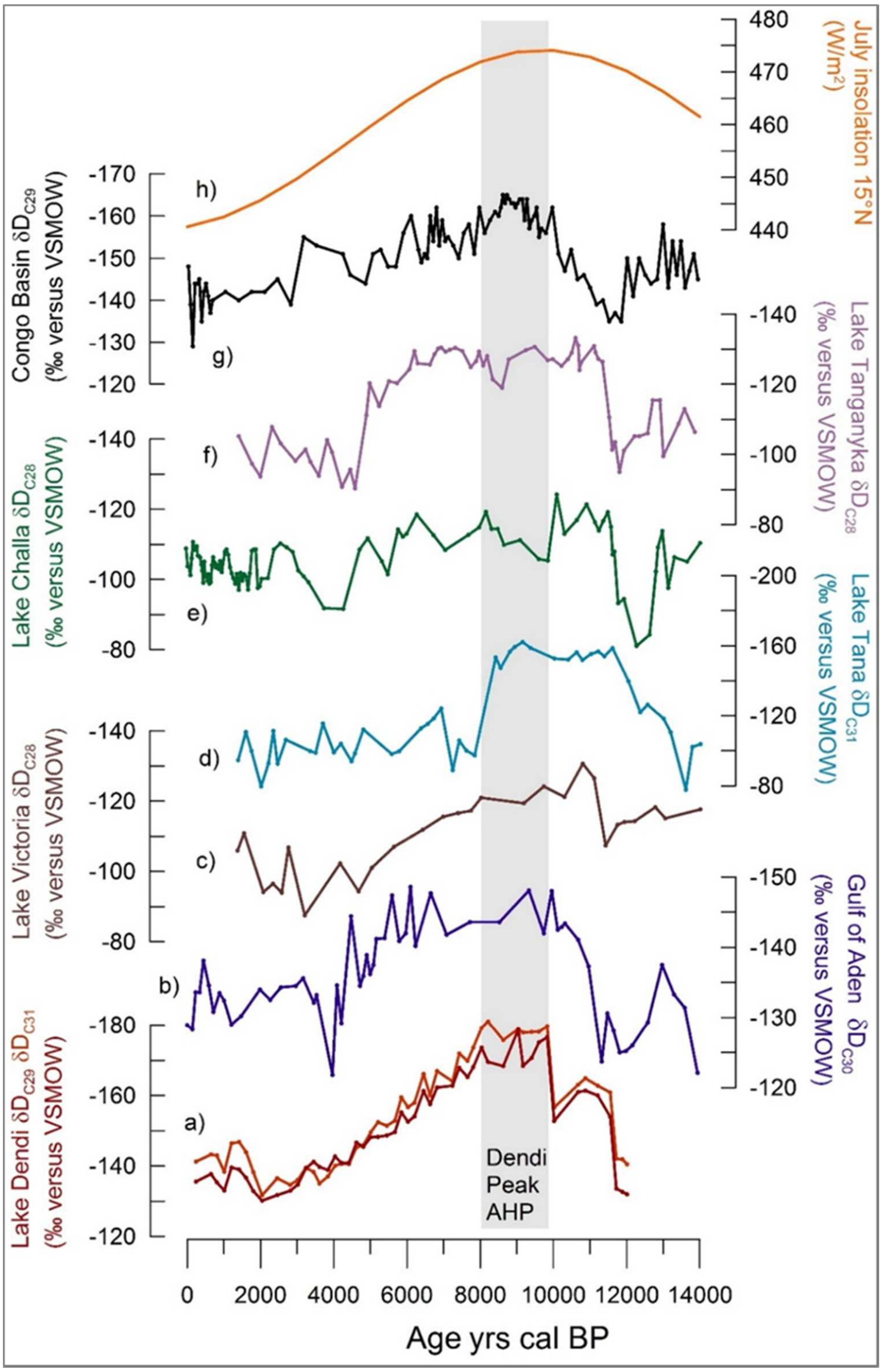

Figure 21. Comparison of African plant leaf wax δD records including: a) Lake Dendi, b) Gulf of Aden (Tierney and deMenocal, 2013), c) Lake Victoria (Berke et al., 2012), d) Lake Tana (Costa et al., 2014), e) Lake Challa (Tierny et al., 2011b), f) Lake Tanganyka (Tierny et al., 2010b), g) Congo Basin (Schefuß et al., 2005). Also shown is h) the mean July insolation at 15°N after Berger and Loutre (1991).

At Lake Dendi, the transition out of the YD period is characterized by a large change in δD of about -40‰ that points to an increase in rainfall due to a re-strengthening of the Indian Ocean atmospheric circulation (Tierney et al., 2010b) but also to an eastwards shift of the CAB and an associated increase in moisture during NH summer from the Congo Basin. The return to full humid AHP conditions at Lake Dendi occurred in two rapid steps (~-20‰), visible from the δD_{wax} record, with the first step between 11,700 yrs cal BP and 11,550 yrs cal BP and the second between 10,000 yrs cal BP and 9,800 yrs cal BP, paralleling the re-strengthening of the monsoonal systems (Fig. 22).

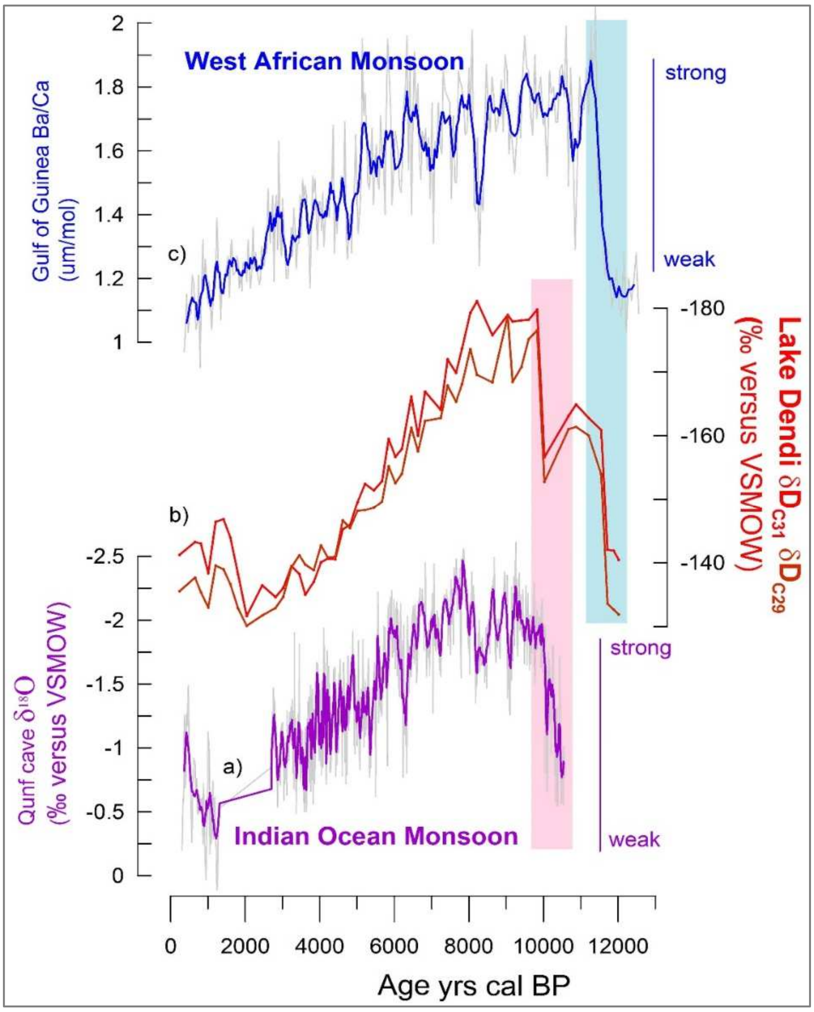

Figure 22. Comparison of b) Lake Dendi plant leaf wax δD data and pace of the a) Indian Ocean Monsoon (Fleitmann et al., 2003) and c) West African Monsoon (Weldeab et al., 2007).

The first step occurred immediately after the YD and simultaneous to the return to peak AHP conditions at Lake Chala (Tierney et al., 2011b) and Tanganyka (Tierney et al., 2010b), that are both dominated by Indian Ocean Moisture. It further coincides with a strong increase in Ba/Ca rations from the Gulf of Guinea, indicating a re-strengthening of the West-African Monsoon (Weldeab et al., 2007) and an associated northward migration of the ITCZ. The second step parallels a rapid decrease in $\delta^{18}O$ values from Qunf cave (Oman), mirroring the onset of the Indian Ocean Monsoon (Fleitmann et al., 2003). The strengthening of the Indian Ocean Monsoon corresponds to an enhanced west–east pressure gradient near the equator (Camberlin, 1997; Junginger et al., 2014) that also leads to advection of moisture from the Congo Basin (shift of the CAB) eastwards to the western part of East Africa (Levin et al., 2009; Kebede and Travi, 2012). The second D-depletion step might therefore mark the advent of the CAB on the Ethiopian Plateau and an increase in D-depleted moisture from the Atlantic/Congo Basin. This also suggests that the isotopic source effect of the CAB cannot be larger than ~-23‰ in δD, without considering any additional D-depletion through the amount effect. Implying a maximum source effect of -14‰ in δD for 100% Congo derived moisture (Costa et al., 2014), the increase in precipitation due to the shift of the CAB must be equal to an amount effect of -9‰. Despite the suggested precipitation increase inferred from δD_{wax}, the BIT index shows relatively low values (0.21 - 0.63) during the Early Holocene (Fig. 24, Tab. 7). However, the high concentrations of Crenarchaeol (relative to brGDGT concentrations), which might be the result of high nutrient input or an increased lake level, strongly bias the BIT values during this phase (Fig. 20). Indeed, the overall high concentrations of brGDGTs during the peak AHP phase point to strong terrestrial input/runoff (Fig. 20). Furthermore, $\delta^{13}C_{31}$ values of up to -21.6‰ indicate an enhanced proportion of C_4 vegetation during the most humid interval. $\delta^{13}C_{29}$ values are slightly more depleted than $\delta^{13}C_{31}$ (~2‰), but also show the most ^{13}C-enriched values during the Early Holocene (Fig. 24, Tab. 7). Vegetational changes at 10,000 yrs cal BP, pointing to a higher percentage of C_3 vegetation, were most likely initiated by a volcanic eruption of the Wenchi crater 12 km to the west of Lake Dendi (Wager et al., in review) and thus do not necessarily carry a climatic signal.

At about 8,600 yrs cal BP we observe a depletion in the $\delta^{13}C_{31}$ record (to -24.2‰) and a slight D-enrichment (~10‰ in C_{29} and ~3‰ in C_{31}), that could be related to a widespread aridity event in tropical and subtropical Africa around 8.5 ka (Gillespie et al., 1983; Gasse, 2000; Jung et al., 2004; Tierney et al., 2011a) and may be linked to the 8.2 ka event observed in other sites (Alley and Ágústsdóttir, 2005). A lake-level low stand and decreasing precipitation between 8.7 and 8.2 cal kyr BP are also suggested by Junginger et al. (2014) for paleo-Lake Suguta in the East African rift. The observed short-term vegetational changes at Lake Dendi (decreased C_4 percentage) and the slight aridification visible from the δD record can be supported by findings of Wagner et al. (in review). The authors report increased terrigenous input around 8.5 ka at Lake Dendi, which is linked to a reduction in vegetation cover.

5.4.3 Middle Holocene - Transition out of the AHP

Starting at about 8,200 yrs cal BP the δD_{wax} records show a gradual long-term increasing aridity trend until ~2,000 yrs cal BP of about +50‰ in accordance to gradually decreasing NH summer insolation (Fig. 21) (Berger and Loutre, 1991) and decreasing strength of the West African Monsoon (Weldeab et al., 2007), Indian Ocean Monsoon (Fleitmann et al., 2003), and the East African Monsoon (Weldeab et al., 2014) (Fig. 22). The BIT index also decreases gradually from about 7,400 yrs cal BP until 650 yrs cal BP, only interrupted by a period of higher values around 4,000 yrs cal BP, indicating a reduction in soil organic matter input (Schouten et al., 2013) most likely due to reduced rainfall runoff over the course of the Middle and Late Holocene. This can be supported by findings from Wagner et al. (in review) who suggest an irregular but rather gradual decline of humidity and rainfall runoff from about 10,000 yrs cal BP until the Late Holocene The MBT/CBT derived annual MAT estimates display a continuously increasing temperature trend from 15.2°C at 7,800 yrs cal BP to 17.2°C at 1,600 yrs cal BP (Fig. 23). The small ΔMAT of 2°C however does not significantly bias the high magnitude of δD values via the temperature effect (Dansgaard, 1964; Majoube, 1971). The general temperature trend at Lake Dendi parallels the trend of the Congo Basin (Weijers et al., 2007c) which might indicate strong atmospheric teleconnections between the regions.

$\delta^{13}C$ values of both the C_{29} and C_{31} *n*-alkanes show more depleted values after 8,200 yrs cal BP indicating a shift towards a higher percentage of C_3 vegetation. This trend, however, is in contrast with other Holocene plant wax $\delta^{13}C$ records from Africa (Tierney et al., 2010b), which mostly show a ^{13}C-enrichment trend and thus a shift towards increased C_4 vegetation during the transition out of the AHP. This discrepancy may result from the high altitude location (~2,800 m) of Lake Dendi in the Ethiopian Highlands. Lake Garba Guracha, situated at a similarly high altitude location in the Bale mountains, (Umer et al., 2007) show a reduction of *Cyperacea/Poacea* (increased C_4) and the establishment of a dry Afromontane forest with *Juniperus/Podocarpus* (C_3 trees) in response to decreased rainfall and humidity during the Mid-Holocene. Thus, assuming similar vegetation types in the Dendi catchment, the decrease in $\delta^{13}C$ and percentage of C_4 vegetation indicate decreasing humidity after ~8,000 yrs cal BP, in agreement with the δD_{wax} records.

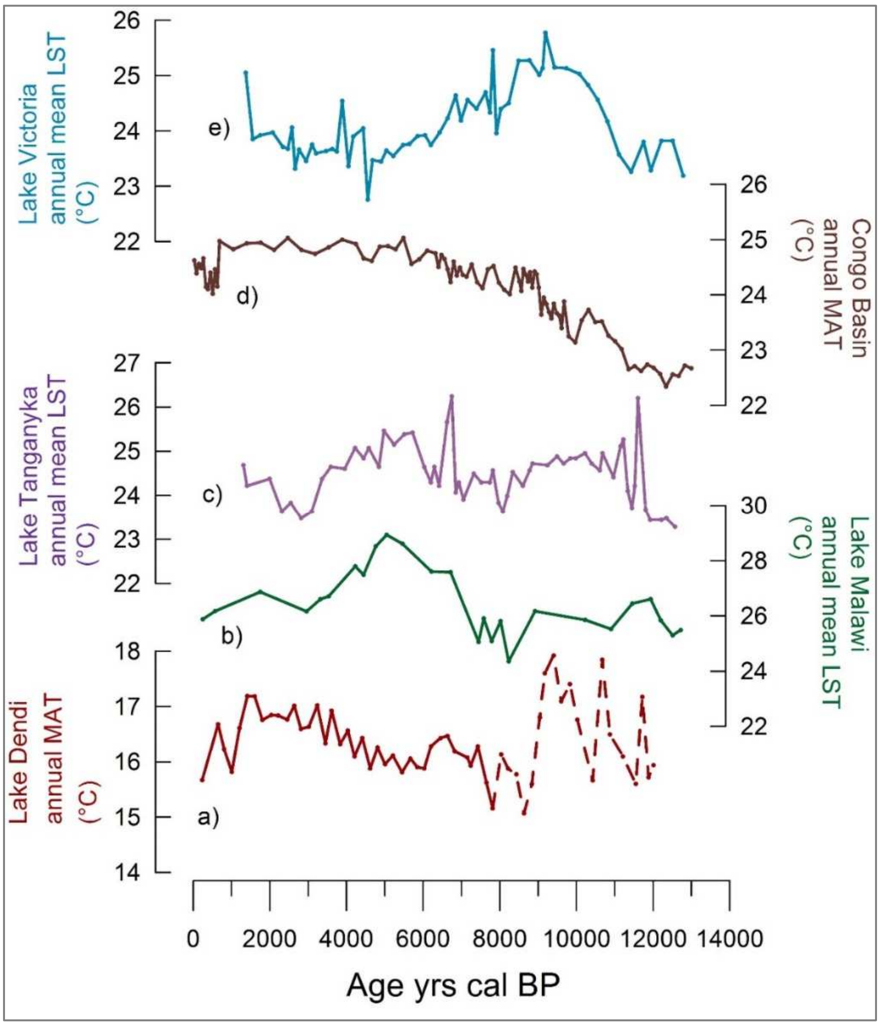

Figure 23. Comparison of African molecular temperature records including: a) Lake Dendi, b) Lake Malawi (Powers et al., 2005), c) Lake Tanganyka (Tierny et al., 2008), d) Congo Basin (Weijers et al., 2007c), e) Lake Victoria (Berke et al., 2012).

$\delta^{13}C_{31}$ values, however, stay relatively enriched until about 5,000 yrs cal BP still indicating a considerable proportion of C_4 vegetation. This vegetation-pattern is also visible in the ACL values, that covariates with the ^{13}C isotopic spread of C_{29} and C_{31} ($r^2 = 0.5$; Fig. 24). Other records from the East African region (Tierney and deMenocal, 2013), that are dominated by Indian Ocean moisture, also indicate relatively wet conditions until ~5 ka BP (Fig. 21). Thus the decrease in moisture after 8,000 yrs cal BP at Lake Dendi must have been only moderate, suggesting that the decreasing δD_{wax} values between 8,000 yrs cal BP and 5,000 yrs cal BP are mainly controlled by a change in moisture sources (less Atlantic Ocean vs. higher Indian Ocean derived moisture) than solely by the amount effect. The decreasing moisture from the Atlantic/Congo Basin could be compensated by increased Indian Ocean derived precipitation, as suggested by Junginger et al. (2014) for lakes from the East-African rift. Junginger (2013; 2014) imply a buffering effect of increased ITCZ related rainfall due to increasing insolation values during September–October after 8,000 yrs cal BP. Indeed, the Dendi region also experienced a Holocene insolation maximum for August-September-October (ASO) around 6,000 yrs cal BP, coinciding with the high percentage of C_4 vegetation indicated by the $\delta^{13}C_{31}$ values (Fig. 24, Table 7).

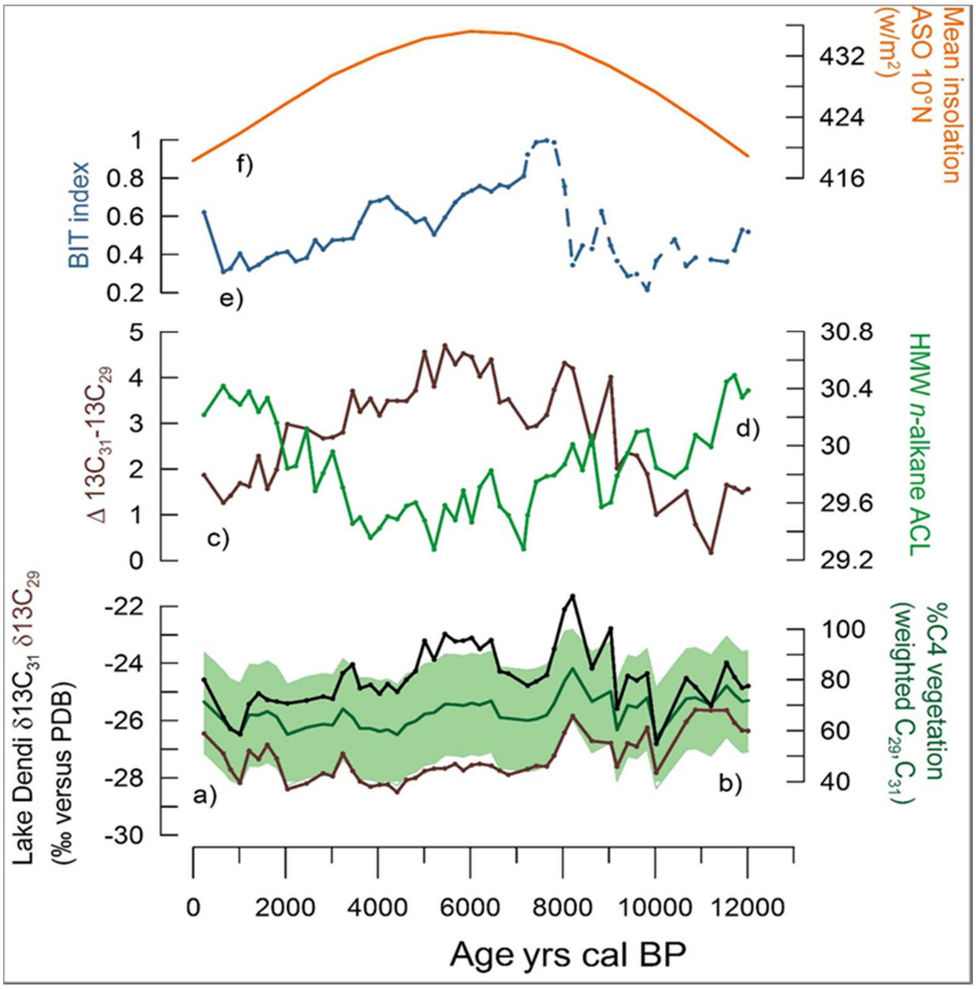

Figure 24. Lake Dendi plant leaf wax a) $\delta^{13}C$, b) $\%C_4$ vegetation estimates, c) $\delta^{13}C_{C29}$-$\delta^{13}C_{C31}$ isotope spread, d) HMW *n*-alkane ACL (C_{27}-C_{33}), e) BIT index. Also shown: f) Mean insolation August-September-October at 10°N after Berger and Loutre (1991).

Other regions, experiencing a more abrupt transition, might in contrast miss suchlike buffering mechanisms. A similar development and timing was also suggested for a geochemical record off Tanzania by Liu et al. (2017), who detected an early phase of the AHP from the beginning of the Holocene to ~8 ka, intensified by additional Atlantic/Congo Basin derived moisture and an eastward position of the CAB. A second, more moderate phase until about 5.5 ka was characterized by a westward shift of the CAB compensated by increased Indian Ocean moisture.

5.4.4 Late Holocene climatic fluctuations and return to wetter conditions

After 2.000 yrs cal BP we observe an overall increasing trend in the δD_{wax} and $\delta^{13}C_{wax}$ values suggesting a return to slightly wetter conditions (Fig. 21; 24). This is in agreement with findings by Wagner et al. (in review), who suggest an increasing but highly fluctuating terrestrial runoff during the last 1.500 yrs cal BP. Furthermore, our MAT estimates show a cooling of ~1.5°C until the present. This overall climatic rebound might be connected to a higher influence of precipitation from the Atlantic/Congo Basin as due to a re-strengthening of the Indian Ocean Monsoon after 1.400 yrs cal BP (Fleitmann et al., 2003). The high fluctuations in runoff reported for Lake Dendi (Wagner et al., in review) are also visible in fluctuations in our biomarker records. These might be related to natural short-term climatic/environmental changes during the last millennium including the Medieval Warm Period (MWP) and the Little Ice Age (LIA). Thus, low δD_{wax} and $\delta^{13}C_{wax}$ values, indicating a decrease in rainfall and in the percentage of C_3 vegetation, coincide with the MWP in Ethiopia around 1.000 yrs, which is frequently associated with a more arid climate, i.e. in central Kenya at Lake Naivasha (Verschuren et al., 2000), or at Lake Bogoria (De Cort et al., 2013). However, Darbyshire et al. (2003) suggested widespread anthropogenic induced environmental change starting at about 500 BC in the northern Ethiopian highlands. Moreover, Umer et al. (2007) detected first anthropogenic activity in the Bale Mountains at about 2,000 cal yrs cal BP, complicating the interpretation of the proxy records during the last two millennia.

5.5 Summary and Conclusions

Based on our plant wax *n*-alkane δD data, the return to full AHP conditions after YD aridity at Lake Dendi occurred in two steps paralleling the re-strengthening of the monsoonal system. The initial step at 11,700 yrs cal BP followed the YD and was characterized by an overall increase in moisture (increase in West African Monsoon strength). The second step at 10,000 yrs cal BP mirrored the eastward shift of the CAB onto the central Ethiopian Plateau most likely due to an enhanced east-west Indian Ocean pressure gradient (increase in Indian Ocean Monsoon strength). Peak AHP conditions at Lake Dendi occurred between 9,800 cal yrs cal BP and 8,000 cal yrs cal BP, interrupted by a short dry spell at 8,600 yrs cal BP, probably linked to the 8.2 ka event (8.5 ka in

East Africa). Peak AHP conditions were followed by a westward shift of the CAB and a resultant moderate decrease in precipitation amounts. Increased moisture export from the Indian Ocean due to enhanced ASO insolation and western Indian Ocean SSTs around 6,000 yrs cal BP partly compensated decreased Congo Basin moisture, leading to a gradual transition out of the AHP. Peak aridity occurred around 2,000 yrs cal BP, followed by a return to a generally wetter climate possibly linked to an increase in the Indian Ocean Monsoon strength. A short dry episode around 1,000 yrs cal BP may coincide with more arid conditions reported for the Medieval Warm period in Ethiopia. However, anthropogenic activities might bias the proxy records during the last two millennia. Our results further highlight, that the nature of the transition out of the AHP seems to be controlled by complex interactions and shifts of wind regimes together with local insolation changes at different geographical positions. Thus, the abrupt ending of the AHP at certain regions might be due to missing buffering mechanisms such as increased Indian Ocean derived moisture during ASO in the Dendi region.

6. Synthesis and outlook

In the following, regional differences of Biomarker proxies that have occurred within this thesis and the potential of multiproxy analysis are discussed. Furthermore a synthesis of the results regarding Holocene climate and environmental variability and a future outlook is given.

6.1 Biomarker from lacustrine sediments in different environments

This thesis underlines the importance of lipid biomarker from lake sedimentary organic matter as a powerful tool for paleo-environmental and -climatic reconstructions of the Holocene. Biomarkers enable the answering of questions about vegetational development, temperatures, erosion processes, hydrology, and anthropogenic impact on the environment. In particular the analyses of compound specific leaf wax hydrogen isotopes has proven to reliably constrain changes in the atmospheric circulation pattern and moisture sourcing throughout the Holocene, as shown in chapter three and five.

Regional differences in biomarker proxies

However, this thesis also highlights that biomarker data must always be interpreted in the regional context considering for example vegetation types, regional climate, land-use, and catchment hydrology and morphology:

For example, as shown in chapter four, the ACL proxy can be used as an indicator for vegetation changes. However, in this case, local pollen data indicate that changes in the ACL rather mirrors changes in the deciduous/coniferous plants ratio rather than in the forest/herbaceous ratio as suggested by other studies (Cranwell, 1973). These findings underline the importance of local vegetation endmember for the application of the ACL proxy.

Another example for the regional differences/complications of biomarker proxies is given in chapter five: The sedimentary record from Lake Dendi shows that vegetational changes towards increased C_3 vegetation derived from leaf wax carbon isotopes cannot automatically be interpreted as being the result of increasing aridity as in other East African lacustrine records (Tierney et al., 2010b; Berke et al., 2012). This results from the specific high altitude setting of Lake Dendi in the Ethiopian Highlands. At this location a drying climate associated with the end of the African Humid Period most likely led to the establishment of a dry Afromontane forest vegetation dominated by J*uniperus/Podocarpus* (C_3) instead of increased C*yperacea/Poacea* (higher C_4 percentage).

Another case (see chapter three) concerns the application of the MBT/CBT paleothermometer to lacustrine sedimentary records. The Lake Torneträsk MBT/CBT derived temperature estimates rather reflect mean summer than annual mean air temperatures like in other studies (Zink et al., 2010; Weijers et al., 2011). This most likely results from limited soil-bacterial production during winter-season, when the ground is frozen, and shows that annual temperature distributions and seasonality have to be considered for the correct interpretation the MBT/CBT paleothermometer values.

Potential of multiproxy analysis

This work also shows that the combination of organic and inorganic multiproxy data facilitates and strengthens the interpretation of biomarker data from sedimentary records.

For example, in regions with only C_3 vegetation such as northern Sweden (see chapter three), palynological analyses provide independent vegetation proxies which can be utilized to evaluate a potential bias on the application of δD as a precipitation proxy. In addition, Lake Torneträsk flood deposit data, derived by radiographic imaging, strengthens the interpretation of δD_{wax} values in the context of changing atmospheric circulation pattern.

Elemental data, derived by XRF and CNS analyses can reveal valuable information regarding terrestrial input and soil erosion processes as well as about redox conditions and preservation/degradation of organic matter in the lake. Thus, the multiproxy dataset from Lake Dendi exhibits decreasing δD_{wax} values while vegetation and sedimentological data still show enhanced moisture availability and runoff. Hence, the Dendi δD values have to be interpreted in terms of changing moisture sources rather than precipitation amount.

Furthermore, archeological evidence can help in the interpretation of lacustrine sedimentary biomarker data through delivering information regarding the degree of human impact in the respective regions. Hence, a rapid drop in ACL values and pollen of coniferous trees at Lake Dojran around ~2,000 yrs cal BP most likely do not result from climatic changes but rather from the anthropogenic intensive lumbering of pine trees during the roman era.

6.2 Holocene climate variability

This thesis strengthens previous interpretation of Holocene NH climatic trends and variability but also enables greater understanding of long-term atmospheric dynamics, as well as of climatic and anthropogenic induced environmental changes (Fig. 25). Furthermore, this thesis gives insight into Holocene centennial to millennial scale rapid climate changes and its possible influence on human civilization.

In the Early Holocene rapidly increasing precipitation amounts indicated by δD_{wax} data obtained from East African Lake Dendi sediments mirror a rapid re-strengthening of the atmospheric circulation (Indian and West African monsoonal system) at ~11,700 yrs cal BP subsequent to the Younger Dryas period. Simultaneously, Early Holocene warming and increasing humidity on the southern Balkan Peninsula is derived from Lake Dojran sedimentary molecular data. Since insolation changes are gradual (Berger and Loutre, 1991), both observations indicate a re-strengthening of the AMOC (weakened during the YD; Chang et al., 2008) which is strongly coupled to the atmospheric circulation and climate in the respective areas by influencing northward heat transport (Rayner et al., 2011) and the intensity of the westerly winds (Wen et al., 2016) (Dojran), and monsoonal flow in Africa (Dendi) (Castañeda et al., 2009). Furthermore, this underlines the strong teleconnections between the high latitudes and the tropics, most likely via the AMOC, since the YD cold event is thought to be initiated in the North-Atlantic region (Broecker, 2006; Carlson, 2010).

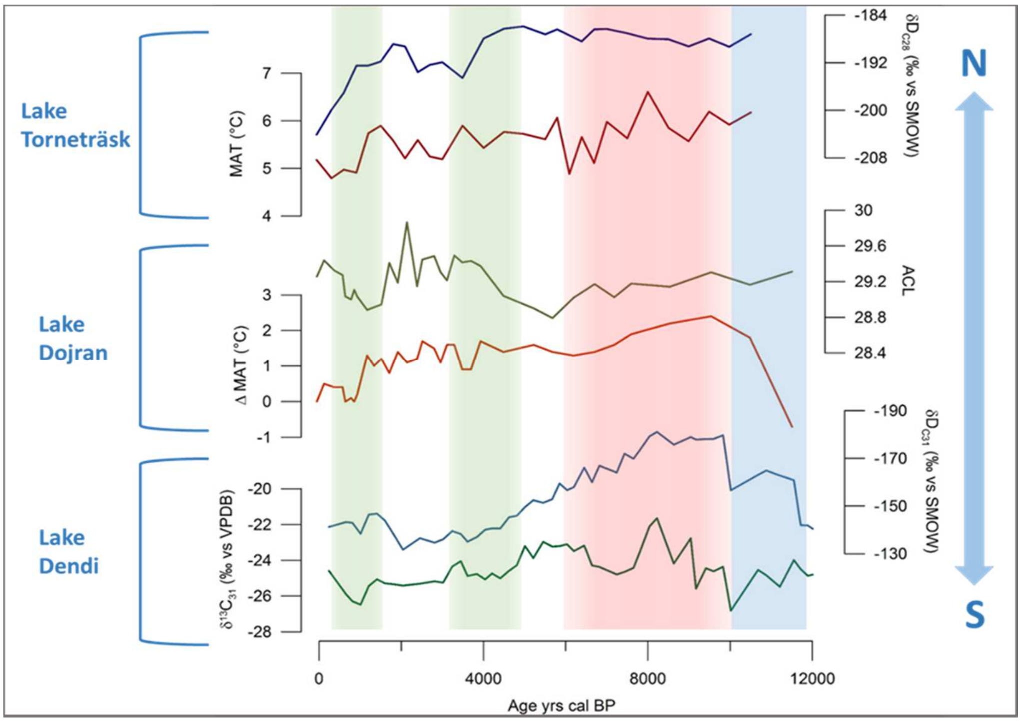

Figure 25. Selected molecular records of Holocene climate change from Lake Torneträsk, Lake Dojran, and Lake Dendi. Blue box marks the onset of the monsoonal circulation and re-strengthening of the AMOC. Red shading marks the Holocene thermal optimum period. Green shading mark periods of Holocene climatic and environmental changes.

Subsequently, peak AHP conditions with high moisture availability and increased C_4 vegetation at Lake Dendi between ~9,800 yrs cal BP and 8,000 yrs cal BP occur synchronously to a temperature maximum at Lake Dojran at 9,500 yrs cal BP, paralleling the maximum in NH summer insolation (Berger and Loutre, 1991) which is responsible for the northernmost position of the ITCZ and maximum monsoonal intensity during this time period. Warmest conditions, related to the HTM period, at Lake Torneträsk were reached about 1,000 yrs later (~8,500 yrs cal BP). This lag is most likely attributed to slow deglaciation and the presence of large ice sheets and glaciers in the high latitude region (glacial aftermath; Mayewski et al., 2004). Starting at ~8,000 yrs cal BP, Lake Dendi biomarker data suggest a rather moderate reduction in precipitation due to decreasing monsoonal activity and an associated southward shift of the ITCZ. Furthermore δD_{wax} data indicate a change in moisture sources at Lake Dendi, driven by an insolation induced gradual weakening west–east pressure gradient near the equator which lead to an eastward shift of the Congo Air Boundary further onto the African continent. Proxies for vegetation and runoff, however still indicate relative high moisture availability until ~4,500 yrs cal BP. This most likely results from enhanced Indian Ocean derived rainfall due to enhanced local insolation (10°N) during summer/fall. The atmospheric reorganization in East Africa is largely paralleled by a (relatively weak) aridification trend, changing seasonality and decreasing temperatures throughout the Middle and Late Holocene at Lake Dojran (Francke et al., 2013 Zhang et al., 2014; Thienemann et al., 2017). This aridification process is a widespread phenomenon in the mid to low latitude desert belt and the SE Mediterranean region (Schilman et al., 2001). Mediterranean aridity can, however not directly be caused by the weakening of the monsoon systems observed at Lake Dendi, as Tzedakis (2007) found that the African monsoon did not extend to the Mediterranean, and that there has been only an indirect effect in terms of Nile discharge and runoff at the North African coast into the Mediterranean Sea. Today, wetter conditions in the Mediterranean are associated with a NAO+ situation leading to enhanced westerlies and moisture transport into southern Europe. Accordingly, Lamy et al. (2006) suggested an atmospheric pressure pattern similar to a more positive AO/NAO as being responsible for Eastern Mediterranean aridity. This, however would be in contrast to previous work (Rimbu et al., 2003; Davis and Brewer, 2009; Wanner et al., 2008), also including this thesis (see chapter three), that rather point to a long-term declining trend in the NAO/AO over the course of the Holocene. Frigola et al. (2007) suggests that the dry conditions in the western Mediterranean resulted directly from the southward migration of the ITCZ and the decrease in the atmospheric pressure gradient and moisture transport, which would be in agreement with Lake Dendi δD_{wax} data.

However, at Lake Dojran local complexity of climate variability such as local vegetation succession and associated changes in catchment processes might exhibit a more severe control than over-regional climate change (Francke et al., 2013; Zhang et al., 2014). Similar to Lake Dojran, Lake Torneträsk biomarker data display a decreasing temperature trend over the course of the Holocene. At Lake Torneträsk, the decreasing temperatures lead to significant environmental changes including a tree-line retreat, the development from a boreal forest to an open sub-alpine woodland, and an associated destabilization of soils and increased catchment erosion. The strong environmental feedback to the declining temperatures most likely results from the lakes sensitivity to experience large biotic shifts (MacDonald et al., 1993; Körner 1998; Barnekow, 1999) due to its location at the present-day tree line. δD_{wax} data, however, suggest a stable northward position of the polar frontal zone until ~4,000 yrs cal BP, indicating that the environmental changes described most likely resulted from decreasing temperatures and not from changing atmospheric circulation pattern.

Around 4,500 yrs cal BP to 4,000 yrs cal BP, the sedimentary records from Lake Dendi, Dojran, Torneträsk all suggest significant climatic/environmental transitions (Fig. 25): At Lake Dendi, vegetational changes (obtained from $\delta^{13}C_{wax}$, ACL) and changes in runoff (BIT), as well as the ongoing D-enrichment trend suggest increasingly arid conditions around 4,500 yrs cal BP to 4,000 yrs cal BP, associated with the end of the AHP. This most likely results from the southwards migration of wind systems, e.g. the ITCZ and the weakening of the West African monsoon system. The general timing is also relatively consistent with the rather abrupt ending of the AHP in other East African records (Tierney et al., 2008; Tierney et al., 2010b; Tierney and deMenocal, 2013). At Lake Dojran, the Mid- to Late Holocene transition is associated with a general trend towards climatic and environmental instability. However, possible anthropogenic impact in the catchment, indicated by biomarker and pollen data since ~4,500 cal yrs BP complicates the identification of natural climatic and environmental changes (Thienemann et al., 2017). Thus, for example the anthropogenic induced deforestation that might have started as early as 4,000 yrs cal BP in the Dojran region, could have contributed to the Late Holocene climatic perturbations via earth-albedo feedbacks, as suggested by a model simulation for southern Europe (Strandberg et al., 2014). At Lake Torneträsk, δD_{wax} data indicate a shift from a dominant zonal to a stronger meridional atmospheric flow starting at ~4,000 yrs cal BP. This shift can be attributed to a southward migration of the polar front and/or a change in NAO/AO like circulation pattern and is consistent with the southward movement of the ITCZ indicated by Lake Dendi δD_{wax} data. Thus, the end of the Middle Holocene, between about 4,500 yrs cal BP and 4,000 yrs cal BP, seems to mark a significant change in the Northern Hemispheric climate and atmospheric system. A similar phase of climatic/atmospheric change is indicated around 2,000 yrs cal BP to 1,500 yrs cal BP with a drop in MAT of ~1°C in all three molecular lake records. Lake Torneträsk δD_{wax} and flood deposit data furthermore suggest a further southward migration of atmospheric circulation systems i.e. the polar frontal zone. A southward shift of the atmospheric circulation would be associated with weakened monsoonal systems and aridity in East Africa. However, at Lake Dendi a return to more humid conditions is observed after ~2,000 yrs cal BP. This discrepancy might be explained by an eastward shift of the CAB and increased Indian Ocean derived precipitation, as Fleitmann et al. (2003) observe a re-strengthening of the Indian Ocean monsoon during the last ~1,500 yrs cal BP. The strength of the West African monsoon, associated with the ITCZ over tropical Africa, on the other hand does show an ongoing decreasing trend (Weldeab et al., 2007).

This thesis further supports the existence of NH Holocene centennial to millennial scale rapid climatic changes commonly referred to as "Bond events" (Bond et al., 1997; Bond et al., 2001). Thus, elemental data from Lake Torneträsk exhibit a clear signal of six rapid climate fluctuations paralleling ice rafted debris maxima from North Atlantic sediment records starting at about 8,000 yrs cal BP. At Lake Torneträsk, these rapid climate changes are associated with colder conditions and northerly/northeasterly winds due to short-term southward shifts of the polar frontal zone. Previous events are not discernible, most likely due to deglaciation and the high turnover of the Torneträsk catchment prior to ~9,000 yrs cal BP. The sedimentary records from Lake Dojran and Lake Dendi, on the other hand only exhibit rapid climate changes associated with the 8.2 ka event and the 4.2 ka event. Lake Dojran data additionally show climatic fluctuations attributed to the Little Ice Age. During these periods, higher aridity and colder conditions are observed at both Lakes that could result, similar to the situation in Fennoscandia, from short-term southwards shifts of the atmospheric circulation cells and/or reduced atmospheric pressure gradients. However, it cannot be resolved if these rapid climate changes are directly initiated by solar variation through for example affecting land–sea contrasts (Shindell et al., 2001), or transmitted from the higher latitudes via atmospheric and/or oceanic linkages (Frigola et al., 2007; Chiang et al., 2008). At present, efficient atmospheric/oceanic teleconnection exist between the Mediterranean/East Africa and the high latitudes that would enable the transitions of climatic signals: Arctic/N.Atlantic climatic signals are transported atmospherically to the northern Mediterranean via orographically channeled winter outbreaks of cold and dry air from high latitudes (Leaman and Schott, 1991; Poulos et al., 1997), while the tropics are connected to the NH via the AMOC (Broecker et al., 1985). Alternatively, internal oscillations in the AMOC could also be the driver for Holocene rapid climate changes (Gupta et al., 2003). However, since these events are most prominent in the sedimentary record from Lake Torneträsk, this thesis indicates that Holocene rapid climate changes might be initiated or at least amplified in the North Atlantic region. Furthermore, it is shown that future recurrences of such climatic fluctuations have the potential to greatly affect not only climate and environmental conditions in the North Atlantic region but also in the middle and lower latitudes. In addition, the importance of greater insight into rapid future climate changes is highlighted by sedimentary biomarker and pollen data from Lake Dojran that suggest a potential influence of Holocene centennial to millennial scale climatic fluctuations on human societies.

6.3 Future outlook

This work demonstrates the value and significance of lipid biomarkers and compound specific leaf wax isotopes for the reconstruction of past climate and environmental variability. However, further research is needed about the documented non-linear feedback mechanisms of the climate system to orbital forcing. In this context, potential tipping points/thresholds, that might play an important role in the climate system, have to be further evaluated. This could be accomplished by additional high resolution stable isotope studies on latitudinal gradients for the exact reconstructions of the timing and nature of the migration of the atmospheric circulation cells. In this context, especially regions such as Fennoscandia that lie in proximity to atmospheric boundaries can be of great interest. Furthermore, past changes in the NAO index could be inferred from the comparison of lake sedimentary $\delta^{18}O$ and δD, as Baldini et al., (2008) observe a present day correlation of the mean winter NAO index and the deuterium-excess in winter precipitation at high-latitude GNIP sites. This, however would require δD analyses of LMW hydrocarbons derived from lacustrine algae, since land-plant δD values from the Torneträsk region are mainly controlled by summer precipitation as documented in this thesis. At Lake Dendi, a more extensive comparison of the molecular records with independent sedimentological and palynological data could greatly improve the understanding of driving factors of δD_{wax}, (e.g. the amount and source effect) and thus about controls and mechanisms of East African climate. In addition, greater insights in D isotopic fractionation factors in different environments and for different plant types/lipids, as well as a more precise knowledge about timing of leaf wax formation and lipid synthesis could greatly improve future studies of compound specific stable isotopes, which have otherwise been shown to be a promising tool to asses Holocene climate variability.

Acknowledgements

I sincerely thank Prof. Dr. Janet Rethemeyer who enabled this thesis and gave me the chance to work in the field of organic geochemistry. She always supported me during my studies and gave me the opportunity to participate in several field campaigns, conferences and workshops. Furthermore, I am very grateful that Prof. Dr. Hans-Rudolf Bork agreed to be my second dissertation chair and that Prof. Dr. Olaf Bubenzer took the chair of my examination committee. Dr. Stephanie Kusch is acknowledged for the great support and productive discussions and for acting as the assessor for my defenses. Furthermore, I want to thank the whole working group of Organic Geochemistry and all other colleagues from the Institute for Geology for the great times and experiences on both a professional and personal level. In particular, I would like to thank Sandra Jivcov and Janna Just for the countless coffees and cigarettes. Thanks go to Bianca Stapper and Stephan John for guidance in the laboratory and to Ilona Steffens for assistance. Thanks also go to Dr. Enno Schefuß and to Ralph Kreutz from MARUM for advice and for running the isotope analyses for this study. Sincere gratitude goes to my family, especially my wife Katja for her constant encouragement and incredible patience.

This work was funded by the German Research Council (DFG) as part of the Collaborative Research Center CRC 806 “Our way to Europe”.

References

Abram NJ, Wolff EW and Curran MAJ. (2013) A review of sea ice proxy information from polar ice cores. *Quaternary Science Reviews* 79: 168-183.

Abrantes F, Voelker A, Sierro FJ, et al. (2012) 1 - Paleoclimate Variability in the Mediterranean Region. In: Lionello P (ed) *The Climate of the Mediterranean Region.* Oxford: Elsevier, 1-86.

ACIA (2005) Arctic Climate Impact Assesment, Camebridge University Press. 1042 p.

Aichner B, Feakins SJ, Lee JE, et al. (2015) High-resolution leaf wax carbon and hydrogen isotopic record of the late Holocene paleoclimate in arid Central Asia. *Clim. Past* 11: 619-633.

Alexandersson, H. and Eggertsson Karlstrom, C. (2001) Temperaturen och nederborden i Sverige 1961–1990, Referensnormaler – utgåva 2, Meteorologi 99, Sveriges Meteorologiska och Hydrologiska Institut, Norrköping.

Allen JRM, Brandt U, Brauer A, et al. (1999) Rapid environmental changes in southern Europe during the last glacial period. *Nature* 400: 740-743.

Alley RB and Ágústsdóttir AM. (2005) The 8k event: cause and consequences of a major Holocene abrupt climate change. *Quaternary Science Reviews* 24: 1123-1149.

Andersen C, Koç N, Jennings A, et al. (2004) Nonuniform response of the major surface currents in the Nordic Seas to insolation forcing: Implications for the Holocene climate variability. *Paleoceanography* 19: PA2003.

Anderson L, Abbott MB, Finney BP, et al. (2005) Regional atmospheric circulation change in the North Pacific during the Holocene inferred from lacustrine carbonate oxygen isotopes, Yukon Territory, Canada. *Quaternary Research* 64: 21-35.

Andersson S, Rosqvist G, leng Mj, et al. (2010) Late Holocene climate change in central Sweden inferred from lacustrine stable isotope data. *Journal of Quaternary Science* 25: 1305-1316.

Andrén H, Jonasson C and Ottosson J. (2002) Deltas in the Abisko area, northern Sweden: the Abiskojokka delta in lake Torneträsk. Geografiska Annaler: Series A, Physical Geography 84: 151-156.

Andreou S, Fotiadis M and Kotsakis K. (1996) Review of Aegean Prehistory V: The Neolithic and Bronze Age of Northern Greece. *American Journal of Archaeology* 100: 537-597.

Ariztegui D, Asioli A, Lowe JJ, et al. (2000) Palaeoclimate and the formation of sapropel S1: inferences from Late Quaternary lacustrine and marine sequences in the central Mediterranean region. *Palaeogeography, Palaeoclimatology, Palaeoecology* 158: 215-240.

Athanasiadis N, Tonkov S, Atanassova J, et al. (2000) Palynological study of Holocene sediments from Lake Doirani in northern Greece. *Journal of Paleolimnology* 24: 331-342.

Aufgebauer A, Panagiotopoulos K, Wagner B, et al. (2012) Climate and environmental change in the Balkans over the last 17 ka recorded in sediments from Lake Prespa (Albania/F.Y.R. of Macedonia/Greece). *Quaternary International* 274: 122-135.

Baek SO, Field RA, Goldstone ME, et al. (1991) A review of atmospheric polycyclic aromatic hydrocarbons: Sources, fate and behavior. *Water, Air, and Soil Pollution* 60: 279-300.

Baldini LM, McDermott F, Foley AM, et al. (2008) Spatial variability in the European winter precipitation $\delta^{18}O$-NAO relationship: Implications for reconstructing NAO-mode climate variability in the Holocene. *Geophysical Research Letters* 35: L04709.

Bar-Matthews M, Ayalon A, Kaufman A, et al. (1999) The Eastern Mediterranean paleoclimate as a reflection of regional events: Soreq cave, Israel. *Earth and Planetary Science Letters* 166: 85-95.

Barnekow L. (1999) Holocene tree-line dynamics and inferred climatic changes in the Abisko area, northern Sweden, based on macrofossil and pollen records. *The Holocene* 9: 253-265.

References

Barnekow L. (2000) Holocene regional and local vegetation history and lake-level changes in the Torneträsk area, northern Sweden. *Journal of Paleolimnology* 23: 399-420.

Barber DC, Dyke A, Hillaire-Marcel C, et al. (1999) Forcing of the cold event of 8,200 years ago by catastrophic drainage of Laurentide lakes. *Nature* 400: 344-348.

Behre K-E. (1988) The rôle of man in European vegetation history. In: Huntley B and Webb T, III (eds) *Vegetation history.* Springer Netherlands, 633-672.

Bendle JAP and Rosell-Melé A. (2007) High-resolution alkenone sea surface temperature variability on the North Icelandic Shelf: implications for Nordic Seas palaeoclimatic development during the Holocene. *The Holocene* 17: 9-24.

Benito G, Macklin MG, Panin A, et al. (2015) Recurring flood distribution patterns related to short-term Holocene climatic variability. *Scientific Reports 5*: 16398.

Berger A and Loutre MF. (1991) Insolation values for the climate of the last 10 million years. *Quaternary Science Reviews* 10: 297-317.

Berke MA, Johnson TC, Werne JP, et al. (2012) Molecular records of climate variability and vegetation response since the Late Pleistocene in the Lake Victoria basin, East Africa. *Quaternary Science Reviews* 55: 59-74.

Bi X, Sheng G, Liu X, et al. (2005) Molecular and carbon and hydrogen isotopic composition of n-alkanes in plant leaf waxes. *Organic Geochemistry* 36: 1405-1417.

Bianchi GG and McCave IN. (1999) Holocene periodicity in North Atlantic climate and deep-ocean flow south of Iceland. *Nature* 397: 515-517.

Bianchi TS and Canuel EA. (2011) *Chemical Biomarkers in Aquatic Ecosystems*: Princeton University Press.

Bigelow NH, Brubaker LB, Edwards ME, et al. (2003) Climate change and Arctic ecosystems: 1. Vegetation changes north of 55°N between the last glacial maximum, mid-Holocene, and present. *Journal of Geophysical Research: Atmospheres* 108: 8170.

Bigg GR and Rohling EJ. (2000) An oxygen isotope data set for marine waters. *Journal of Geophysical Research: Oceans* 105: 8527-8535.

Bigler C, Grahn E, Larocque I, et al. (2003) Holocene environmental change at Lake Njulla (999 m a.s.l.), northern Sweden: a comparison with four small nearby lakes alongan altitudinal gradient. *Journal of Paleolimnology* 29: 13-29.

Bird MI, Summons RE, Gagan MK, et al. (1995) Terrestrial vegetation change inferred from *n*-alkane $\delta_{13}C$ analysis in the marine environment. *Geochimica et Cosmochimica Acta* 59: 2853-2857.

Bjørseth A. (1983) Handbook of polycyclic aromatic hydrocarbons.

Blackford J. (2000) Palaeoclimatic records from peat bogs. *Trends in Ecology & Evolution* 15: 193-198.

Blaga CI, Reichart G-J, Heiri O, et al. (2009) Tetraether membrane lipid distributions in water-column particulate matter and sediments: a study of 47 European lakes along a north–south transect. *Journal of Paleolimnology* 41: 523-540.

Blaga CI, Reichart G-J, Lotter AF, et al. (2013) A TEX_{86} lake record suggests simultaneous shifts in temperature in Central Europe and Greenland during the last deglaciation. *Geophysical Research Letters* 40: 948-953.

Blaauw M and Christen JA. (2011) Flexible paleoclimate age-depth models using an autoregressive gamma process. *Bayesian Analysis* 6: 457-474.

Bocquet-Appel J-P, Naji S, Linden MV, et al. (2009) Detection of diffusion and contact zones of early farming in Europe from the space-time distribution of ^{14}C dates. *Journal of Archaeological Science* 36: 807-820.

Boehm PD. (2005) 15 - Polycyclic Aromatic Hydrocarbons (PAHs). In: Morrison RD and Murphy BL (eds) *Environmental Forensics.* Burlington: Academic Press, 313-337.

References

Bonafini M, Pellegrini M, Ditchfield P, et al. (2013) Investigation of the 'canopy effect' in the isotope ecology of temperate woodlands. *Journal of Archaeological Science* 40: 3926-3935.

Bond G, Kromer B, Beer J, et al. (2001) Persistent Solar Influence on North Atlantic Climate During the Holocene. *Science* 294: 2130-2136.

Bond G, Showers W, Cheseby M, et al. (1997) A Pervasive Millennial-Scale Cycle in North Atlantic Holocene and Glacial Climates. *Science* 278: 1257-1266.

Bordon A, Peyron O, Lézine A-M, et al. (2009) Pollen-inferred Late-Glacial and Holocene climate in southern Balkans (Lake Maliq). *Quaternary International* 200: 19-30.

Bowen GJ. (2008) Spatial analysis of the intra-annual variation of precipitation isotope ratios and its climatological corollaries. *Journal of Geophysical Research: Atmospheres* 113: D05113.

Bowling DR, Pataki DE and Randerson JT. (2008) Carbon isotopes in terrestrial ecosystem pools and CO2 fluxes. *New Phytologist* 178: 24-40.

Bradley RS and Jonest PD. (1993) 'Little Ice Age' summer temperature variations: their nature and relevance to recent global warming trends. *The Holocene* 3: 367-376.

Braun H, Christl M, Rahmstorf S, et al. (2005) Possible solar origin of the 1,470-year glacial climate cycle demonstrated in a coupled model. *Nature* 438: 208-211.

Bray EE and Evans ED. (1961) Distribution of n-paraffins as a clue to recognition of source beds. *Geochimica et Cosmochimica Acta* 22: 2-15.

Brocks JJ and Pearson A. (2005) Building the Biomarker Tree of Life. *Reviews in Mineralogy and Geochemistry* 59: 233-258.

Broecker WS. (2006) Was the Younger Dryas Triggered by a Flood? *Science* 312: 1146-1148.

Broecker WS, Denton GH, Edwards RL, et al. (2010) Putting the Younger Dryas cold event into context. *Quaternary Science Reviews* 29: 1078-1081.

Broecker WS, Peteet DM and Rind D. (1985) Does the ocean-atmosphere system have more than one stable mode of operation? *Nature* 315: 21-26.

Brown KJ, Clark JS, Grimm EC, et al. (2005) Fire cycles in North American interior grasslands and their relation to prairie drought. *Proceedings of the National Academy of Sciences of the United States of America* 102: 8865-8870.

Bull ID, Lockheart MJ, Elhmmali MM, et al. (2002) The origin of faeces by means of biomarker detection. *Environment International* 27: 647-654.

Camberlin P. (1997) Rainfall Anomalies in the Source Region of the Nile and Their Connection with the Indian Summer Monsoon. *Journal of Climate* 10: 1380-1392.

Carlson AE. (2010) What Caused the Younger Dryas Cold Event? *Geology* 38: 383-384.

Carreira RS, Wagener ALR and Readman JW. (2004) Sterols as markers of sewage contamination in a tropical urban estuary (Guanabara Bay, Brazil): space–time variations. *Estuarine, Coastal and Shelf Science* 60: 587-598.

Casford JSL, Abu-Zied R, Rohling EJ, et al. (2001) Mediterranean climate variability during the Holocene. *Mediterranean Marine Science* 2(1): 45–55.

Castañeda IS, Mulitza S, Schefuß E, et al. (2009) Wet phases in the Sahara/Sahel region and human migration patterns in North Africa. *Proceedings of the National Academy of Sciences* 106: 20159-20163.

Castañeda I. S. and Schouten S. (2011). A review of molecular organic proxies for examining modern and ancient lacustrine environments. *Quaternary Science Reviews* 30, 2851–2891.

Castañeda IS, Schouten S, Pätzold J, et al. (2016) Hydroclimate variability in the Nile River Basin during the past 28,000 years. *Earth and Planetary Science Letters* 438: 47-56.

Chang P, Zhang R, Hazeleger W, et al. (2008) Oceanic link between abrupt changes in the North Atlantic Ocean and the African monsoon. *Nature Geoscience* 1: 444-448.

References

Chen S, Huang Y, Zou J, et al. (2013) Mean residence time of global topsoil organic carbon depends on temperature, precipitation and soil nitrogen. *Global and Planetary Change* 100: 99-108.

Cheng W, Sun L, Kimpe LE, et al. (2016) Sterols and Stanols Preserved in Pond Sediments Track Seabird Biovectors in a High Arctic Environment. *Environmental Science & Technology* 50: 9351-9360.

Chikaraishi Y and Naraoka H. (2003) Compound-specific δD–δ^{13}C analyses of *n*-alkanes extracted from terrestrial and aquatic plants. *Phytochemistry* 63: 361-371.

Chikaraishi Y and Naraoka H. (2007) δ^{13}C and δD relationships among three *n*-alkyl compound classes (*n*-alkanoic acid, *n*-alkane and *n*-alkanol) of terrestrial higher plants. *Organic Geochemistry* 38: 198-215.

Chikaraishi Y, Naraoka H and Poulson SR. (2004) Hydrogen and carbon isotopic fractionations of lipid biosynthesis among terrestrial (C3, C4 and CAM) and aquatic plants. *Phytochemistry* 65: 1369-1381.

Clark PU, Pisias NG, Stocker TF, et al. (2002) The role of the thermohaline circulation in abrupt climate change. *Nature* 415: 863-869.

Claussen M and Gayler V. (1997) The Greening of the Sahara during the Mid-Holocene: Results of an Interactive Atmosphere-Biome Model. *Global Ecology and Biogeography Letters* 6: 369-377.

Coffinet S, Huguet A, Pedentchouk N, et al. (2017) Evaluation of branched GDGTs and leaf wax *n*-alkane δ^{2}H as (paleo) environmental proxies in East Africa. *Geochimica et Cosmochimica Acta* 198: 182-193.

Cohen AS. (2003) *Paleolimnology: the history and evolution of lake systems*: Oxford University Press.

Cohen ER. (2007) *Quantities, units and symbols in physical chemistry*: Royal Society of Chemistry.

COHMAP-Members. (1988) Climatic Changes of the Last 18,000 Years: Observations and Model Simulations. *Science* 241: 1043-1052.

Connor SE, Ross SA, Sobotkova A, et al. (2013) Environmental conditions in the SE Balkans since the Last Glacial Maximum and their influence on the spread of agriculture into Europe. *Quaternary Science Reviews* 68: 200-215.

Costa K, Russell J, Konecky B, et al. (2014) Isotopic reconstruction of the African Humid Period and Congo Air Boundary migration at Lake Tana, Ethiopia. *Quaternary Science Reviews* 83: 58-67.

Craig H. (1961) Isotopic Variations in Meteoric Waters. *Science* 133: 1702-1703.

Cranwell PA. (1973) Chain-length distribution of n-alkanes from lake sediments in relation to post-glacial environmental change. *Freshwater Biology* 3: 259-265.

Cullen HM, deMenocal PB, Hemming S, et al. (2000) Climate change and the collapse of the Akkadian empire: Evidence from the deep sea. *Geology* 28: 379-382.

D'Anjou RM, Bradley RS, Balascio NL, et al. (2012) Climate impacts on human settlement and agricultural activities in northern Norway revealed through sediment biogeochemistry. *Proceedings of the National Academy of Sciences* 109 (50): 20332-20337.

Dalfes HN, Kukla G and Weiss H. (2013) *Third millennium BC climate change and old world collapse*: Springer Science & Business Media.

Dansgaard W. (1964) Stable isotopes in precipitation. *Tellus* 16: 436-468.

Dansgaard W, Johnsen S, Clausen H, et al. (1993) Evidence for general instability of past climate from a 250-kyr. *Nature* 364: 15.

Darbyshire I, Lamb H and Umer M. (2003) Forest clearance and regrowth in northern Ethiopia during the last 3000 years. *The Holocene* 13: 537-546.

Davies O, Heurtley WA and Cuttle WL. (1926) Report on Excavations at the Toumba and Tables of Vardaróftsa, Macedonia, 1925, 1926. *The Annual of the British School at Athens* 28: 195-242.

Davis BAS, Brewer S, Stevenson AC, et al. (2003) The temperature of Europe during the Holocene reconstructed from pollen data. *Quaternary Science Reviews* 22: 1701-1716.

References

Dearing JA. (2006) Climate-human-environment interactions: resolving our past. *Climate of the Past Discussions* 2: 563-604.

De Cort G, Bessems I, Keppens E, et al. (2013) Late-Holocene and recent hydroclimatic variability in the central Kenya Rift Valley: The sediment record of hypersaline lakes Bogoria, Nakuru and Elementeita. *Palaeogeography, Palaeoclimatology, Palaeoecology* 388: 69-80.

Degefu F and Schagerl M. (2015) Zooplankton abundance, species composition and ecology of tropical high-mountain crater lake Wonchi, Ethiopia. J. *Limnol*., 72: 324-334.

Degefu, F., Herzig, A., Jirsa, F., and Schagerl, M., 2014: First limnological records of highly threatened tropical high-mountain crater lakes in Ethiopia. *Trop. Conserv. Sci*., 7: 365-381.

De Jonge C, Hopmans EC, Zell CI, et al. (2014) Occurrence and abundance of 6-methyl branched glycerol dialkyl glycerol tetraethers in soils: Implications for palaeoclimate reconstruction. *Geochimica et Cosmochimica Acta* 141: 97-112.

Debret M, Bout-Roumazeilles V, Grousset F, et al. (2007) The origin of the 1500-year climate cycles in Holocene North-Atlantic records. *Clim. Past* 3: 569-575.

DeMenocal P, Ortiz J, Guilderson T, et al. (2000) Abrupt onset and termination of the African Humid Period:: rapid climate responses to gradual insolation forcing. *Quaternary Science Reviews* 19: 347-361.

DeMenocal PB. (2001) Cultural responses to climate change during the late Holocene. *Science (New York, N.Y.)* 292: 667-673.

Devane M, Wood D, Chappell A, et al. (2015) Identifying avian sources of faecal contamination using sterol analysis. *Environmental Monitoring and Assessment* 187: 1-19.

De Vernal A, Hillaire-Marcel C and Darby DA. (2005) Variability of sea ice cover in the Chukchi Sea (western Arctic Ocean) during the Holocene. *Paleoceanography* 20: PA4018.

Dickson RR, Osborn TJ, Hurrell JW, et al. (2000) The Arctic Ocean Response to the North Atlantic Oscillation. *Journal of Climate* 13: 2671-2696.

Diefendorf AF, Mueller KE, Wing SL, et al. (2010) Global patterns in leaf ^{13}C discrimination and implications for studies of past and future climate. *Proceedings of the National Academy of Sciences* 107: 5738-5743.

Diffenbaugh NS and Field CB. (2013) Changes in Ecologically Critical Terrestrial Climate Conditions. *Science* 341: 486-492.

Dormoy I, Peyron O, Combourieu Nebout N, et al. (2009) Terrestrial climate variability and seasonality changes in the Mediterranean region between 15 000 and 4000 years BP deduced from marine pollen records. Clim. Past 5: 615-632.

Doyen É, Vannière B, Rius D, et al. (2015) Climate and biomass control on fire activity during the late-glacial/early-Holocene transition in temperate ecosystems of the upper Rhone valley (France). *Quaternary Research* 83: 94-104.

Dubois N and Jacob J. (2016) Molecular Biomarkers of Anthropic Impacts in Natural Archives: A Review. *Frontiers in Ecology and Evolution* 4: Article 92 (16 pp.)

Eddy JA. (1976) The Maunder Minimum. *Science* 192: 1189-1202.

Eglinton G and Hamilton R. (1963) The distribution of alkanes. *Chemical plant taxonomy* 187: 217.

Eglinton G. and Hamilton R. J. (1967) Leaf Epicuticular Waxes. *Science* 156, 1322–1335.

Eglinton G and Pancost RD. (2004) Immortal Molecules, 'Superfeature'.

Eglinton G, Scott PM, Belsky T, et al. (1964) Hydrocarbons of Biological Origin from a One-Billion-Year-Old Sediment. *Science* 145: 263-264.

Eglinton TI and Eglinton G. (2008) Molecular proxies for paleoclimatology. *Earth and Planetary Science Letters* 275: 1-16.

Elias S. (2006) *Encyclopedia of Quaternary science*: Elsevier.

References

Ellis EC. (2011) Anthropogenic transformation of the terrestrial biosphere. *Philosophical Transactions of the Royal Society of London A: Mathematical, Physical and Engineering Sciences* 369: 1010-1035.

Ellison CRW, Chapman MR and Hall IR. (2006) Surface and Deep Ocean Interactions During the Cold Climate Event 8200 Years Ago. *Science* 312: 1929-1932.

Fairchild IJ and Baker A. (2012) Introduction to Speleothems and Systems. *Speleothem Science.* John Wiley & Sons, Ltd, 1-27.

Feakins SJ and Sessions AL. (2010) Controls on the D/H ratios of plant leaf waxes in an arid ecosystem. *Geochimica et Cosmochimica Acta* 74: 2128-2141.

Felis T, Patzold J, Loya Y, et al. (2000) A coral oxygen isotope record from the northern Red Sea documenting NAO, ENSO, and North Pacific teleconnections on Middle East climate variability since the year 1750 (Paper 1999PA000477). *Paleoceanography* 15: 679-694.

Feng X and Epstein S. (1995) Carbon isotopes of trees from arid environments and implications for reconstructing atmospheric CO_2 concentration. *Geochimica et Cosmochimica Acta* 59: 2599-2608.

Feynman J and Ruzmaikin A. (2007) Climate stability and the development of agricultural societies. *Climatic Change* 84: 295-311.

Ficken KJ, Li B, Swain DL, et al. (2000) An n-alkane proxy for the sedimentary input of submerged/floating freshwater aquatic macrophytes. *Organic Geochemistry* 31: 745-749.

Fietz S, Martínez-Garcia A, Huguet C, et al. (2011) Constraints in the application of the Branched and Isoprenoid Tetraether index as a terrestrial input proxy. *Journal of Geophysical Research: Oceans* 116: C10032.

Finné M, Holmgren K, Sundqvist HS, et al. (2011) Climate in the eastern Mediterranean, and adjacent regions, during the past 6000 years – A review. *Journal of Archaeological Science* 38: 3153-3173.

Fleitmann D, Burns SJ, Mangini A, et al. (2007) Holocene ITCZ and Indian monsoon dynamics recorded in stalagmites from Oman and Yemen (Socotra). *Quaternary Science Reviews* 26: 170-188.

Fleitmann D, Burns SJ, Mudelsee M, et al. (2003) Holocene forcing of the Indian monsoon recorded in a stalagmite from southern Oman. *Science* 300: 1737-1739.

Foerster V, Junginger A, Langkamp O, et al. (2012) Climatic change recorded in the sediments of the Chew Bahir basin, southern Ethiopia, during the last 45,000 years. *Quaternary International* 274: 25-37.

Folland CK, Colman AW, Rowell DP, et al. (2001) Predictability of Northeast Brazil Rainfall and Real-Time Forecast Skill, 1987–98. *Journal of Climate* 14: 1937-1958.

Fontugne MR and Calvert SE. (1992) Late Pleistocene Variability of the Carbon Isotopic Composition of Organic Matter in the Eastern Mediterranean: Monitor of Changes in Carbon Sources and Atmospheric CO2 Concentrations. *Paleoceanography* 7: 1-20.

Fouache E and Pavlopoulos K. (2011) The Interplay between Environment and People from Neolithic to Classical Times in Greece and Albania. In: Martini IP and Chesworth W (eds) *Landscapes and Societies.* Springer Netherlands, 155-166.

Fouache E, Desruelles S, Magny M, et al. (2010) Palaeogeographical reconstructions of Lake Maliq (Korça Basin, Albania) between 14,000 BP and 2000 BP. *Journal of Archaeological Science 37*: 525-535.

Francke A, Wagner B, Leng MJ, et al. (2013) A Late Glacial to Holocene record of environmental change from Lake Dojran (Macedonia, Greece). *Clim. Past* 9: 481-498.

Frankignoul C, Gastineau G and Kwon Y-O. (2013) The Influence of the AMOC Variability on the Atmosphere in CCSM3. *Journal of Climate* 26: 9774-9790.

Frigola J, Moreno A, Cacho I, et al. (2007) Holocene climate variability in the western Mediterranean region from a deepwater sediment record. *Paleoceanography* 22: PA2209.

Frisia S, Borsato A, SpÖTl C, et al. (2005) Climate variability in the SE Alps of Italy over the past 17 000 years reconstructed from a stalagmite record. *Boreas* 34: 445-455.

References

Fritzsche, F., Zech, W., and Guggenberger, G. (2007) Soils of the Main Ethiopian Rift Valley escarpment: A transect study, Catena, 70, 209-219.

Gagosian RB and Peltzer ET. (1986) The importance of atmospheric input of terrestrial organic material to deep sea sediments. *Organic Geochemistry* 10: 661-669.

Ganopolski A and Rahmstorf S. (2001) Rapid changes of glacial climate simulated in a coupled climate model. *Nature* 409: 153-158.

Garcin Y, Williamson D, Taieb M, et al. (2006) Centennial to millennial changes in maar-lake deposition during the last 45,000 years in tropical Southern Africa (Lake Masoko, Tanzania). *Palaeogeography, Palaeoclimatology, Palaeoecology* 239: 334-354.

Gasse F. (2000) Hydrological changes in the African tropics since the Last Glacial Maximum. *Quaternary Science Reviews* 19: 189-211.

Giesecke T, Bjune AE, Chiverrell RC, et al. (2008) Exploring Holocene continentality changes in Fennoscandia using present and past tree distributions. *Quaternary Science Reviews* 27: 1296-1308.

Gillespie R, Street-Perrott FA and Switsur R. (1983) Post-glacial arid episodes in Ethiopia have implications for climate prediction. *Nature* 306: 680-683.

Gimbutas M. (1974) Anza, ca. 6500-5000 B. C.: A Cultural Yardstick for the Study of Neolithic Southeast Europe. *Journal of Field Archaeology* 1: 27-66.

Glur L, Wirth SB, Büntgen U, et al. (2013) Frequent floods in the European Alps coincide with cooler periods of the past 2500 years. *Scientific Reports* 3: 2770.

Goudie AS. (2013) *The Human Impact on the Natural Environment: Past, Present, and Future*: Wiley.

Grice RE, Locksley HD and Scheinmann F. (1968) Alkane Distribution as Biological Markers: Presence and Possible Origin of *n*-alkanes in Guttiferae Heartwoods. *Nature* 218: 892-893.

Grimalt JO, Fernandez P, Bayona JM, et al. (1990) Assessment of fecal sterols and ketones as indicators of urban sewage inputs to coastal waters. *Environmental Science & Technology* 24: 357-363.

Gupta AK, Anderson DM and Overpeck JT. (2003) Abrupt changes in the Asian southwest monsoon during the Holocene and their links to the North Atlantic Ocean. *Nature* 421: 354-357.

Gustafsson M, Rayner D and Chen D. (2010) Extreme rainfall events in southern Sweden: where does the moisture come from? *Tellus A* 62: 605-616.

Häggi C, Sawakuchi AO, Chiessi CM, et al. (2016) Origin, transport and deposition of leaf-wax biomarkers in the Amazon Basin and the adjacent Atlantic. *Geochimica et Cosmochimica Acta* 192: 149-165.

Hammarlund D, Barnekow L, Birks HJB, et al. (2002) Holocene changes in atmospheric circulation recorded in the oxygen-isotope stratigraphy of lacustrine carbonates from northern Sweden. *The Holocene* 12: 339-351.

Hammarlund D, Björck S, Buchardt B, et al. (2003) Rapid hydrological changes during the Holocene revealed by stable isotope records of lacustrine carbonates from Lake Igelsjön, southern Sweden. *Quaternary Science Reviews* 22: 353-370.

Hammond N. (1972) *A History of Macedonia. Vol. I.*: Oxford Univ. Press.

Harrison SP, Prentice IC and Bartlein PJ. (1992) Influence of insolation and glaciation on atmospheric circulation in the North Atlantic sector: Implications of general circulation model experiments for the Late Quaternary climatology of Europe. *Quaternary Science Reviews* 11: 283-299.

Harris WV. (2013) Defining and Detecting Mediterranean Deforestation, 800BCE to 700CE. *The Ancient Mediterranean Environment between Science and History.* Brill, 173-194.

Haug GH, Hughen KA, Sigman DM, et al. (2001) Southward Migration of the Intertropical Convergence Zone Through the Holocene. *Science* 293: 1304-1308.

Hays JD, Imbrie J and Shackleton NJ. (1976) Variations in the Earth's Orbit: Pacemaker of the Ice Ages. *Science* 194: 1121-1132.

References

Hedges JI and Keil RG. (1995) Sedimentary organic matter preservation: an assessment and speculative synthesis. *Marine Chemistry* 49: 81-115.

Helliker BR and Ehleringer JR. (2000) Establishing a grassland signature in veins: ^{18}O in the leaf water of C_3 and C_4 grasses. *Proceedings of the National Academy of Sciences of the United States of America* 97: 7894-7898.

Hellström C. (2005) Atmospheric conditions during extreme and non-extreme precipitation events in Sweden. *International Journal of Climatology* 25: 631-648.

Herold M and Lohmann G. (2009) Eemian tropical and subtropical African moisture transport: an isotope modelling study. *Climate Dynamics* 33: 1075-1088.

Herren P-A, Eichler A, Machguth H, et al. (2013) The onset of Neoglaciation 6000 years ago in western Mongolia revealed by an ice core from the Tsambagarav mountain range. *Quaternary Science Reviews* 69: 59-68.

Heslop-Harrison JS. (2011) Atlas of the potential vegetation of Ethiopia. *Annals of Botany* 107: vi-vii.

Hodell DA, Curtis JH and Brenner M. (1995) Possible role of climate in the collapse of Classic Maya civilization. *Nature* 375: 391-394.

Höfle S, Rethemeyer J, Mueller CW, et al. (2013) Organic matter composition and stabilization in a polygonal tundra soil of the Lena Delta. *Biogeosciences* 10: 3145-3158.

Hoefs J. (2008) *Stable isotope geochemistry*: Springer Science & Business Media.

Holdsworth G, Fogarasi S and Krouse HR. (1991) Variation of the stable isotopes of water with altitude in the Saint Elias Mountains of Canada. *Journal of Geophysical Research: Atmospheres* 96: 7483-7494.

Holtvoeth J, Rushworth D, Copsey H, et al. (2016) Improved end-member characterisation of modern organic matter pools in the Ohrid Basin (Albania, Macedonia) and evaluation of new palaeoenvironmental proxies. *Biogeosciences* 13: 795-816.

Holtvoeth J, Vogel H, Wagner B, et al. (2010) Lipid biomarkers in Holocene and glacial sediments from ancient Lake Ohrid (Macedonia, Albania). *Biogeosciences* 7: 3473-3489.

Hopmans EC, Weijers JWH, Schefuß E, et al. (2004) A novel proxy for terrestrial organic matter in sediments based on branched and isoprenoid tetraether lipids. *Earth and Planetary Science Letters* 224: 107-116.

Hou J, D’Andrea WJ and Huang Y. (2008) Can sedimentary leaf waxes record D/H ratios of continental precipitation? Field, model, and experimental assessments. *Geochimica et Cosmochimica Acta* 72: 3503-3517.

Hou J, D’Andrea WJ, MacDonald D, et al. (2007) Hydrogen isotopic variability in leaf waxes among terrestrial and aquatic plants around Blood Pond, Massachusetts (USA). *Organic Geochemistry* 38: 977-984.

Huguet A, Fosse C, Metzger P, et al. (2010) Occurrence and distribution of non-extractable glycerol dialkyl glycerol tetraethers in temperate and tropical podzol profiles. *Organic Geochemistry* 41: 833-844.

Huguet C, Schimmelmann A, Thunell R, et al. (2007) A study of the TEX_{86} paleothermometer in the water column and sediments of the Santa Barbara Basin, California. *Paleoceanography* 22: PA3203.

Hurrell JW, Kushnir Y, Ottersen G, et al. (2013) An Overview of the North Atlantic Oscillation. *The North Atlantic Oscillation: Climatic Significance and Environmental Impact.* American Geophysical Union, 1-35.

IAEA/WMO: Global Network of Isotopes in Precipitation. The GNIP Database http://isohis.iaea.org /, last access: 12 August 2016.

Jessen CA, Solignac S, Nørgaard-Pedersen N, et al. (2011) Exotic pollen as an indicator of variable atmospheric circulation over the Labrador Sea region during the mid to late Holocene. *Journal of Quaternary Science* 26: 286-296.

Joannin S, Brugiapaglia E, de Beaulieu JL, et al. (2012) Pollen-based reconstruction of Holocene vegetation and climate in southern Italy: the case of Lago Trifoglietti. *Clim. Past* 8: 1973-1996.
Johnsen SJ, Clausen HB, Dansgaard W, et al. (1997) The $\delta^{18}O$ record along the Greenland Ice Core Project deep ice core and the problem of possible Eemian climatic instability. *Journal of Geophysical Research: Oceans* 102: 26397-26410.
Jonasson C and Nyberg R. (1999) The Rainstorm of August 1998 in the Abisko Area, Northern Sweden: Preliminary Report on Observations of Erosion and Sediment Transport. *Geografiska Annaler: Series A, Physical Geography* 81: 387-390.
Jonsson CE, Andersson S, Rosqvist GC, et al. (2010) Reconstructing past atmospheric circulation changes using oxygen isotopes in lake sediments from Sweden. *Clim. Past* 6: 49-62.
Jonsson CE, Leng MJ, Rosqvist GC, et al. (2009) Stable oxygen and hydrogen isotopes in sub-Arctic lake waters from northern Sweden. *Journal of Hydrology* 376: 143-151.
Junginger A, Roller S, Olaka LA, et al. (2014) The effects of solar irradiation changes on the migration of the Congo Air Boundary and water levels of paleo-Lake Suguta, Northern Kenya Rift, during the African Humid Period (15–5 ka BP). *Palaeogeography, Palaeoclimatology, Palaeoecology* 396: 1-16.
Jung SJA, Davies GR, Ganssen GM, et al. (2004) Stepwise Holocene aridification in NE Africa deduced from dust-borne radiogenic isotope records. *Earth and Planetary Science Letters* 221: 27-37.
Kaiser T and Voytek B. (1983) Sedentism and economic change in the Balkan Neolithic. *Journal of Anthropological Archaeology* 2: 323-353.
Kallel N, Paterne M, Labeyrie L, et al. (1997) Temperature and salinity records of the Tyrrhenian Sea during the last 18,000 years. *Palaeogeography, Palaeoclimatology, Palaeoecology* 135: 97-108.
Karlén W and Kuylenstierna J. (1996) On solar forcing of Holocene climate: evidence from Scandinavia. *The Holocene* 6: 359-365.
Kebede S and Travi Y. (2012) Origin of the $\delta^{18}O$ and $\delta^{2}H$ composition of meteoric waters in Ethiopia. *Quaternary International* 257: 4-12.
Keeling CD. (1979) The Suess effect: ^{13}Carbon-^{14}Carbon interrelations. *Environment International* 2: 229-300.
Kendall C and Caldwell EA. (1998) Chapter 2 - Fundamentals of Isotope Geochemistry. *Isotope Tracers in Catchment Hydrology.* Amsterdam: Elsevier, 51-86.
Kerr RA. (2000) A North Atlantic Climate Pacemaker for the Centuries. *Science* 288: 1984-1985.
Killops S, Killops V, Killops S, et al. (2004a) Carbon, the Earth and Life. *Introduction to Organic Geochemistry.* Blackwell Publishing Ltd., 1-29.
Killops S, Killops V, Killops S, et al. (2004b) Chemical Composition of Organic Matter. *Introduction to Organic Geochemistry.* Blackwell Publishing Ltd., 30-70.
Kim J-H, Schouten S, Hopmans EC, et al. (2008) Global sediment core-top calibration of the TEX_{86} paleothermometer in the ocean. *Geochimica et Cosmochimica Acta* 72: 1154-1173.
Knight JR, Allan RJ, Folland CK, et al. (2005) A signature of persistent natural thermohaline circulation cycles in observed climate. *Geophysical Research Letters* 32: L20708.
Knudsen MF, Seidenkrantz M-S, Jacobsen BH, et al. (2011) Tracking the Atlantic Multidecadal Oscillation through the last 8,000 years. *Nature Communications* 2: 178.
Kobashi T, Severinghaus JP, Brook EJ, et al. (2007) Precise timing and characterization of abrupt climate change 8200 years ago from air trapped in polar ice. *Quaternary Science Reviews* 26: 1212-1222.
Körner C. (1998) A re-assessment of high elevation treeline positions and their explanation. *Oecologia* 115: 445-459.
Kokkinidou D and Trantalidou K. (1991) Neolithic and Bronze Age Settlement in Western Macedonia. *Annual of the British School at Athens* 86: 93-106.

References

Kotthoff U, Koutsodendris A, Pross J, et al. (2011) Impact of Lateglacial cold events on the northern Aegean region reconstructed from marine and terrestrial proxy data. *Journal of Quaternary Science* 26: 86-96.

Kotthoff U, Müller UC, Pross J, et al. (2008) Lateglacial and Holocene vegetation dynamics in the Aegean region: an integrated view based on pollen data from marine and terrestrial archives. *The Holocene* 18: 1019-1032.

Kröpelin S, Verschuren D, Lézine A-M, et al. (2008) Climate-Driven Ecosystem Succession in the Sahara: The Past 6000 Years. *Science* 320: 765-768.

Kuhnert H, Kuhlmann H, Mohtadi M, et al. (2014) Holocene tropical western Indian Ocean sea surface temperatures in covariation with climatic changes in the Indonesian region. *Paleoceanography* 29: 423-437.

Kumar R. (2011) Neoglaciation. In: Singh VP, Singh P and Haritashya UK (eds) *Encyclopedia of Snow, Ice and Glaciers.* Dordrecht: Springer Netherlands, 775-775.

Laaksonen, K., (1976) The dependence of mean air temperature upon latitude and altitude in Fennoscandia (1921-1950). *Annales Academiae Scientiarium Fennice* 119 (Series AIII): 5-19.

Lamy F, Arz HW, Bond GC, et al. (2006) Multicentennial-scale hydrological changes in the Black Sea and northern Red Sea during the Holocene and the Arctic/North Atlantic Oscillation. *Paleoceanography* 21: PA1008.

Lashof and DA, DeAngelo BJ, Saleska and SR, et al. (1997) Terrestrial ecosystem feedbacks to global climate change. *Annual Review of Energy and the Environment* 22: 75-118.

Leaman KD and Schott FA. (1991) Hydrographic Structure of the Convection Regime in the Gulf of Lions: Winter 1987. *Journal of Physical Oceanography* 21: 575-598.

Leeming R, Ball A, Ashbolt N, et al. (1996) Using faecal sterols from humans and animals to distinguish faecal pollution in receiving waters. *Water Research* 30: 2893-2900.

LeGrande AN and Schmidt GA. (2006) Global gridded data set of the oxygen isotopic composition in seawater. *Geophysical Research Letters* 33: L12604.

Leng MJ and Marshall JD. (2004) Palaeoclimate interpretation of stable isotope data from lake sediment archives. *Quaternary Science Reviews* 23: 811-831.

Levin NE, Zipser EJ and Cerling TE. (2009) Isotopic composition of waters from Ethiopia and Kenya: Insights into moisture sources for eastern Africa. *Journal of Geophysical Research: Atmospheres* 114: D23306.

Lézine A-M, Casanova J and Hillaire-Marcel C. (1990) Across an early Holocene humid phase in western Sahara: Pollen and isotope stratigraphy. *Geology* 18: 264-267.

Liepert BG and Previdi M. (2009) Do Models and Observations Disagree on the Rainfall Response to Global Warming? *Journal of Climate* 22: 3156-3166.

Lima ALC, Farrington JW and Reddy CM. (2005) Combustion-Derived Polycyclic Aromatic Hydrocarbons in the Environment—A Review. *Environmental Forensics* 6: 109-131.

Liu W, Huang Y, An Z, et al. (2005) Summer monsoon intensity controls C_4/C_3 plant abundance during the last 35 ka in the Chinese Loess Plateau: Carbon isotope evidence from bulk organic matter and individual leaf waxes. *Palaeogeography, Palaeoclimatology, Palaeoecology* 220: 243-254.

Liu X, Rendle-Bühring R, Kuhlmann H, et al. (2017) Two phases of the Holocene East African Humid Period: Inferred from a high-resolution geochemical record off Tanzania. *Earth and Planetary Science Letters* 460: 123-134.

Liu Y, Beckingham B, Ruegner H, et al. (2013) Comparison of Sedimentary PAHs in the Rivers of Ammer (Germany) and Liangtan (China): Differences between Early- and Newly-Industrialized Countries. *Environmental Science & Technology* 47: 701-709.

Liu Z, Zhu J, Rosenthal Y, et al. (2014) The Holocene temperature conundrum. *Proceedings of the National Academy of Sciences* 111: E3501-E3505.

MacDonald GM, Edwards TWD, Moser KA, et al. (1993) Rapid response of treeline vegetation and lakes to past climate warming. *Nature* 361: 243-246.

Maffei M. (1996) Chemotaxonomic significance of leaf wax alkanes in the gramineae. *Biochemical Systematics and Ecology* 24: 53-64.

Maffei M, Badino S, Bossi S (2004) Chemotaxonomic significance of leaf wax *n*-alkanes in the Pinales (Coniferales). *Journal of Biological Research* 1: 3-19.

Magny M, Vannière B, Zanchetta G, et al. (2009) Possible complexity of the climatic event around 4300—3800 cal. BP in the central and western Mediterranean. *The Holocene* 19: 823-833.

Mahajan S, Zhang R and Delworth TL. (2011) Impact of the Atlantic Meridional Overturning Circulation (AMOC) on Arctic Surface Air Temperature and Sea Ice Variability. *Journal of Climate* 24: 6573-6581.

Majoube M. (1971) Fractionnement en oxygene-18 et en deuterium entre l'eau et sa vapeur. *J. Chim. phys* 68: 1423-1436.

Marcott SA, Shakun JD, Clark PU, et al. (2013) A Reconstruction of Regional and Global Temperature for the Past 11,300 Years. *Science* 339: 1198-1201.

Marini C and Frankignoul C. (2014) An attempt to deconstruct the Atlantic Multidecadal Oscillation. *Climate Dynamics* 43: 607-625.

Marinova E, Tonkov S, Bozilova E, et al. (2012) Holocene anthropogenic landscapes in the Balkans: the palaeobotanical evidence from southwestern Bulgaria. *Vegetation History and Archaeobotany* 21: 413-427.

Marshall J, Kushnir Y, Battisti D, et al. (2001) North Atlantic climate variability: phenomena, impacts and mechanisms. *International Journal of Climatology* 21: 1863-1898.

Martin WJ, Ravi Subbiah MT, Kottke BA, et al. (1973) Nature of fecal sterols and intestinal bacterial flora. *Lipids* 8: 208-215.

Masi A, Sadori L and Zanchetta G. (2013) Climatic interpretation of carbon isotope content of Mid-Holocene archaeological charcoals from eastern Anatolia. *Quaternary International* 303: 64-72.

Mattfeld J. (1927) Aus Wald und Macchie in Griechenland. *Mitt. Deutsch. Dendrol. Gess.* 38: 106–151.

Matthews JA and Briffa KR. (2005) THE 'LITTLE ICE AGE': RE-EVALUATION OF AN EVOLVING CONCEPT. *Geografiska Annaler: Series A, Physical Geography* 87: 17-36.

Mayewski PA, Meeker LD, Twickler MS, et al. (1997) Major features and forcing of high-latitude northern hemisphere atmospheric circulation using a 110,000-year-long glaciochemical series. *Journal of Geophysical Research: Oceans* 102: 26345-26366.

Mayewski PA, Rohling EE, Curt Stager J, et al. (2004) Holocene climate variability. *Quaternary Research* 62: 243-255.

McCarroll D and Loader NJ. (2004) Stable isotopes in tree rings. *Quaternary Science Reviews* 23: 771-801.

McInerney FA, Helliker BR and Freeman KH. (2011) Hydrogen isotope ratios of leaf wax *n*-alkanes in grasses are insensitive to transpiration. *Geochimica et Cosmochimica Acta* 75: 541-554.

Meehl GA, Washington WM, Collins WD, et al. (2005) How Much More Global Warming and Sea Level Rise? *Science* 307: 1769-1772.

Meyer-Jacob et al., (in review) Lake ontogeny and regional Holocene climate and landscape changes in the first biogeochemical record of the subarctic lake Torneträsk, N Fennoscandia.

Meyers PA. (1997) Organic geochemical proxies of paleoceanographic, paleolimnologic, and paleoclimatic processes. *Organic Geochemistry* 27: 213-250.

Meyers PA and Ishiwatari R. (1993) Lacustrine organic geochemistry—an overview of indicators of organic matter sources and diagenesis in lake sediments. *Organic Geochemistry* 20: 867-900.

References

Michener R and Lajtha K. (2008) *Stable isotopes in ecology and environmental science*: John Wiley & Sons.

Milankovitch M. (1941) *Kanon der Erdebestrahlung und seine Anwendung auf das Eiszeitenproblem*: Königlich Serbische Akademie.

Miller GH, Alley RB, Brigham-Grette J, et al. (2010a) Arctic amplification: can the past constrain the future? *Quaternary Science Reviews* 29: 1779-1790.

Miller GH, Brigham-Grette J, Alley RB, et al. (2010b) Temperature and precipitation history of the Arctic. *Quaternary Science Reviews* 29: 1679-1715.

Mitchell, T. D. and Jones, P. D. (2005) An improved method of constructing a database of monthly climate observations and associated high-resolution grids. *Int. J. Climatol*. 25: 693-712.

Mitrevski D. (2009a) Bay of the Bones, Archaeological sites, Cultural heritage protection office, Skopje, 61.

Mitrevski D. (2009b) Vardarski Rid, Archaeological sites, Cultural heritage protection office, Skopje, 62-65.

MØller JJ. (1987) Shoreline relation and prehistoric settlement in northern Norway. Norsk Geografisk Tidsskrift - *Norwegian Journal of Geography* 41: 45-60.

Morrissey A, Scholz CA and Russell JM. (2017) Late Quaternary TEX_{86} paleotemperatures from the world's largest desert lake, Lake Turkana, Kenya. *Journal of Paleolimnology*: 1-15.

Moulin C, Lambert CE, Dulac F, et al. (1997) Control of atmospheric export of dust from North Africa by the North Atlantic Oscillation. *Nature* 387: 691.

Nederbragt AJ and Thurow J. (2005) Geographic coherence of millennial-scale climate cycles during the Holocene. *Palaeogeography, Palaeoclimatology, Palaeoecology* 221: 313-324.

Nesje A, Matthews JA, Dahl SO, et al. (2001) Holocene glacier fluctuations of Flatebreen and winter-precipitation changes in the Jostedalsbreen region, western Norvay, based on glaciolacustrine sediment records. *The Holocene* 11: 267-280.

O'Leary MH. (1988) Carbon Isotopes in Photosynthesis. *BioScience* 38: 328-336.

Okajima H, Xie S-P and Numaguti A. (2003) Interhemispheric Coherence of Tropical Climate Variability: Effect of the Climatological ITCZ. *Journal of the Meteorological Society of Japan. Ser. II* 81: 1371-1386.

Oreskes N. (2004) The Scientific Consensus on Climate Change. *Science* 306: 1686-1686.

Ottera OH, Bentsen M, Drange H, et al. (2010) External forcing as a metronome for Atlantic multidecadal variability. *Nature Geosci* 3: 688-694.

Panagiotopoulos K, Aufgebauer A, Schäbitz F, et al. (2013) Vegetation and climate history of the Lake Prespa region since the Lateglacial. *Quaternary International* 293: 157-169.

Pedentchouk N, Sumner W, Tipple B, et al. (2008) $\delta^{13}C$ and δD compositions of *n*-alkanes from modern angiosperms and conifers: An experimental set up in central Washington State, USA. *Organic Geochemistry* 39: 1066-1071.

Peristykh AN and Damon PE. (2003) Persistence of the Gleissberg 88-year solar cycle over the last∼ 12,000 years: Evidence from cosmogenic isotopes. *Journal of Geophysical Research: Space Physics* 108.

Peters KE, Walters CC and Moldowan JM. (2005) *The biomarker guide*: Cambridge University Press.

Peterse F, van der Meer J, Schouten S, et al. (2012) Revised calibration of the MBT–CBT paleotemperature proxy based on branched tetraether membrane lipids in surface soils. *Geochimica et Cosmochimica Acta* 96: 215-229.

Peyron O, Goring S, Dormoy I, et al. (2011) Holocene seasonality changes in the central Mediterranean region reconstructed from the pollen sequences of Lake Accesa (Italy) and Tenaghi Philippon (Greece). *The Holocene* 21: 131-146.

Piva A, Asioli A, Trincardi F, et al. (2008) Late-Holocene climate variability in the Adriatic Sea (Central Mediterranean). *The Holocene* 18: 153-167.

Polyakov IV, Alexeev VA, Bhatt US, et al. (2010) North Atlantic warming: patterns of long-term trend and multidecadal variability. *Climate Dynamics* 34: 439-457.

Poto L, Gabrieli J, Crowhurst SJ, et al. (2013) The first continuous Late Glacial – Holocene peat bog multi-proxy record from the Dolomites (NE Italian Alps). *Quaternary International* 306: 71-79.

Poulos SE, Drakopoulos PG and Collins MB. (1997) Seasonal variability in sea surface oceanographic conditions in the Aegean Sea (Eastern Mediterranean): an overview. *Journal of Marine Systems* 13: 225-244.

Powers L, Werne JP, Vanderwoude AJ, et al. (2010) Applicability and calibration of the TEX_{86} paleothermometer in lakes. *Organic Geochemistry* 41: 404-413.

Powers LA, Werne JP, Johnson TC, et al. (2004) Crenarchaeotal membrane lipids in lake sediments: A new paleotemperature proxy for continental paleoclimate reconstruction? *Geology* 32: 613-616.

Poynter JG, Farrimond P, Robinson N, et al. (1989) Aeolian-Derived Higher Plant Lipids in the Marine Sedimentary Record: Links with Palaeoclimate. In: Leinen M and Sarnthein M (eds). *Paleoclimatology and Paleometeorology: Modern and Past Patterns of Global Atmospheric Transport.* Dordrecht: Springer Netherlands, 435-462.

Prabu, P.C., Wondimu, L., Tesso, M., 2010. Assessment of water quality of Huluka and Alaltu rivers of Ambo, Ethiopia. *Journal of Agricultural Science and Technology* 13: 131–138.

Rahmstorf S. (2003a) Thermohaline circulation: The current climate. *Nature* 421: 699-699.

Rahmstorf S. (2003b) Timing of abrupt climate change: A precise clock. *Geophysical Research Letters* 30: 1510.

Rayner D, Hirschi JJM, Kanzow T, et al. (2011) Monitoring the Atlantic meridional overturning circulation. Deep Sea Research Part II: *Topical Studies in Oceanography* 58: 1744-1753.

Readman JW, Mantoura RF and Rhead MM. (1987) A record of polycyclic aromatic hydrocarbon (PAH) pollution obtained from accreting sediments of the Tamar Estuary, U.K.: evidence for non-equilibrium behaviour of PAH. *Sci Total Environ* 66: 73-94.

Reimer, P.J., Baillie, M.G.L., Bard, E., Bayliss, A., Beck, J.W., Blackwell, P.G., Bronk Ramsey, C., Buck, C.E., Burr, G.S., Edwards, R.L., Friedrich, M., Grootes, P.M., Guilderson, T.P., Hajdas, I., Hea-ton, T.J., Hogg, A.G., Hughen, K.A., Kaiser, K.F., Kromer, B., McCormac, F.G., Manning, S.W., Reimer, R.W., Richards, D.A., Southon, J.R., Talamo, S., Turney, C.S.M., van der Plicht, J., Weyhenmeyer, C.E., (2009): IntCal09 and Marine09 radiocarbon age calibration curves, 0-50,000 years cal BP. - *Radiocarbon* 51: 1111-1150

Renssen H, Seppä H, Crosta X, et al. (2012) Global characterization of the Holocene Thermal Maximum. *Quaternary Science Reviews* 48: 7-19.

Revel M, Ducassou E, Grousset FE, et al. (2010) 100,000 Years of African monsoon variability recorded in sediments of the Nile margin. *Quaternary Science Reviews* 29: 1342-1362.

Richerson PJ, Boyd R and Bettinger RL. (2001) Was Agriculture Impossible during the Pleistocene but Mandatory during the Holocene? A Climate Change Hypothesis. *American Antiquity* 66: 387-411.

Rimbu N, Lohmann G, Kim JH, et al. (2003) Arctic/North Atlantic Oscillation signature in Holocene sea surface temperature trends as obtained from alkenone data. *Geophysical Research Letters* 30: 1280.

Rius D, Vannière B and Galop D. (2009) Fire frequency and landscape management in the northwestern Pyrenean piedmont, France, since the early Neolithic (8000 cal. BP). *The Holocene* 19: 847-859.

Roberts N, Jones MD, Benkaddour A, et al. (2008) Stable isotope records of Late Quaternary climate and hydrology from Mediterranean lakes: the ISOMED synthesis. *Quaternary Science Reviews* 27: 2426-2441.

Rodwell MJ, Rowell DP and Folland CK. (1999) Oceanic forcing of the wintertime North Atlantic Oscillation and European climate. *Nature* 398: 320-323.

Rosen AM. (1997) Environmental Change and Human Adaptational Failure at the End of the Early Bronze Age in the Southern Levant. In: Dalfes HN, Kukla G and Weiss H (eds) *Third Millennium BC Climate Change and Old World Collapse.* Berlin, Heidelberg: Springer Berlin Heidelberg, 25-38.

Rosenzweig C, Karoly D, Vicarelli M, et al. (2008) Attributing physical and biological impacts to anthropogenic climate change. *Nature* 453: 353-357.

Rosqvist GC, Leng MJ and Jonsson C. (2007) North Atlantic region atmospheric circulation dynamics inferred from a late-Holocene lacustrine carbonate isotope record, northern Swedish Lapland. *The Holocene* 17: 867-873.

Rosqvist G, Jonsson C, Yam R, et al. (2004) Diatom oxygen isotopes in pro-glacial lake sediments from northern Sweden: a 5000 year record of atmospheric circulation. Quaternary Science Reviews 23: 851-859.

Rothwell RG and Croudace Iw. (2015) Twenty Years of XRF Core Scanning Marine Sediments: What Do Geochemical Proxies Tell Us? In: Croudace IW and Rothwell RG (eds) *Micro-XRF Studies of Sediment Cores: Applications of a non-destructive tool for the environmental sciences.* Dordrecht: Springer Netherlands, 25-102.

Rowell DP, Folland CK, Maskell K, et al. (1995) Variability of summer rainfall over tropical north Africa (1906–92): Observations and modelling. *Quarterly Journal of the Royal Meteorological Society* 121: 669-704.

Rozanski K, Araguás-Araguás L and Gonfiantini R. (1993) Isotopic Patterns in Modern Global Precipitation. *Climate Change in Continental Isotopic Records.* American Geophysical Union, 1-36.

Rueda G, Rosell-Melé A, Escala M, et al. (2009) Comparison of instrumental and GDGT-based estimates of sea surface and air temperatures from the Skagerrak. *Organic Geochemistry* 40: 287-291.

Ryder JM and Thomson B. (1986) Neoglaciation in the southern Coast Mountains of British Columbia: chronology prior to the late Neoglacial maximum. *Canadian Journal of Earth Sciences* 23: 273-287.

Sachse D, Billault I, Bowen GJ, et al. (2012) Molecular Paleohydrology: Interpreting the Hydrogen-Isotopic Composition of Lipid Biomarkers from Photosynthesizing Organisms. *Annual Review of Earth and Planetary Sciences* 40: 221-249.

Sachse D, Radke J and Gleixner G. (2004) Hydrogen isotope ratios of recent lacustrine sedimentary *n*-alkanes record modern climate variability. *Geochimica et Cosmochimica Acta* 68: 4877-4889.

Sadori L and Giardini M. (2007) Charcoal analysis, a method to study vegetation and climate of the Holocene: The case of Lago di Pergusa (Sicily, Italy). *Geobios* 40: 173-180.

Sadori L and Giardini M. (2008) Environmental history in the Mediterranean basin: microcharcoal as a tool to disentangle human impact and climate change. In: Fiorentino G., Magri, D., editors. Charcoals from the Past: Cultural and Palaeoenvironmental Implications. BAR International Series 1807, 229-236.

Sadori L, Giardini M, Gliozzi E, et al. (2015a) Vegetation, climate and environmental history of the last 4500 years at lake Shkodra (Albania/Montenegro). *The Holocene* 25: 435-444.

Sadori L, Giardini M, Masi A, et al. (2016) Climate, environment and society in southern Italy during the last 2000 years. A review of the environmental, historical and archaeological evidence. *Quaternary Science Reviews* 136: 173-188.

Sadori L, Giraudi C, Petitti P and Ramrath A. (2004) Human impact at Lago di Mezzano (central Italy) during the Bronze Age: a multidisciplinary approach. *Quaternary International* 113: 5-17.

Sadori L, Jahns S and Peyron O. (2011) Mid-Holocene vegetation history of the central Mediterranean. *The Holocene* 21: 117-129.

Sadori L, Masi A and Ricotta C. (2015b) Climate driven past fires in central Sicily. *Plant Biosystems* 149: 166-173.

References

Sadori L and Narcisi B. (2001) The Postglacial record of environmental history from Lago di Pergusa, Sicily. *The Holocene* 11: 655-671.

Sadori L, Ortu E, Peyron O, et al. (2013) The last 7 millennia of vegetation and climate changes at Lago di Pergusa (central Sicily, Italy). *Climate of the Past* 9: 1969–1984.

SAHRA (2014), 'Isotopes & Hydrology'. URL: http://web.sahra.arizona.edu/programs/isotopes/oxygen.html#4

Sander LC and Wise SA. (1997) *Polycyclic aromatic hydrocarbon structure index*: US Department of Commerce, Technology Administration, National Institute of Standards and Technology Gaithersburg, MD.

Sanders G, Jones KC, Hamilton-Taylor J, et al. (1995) PCB and PAH fluxes to a dated UK peat core. *Environmental Pollution* 89: 17-25.

Sauer PE, Eglinton TI, Hayes JM, et al. (2001) Compound-specific D/H ratios of lipid biomarkers from sediments as a proxy for environmental and climatic conditions. *Geochimica et Cosmochimica Acta* 65: 213-222.

Schefuß E, Ratmeyer V, Stuut J-BW, et al. (2003) Carbon isotope analyses of *n*-alkanes in dust from the lower atmosphere over the central eastern Atlantic. *Geochimica et Cosmochimica Acta* 67: 1757-1767.

Schefuß E, Schouten S and Schneider RR. (2005) Climatic controls on central African hydrology during the past 20,000 years. *Nature* 437: 1003-1006.

Schilman B, Bar-Matthews M, Almogi-Labin A, et al. (2001) Global climate instability reflected by Eastern Mediterranean marine records during the late Holocene. *Palaeogeography, Palaeoclimatology, Palaeoecology* 176: 157-176.

Schimmelmann A, Sessions AL and Mastalerz M. (2006) Hydrogen isotopic (D/H) composition of organic matter during diagenesis and thermal maturation. *Annu. Rev. Earth Planet. Sci.* 34: 501-533.

Shindell DT, Schmidt GA, Mann ME, et al. (2001) Solar Forcing of Regional Climate Change During the Maunder Minimum. *Science* 294: 2149-2152.

Schouten S, Hopmans EC, Forster A, et al. (2003) Extremely high sea-surface temperatures at low latitudes during the middle Cretaceous as revealed by archaeal membrane lipids. *Geology* 31: 1069-1072.

Schouten S, Hopmans EC, Schefuß E, et al. (2002) Distributional variations in marine crenarchaeotal membrane lipids: a new tool for reconstructing ancient sea water temperatures? *Earth and Planetary Science Letters* 204: 265-274.

Schouten S, Hopmans EC and Sinninghe Damsté JS. (2013) The organic geochemistry of glycerol dialkyl glycerol tetraether lipids: A review. *Organic Geochemistry* 54: 19-61.

Sejrup HP, Seppä H, McKay NP, et al. North Atlantic-Fennoscandian Holocene climate trends and mechanisms. *Quaternary Science Reviews* 147: 365-378.

Seppä H and Birks HJB. (2001) July mean temperature and annual precipitation trends during the Holocene in the Fennoscandian tree-line area: pollen-based climate reconstructions. *The Holocene* 11: 527-539.

Seppä H and Poska A. (2004) Holocene annual mean temperature changes in Estonia and their relationship to solar insolation and atmospheric circulation patterns. *Quaternary Research* 61: 22-31.

Shah VG, Hugh Dunstan R, Geary PM, et al. (2007) Evaluating potential applications of faecal sterols in distinguishing sources of faecal contamination from mixed faecal samples. *Water Research* 41: 3691-3700.

Shanahan TM, Hughen KA and Van Mooy BAS. (2013) Temperature sensitivity of branched and isoprenoid GDGTs in Arctic lakes. *Organic Geochemistry* 64: 119-128.

Shanahan TM, McKay NP, Hughen KA, et al. (2015) The time-transgressive termination of the African Humid Period. *Nature Geosci* 8: 140-144.

Shangcheng J. (1988) The climatic characteristics of the ITCZ all over the globe. *Acta Meteorologica Sinica* 2: 015.

Shemesh A, Rosqvist G, Rietti-Shati M, et al. (2001) Holocene climatic change in Swedish Lapland inferred from an oxygen-isotope record of lacustrine biogenic silica. *The Holocene* 11: 447-454.

Sinninghe Damsté JS, Ossebaar J, Schouten S, et al. (2008) Altitudinal shifts in the branched tetraether lipid distribution in soil from Mt. Kilimanjaro (Tanzania): Implications for the MBT/CBT continental palaeothermometer. *Organic Geochemistry* 39: 1072-1076.

Sinninghe Damsté JS, Rijpstra WIC, Hopmans EC, et al. (2002) Distribution of Membrane Lipids of Planktonic Crenarchaeota in the Arabian Sea. *Applied and Environmental Microbiology* 68: 2997-3002.

Sinninghe Damsté JS, Verschuren D, Ossebaar J, et al. (2011) A 25,000-year record of climate-induced changes in lowland vegetation of eastern equatorial Africa revealed by the stable carbon-isotopic composition of fossil plant leaf waxes. *Earth and Planetary Science Letters* 302: 236-246.

Slonosky VC, Jones PD and Davies TD. (2001) Atmospheric circulation and surface temperature in Europe from the 18th century to 1995. *International Journal of Climatology* 21: 63-75.

Sotiria K and Petkovski S. (2004) Lake Doiran – An overview of the current situation. *Greek Biotope/Wetland Centre (EKBY), Society for the Investigation and Conservation of Biodiversity and the Sustainable Development of Natural Ecosystems (BIOECO), Thermi*: 1–117.

Stocker T. (2014) *Climate change 2013: the physical science basis: Working Group I contribution to the Fifth assessment report of the Intergovernmental Panel on Climate Change*: Cambridge University Press.

Stockmarr J. (1971) Tables with spores used in absolute pollen analysis. *Pollen and Spores* 13: 614-621.

Stojanov R and Micevski E. (1989) Geology of Lake Doiran and its surrounding. *Contributions of the Macedonian Academy of Sciences and Arts, Section of Biological and Medical Sciences* 10: 37–52.

Strandberg G, Kjellström E, Poska A, et al. (2014) Regional climate model simulations for Europe at 6 and 0.2 k BP: sensitivity to changes in anthropogenic deforestation. *Clim. Past* 10: 661-680.

Stroeven AP, Fabel D, Harbor J, et al. (2002) Quantifying the erosional impact of the Fennoscandian ice sheet in the Torneträsk–Narvik corridor, northern Sweden, based on cosmogenic radionuclide data. *Geografiska Annaler: Series A, Physical Geography* 84: 275-287.

Stuiver M and Braziunas TF. (1989) Atmospheric ^{14}C and century-scale solar oscillations. *Nature* 338: 405-408.

Sugano M. (1967) Steroid-C^{14} Excretion in the Chickens Following Intravenous Administration of Cholesterol-4-C^{14} in Lipoprotein. *Agricultural and Biological Chemistry* 31: 378-381.

Sutton RT and Hodson DLR. (2005) Atlantic Ocean Forcing of North American and European Summer Climate. *Science* 309: 115-118.

Talbot M and Allen P. (1996) Lakes. *Sedimentary Environments: processes, facies and stratigraphy* 3: 83-124.

Talbot MR, Filippi ML, Jensen NB, et al. (2007) An abrupt change in the African monsoon at the end of the Younger Dryas. *Geochemistry, Geophysics, Geosystems* 8: *Q03005* .

Tegelaar EW, de Leeuw JW, Derenne S, et al. (1989) A reappraisal of kerogen formation. *Geochimica et Cosmochimica Acta* 53: 3103-3106.

Thienemann A. (1941) Leben und Umwelt. Leipzig

Thienemann M, Masi A, Kusch S, et al. (2017) Organic geochemical and palynological evidence for Holocene natural and anthropogenic environmental change at Lake Dojran (Macedonia/Greece). *The Holocene*: 27: 1103-1114.

Tierney JE and deMenocal PB. (2013) Abrupt Shifts in Horn of Africa Hydroclimate Since the Last Glacial Maximum. *Science* 342, Issue 6160: 843-846.

Tierney JE and Russell JM. (2009) Distributions of branched GDGTs in a tropical lake system: Implications for lacustrine application of the MBT/CBT paleoproxy. *Organic Geochemistry* 40: 1032-1036.

Tierney JE, Lewis SC, Cook BI, et al. (2011a) Model, proxy and isotopic perspectives on the East African Humid Period. *Earth and Planetary Science Letters* 307: 103-112.

Tierney JE, Pausata FSR and deMenocal PB. (2017) Rainfall regimes of the Green Sahara. *Science Advances* 3, no. 1: e1601503.

Tierney JE, Russell JM, Sinninghe Damsté JS, et al. (2011b) Late Quaternary behavior of the East African monsoon and the importance of the Congo Air Boundary. *Quaternary Science Reviews* 30: 798-807.

Tierney JE, Russell JM, Eggermont H, et al. (2010a) Environmental controls on branched tetraether lipid distributions in tropical East African lake sediments. *Geochimica et Cosmochimica Acta* 74: 4902-4918.

Tierney JE, Russell JM and Huang Y. (2010b) A molecular perspective on Late Quaternary climate and vegetation change in the Lake Tanganyika basin, East Africa. *Quaternary Science Reviews* 29: 787-800.

Tierney JE, Russell JM, Huang Y, et al. (2008) Northern Hemisphere Controls on Tropical Southeast African Climate During the Past 60,000 Years. *Science* 322: 252-255.

Tipple BJ and Pagani M. (2010) A 35 Myr North American leaf-wax compound-specific carbon and hydrogen isotope record: Implications for C_4 grasslands and hydrologic cycle dynamics. *Earth and Planetary Science Letters* 299: 250-262.

Trenberth KE and Caron JM. (2001) Estimates of Meridional Atmosphere and Ocean Heat Transports. *Journal of Climate* 14: 3433-3443.

Trigo RM, Osborn TJ and Corte-Real JM. (2002) The North Atlantic Oscillation influence on Europe: climate impacts and associated physical mechanisms. *Climate Research* 20: 9-17.

Turney C, Baillie M, Clemens S, et al. (2005) Testing solar forcing of pervasive Holocene climate cycles. *Journal of Quaternary Science* 20: 511-518.

Tzedakis PC. (2007) Seven ambiguities in the Mediterranean palaeoenvironmental narrative. *Quaternary Science Reviews* 26: 2042-2066.

Umer M, Lamb HF, Bonnefille R, et al. (2007) Late Pleistocene and Holocene vegetation history of the Bale Mountains, Ethiopia. *Quaternary Science Reviews* 26: 2229-2246.

Valsecchi V, Sanchez Goñi MF and Londeix L. (2012) Vegetation dynamics in the Northeastern Mediterranean region during the past 23 000 yr: insights from a new pollen record from the Sea of Marmara. *Clim. Past* 8: 1941-1956.

Van Andel TH and Runnels CN. (1995) The earliest farmers in Europe. *Antiquity* 69: 481-500.

Van der Merwe NJ and Medina E. (1991) The canopy effect, carbon isotope ratios and foodwebs in amazonia. *Journal of Archaeological Science* 18: 249-259.

Vannière B, Colombaroli D, Chapron E, et al. (2008) Climate versus human-driven fire regimes in Mediterranean landscapes: the Holocene record of Lago dell'Accesa (Tuscany, Italy). *Quaternary Science Reviews* 27: 1181-1196.

Velevski M, Hallmann B, Grubač B, et al. (2010) Important Bird Areas in Macedonia: Sites of Global and European Importance. *Acrocephalus*. 147: 181–282.

Verschuren D, Laird KR and Cumming BF. (2000) Rainfall and drought in equatorial east Africa during the past 1,100 years. *Nature* 403: 410-414.

Verschuren D, Sinninghe Damste JS, Moernaut J, et al. (2009) Half-precessional dynamics of monsoon rainfall near the East African Equator. *Nature* 462: 637-641.

Visbeck MH, Hurrell JW, Polvani L, et al. (2001) The North Atlantic Oscillation: Past, present, and future. *Proceedings of the National Academy of Sciences* 98: 12876-12877.

References

Vogel H, Wagner B and Rosén P. (2013) Lake Floor Morphology and Sediment Architecture of Lake Torneträsk, Northern Sweden. *Geografiska Annaler: Series A, Physical Geography* 95: 159-170.

Vogel H, Wagner B, Zanchetta G, et al. (2010) A paleoclimate record with tephrochronological age control for the last glacial-interglacial cycle from Lake Ohrid, Albania and Macedonia. *Journal of Paleolimnology* 44: 295-310.

Wagner B, et al. (in-review) Holocene evolution of the River Nile drainage system as revealed from the Lake Dendi sediment record, central Ethiopian highlands. *Global and Planetary Change.*

Wagner B, Lotter A, Nowaczyk N, et al. (2009) A 40,000-year record of environmental change from ancient Lake Ohrid (Albania and Macedonia). *Journal of Paleolimnology* 41: 407-430.

Wagner G, Beer J, Masarik J, et al. (2001) Presence of the solar de Vries cycle (-205 years) during the last ice age.

Walker MJC, Berkelhammer M, Björck S, et al. (2012) Formal subdivision of the Holocene Series/Epoch: a Discussion Paper by a Working Group of INTIMATE (Integration of ice-core, marine and terrestrial records) and the Subcommission on Quaternary Stratigraphy (International Commission on Stratigraphy). *Journal of Quaternary Science* 27: 649-659.

Walther G-R, Post E, Convey P, et al. (2002) Ecological responses to recent climate change. *Nature* 416: 389-395.

Wang C and Zhang L. (2013) Multidecadal Ocean Temperature and Salinity Variability in the Tropical North Atlantic: Linking with the AMO, AMOC, and Subtropical Cell. *Journal of Climate* 26: 6137-6162.

Wanner H, Beer J, Bütikofer J, et al. (2008) Mid- to Late Holocene climate change: an overview. *Quaternary Science Reviews* 27: 1791-1828.

Weber ME, Reichelt L, Kuhn G, et al. (2010) BMPix and PEAK tools: New methods for automated laminae recognition and counting—Application to glacial varves from Antarctic marine sediment. *Geochemistry, Geophysics, Geosystems* 11: Q0AA05.

Weijers JWH, Lim KLH, Aquilina A, et al. (2011) Biogeochemical controls on glycerol dialkyl glycerol tetraether lipid distributions in sediments characterized by diffusive methane flux. *Geochemistry, Geophysics, Geosystems* 12: Q10010.

Weijers JWH, Schefuß E, Schouten S, et al. (2007c) Coupled Thermal and Hydrological Evolution of Tropical Africa over the Last Deglaciation. *Science* 315: 1701-1704.

Weijers JWH, Schouten S, Sluijs A, et al. (2007a) Warm arctic continents during the Palaeocene–Eocene thermal maximum. *Earth and Planetary Science Letters* 261: 230-238.

Weijers JWH, Schouten S, Spaargaren OC, et al. (2006) Occurrence and distribution of tetraether membrane lipids in soils: Implications for the use of the TEX_{86} proxy and the BIT index. *Organic Geochemistry* 37: 1680-1693.

Weijers JWH, Schouten S, van den Donker JC, et al. (2007b) Environmental controls on bacterial tetraether membrane lipid distribution in soils. *Geochimica et Cosmochimica Acta* 71: 703-713.

Weiss H and Bradley RS. (2001) What Drives Societal Collapse? *Science* 291: 609-610.

Weldeab S, Lea DW, Schneider RR, et al. (2007) 155,000 Years of West African Monsoon and Ocean Thermal Evolution. *Science* 316: 1303-1307.

Weldeab S, Menke V and Schmiedl G. (2014) The pace of East African monsoon evolution during the Holocene. *Geophysical Research Letters* 41: 2014GL059361.

Wen N, Frankignoul C and Gastineau G. (2016) Active AMOC–NAO coupling in the IPSL-CM5A-MR climate model. *Climate Dynamics* 47: 2105-2119.

White S. (2011) *The Climate of Rebellion in the Early Modern Ottoman Empire*: Cambridge University Press.

Whitlock C and Millspaugh SH. (1996) Testing assumption of fire history studies: an examination of modern charcoal accumulation in Yellowstone National Park. The Holocene 6: 7–15.

References

Wick L, Lemcke G and Sturm M. (2003) Evidence of Lateglacial and Holocene climatic change and human impact in eastern Anatolia: high-resolution pollen, charcoal, isotopic and geochemical records from the laminated sediments of Lake Van, Turkey. The Holocene 13: 665-675.

Wilkie KMK, Chapligin B, Meyer H, et al. (2013) Modern isotope hydrology and controls on δD of plant leaf waxes at Lake El'gygytgyn, NE Russia. *Clim. Past* 9: 335-352.

Williams, S. D., Vivero, J. L., Spawls, S., Anteneh, S., and Ensermu, K. (2004) The Ethiopian Highlands, in: Hotspots Revisited: Earth´s Biologically Richest and Most Endangered Ecoregions, Mittermeier, R. A., Robles¬ Gil, P., Hoffmann, M., Pilgrim, J. D., Brooks, T. M., Mittermeier, C. G., and Fonseca, G. (eds.), 262-¬273, CEMEX, Mexico city, Mexico.

Willis KJ and Bennett KD. (1994) The Neolithic transition - fact or fiction? Palaeoecological evidence from the Balkans. *The Holocene* 4: 326-330.

Wilson R, Anchukaitis K, Briffa KR, et al. (2016) Last millennium northern hemisphere summer temperatures from tree rings: Part I: The long term context. *Quaternary Science Reviews* 134: 1-18.

Wirth SB, Glur L, Gilli A, et al. (2013) Holocene flood frequency across the Central Alps – solar forcing and evidence for variations in North Atlantic atmospheric circulation. *Quaternary Science Reviews* 80: 112-128.

Wuchter C, Schouten S, Wakeham SG, et al. (2005) Temporal and spatial variation in tetraether membrane lipids of marine Crenarchaeota in particulate organic matter: Implications for TEX_{86} paleothermometry. *Paleoceanography* 20: PA3013.

Xing L, Jiang Y, Yuan Z, et al. (2013) Holocene temperature records from the East China sea mud area southwest of the Cheju Island reconstructed by the $U_{37}^{K'}$ and TEX_{86} paleothermometers. *Journal of Ocean University of China* 12: 599-604.

Yang H and Leng Q. (2009) Molecular hydrogen isotope analysis of living and fossil plants—Metasequoia as an example. *Progress in Natural Science* 19: 901-912.

Zacharias I, Bertachas I, Skoulikidis N, et al. (2002) Greek Lakes: Limnological overview. *Lakes & Reservoirs: Research & Management* 7: 55-62.

Zhang X, Reed J, Wagner B, et al. (2014) Lateglacial and Holocene climate and environmental change in the northeastern Mediterranean region: diatom evidence from Lake Dojran (Republic of Macedonia/Greece). *Quaternary Science Reviews* 103: 51-66.

Zhang Z and Sachs JP. (2007) Hydrogen isotope fractionation in freshwater algae: I. Variations among lipids and species. *Organic Geochemistry* 38: 582-608.

Zhuang G, Brandon MT, Pagani M, et al. (2014) Leaf wax stable isotopes from Northern Tibetan Plateau: Implications for uplift and climate since 15 Ma. *Earth and Planetary Science Letters* 390: 186-198.

Zink K-G, Vandergoes MJ, Mangelsdorf K, et al. (2010) Application of bacterial glycerol dialkyl glycerol tetraethers (GDGTs) to develop modern and past temperature estimates from New Zealand lakes. *Organic Geochemistry* 41: 1060-1066.

Appendix

Torneträsk elemental data

Depth (cm)	Age yrs cal BP	Ca	Ti	Fe	Depth (cm)	Age yrs cal BP	Ca	Ti	Fe	Depth (cm)	Age yrs cal BP	Ca	Ti	Fe	Depth (cm)	Age yrs cal BP	Ca	Ti	Fe	Depth (cm)	Age yrs cal BP	Ca	Ti	Fe
0	-62	2058	1143	60180	13	96	3822	1998	85714	26	261	3624	1921	85870	39	438	3767	2105	90495	52	635	3951	2157	90155
0.2	-60	3169	1648	76683	13.2	99	3580	1826	82720	26.2	263	3231	1733	85464	39.2	441	3751	1943	89787	52.2	638	3850	2068	89765
0.4	-57	3012	1446	75299	13.4	101	3653	1820	82165	26.4	266	3448	1843	87286	39.4	444	3500	1860	88671	52.4	642	3794	1903	89115
0.6	-55	3175	1594	77101	13.6	104	3448	1862	84143	26.6	269	3510	1833	87508	39.6	447	3574	1814	89074	52.6	645	3957	1989	89447
0.8	-52	3735	2071	81190	13.8	106	3051	1565	79252	26.8	271	3489	1861	85133	39.8	450	3372	1865	88152	52.8	648	4139	2135	90425
1	-50	3662	1857	86451	14	108	3257	1658	81834	27	274	3145	1833	83003	40	453	3329	1895	87734	53	651	4476	2239	91943
1.2	-47	4002	2035	83988	14.2	111	3694	2021	84121	27.2	276	3681	2026	83254	40.2	455	3338	1919	86841	53.2	654	4687	2433	93669
1.4	-45	3941	2049	85093	14.4	113	3715	2147	85118	27.4	279	4049	1978	88639	40.4	458	3127	1784	87774	53.4	658	4681	2280	94457
1.6	-43	3825	2036	86523	14.6	116	3483	1951	81874	27.6	282	3420	1860	84674	40.6	461	3346	2000	88571	53.6	661	4370	2241	93891
1.8	-40	3889	2106	91069	14.8	118	4033	2042	85571	27.8	284	3460	1932	84016	40.8	464	3105	1690	88779	53.8	664	4682	2316	94539
2	-38	3362	1803	86880	15	121	3735	2112	84806	28	287	3347	1876	84674	41	467	3531	1997	89392	54	667	4751	2332	95946
2.2	-35	3222	1645	80110	15.2	123	3852	2066	86281	28.2	290	3135	1982	83855	41.2	470	3502	2037	90263	54.2	671	4370	2356	93018
2.4	-33	3169	1486	77185	15.4	126	4077	2186	87448	28.4	292	3132	1817	86964	41.4	473	3449	1918	86391	54.4	674	4363	2262	93082
2.6	-31	3487	1749	80283	15.6	128	3869	2105	86020	28.6	295	3363	1884	88007	41.6	476	3257	1878	87880	54.6	677	4337	2269	94493
2.8	-28	3513	1743	82686	15.8	131	3165	1510	82321	28.8	298	3595	1934	87522	41.8	479	3271	1861	86316	54.8	681	4327	2385	92687
3	-26	3432	1906	81274	16	133	3807	1914	84312	29	300	3310	1909	86975	42	482	3823	2233	89980	55	684	3723	2014	90856
3.2	-23	3948	1872	83757	16.2	136	2917	1558	80540	29.2	303	3463	1921	86294	42.2	485	3832	2100	90123	55.2	687	3552	1981	91350
3.4	-21	3677	1971	83349	16.4	138	3417	1719	82654	29.4	306	3664	1827	86074	42.4	488	3636	2040	88332	55.4	691	3706	1981	91282
3.6	-18	3897	1981	85557	16.6	141	3485	1970	85824	29.6	308	3640	1925	86909	42.6	490	3577	2078	90856	55.6	694	3746	2050	89445
3.8	-16	4738	2141	87966	16.8	143	3326	1979	84043	29.8	311	3302	2016	82964	42.8	493	3387	2081	87203	55.8	697	3928	2036	93413
4	-14	4345	2228	90088	17	146	3735	2063	86233	30	314	3421	1931	83979	43	496	3341	1919	88978	56	701	4387	2148	91153
4.2	-11	4815	2249	93051	17.2	148	3911	1920	85955	30.2	316	3613	1922	85385	43.2	499	3279	2131	88998	56.2	704	4447	2071	92408
4.4	-9	4750	2226	92007	17.4	151	3929	2171	86865	30.4	319	3418	1951	85152	43.4	502	3337	1912	89311	56.4	707	4271	2108	89948
4.6	-6	2998	1435	73670	17.6	153	3963	2034	89843	30.6	322	3440	1973	84387	43.6	505	3448	1974	91434	56.6	711	3922	1957	88120
4.8	-4	4223	2004	87726	17.8	156	4090	2011	85659	30.8	324	3146	1852	86741	43.8	508	3363	2008	89407	56.8	714	3663	2139	88300
5	-1	3768	1932	86111	18	158	4414	2274	90415	31	327	3261	1916	85500	44	511	3360	1949	88897	57	717	3515	2146	87285
5.2	1	3176	1802	80798	18.2	161	4144	1956	89152	31.2	330	3602	2052	87702	44.2	514	3465	1937	88674	57.2	721	3511	1905	87578
5.4	3	2673	1519	75969	18.4	163	3985	2069	87679	31.4	332	3413	1895	88654	44.4	517	3191	1808	89217	57.4	724	3548	1913	86810
5.6	6	2565	1474	77280	18.6	166	3958	1956	88352	31.6	335	3795	1810	87369	44.6	520	3469	1943	90617	57.6	727	3118	1811	86711
5.8	8	2664	1608	77904	18.8	168	3968	2176	89318	31.8	338	3504	1785	87265	44.8	523	3747	2155	90229	57.8	731	3350	1878	86983
6	11	2350	1392	68384	19	171	3917	2028	88570	32	341	3441	1825	85438	45	526	3672	2140	87642	58	734	3332	2014	89269
6.2	13	2214	1518	71762	19.2	173	3522	2003	85524	32.2	343	3672	2119	86120	45.2	529	3338	1969	87164	58.2	737	3369	2028	85330
6.4	15	2200	1407	73911	19.4	176	3265	1830	87374	32.4	346	4094	2192	86247	45.4	532	3371	2024	87026	58.4	741	3612	1997	85328
6.6	18	2313	1461	73331	19.6	178	3207	1620	83464	32.6	349	3532	2156	86664	45.6	535	3382	2166	87718	58.6	744	3159	1862	83048
6.8	20	1881	1375	73351	19.8	181	3613	1925	87249	32.8	351	3305	1739	85040	45.8	538	3499	1984	85215	58.8	748	3313	1838	84448
7	23	1590	1163	69871	20	184	3545	1898	85654	33	354	3620	1730	86387	46	541	3036	1727	82710	59	751	3169	1882	83291
7.2	25	2617	1616	77460	20.2	186	3587	1949	85815	33.2	357	3295	1922	84393	46.2	544	2902	1858	81104	59.2	755	2885	1627	77223
7.4	28	2933	1798	82451	20.4	189	3783	1993	85761	33.4	360	3256	1765	85370	46.4	547	3230	1814	83103	59.4	758	3026	1561	77709
7.6	30	3057	1560	83854	20.6	191	4328	2197	90620	33.6	362	3298	1819	86518	46.6	551	3426	1921	85204	59.6	761	2900	1559	74085
7.8	33	3049	1819	82407	20.8	194	3905	2111	88108	33.8	365	3646	2049	87020	46.8	554	3441	1991	84703	59.8	765	2922	1690	76415
8	35	3257	1947	83627	21	196	3716	1971	89315	34	368	3792	2143	87938	47	557	3387	1888	88634	60	768	2732	1585	75786
8.2	37	3511	1904	85790	21.2	199	4063	1943	86730	34.2	371	3446	1792	87966	47.2	560	3444	1947	88766	60.2	772	2869	1579	74993
8.4	40	3425	1807	83393	21.4	201	3943	2279	85445	34.4	373	3700	2049	89098	47.4	563	3662	2145	86671	60.4	775	3289	1761	78009
8.6	42	3241	1883	82055	21.6	204	4080	1997	86931	34.6	376	3751	2036	90154	47.6	566	3542	1962	88401	60.6	779	3290	1928	81199
8.8	45	3118	1695	84188	21.8	206	3807	2077	84558	34.8	379	3940	2008	91970	47.8	569	3566	2107	87868	60.8	782	2958	1638	80255
9	47	3445	1863	85049	22	209	3755	2030	83884	35	382	3807	2013	92896	48	572	3590	1968	87391	61	786	3242	1945	80259
9.2	50	3126	1650	81798	22.2	212	3136	1657	80664	35.2	385	3434	1828	88640	48.2	575	3691	2017	87991	61.2	789	2970	1552	78677
9.4	52	3547	1887	82458	22.4	214	3683	1909	84183	35.4	387	3588	2206	90452	48.4	578	3537	2004	85519	61.4	793	3068	1859	79065
9.6	54	3434	1721	81310	22.6	217	3466	1690	81985	35.6	390	3376	1871	86743	48.6	581	3781	2041	86963	61.6	796	3052	1766	78511
9.8	57	3716	2050	84601	22.8	219	3453	1915	83342	35.8	393	3545	2104	82309	48.8	584	3749	1936	88478	61.8	800	3296	1846	78452
10	59	4140	2056	90060	23	222	3444	1706	83089	36	396	3430	2153	85837	49	588	3758	2056	89156	62	803	3524	1924	80793
10.2	62	3213	1740	82706	23.2	224	3690	1881	86238	36.2	399	3569	1869	87142	49.2	591	3982	2282	90197	62.2	807	3277	1865	78884
10.4	64	3590	1956	83846	23.4	227	3847	1901	84570	36.4	401	3867	2214	88445	49.4	594	4030	2250	91675	62.4	810	3318	1741	78698
10.6	67	3377	1932	82083	23.6	230	3879	1800	87787	36.6	404	3664	1990	88109	49.6	597	3716	2058	89035	62.6	814	3147	1928	78810
10.8	69	3516	1887	84052	23.8	232	3890	2117	87637	36.8	407	3499	1972	87431	49.8	600	3822	2047	89092	62.8	817	2968	1633	75020
11	72	3319	1995	84613	24	235	3929	1951	89645	37	410	3704	1893	88774	50	603	3186	1846	85427	63	821	3295	2088	77955
11.2	74	3133	1715	78018	24.2	237	3927	2002	88929	37.2	413	3146	1891	86856	50.2	606	3449	1951	86111	63.2	824	3061	1678	76852
11.4	76	2771	1656	77344	24.4	240	4225	2117	88230	37.4	415	3380	1850	87269	50.4	610	3385	1867	87432	63.4	828	3221	1780	78742
11.6	79	2436	1686	73252	24.6	242	3943	1956	87879	37.6	418	3233	1917	86410	50.6	613	3625	1869	87521	63.6	831	3526	1944	82029
11.8	81	3180	1642	77879	24.8	245	3655	1953	84466	37.8	421	3284	2009	84710	50.8	616	3997	2152	88684	63.8	835	3536	1827	82475
12	84	3626	2010	84624	25	248	4222	2351	88672	38	424	2899	1857	83778	51	619	3845	2139	89053	64	838	3814	2084	84533
12.2	86	3643	1748	83678	25.2	250	3981	1968	89167	38.2	427	3087	1732	85742	51.2	622	3634	1956	87079	64.2	842	3762	2129	83060
12.4	89	3593	1797	83524	25.4	253	3776	1924	87292	38.4	430	3292	1889	88086	51.4	625	4011	2328	90223	64.4	846	3543	2029	81925
12.6	91	3292	1693	84450	25.6	255	3781	1962	87428	38.6	432	3481	1972	90642	51.6	629	3784	2064	87909	64.6	849	3699	2030	81311
12.8	94	3773	2066	84887	25.8	258	3750	1989	85307	38.8	435	3277	1970	89167	51.8	632	3644	2043	86556	64.8	853	3827	2025	82562

Appendix

Depth (cm)	Age yrs cal BP	Ca	Ti	Fe	Depth (cm)	Age yrs cal BP	Ca	Ti	Fe	Depth (cm)	Age yrs cal BP	Ca	Ti	Fe	Depth (cm)	Age yrs cal BP	Ca	Ti	Fe	Depth (cm)	Age yrs cal BP	Ca	Ti	Fe
65	856	3846	2205	82744	78	1101	4252	2172	86817	91	1369	4166	2201	92559	104	1658	5671	2567	94618	117	1966	4175	2104	87733
65.2	860	3807	2144	83514	78.2	1105	4570	2508	89375	91.2	1373	4243	2091	91479	104.2	1662	5650	2614	94932	117.2	1971	4129	2217	86575
65.4	863	4013	2073	86287	78.4	1109	4784	2333	89282	91.4	1378	4052	2101	87345	104.4	1667	5352	2351	94502	117.4	1976	4320	2162	87312
65.6	867	4148	2145	89276	78.6	1113	4156	2132	89258	91.6	1382	4050	1916	86937	104.6	1672	5407	2457	95582	117.6	1981	4256	2216	87377
65.8	871	4150	2112	88185	78.8	1117	3843	1996	86655	91.8	1386	3975	2070	87757	104.8	1676	5053	2191	94532	117.8	1986	4249	2167	86952
66	874	4087	2178	87258	79	1121	3866	1958	87174	92	1391	3834	2037	86295	105	1681	4902	2333	91170	118	1991	4235	1973	85093
66.2	878	3940	1968	84863	79.2	1125	4037	2064	87018	92.2	1395	3710	1974	86202	105.2	1685	4612	2174	86684	118.2	1996	3897	1991	83955
66.4	882	3634	2066	83669	79.4	1129	4005	2173	88947	92.4	1399	3697	1975	85215	105.4	1690	4365	2165	84775	118.4	2001	3869	2007	83251
66.6	885	3746	1947	82707	79.6	1133	4273	2418	87068	92.6	1403	3930	1960	85660	105.6	1695	4255	2023	87238	118.6	2005	4038	2169	84665
66.8	889	3541	1811	82175	79.8	1137	4200	2263	86117	92.8	1408	3745	2090	84306	105.8	1699	4188	1849	88786	118.8	2010	3909	2184	83604
67	892	3353	2009	80924	80	1141	4324	2132	85735	93	1412	4005	1942	85830	106	1704	4031	2003	86980	119	2015	4063	2124	83948
67.2	896	3502	2064	83381	80.2	1145	3961	1967	85451	93.2	1416	4126	2019	87046	106.2	1709	3874	2168	86536	119.2	2020	4036	2088	84095
67.4	900	3634	2007	83492	80.4	1149	4197	1945	88339	93.4	1421	4014	2016	85312	106.4	1713	4067	2174	85655	119.4	2025	4051	2028	84401
67.6	903	3657	1930	83168	80.6	1153	4163	2433	87767	93.6	1425	4250	2234	88770	106.6	1718	4096	2083	86189	119.6	2030	4061	2051	84777
67.8	907	3598	1892	82662	80.8	1157	4040	2182	87525	93.8	1429	4337	2322	90676	106.8	1723	4186	2020	85066	119.8	2035	4248	2208	85245
68	911	3556	2162	83282	81	1161	4015	2281	87503	94	1434	4434	2345	90459	107	1727	3829	2173	83125	120	2040	4380	2239	85852
68.2	914	3521	2141	81734	81.2	1165	4014	1973	88287	94.2	1438	4447	2281	89771	107.2	1732	3858	2006	84413	120.2	2045	4228	2157	85127
68.4	918	3453	1980	81827	81.4	1169	3825	2119	84619	94.4	1443	4557	2390	89631	107.4	1737	3690	2088	81969	120.4	2050	4102	2151	83000
68.6	922	3291	1840	82239	81.6	1173	4019	2053	89361	94.6	1447	4419	2183	89634	107.6	1741	3639	2123	82480	120.6	2055	4184	2167	85149
68.8	926	3308	1861	81576	81.8	1177	4063	2115	87473	94.8	1451	4460	2400	90359	107.8	1746	3692	1973	84998	120.8	2060	4469	2316	85074
69	929	3761	1974	85067	82	1181	4213	2148	89492	95	1456	4535	2325	91237	108	1751	3705	2145	85583	121	2065	4256	2180	85689
69.2	933	3742	2031	83596	82.2	1185	4067	2408	89408	95.2	1460	4514	2148	90801	108.2	1755	3920	2125	83424	121.2	2070	4317	2258	85201
69.4	937	3721	2152	85190	82.4	1190	4131	2286	87429	95.4	1464	4600	2278	91054	108.4	1760	3790	2027	80339	121.4	2075	4223	2227	85465
69.6	940	3556	2024	83431	82.6	1194	4086	2156	88082	95.6	1469	4588	2389	90984	108.6	1765	3681	1966	82156	121.6	2080	4485	2114	86374
69.8	944	3488	1992	80696	82.8	1198	3530	1945	74707	95.8	1473	4159	2134	88959	108.8	1769	3903	2033	82205	121.8	2085	4265	2147	87388
70	948	3624	1933	80737	83	1202	3961	2137	83918	96	1478	4324	2307	91087	109	1774	3825	2048	82135	122	2090	4413	2262	87776
70.2	952	3063	1664	77601	83.2	1206	3890	1915	86308	96.2	1482	4264	2215	88468	109.2	1779	3836	2061	80274	122.2	2095	4426	2393	88053
70.4	955	3373	1781	82022	83.4	1210	3947	2025	87731	96.4	1486	4276	2199	88578	109.4	1784	3669	1917	80576	122.4	2100	4331	1966	84803
70.6	959	3296	1956	81641	83.6	1214	3841	2151	87382	96.6	1491	4364	2091	89201	109.6	1788	3595	1920	80543	122.6	2105	4173	2045	85376
70.8	963	3168	2036	81036	83.8	1218	3649	2027	81798	96.8	1495	4188	2136	86468	109.8	1793	3764	1875	80342	122.8	2110	4074	1978	83523
71	967	3241	1889	82579	84	1222	3913	2046	86312	97	1500	4343	2209	87367	110	1798	3718	1916	83418	123	2115	3539	1872	81792
71.2	970	3318	2082	80879	84.2	1226	4023	2215	87739	97.2	1504	4207	2326	87789	110.2	1802	3413	1811	82669	123.2	2120	3506	1945	80682
71.4	974	3320	2086	81688	84.4	1230	4208	2220	91059	97.4	1509	4251	2231	88374	110.4	1807	3479	1944	83357	123.4	2125	3728	2115	81811
71.6	978	3318	2016	80516	84.6	1235	3928	2082	90485	97.6	1513	4322	2279	90907	110.6	1812	3492	1927	81958	123.6	2130	3432	2065	80140
71.8	982	3003	1876	80472	84.8	1239	3978	2094	89114	97.8	1518	4229	2268	88310	110.8	1817	3783	1987	83054	123.8	2135	3379	1703	80910
72	985	3157	1817	80363	85	1243	4092	2278	87685	98	1522	4344	2236	88347	111	1821	3859	2158	83166	124	2140	3303	1831	80031
72.2	989	3428	1987	79737	85.2	1247	4054	2024	87525	98.2	1526	4330	2201	90107	111.2	1826	3729	2235	82399	124.2	2145	3191	1991	80423
72.4	993	3448	2030	82463	85.4	1251	4255	2156	87564	98.4	1531	4407	2337	88342	111.4	1831	3842	2126	84131	124.4	2150	3222	1792	78863
72.6	997	3481	1958	81737	85.6	1255	4194	2505	88416	98.6	1535	4464	2345	89608	111.6	1836	3957	2115	85030	124.6	2155	3109	1747	78494
72.8	1001	3656	2143	85086	85.8	1259	4351	2255	89397	98.8	1540	4434	2482	90241	111.8	1841	4076	2029	84138	124.8	2160	3373	1799	80990
73	1004	3664	1999	86421	86	1264	4262	2248	89393	99	1544	4695	2430	92930	112	1845	3982	2038	81860	125	2165	3413	1755	81013
73.2	1008	3762	1977	85332	86.2	1268	4381	2341	89592	99.2	1549	4644	2266	91620	112.2	1850	3887	2078	83006	125.2	2170	3161	1817	79394
73.4	1012	3615	1840	82932	86.4	1272	4429	2486	91546	99.4	1553	4618	2374	91248	112.4	1855	3793	1863	80651	125.4	2175	3363	1856	79723
73.6	1016	3286	1706	82562	86.6	1276	4197	2453	88748	99.6	1558	4574	2294	92457	112.6	1860	3798	1920	80392	125.6	2180	3397	1872	78754
73.8	1020	3600	1927	86203	86.8	1280	4616	2513	92070	99.8	1562	4468	2453	89592	112.8	1864	4208	2201	83528	125.8	2185	3474	1870	78257
74	1024	3863	2155	84856	87	1284	4490	2187	92205	100	1567	4572	2388	91606	113	1869	3856	1919	82743	126	2191	3508	1922	77449
74.2	1027	3525	1990	84068	87.2	1289	4407	2219	89072	100.2	1571	4772	2219	91965	113.2	1874	3711	2006	82868	126.2	2196	3240	1709	76813
74.4	1031	3695	2056	82975	87.4	1293	3984	1999	82786	100.4	1576	4731	2281	91671	113.4	1879	3174	1677	78861	126.4	2201	3047	1670	77865
74.6	1035	3773	2165	86009	87.6	1297	3953	1961	83712	100.6	1580	4649	2484	91607	113.6	1884	3585	1801	81385	126.6	2206	3093	1658	76823
74.8	1039	4089	2377	84745	87.8	1301	4286	2387	86088	100.8	1585	4982	2389	92025	113.8	1889	4106	2023	85240	126.8	2211	3252	1840	78115
75	1043	4450	2214	86956	88	1305	4087	2093	88164	101	1589	5165	2549	92921	114	1893	4363	2301	84735	127	2216	3191	1917	77831
75.2	1047	4455	2383	87699	88.2	1310	4024	2282	84760	101.2	1594	4854	2436	90696	114.2	1898	4557	2160	88339	127.2	2221	3474	1872	77841
75.4	1051	4444	2229	89953	88.4	1314	3851	2154	83758	101.4	1598	4868	2265	90139	114.4	1903	3777	1791	77389	127.4	2226	3324	1864	75636
75.6	1054	3644	1908	76596	88.6	1318	4226	2062	86783	101.6	1603	5307	2444	92041	114.6	1908	4111	2036	80463	127.6	2231	3159	1847	74375
75.8	1058	3346	1634	72886	88.8	1322	4217	2299	86368	101.8	1607	5100	2403	91355	114.8	1913	4292	2169	86369	127.8	2236	3229	1906	76869
76	1062	4536	2189	86335	89	1326	4189	2177	85228	102	1612	5304	2505	91211	115	1918	4055	2186	85528	128	2242	3175	1886	77299
76.2	1066	4777	2314	88591	89.2	1331	4395	2316	89454	102.2	1617	5058	2320	91637	115.2	1922	4579	2187	88137	128.2	2247	3305	1772	75719
76.4	1070	4660	2395	89377	89.4	1335	4208	2243	89182	102.4	1621	5188	2392	91832	115.4	1927	4143	2197	87629	128.4	2252	2995	1652	77593
76.6	1074	4903	2617	90925	89.6	1339	4322	2236	90981	102.6	1626	4787	2342	92750	115.6	1932	4289	2137	90044	128.6	2257	3430	1797	79174
76.8	1078	4941	2474	90915	89.8	1343	4107	2346	91525	102.8	1630	4541	2159	88523	115.8	1937	4453	2367	87832	128.8	2262	3571	1865	82359
77	1082	4931	2415	90926	90	1348	4454	2225	89288	103	1635	5059	2355	92207	116	1942	4232	2187	88553	129	2267	3549	1929	78377
77.2	1086	4893	2185	91666	90.2	1352	4337	2406	89388	103.2	1639	5086	2425	91020	116.2	1947	4188	2372	87587	129.2	2272	3263	1873	78850
77.4	1090	4539	2286	91156	90.4	1356	4170	2023	87124	103.4	1644	5162	2617	92207	116.4	1952	4152	1924	86322	129.4	2277	3237	2020	78395
77.6	1094	4287	2075	88740	90.6	1360	4334	2182	88746	103.6	1649	5207	2342	93441	116.6	1956	4316	2108	85956	129.6	2283	3150	1886	78251
77.8	1097	4504	2248	87379	90.8	1365	4335	2101	89721	103.8	1653	5384	2454	93384	116.8	1961	4575	2170	87091	129.8	2288	3267	1956	78691

Appendix

Depth (cm)	Age yrs cal BP	Ca	Ti	Fe
130	2293	3437	1966	78818
130.2	2298	3446	1875	79461
130.4	2303	3307	1922	79497
130.6	2308	3425	1913	77971
130.8	2314	3355	1767	79219
131	2319	3406	1923	79324
131.2	2324	3425	1972	78515
131.4	2329	3152	1995	77394
131.6	2334	3326	1752	78985
131.8	2340	3439	1872	81438
132	2345	3344	2012	81135
132.2	2350	3310	1831	90849
132.4	2355	3039	1796	92547
132.6	2360	2934	1732	88215
132.8	2366	3276	1915	83304
133	2371	3551	1889	82028
133.2	2376	3028	1766	78407
133.4	2381	3184	1787	76555
133.6	2386	3368	1940	76049
133.8	2392	3377	1927	77145
134	2397	3419	1832	76408
134.2	2402	3522	1915	77636
134.4	2407	3411	1961	78185
134.6	2413	3513	1832	79364
134.8	2418	3700	1958	80366
135	2423	3764	1896	81806
135.2	2428	3484	1900	77693
135.4	2434	3382	1753	78267
135.6	2439	3304	1873	77112
135.8	2444	3530	2101	74800
136	2450	3717	2020	81260
136.2	2455	3523	1932	81237
136.4	2460	3509	1957	80570
136.6	2465	3446	1868	79357
136.8	2471	3465	1906	80299
137	2476	3421	1911	81344
137.2	2481	3307	1851	80442
137.4	2487	3234	1945	79970
137.6	2492	3192	1860	77684
137.8	2497	3337	1804	77532
138	2502	3510	1891	77828
138.2	2508	3382	1921	78311
138.4	2513	3366	1936	79244
138.6	2518	3509	2030	80225
138.8	2524	3558	2095	81828
139	2529	3368	1875	77869
139.2	2534	3566	1860	78608
139.4	2540	3671	1930	78794
139.6	2545	3628	1953	76615
139.8	2550	3979	1957	80640
140	2556	4107	2195	80634
140.2	2561	3901	2020	80404
140.4	2567	3785	2048	81369
140.6	2572	3884	2052	82522
140.8	2577	4077	2215	82602
141	2583	3822	2207	81823
141.2	2588	3757	1884	80425
141.4	2593	3939	2058	82088
141.6	2599	3637	2017	81448
141.8	2604	3773	1912	80733
142	2610	3792	2048	82582
142.2	2615	3923	1940	81445
142.4	2620	3689	1938	79666
142.6	2626	3664	1993	78734
142.8	2631	3637	1924	76862
143	2637	3672	1857	74376
143.2	2642	3495	2038	76145
143.4	2647	3577	2094	75666
143.6	2653	3245	1868	72505
143.8	2658	3181	1876	71755
144	2664	3232	1923	72500
144.2	2669	3618	1981	69904
144.4	2675	3370	2066	69275
144.6	2680	3378	1958	72152
144.8	2685	3557	1900	75767
145	2691	3611	1901	75994
145.2	2696	3750	1981	80637
145.4	2702	3815	2132	78964
145.6	2707	3659	2024	79521
145.8	2713	3713	2002	79729
146	2718	3749	2080	80335
146.2	2724	3559	2003	79074
146.4	2729	3392	1950	76988
146.6	2735	3311	1868	74962
146.8	2740	3267	1941	76315
147	2745	3248	1748	75873
147.2	2751	3059	1843	73560
147.4	2756	3311	1937	73874
147.6	2762	3410	1864	74193
147.8	2767	3558	1959	75010
148	2773	3385	2089	75525
148.2	2778	3332	1798	76741
148.4	2784	3493	1837	78262
148.6	2789	3500	1873	79454
148.8	2795	3396	1841	76305
149	2800	3367	1796	73890
149.2	2806	3273	2094	74292
149.4	2812	3318	1947	73045
149.6	2817	3475	1862	74651
149.8	2823	3601	1905	75308
150	2828	3647	2002	77797
150.2	2834	3462	2012	80071
150.4	2839	3772	1945	78477
150.6	2845	3895	2153	79496
150.8	2850	4061	2292	82133
151	2856	3831	2105	82785
151.2	2861	3949	2132	82244
151.4	2867	3896	2057	82195
151.6	2872	4093	2173	82365
151.8	2878	4143	2055	81603
152	2884	4000	2267	83148
152.2	2889	3946	1999	80892
152.4	2895	3668	2101	81120
152.6	2900	3977	1944	81933
152.8	2906	4108	2142	84024
153	2912	4007	2258	81432
153.2	2917	3910	1975	80534
153.4	2923	4216	2088	82411
153.6	2928	4483	2280	85118
153.8	2934	4450	2200	86591
154	2939	4419	2046	85150
154.2	2945	4437	2066	84974
154.4	2951	4490	2379	85102
154.6	2956	4293	2218	85837
154.8	2962	4457	2174	84561
155	2968	4209	2103	83454
155.2	2973	4352	2141	82160
155.4	2979	4396	2255	83512
155.6	2984	4385	2182	83257
155.8	2990	4170	2001	82070
156	2996	4078	2097	83557
156.2	3001	4038	2157	80797
156.4	3007	3879	2235	80622
156.6	3013	4000	2145	79999
156.8	3018	3757	2073	80151
157	3024	4088	2177	81660
157.2	3030	4035	2094	79520
157.4	3035	3937	2072	79111
157.6	3041	3992	2230	81244
157.8	3047	4034	2096	80707
158	3052	3926	2039	78932
158.2	3058	3777	2041	80600
158.4	3064	3872	2080	79156
158.6	3069	3919	2202	80623
158.8	3075	3907	2153	80928
159	3081	3608	1898	79578
159.2	3086	3724	2118	79986
159.4	3092	3870	2189	81780
159.6	3098	4094	1951	81613
159.8	3103	3941	2160	82461
160	3109	3969	2178	82763
160.2	3115	3978	2014	82294
160.4	3120	4236	2100	83001
160.6	3126	4204	2005	83100
160.8	3132	4379	2166	84605
161	3138	4008	1998	83213
161.2	3143	4138	2109	82206
161.4	3149	4112	2206	82618
161.6	3155	4347	2269	84076
161.8	3161	4062	2122	82689
162	3166	4143	2022	82952
162.2	3172	4288	2018	82169
162.4	3178	4308	2198	84229
162.6	3183	4546	2238	83219
162.8	3189	4238	2154	82208
163	3195	4116	2046	82686
163.2	3201	4547	2136	83852
163.4	3206	4612	2342	85675
163.6	3212	4904	2256	87379
163.8	3218	4718	2558	85008
164	3224	4542	2326	84810
164.2	3230	4434	2191	86471
164.4	3235	4446	2191	84674
164.6	3241	4771	2178	86584
164.8	3247	4499	2278	86303
165	3253	4579	2166	84310
165.2	3258	4405	2171	84783
165.4	3264	3931	2070	82361
165.6	3270	3852	2176	82450
165.8	3276	3546	1886	75660
166	3282	3615	1820	79006
166.2	3287	3218	1705	78457
166.4	3293	3513	1779	80637
166.6	3299	3571	2011	79115
166.8	3305	3547	1827	80593
167	3311	3550	1848	82264
167.2	3316	3604	2111	82877
167.4	3322	3667	1938	81190
167.6	3328	3227	1639	72188
167.8	3334	2392	1432	73134
168	3340	2847	1570	73065
168.2	3346	2662	1439	72279
168.4	3351	2729	1453	71123
168.6	3357	2755	1577	71843
168.8	3363	3121	1638	73667
169	3369	3076	1688	70499
169.2	3375	2744	1636	70986
169.4	3381	2897	1526	71211
169.6	3386	2906	1596	72586
169.8	3392	2850	1586	72692
170	3398	3199	1630	73950
170.2	3404	3134	1619	73288
170.4	3410	3071	1616	72577
170.6	3416	3331	1877	72852
170.8	3422	3059	1798	72885
171	3427	2983	1742	71370
171.2	3433	3008	1663	71666
171.4	3439	2917	1651	72107
171.6	3445	2959	1585	71054
171.8	3451	2805	1715	69281
172	3457	2915	1683	71077
172.2	3463	2794	1657	70260
172.4	3469	2827	1587	69860
172.6	3475	2950	1581	69954
172.8	3480	2888	1641	70829
173	3486	2890	1723	66865
173.2	3492	2858	1756	70489
173.4	3498	2811	1605	68534
173.6	3504	2872	1698	68560
173.8	3510	2979	1751	70614
174	3516	3036	1661	71402
174.2	3522	2881	1765	70920
174.4	3528	2788	1671	66897
174.6	3534	2939	1656	71351
174.8	3540	2981	1592	71152
175	3545	2748	1681	68740
175.2	3551	2854	1529	69207
175.4	3557	2667	1526	68385
175.6	3563	2932	1636	69616
175.8	3569	3157	1843	73011
176	3575	2979	1758	69823
176.2	3581	2919	1594	70931
176.4	3587	2655	1559	68951
176.6	3593	3056	1611	70754
176.8	3599	3158	1680	72116
177	3605	3015	1789	71690
177.2	3611	2846	1638	70314
177.4	3617	2033	1216	56003
177.6	3623	1938	1134	49791
177.8	3629	2537	1380	61434
178	3635	2740	1517	68494
178.2	3641	2877	1548	71020
178.4	3647	2955	1728	71351
178.6	3653	2713	1545	69159
178.8	3659	2884	1540	69375
179	3665	3032	1636	72232
179.2	3671	2927	1568	68250
179.4	3677	2769	1565	69353
179.6	3683	2903	1576	70411
179.8	3689	2850	1487	69576
180	3695	2775	1585	68274
180.2	3701	2813	1644	67451
180.4	3707	2321	1413	63733
180.6	3713	2531	1538	65637
180.8	3719	2648	1585	65982
181	3725	2746	1610	67669
181.2	3731	2926	1595	68645
181.4	3737	2398	1473	65177
181.6	3743	2338	1465	64321
181.8	3749	2640	1615	65964
182	3755	2793	1699	67431
182.2	3761	2788	1668	67008
182.4	3767	2669	1606	68763
182.6	3773	3055	1669	69483
182.8	3779	3398	1896	71986
183	3785	2949	1732	71539
183.2	3791	2885	1778	67554
183.4	3797	3098	1803	71618
183.6	3803	2895	1723	71423
183.8	3809	3195	1910	75054
184	3815	3108	1802	71905
184.2	3821	3160	1744	72046
184.4	3827	3213	1906	71913
184.6	3833	3318	1951	71848
184.8	3839	3229	1803	69625
185	3845	3340	1761	68636
185.2	3851	2918	1870	64042
185.4	3858	2806	1614	63843
185.6	3864	2864	1659	64805
185.8	3870	3187	1868	68866
186	3876	3232	1789	70333
186.2	3882	3257	1828	71514
186.4	3888	3118	1843	70911
186.6	3894	3176	1745	73927
186.8	3900	3517	1842	75846
187	3906	3235	1852	74499
187.2	3912	3301	1962	74887
187.4	3918	3304	2014	75119
187.6	3924	3173	1767	73947
187.8	3931	3539	1839	76456
188	3937	3468	2015	77484
188.2	3943	3084	1872	76511
188.4	3949	3119	1896	73625
188.6	3955	2978	1612	70504
188.8	3961	3187	1628	70171
189	3967	3142	1753	73682
189.2	3973	2963	1630	72697
189.4	3979	2916	1663	70219
189.6	3986	3062	1720	70464
189.8	3992	3137	1673	71544
190	3998	2908	1563	70859
190.2	4004	2941	1790	71671
190.4	4010	3063	1762	74075
190.6	4016	3495	1937	76135
190.8	4022	3285	1796	75049
191	4029	3171	1779	73395
191.2	4035	3127	1632	72981
191.4	4041	2898	1424	73112
191.6	4047	2944	1751	71711
191.8	4053	3070	1807	72492
192	4059	3222	1724	72060
192.2	4065	3218	1667	74424
192.4	4072	3287	1775	74921
192.6	4078	3353	1967	76343
192.8	4084	3855	2074	81815
193	4090	3621	2058	78025
193.2	4096	3408	1997	75381
193.4	4102	3524	1831	75440
193.6	4109	3273	1736	75132
193.8	4115	3679	1870	75411
194	4121	3537	1989	74623
194.2	4127	3214	1715	73213
194.4	4133	2992	1656	72096
194.6	4139	3080	1635	71967
194.8	4146	3155	1758	73347

Appendix

Depth (cm)	Age yrs cal BP	Ca	Ti	Fe
195	4152	3021	1783	73227
195.2	4158	3016	1673	72435
195.4	4164	2947	1675	69739
195.6	4170	2973	1661	69354
195.8	4177	3168	1789	72919
196	4183	3265	1741	75029
196.2	4189	3167	1913	77246
196.4	4195	3141	1763	76007
196.6	4201	3152	1712	76646
196.8	4208	3536	1907	77860
197	4214	3313	1734	75744
197.2	4220	3557	2032	78665
197.4	4226	3804	1891	78405
197.6	4232	3710	1967	78566
197.8	4239	3968	2099	79553
198	4245	3753	1947	79393
198.2	4251	3518	1803	77590
198.4	4257	3283	1609	76570
198.6	4264	3426	1894	78228
198.8	4270	3598	1847	78015
199	4276	3441	1795	78815
199.2	4282	3515	1919	78735
199.4	4289	3833	1908	79588
199.6	4295	3906	1960	82390
199.8	4301	3947	1980	81106
200	4307	3532	1930	78754
200.2	4314	3297	1691	75630
200.4	4320	3184	1724	72896
200.6	4326	3429	1722	74692
200.8	4332	3750	1877	75982
201	4339	3489	1876	77454
201.2	4345	3635	1998	78704
201.4	4351	3908	2033	79926
201.6	4357	3745	2022	78780
201.8	4364	3930	1920	79338
202	4370	3882	1953	80803
202.2	4376	3874	1862	81003
202.4	4382	3807	1850	78546
202.6	4389	3551	2068	77200
202.8	4395	3350	1754	76886
203	4401	3703	2096	80797
203.2	4408	3610	1984	81227
203.4	4414	3661	1990	80320
203.6	4420	3619	1964	76292
203.8	4426	3662	1967	77467
204	4433	3627	2114	78230
204.2	4439	3151	1684	75214
204.4	4445	3368	1892	74113
204.6	4452	3347	1871	71241
204.8	4458	3504	2007	76891
205	4464	3540	1906	76662
205.2	4470	3301	1679	76193
205.4	4477	3258	2042	73651
205.6	4483	3551	1899	75353
205.8	4489	3497	1757	74625
206	4496	3370	1701	73850
206.2	4502	3268	1628	72026
206.4	4508	2960	1752	74037
206.6	4515	3100	1713	73235
206.8	4521	3216	1814	75779
207	4527	3289	1783	75704
207.2	4534	2937	1541	74421
207.4	4540	3126	1702	73416
207.6	4546	3359	1772	74681
207.8	4553	3268	1806	77297

Depth (cm)	Age yrs cal BP	Ca	Ti	Fe
208	4559	3415	1810	75577
208.2	4565	3755	1881	78080
208.4	4571	3513	1820	77638
208.6	4578	3741	1826	77563
208.8	4584	3823	1922	77933
209	4591	3780	1888	78545
209.2	4597	3793	1953	79320
209.4	4603	3771	1981	79590
209.6	4610	3638	1833	78015
209.8	4616	3694	1862	79118
210	4622	3827	1920	81321
210.2	4629	3954	2052	82749
210.4	4635	2376	1332	71233
210.6	4641	1553	856	57405
210.8	4648	2786	1538	68750
211	4654	3260	1678	77345
211.2	4660	3215	1779	81612
211.4	4667	3248	1808	79491
211.6	4673	3409	1722	78515
211.8	4679	3457	1815	78997
212	4686	3490	1821	77740
212.2	4692	3402	1922	75817
212.4	4699	3375	1755	76490
212.6	4705	3253	1733	74446
212.8	4711	3372	1639	74992
213	4718	3454	1742	75326
213.2	4724	3708	2007	77713
213.4	4730	3679	1962	78365
213.6	4737	3906	1901	78052
213.8	4743	4309	2180	82018
214	4750	4406	2134	82445
214.2	4756	4921	2396	84967
214.4	4762	4345	2069	81391
214.6	4769	4189	2099	80591
214.8	4775	4303	2169	82326
215	4782	4213	2096	83399
215.2	4788	4472	2089	83908
215.4	4794	4334	2170	82070
215.6	4801	4030	2080	81570
215.8	4807	3985	2071	78873
216	4814	4250	2116	79325
216.2	4820	4182	2008	78239
216.4	4826	3555	1862	74864
216.6	4833	3169	1709	73546
216.8	4839	3311	1687	73892
217	4846	3159	1559	72968
217.2	4852	3034	1691	72819
217.4	4858	2783	1542	73240
217.6	4865	2803	1542	76687
217.8	4871	3238	1581	76832
218	4878	3172	1635	76411
218.2	4884	3078	1602	73864
218.4	4891	2757	1550	69046
218.6	4897	3507	1788	73680
218.8	4903	3356	1755	76286
219	4910	3464	1859	73483
219.2	4916	3488	1762	74549
219.4	4923	3005	1606	72458
219.6	4929	2843	1666	71383
219.8	4936	3232	1865	74193
220	4942	3068	1692	71785
220.2	4948	2977	1726	69203
220.4	4955	2633	1455	66426
220.6	4961	2466	1476	65562
220.8	4968	2888	1727	67750

Depth (cm)	Age yrs cal BP	Ca	Ti	Fe
221	4974	2602	1671	65108
221.2	4981	2599	1451	65249
221.4	4987	2593	1488	66700
221.6	4994	2705	1556	68484
221.8	5000	2800	1737	69164
222	5007	2693	1526	68761
222.2	5013	2940	1585	66889
222.4	5019	2898	1616	68269
222.6	5026	2563	1429	65346
222.8	5032	2872	1591	69612
223	5039	2880	1572	68870
223.2	5045	2982	1640	68592
223.4	5052	3035	1524	70811
223.6	5058	3073	1706	72622
223.8	5065	3231	1724	76265
224	5071	3263	1719	75912
224.2	5078	3344	1791	76562
224.4	5084	3579	1848	77949
224.6	5091	3152	1725	74672
224.8	5097	3199	1711	73270
225	5104	2916	1450	69993
225.2	5110	3168	1700	73646
225.4	5117	3272	1572	72743
225.6	5123	3246	1548	73736
225.8	5130	3262	1860	74150
226	5136	3181	1764	73041
226.2	5143	3277	1970	74508
226.4	5149	2956	1655	73579
226.6	5155	2998	1520	73295
226.8	5162	3387	1842	73703
227	5168	3137	1650	72761
227.2	5175	2832	1704	72231
227.4	5181	2522	1490	67734
227.6	5188	2761	1498	69381
227.8	5194	2924	1681	71544
228	5201	2888	1548	70433
228.2	5207	3170	1753	72571
228.4	5214	3054	1682	71949
228.6	5221	3068	1768	73025
228.8	5227	3194	1767	73590
229	5234	2957	1620	71904
229.2	5240	3111	1629	73312
229.4	5247	3287	1752	74345
229.6	5253	3053	1626	72137
229.8	5260	3451	1780	73189
230	5266	3501	1753	73255
230.2	5273	3510	1842	75469
230.4	5279	3089	1723	74010
230.6	5286	2755	1559	70373
230.8	5292	3088	1588	73065
231	5299	3644	1892	75750
231.2	5305	3694	1874	75575
231.4	5312	3408	1745	73624
231.6	5318	2976	1708	70382
231.8	5325	3136	1736	72112
232	5331	2942	1738	70716
232.2	5338	3124	1761	71081
232.4	5344	2991	1788	70274
232.6	5351	3237	1720	72301
232.8	5358	3185	1972	72393
233	5364	3025	1809	72635
233.2	5371	2934	1560	72383
233.4	5377	2988	1770	71121
233.6	5384	2894	1581	69611
233.8	5390	2891	1668	70996

Depth (cm)	Age yrs cal BP	Ca	Ti	Fe
234	5397	2717	1617	70159
234.2	5403	2845	1538	68986
234.4	5410	2516	1438	67491
234.6	5416	2622	1432	68244
234.8	5423	2842	1605	69024
235	5430	3096	1762	73425
235.2	5436	3352	1813	73622
235.4	5443	3121	1725	72646
235.6	5449	3333	1837	74707
235.8	5456	3537	1924	78107
236	5462	3421	1798	77390
236.2	5469	3783	1830	78481
236.4	5475	3759	1910	79417
236.6	5482	3732	1940	81244
236.8	5489	3893	2022	79871
237	5495	3924	2187	81278
237.2	5502	4096	2034	81242
237.4	5508	3754	1923	80394
237.6	5515	3668	2009	79175
237.8	5521	4187	2073	83045
238	5528	4208	1955	80907
238.2	5535	4223	2217	81329
238.4	5541	4440	2072	81932
238.6	5548	4540	2198	83953
238.8	5554	4480	2151	84059
239	5561	4471	2165	84158
239.2	5567	4543	2188	84056
239.4	5574	4231	1954	82557
239.6	5581	4364	2043	82662
239.8	5587	3886	1847	77883
240	5594	4419	2177	80663
240.2	5600	4417	2268	81277
240.4	5607	4109	2040	79252
240.6	5614	4207	1889	78371
240.8	5620	4366	2087	79868
241	5627	4090	2005	80109
241.2	5633	4227	2171	80500
241.4	5640	3918	1856	76965
241.6	5646	3940	2098	80043
241.8	5653	4093	1923	78839
242	5660	4278	2141	80024
242.2	5666	4367	2145	80665
242.4	5673	4402	2092	79544
242.6	5679	4392	2295	81868
242.8	5686	5451	2316	87764
243	5693	4786	2320	85361
243.2	5699	4286	2195	83590
243.4	5706	2356	1260	69570
243.6	5712	438	383	36902
243.8	5719	677	379	32063
244	5726	1274	625	38233
244.2	5732	1374	623	36972
244.4	5739	840	446	30258
244.6	5745	925	439	27529
244.8	5752	2314	1146	44956
245	5759	2279	1156	58737
245.2	5765	2412	1241	62235
245.4	5772	2474	1350	63856
245.6	5779	3969	1820	75122
245.8	5785	3572	1808	75146
246	5792	3481	1780	71226
246.2	5798	3072	1723	66039
246.4	5805	3181	1684	67105
246.6	5812	2870	1637	66333
246.8	5818	2867	1661	65810

Depth (cm)	Age yrs cal BP	Ca	Ti	Fe
247	5825	3130	1679	69411
247.2	5832	3210	1749	70774
247.4	5838	3473	1801	71367
247.6	5845	3220	1759	69736
247.8	5851	2963	1578	67350
248	5858	3164	1711	68754
248.2	5865	3207	1762	69068
248.4	5871	3213	1603	70094
248.6	5878	3114	1665	70627
248.8	5885	3076	1610	68020
249	5891	3356	1625	71434
249.2	5898	3450	1922	71759
249.4	5904	3639	1810	71727
249.6	5911	3398	1689	71357
249.8	5918	3234	1748	70578
250	5924	3281	1670	71736
250.2	5931	3358	1683	74917
250.4	5938	3634	1873	76295
250.6	5944	3726	1854	78086
250.8	5951	3869	2007	78795
251	5958	3664	1959	77976
251.2	5964	3983	1901	78699
251.4	5971	3816	1879	77499
251.6	5977	3807	1961	75997
251.8	5984	3562	1657	73360
252	5991	3180	1692	71740
252.2	5997	3201	1760	70718
252.4	6004	3064	1636	70343
252.6	6011	2959	1663	68157
252.8	6017	2659	1476	64835
253	6024	2673	1630	60637
253.2	6031	2754	1526	63192
253.4	6037	2787	1568	65565
253.6	6044	2863	1527	65134
253.8	6051	3079	1764	68032
254	6057	3136	1667	69589
254.2	6064	2944	1643	67825
254.4	6071	3174	1821	69414
254.6	6077	3009	1757	71289
254.8	6084	3244	1679	70861
255	6091	3276	1755	72431
255.2	6097	3796	1877	75046
255.4	6104	3748	1982	78131
255.6	6111	3839	1861	80106
255.8	6117	3806	1855	78979
256	6124	4075	1966	84972
256.2	6131	3927	1959	85433
256.4	6137	3918	1823	80889
256.6	6144	3750	1845	78044
256.8	6151	3686	1964	78107
257	6157	3365	1849	73927
257.2	6164	3539	1918	75162
257.4	6171	3366	1882	73054
257.6	6177	3333	1941	72044
257.8	6184	3425	1774	74299
258	6191	3414	1812	71525
258.2	6197	3373	1861	70729
258.4	6204	3130	1733	70509
258.6	6211	3027	1604	66803
258.8	6217	2693	1471	65330
259	6224	1969	1134	56617
259.2	6231	2571	1514	63916
259.4	6237	3009	1646	67986
259.6	6244	2746	1584	66268
259.8	6251	2868	1560	65542

Appendix

Depth (cm)	Age yrs cal BP	Ca	Ti	Fe
260	6257	2904	1569	63817
260.2	6264	3005	1673	68445
260.4	6271	3130	1837	68966
260.6	6277	3307	1833	70321
260.8	6284	3296	1860	69864
261	6291	3165	1832	69774
261.2	6297	3227	1731	70477
261.4	6304	3430	1985	71917
261.6	6311	3740	1975	73487
261.8	6317	3767	1903	74602
262	6324	3771	2113	75215
262.2	6331	3641	1874	74459
262.4	6337	3695	1896	73187
262.6	6344	3691	1863	72891
262.8	6351	3628	1908	73556
263	6357	3671	1837	72937
263.2	6364	3679	1779	72706
263.4	6371	3565	1801	72251
263.6	6378	3297	1768	69823
263.8	6384	2974	1656	67653
264	6391	2915	1751	66846
264.2	6398	2955	1755	66098
264.4	6404	2981	1721	66264
264.6	6411	2807	1679	63318
264.8	6418	2931	1619	66796
265	6424	3091	1680	70466
265.2	6431	3072	1734	69370
265.4	6438	3289	1779	71224
265.6	6444	3219	1717	70186
265.8	6451	3228	1660	68446
266	6458	3071	1673	67553
266.2	6465	2957	1830	68603
266.4	6471	2964	1707	68433
266.6	6478	2859	1653	65921
266.8	6485	2601	1618	61605
267	6491	2665	1617	60850
267.2	6498	2848	1727	65753
267.4	6505	2912	1698	66621
267.6	6511	2953	1683	67860
267.8	6518	2964	1585	69451
268	6525	2829	1512	69112
268.2	6532	3082	1686	69534
268.4	6538	2957	1687	67666
268.6	6545	2918	1711	67065
268.8	6552	2701	1628	64864
269	6558	2710	1476	65765
269.2	6565	2575	1585	65557
269.4	6572	2801	1570	66570
269.6	6578	2865	1584	65118
269.8	6585	2836	1624	66251
270	6592	2636	1546	63445
270.2	6599	2753	1499	64427
270.4	6605	2814	1523	67283
270.6	6612	3018	1567	68588
270.8	6619	2828	1608	67092
271	6625	2764	1583	65349
271.2	6632	2910	1506	66811
271.4	6639	2697	1530	62581
271.6	6646	3039	1584	66293
271.8	6652	3111	1668	66807
272	6659	3227	1699	67951
272.2	6666	3343	1734	70107
272.4	6672	3263	1695	71119
272.6	6679	3227	1606	68788
272.8	6686	3567	1865	69104

Depth (cm)	Age yrs cal BP	Ca	Ti	Fe
273	6692	3463	1725	67878
273.2	6699	3494	1872	69993
273.4	6706	3296	1832	67835
273.6	6713	3034	1715	65483
273.8	6719	2896	1644	62528
274	6726	2850	1523	63194
274.2	6733	2736	1540	62797
274.4	6739	2761	1593	62321
274.6	6746	2434	1424	60058
274.8	6753	2575	1564	62272
275	6760	2961	1671	67128
275.2	6766	2925	1642	68577
275.4	6773	2938	1624	67610
275.6	6780	3354	1622	71874
275.8	6786	3146	1665	67814
276	6793	3092	1619	67330
276.2	6800	2889	1625	66764
276.4	6807	2787	1459	62458
276.6	6813	3182	1842	66099
276.8	6820	2744	1623	64043
277	6827	2727	1623	63689
277.2	6833	2898	1591	63151
277.4	6840	2815	1528	62065
277.6	6847	2891	1657	63653
277.8	6854	3122	1585	62213
278	6860	2779	1610	61832
278.2	6867	2687	1520	59539
278.4	6874	2529	1537	59341
278.6	6880	2706	1555	61996
278.8	6887	2663	1526	59635
279	6894	2731	1596	60261
279.2	6901	2822	1554	62498
279.4	6907	2919	1565	64966
279.6	6914	2926	1681	65844
279.8	6921	2787	1557	64580
280	6927	2883	1639	64957
280.2	6934	2894	1661	65930
280.4	6941	3000	1634	65476
280.6	6948	3007	1693	65499
280.8	6954	2924	1768	62139
281	6961	3139	1927	66055
281.2	6968	3061	1946	65821
281.4	6975	3088	1866	66801
281.6	6981	2972	1714	66257
281.8	6988	3051	1610	65098
282	6995	2858	1559	65379
282.2	7001	2607	1405	62144
282.4	7008	2853	1472	64645
282.6	7015	2709	1566	62262
282.8	7022	2550	1356	61816
283	7028	2565	1489	63175
283.2	7035	2656	1509	63011
283.4	7042	2415	1437	62331
283.6	7048	2249	1360	60499
283.8	7055	2445	1410	61987
284	7062	2621	1468	64580
284.2	7069	2955	1578	64830
284.4	7075	3048	1802	65407
284.6	7082	3226	1818	66486
284.8	7089	2970	1811	67182
285	7095	2894	1646	66225
285.2	7102	2788	1686	67983
285.4	7109	3265	1851	71844
285.6	7116	3064	1818	68569
285.8	7122	3169	1941	68984

Depth (cm)	Age yrs cal BP	Ca	Ti	Fe
286	7129	2941	1937	68782
286.2	7136	2241	1282	50892
286.4	7143	1840	1261	44947
286.6	7149	1948	1173	44837
286.8	7156	2004	1258	45968
287	7163	1210	1095	36402
287.2	7169	385	200	10598
287.4	7176	2416	1562	60409
287.6	7183	2532	1552	64528
287.8	7190	2486	1592	63906
288	7196	2601	1598	62023
288.2	7203	2712	1641	69070
288.4	7210	1528	885	43083
288.6	7216	2001	1151	52095
288.8	7223	2434	1399	60536
289	7230	2537	1560	63595
289.2	7237	2783	1488	64459
289.4	7243	2653	1763	65434
289.6	7250	2814	1780	65603
289.8	7257	2785	1578	63848
290	7264	2808	1625	63198
290.2	7270	2811	1626	62716
290.4	7277	2924	1704	62980
290.6	7284	2727	1675	60947
290.8	7290	2645	1656	58907
291	7297	2765	1693	57238
291.2	7304	2684	1548	58889
291.4	7311	2822	1746	61418
291.6	7317	2898	1964	61518
291.8	7324	3127	1826	62362
292	7331	3089	1657	61136
292.2	7337	2971	1804	61484
292.4	7344	2845	1712	61077
292.6	7351	2720	1590	62051
292.8	7358	3011	1636	64066
293	7364	3150	1829	65336
293.2	7371	3027	1770	66590
293.4	7378	2918	1581	62875
293.6	7384	3097	1797	65213
293.8	7391	3043	1891	65911
294	7398	3179	1703	64768
294.2	7405	3107	1861	65180
294.4	7411	3087	1775	64575
294.6	7418	3394	1897	67377
294.8	7425	3393	1877	67832
295	7431	3697	1902	69466
295.2	7438	3462	1835	68642
295.4	7445	3494	1867	69468
295.6	7452	3199	1899	68200
295.8	7458	3451	1789	68095
296	7465	3521	1804	68240
296.2	7472	3230	1784	66761
296.4	7478	3164	1877	66514
296.6	7485	3203	1687	66048
296.8	7492	3198	1887	65285
297	7499	3116	1757	68088
297.2	7505	2890	1633	65487
297.4	7512	3102	1689	68282
297.6	7519	3287	1878	70409
297.8	7525	3170	1767	71838
298	7532	3114	1791	69946
298.2	7539	3328	1978	70921
298.4	7546	3289	2059	71606
298.6	7552	3109	1918	68912
298.8	7559	3381	2059	69216

Depth (cm)	Age yrs cal BP	Ca	Ti	Fe
299	7566	3495	1856	68711
299.2	7572	3144	1972	67723
299.4	7579	3216	1954	69175
299.6	7586	3170	1807	69091
299.8	7593	3454	1903	70175
300	7599	3633	1907	72512
300.2	7606	3683	1873	73593
300.4	7613	3743	2081	75869
300.6	7619	3762	1914	77095
300.8	7626	3603	1850	74615
301	7633	3677	1998	75541
301.2	7640	3806	1946	75699
301.4	7646	3748	1970	76016
301.6	7653	3718	1931	76514
301.8	7660	3868	2090	77140
302	7666	3891	2191	75830
302.2	7673	3590	1906	73793
302.4	7680	3439	1982	71825
302.6	7686	3228	1820	69790
302.8	7693	3462	1995	69579
303	7700	3504	1885	71932
303.2	7707	3820	1959	73986
303.4	7713	4014	2138	74651
303.6	7720	4413	2328	75578
303.8	7727	4336	2120	77881
304	7733	4325	2253	79832
304.2	7740	4987	2294	80391
304.4	7747	5678	2845	86116
304.6	7753	5413	2554	84565
304.8	7760	4911	2575	80174
305	7767	5107	2529	81839
305.2	7774	4616	2308	79072
305.4	7780	4995	2419	80322
305.6	7787	4976	2432	81052
305.8	7794	4551	2276	78469
306	7800	4815	2504	82099
306.2	7807	5027	2294	80848
306.4	7814	4976	2230	81557
306.6	7820	5081	2492	80778
306.8	7827	5010	2239	78932
307	7834	5360	2525	80488
307.2	7841	5249	2609	80201
307.4	7847	5115	2527	81077
307.6	7854	5208	2421	80450
307.8	7861	4847	2423	78194
308	7867	4644	2384	78117
308.2	7874	4748	2111	78090
308.4	7881	5035	2575	78628
308.6	7887	4960	2456	78934
308.8	7894	4675	2210	78457
309	7901	4653	2266	78861
309.2	7907	4774	2284	78695
309.4	7914	4824	2318	79169
309.6	7921	4828	2221	79763
309.8	7927	4488	2331	77570
310	7934	4964	2560	79069
310.2	7941	4862	2445	79732
310.4	7948	4588	2424	79777
310.6	7954	4812	2506	79321
310.8	7961	4702	2194	79425
311	7968	4817	2473	78951
311.2	7974	4815	2537	78921
311.4	7981	4803	2456	78907
311.6	7988	4678	2362	77802
311.8	7994	4703	2194	80416

Depth (cm)	Age yrs cal BP	Ca	Ti	Fe
312	8001	3956	2017	72783
312.2	8008	4145	1980	74757
312.4	8014	4737	2374	79811
312.6	8021	4741	2340	81256
312.8	8028	5030	2222	82447
313	8034	5307	2631	83932
313.2	8041	5411	2679	83751
313.4	8048	5455	2559	84953
313.6	8054	5175	2355	85064
313.8	8061	5002	2455	81475
314	8068	5576	2677	85876
314.2	8074	5705	2585	87000
314.4	8081	5414	2500	84517
314.6	8088	5545	2647	87387
314.8	8094	5293	2407	85623
315	8101	5237	2371	83927
315.2	8108	5093	2596	84200
315.4	8114	5158	2395	83878
315.6	8121	5071	2596	84970
315.8	8128	5493	2671	88296
316	8134	5483	2564	86764
316.2	8141	5239	2494	84737
316.4	8148	4982	2231	83269
316.6	8154	5292	2564	84652
316.8	8161	5528	2675	86581
317	8168	5479	2571	85903
317.2	8174	5540	2567	86912
317.4	8181	4598	2241	78635
317.6	8188	3751	1765	69405
317.8	8194	4675	2318	80680
318	8201	4535	2243	82139
318.2	8208	4532	2453	80670
318.4	8214	4015	2168	78441
318.6	8221	4137	2186	79455
318.8	8228	4350	2205	79894
319	8234	4040	2089	79751
319.2	8241	4475	2084	78424
319.4	8248	4083	2230	77419
319.6	8254	4124	2136	77871
319.8	8261	4154	2103	78234
320	8268	4392	2176	79895
320.2	8274	4436	2200	80347
320.4	8281	4473	2133	79358
320.6	8287	4080	1906	77004
320.8	8294	3745	1944	75832
321	8301	4213	2151	75497
321.2	8307	4343	2364	77340
321.4	8314	4762	2417	77853
321.6	8321	4333	2296	78202
321.8	8327	3922	2163	74582
322	8334	3967	1963	73179
322.2	8341	3714	2182	72361
322.4	8347	2990	1473	64241
322.6	8354	3382	1790	65565
322.8	8361	3425	1691	68293
323	8367	3912	2033	72886
323.2	8374	3732	2024	73993
323.4	8380	4248	2240	76979
323.6	8387	4343	2145	76257
323.8	8394	4503	2046	74514
324	8400	4422	2210	74403
324.2	8407	4031	1913	73383
324.4	8414	3658	1804	72587
324.6	8420	3880	2188	73849
324.8	8427	3951	2039	74739

Appendix

Depth (cm)	Age yrs cal BP	Ca	Ti	Fe	Depth (cm)	Age yrs cal BP	Ca	Ti	Fe	Depth (cm)	Age yrs cal BP	Ca	Ti	Fe	Depth (cm)	Age yrs cal BP	Ca	Ti	Fe	Depth (cm)	Age yrs cal BP	Ca	Ti	Fe
325	8433	3775	1997	74931	338	8863	4579	2409	79621	351	9290	3891	1792	75196	364	9714	4642	2096	80998	377	10138	4582	2262	81999
325.2	8440	3703	1877	74572	338.2	8869	4351	2279	77732	351.2	9296	4231	2062	78574	364.2	9721	4470	2370	79719	377.2	10144	4556	2236	80226
325.4	8447	3646	1925	71981	338.4	8876	4296	2121	79715	351.4	9303	4365	2217	78010	364.4	9727	4462	2176	79228	377.4	10151	4144	2048	78347
325.6	8453	3902	2031	73593	338.6	8883	4779	2288	83474	351.6	9309	4430	2196	78556	364.6	9734	4340	2206	77583	377.6	10157	4145	2165	78022
325.8	8460	4715	2403	78901	338.8	8889	4955	2407	83788	351.8	9316	4332	2067	77643	364.8	9740	4455	2200	77094	377.8	10164	4315	2221	78530
326	8467	4818	2282	79556	339	8896	5416	2592	83583	352	9322	4253	2210	77033	365	9747	4722	2243	78729	378	10170	4521	2351	81834
326.2	8473	4948	2493	78817	339.2	8902	5297	2377	83659	352.2	9329	4444	2081	78759	365.2	9754	5013	2442	78214	378.2	10177	4779	2391	80956
326.4	8480	5363	2456	82803	339.4	8909	5045	2450	83112	352.4	9335	4320	2172	79126	365.4	9760	5069	2289	79866	378.4	10183	4784	2583	81882
326.6	8486	5343	2486	83036	339.6	8915	4921	2530	81684	352.6	9342	4235	1961	77776	365.6	9767	5269	2293	79529	378.6	10190	4654	2377	81261
326.8	8493	5351	2401	84680	339.8	8922	4438	2215	81749	352.8	9348	3859	1992	76600	365.8	9773	5169	2388	79208	378.8	10197	4716	2130	80769
327	8500	4267	1837	73850	340	8929	4623	2404	81870	353	9355	4246	2203	79664	366	9780	5110	2152	80224	379	10203	4414	2197	79114
327.2	8506	4974	2168	81113	340.2	8935	4773	2232	81423	353.2	9362	4655	2209	81742	366.2	9786	5088	2205	78863	379.2	10210	4796	2266	81304
327.4	8513	5106	2209	80328	340.4	8942	4621	2280	80155	353.4	9368	5094	2400	82697	366.4	9793	5290	2284	79501	379.4	10216	4878	2304	80484
327.6	8520	5200	2108	82131	340.6	8948	5084	2267	82507	353.6	9375	5404	2440	82862	366.6	9799	5140	2320	79863	379.6	10223	4409	2289	78195
327.8	8526	5170	2196	82636	340.8	8955	5422	2353	85228	353.8	9381	5326	2363	82221	366.8	9806	5105	2343	81589	379.8	10229	4498	2179	78736
328	8533	5310	2555	81414	341	8961	5335	2545	84149	354	9388	5056	2481	81927	367	9812	4900	2345	81789	380	10236	4650	2227	79341
328.2	8539	5181	2462	81836	341.2	8968	5110	2656	83033	354.2	9394	5009	2197	80694	367.2	9819	4871	2208	81350	380.2	10242	4538	2098	80778
328.4	8546	5325	2449	83001	341.4	8975	4821	2381	82445	354.4	9401	4344	2302	78197	367.4	9825	4725	2279	82605	380.4	10249	4950	2270	82074
328.6	8553	5134	2607	82708	341.6	8981	4597	2281	81677	354.6	9407	4274	2037	77389	367.6	9832	4745	2168	80560	380.6	10255	4929	2216	83787
328.8	8559	5287	2499	82359	341.8	8988	5036	2415	83150	354.8	9414	4123	1860	74431	367.8	9838	4779	2276	81917	380.8	10262	5091	2265	84676
329	8566	5124	2408	83927	342	8994	4775	2282	81231	355	9420	4350	2026	76171	368	9845	4767	2324	82241	381	10268	5183	2497	86961
329.2	8573	5141	2454	82906	342.2	9001	4620	2284	80855	355.2	9427	4274	1963	76814	368.2	9851	4752	2167	80527	381.2	10275	5236	2413	86554
329.4	8579	5078	2348	81084	342.4	9007	4371	2229	79254	355.4	9434	4098	2022	76183	368.4	9858	4361	2087	75062	381.4	10281	5230	2354	84892
329.6	8586	5169	2318	81529	342.6	9014	4361	2272	77034	355.6	9440	4150	2021	76923	368.6	9864	4006	2008	73637	381.6	10288	5029	2163	81308
329.8	8592	4976	2445	81378	342.8	9021	4355	2160	77843	355.8	9447	4056	2191	75630	368.8	9871	3734	1808	70709	381.8	10294	5071	2217	82902
330	8599	4774	2251	80692	343	9027	4122	2278	77416	356	9453	4241	2138	75642	369	9877	3612	1788	71044	382	10301	4596	1979	79880
330.2	8606	4880	2488	80177	343.2	9034	4202	2136	76798	356.2	9460	4299	2144	74924	369.2	9884	3585	2038	72044	382.2	10307	4633	2007	77217
330.4	8612	4383	2164	77251	343.4	9040	4528	2150	78566	356.4	9466	3851	1935	73109	369.4	9890	3516	1912	72789	382.4	10314	4351	2168	75956
330.6	8619	4675	2296	80085	343.6	9047	4300	2183	76991	356.6	9473	3876	1914	70919	369.6	9897	3830	2042	74034	382.6	10320	4035	2086	76002
330.8	8625	4605	2271	78505	343.8	9053	4122	2036	76269	356.8	9479	3631	1933	70288	369.8	9903	3939	2133	73813	382.8	10327	4047	2082	75183
331	8632	4780	2303	78151	344	9060	4827	2437	80785	357	9486	3241	1762	66176	370	9910	3919	1935	73737	383	10333	3970	2015	75617
331.2	8639	4495	2287	77438	344.2	9067	5200	2552	83645	357.2	9492	3048	1729	63100	370.2	9916	3983	1999	75018	383.2	10340	3882	2116	76800
331.4	8645	4669	2436	80164	344.4	9073	5053	2673	82216	357.4	9499	3112	1696	65033	370.4	9923	3871	1956	75066	383.4	10346	4293	2066	77966
331.6	8652	5071	2280	82053	344.6	9080	4808	2226	81137	357.6	9505	2854	1573	65607	370.6	9930	4094	2141	75822	383.6	10353	4228	2046	78877
331.8	8658	4195	1891	71028	344.8	9086	4909	2364	83036	357.8	9512	2756	1654	65331	370.8	9936	4002	1976	75443	383.8	10359	4485	2127	79942
332	8665	4461	2042	76633	345	9093	4557	2117	79955	358	9518	3140	1709	66301	371	9943	4151	2271	77610	384	10366	4542	2163	81136
332.2	8672	4334	1940	77339	345.2	9099	5172	2295	83911	358.2	9525	3503	1880	71104	371.2	9949	4070	2067	76714	384.2	10372	4591	2172	82425
332.4	8678	4214	2028	75241	345.4	9106	4659	2089	81179	358.4	9532	3667	1789	72444	371.4	9956	3839	2044	76543	384.4	10379	4779	2321	82148
332.6	8685	3860	1886	73513	345.6	9113	4314	1977	76743	358.6	9538	3555	1880	71566	371.6	9962	3721	1934	74541	384.6	10385	4856	2180	83687
332.8	8691	3985	1909	73615	345.8	9119	4441	2147	77190	358.8	9545	3449	1905	68131	371.8	9969	3507	1867	72747	384.8	10392	4855	2294	82298
333	8698	3795	1892	72725	346	9126	4012	2030	77425	359	9551	3529	1712	71382	372	9975	3558	1960	72592	385	10398	4780	2216	82655
333.2	8705	3984	2010	75351	346.2	9132	4527	2177	80215	359.2	9558	3537	1978	72005	372.2	9982	3897	2008	75973	385.2	10405	4978	2238	82872
333.4	8711	4217	2187	78248	346.4	9139	4558	2063	78818	359.4	9564	3665	1913	71354	372.4	9988	4139	2115	77071	385.4	10411	4897	2310	82894
333.6	8718	3762	1890	72667	346.6	9145	4481	2275	78277	359.6	9571	3825	2065	73868	372.6	9995	4225	2112	77313	385.6	10418	4643	2186	82102
333.8	8724	4162	2063	75622	346.8	9152	4579	2215	79173	359.8	9577	3663	1960	72343	372.8	10001	4331	2156	78068	385.8	10424	4583	2160	79372
334	8731	3870	1933	76091	347	9158	4365	2186	79197	360	9584	3742	2022	72851	373	10008	4405	2290	78590	386	10431	4979	2218	80302
334.2	8738	3668	1876	74586	347.2	9165	4241	2160	77685	360.2	9590	3928	1948	74819	373.2	10014	4288	2068	78827	386.2	10437	4816	2240	83157
334.4	8744	3640	1948	74647	347.4	9172	4550	2259	79887	360.4	9597	4164	2024	77158	373.4	10021	4338	2070	80345	386.4	10444	4931	2112	84047
334.6	8751	3511	2050	75626	347.6	9178	4931	2279	81820	360.6	9603	4011	2071	74107	373.6	10027	4248	2128	79010	386.6	10450	4905	2224	83286
334.8	8757	3553	1833	75178	347.8	9185	4939	2289	82131	360.8	9610	4202	2142	75907	373.8	10034	4183	2144	79428	386.8	10457	4905	2141	83086
335	8764	3917	1938	76285	348	9191	4935	2378	81264	361	9616	3983	2070	77403	374	10040	4175	2051	79846	387	10463	4531	2163	79517
335.2	8771	3846	2189	76970	348.2	9198	4933	2461	82486	361.2	9623	4180	2213	78604	374.2	10047	4303	2043	80222	387.2	10470	4454	2038	78635
335.4	8777	3701	1878	77946	348.4	9204	4681	2429	81094	361.4	9630	4287	2247	78244	374.4	10053	4486	2102	80509	387.4	10476	4075	1846	75978
335.6	8784	3179	1737	74880	348.6	9211	4673	2390	79712	361.6	9636	4191	2175	74740	374.6	10060	4445	2041	79228	387.6	10483	4358	2028	78265
335.8	8790	3000	1747	71849	348.8	9217	4868	2250	81338	361.8	9643	4000	2184	74577	374.8	10066	4399	2274	78000	387.8	10489	4227	1907	78951
336	8797	3696	1872	75232	349	9224	4827	2352	80289	362	9649	4093	2068	74768	375	10073	4497	2149	78508	388	10496	4359	2035	77161
336.2	8804	4052	1884	77225	349.2	9231	3822	1887	74924	362.2	9656	4056	2124	74554	375.2	10079	4598	2186	80773	388.2	10502	3924	1992	77351
336.4	8810	4540	2033	79407	349.4	9237	3650	1865	73692	362.4	9662	4081	2111	75910	375.4	10086	4609	2373	81720					
336.6	8817	4767	2438	80652	349.6	9244	3800	1988	73948	362.6	9669	4192	2229	77176	375.6	10092	4798	2391	82400					
336.8	8823	4844	2400	82321	349.8	9250	3631	1940	73620	362.8	9675	4356	2157	80177	375.8	10099	4995	2335	83679					
337	8830	4732	2235	80750	350	9257	3755	1875	75171	363	9682	4664	2278	81396	376	10105	4890	2280	82980					
337.2	8836	4478	2124	82011	350.2	9263	3486	1872	74737	363.2	9688	4755	2342	83054	376.2	10112	4916	2312	82517					
337.4	8843	4612	2295	81877	350.4	9270	3733	1961	74759	363.4	9695	4768	2373	85361	376.4	10118	4751	2300	81967					
337.6	8850	4823	2377	80209	350.6	9276	4182	2130	77235	363.6	9701	4578	2261	81165	376.6	10125	4746	2346	81950					
337.8	8856	4668	2282	80396	350.8	9283	4222	2111	76755	363.8	9708	4550	2201	79623	376.8	10131	4624	2301	80818					

Appendix

Dojran pollen and microcharcoal data

Depth (cm)	Age cal yrs BP	conifer	deciduous	poaceae	mediterranean	cultivated	ruderals	tot pollen	charcoal 10-50	charcoal 50-125	charcoal >125	NAP	AP
1	-54	12.83095723	21.99592668	10.59063136	21.18126273	7.739307536	1.221995927	9321.3	1177	0		31.36456212	68.63543788
9	3	19.43095856	22.76165745	7.948515299	18.7873998	5.058146099	0	9013.1	1856.2	293.1	500	28.903692	71.096308
17	61	19.20917698	26.38067691	13.42588021	8.479503291	2.355417581	2.119875823	7495.7	53	0		39.80655712	60.19344288
25	120	17.03360371	31.5179606	21.32097335	5.098493627	2.780996524	1.622247972	7356.2	85.2	0		38.93395133	61.06604867
33	181	18.37209302	34.65116279	12.79069767	4.418604651	3.488372093	0.697674419	8556.4	179.1	0		34.41860465	65.58139535
41	242	27.06333973	26.10364683	13.81957774	2.303262956	6.909788868	1.151631478	10865	41.7	41.7		38.38771593	61.61228407
49	304	23.92502756	30.20948181	12.12789416	6.615214994	5.733186329	0.661521499	10682.1	0	0		32.41455347	67.58544653
59	384	24.59425718	37.45318352	9.488139825	2.746566792	3.495630462	0.24968789	13939.3	139.2	0		30.21223471	69.78776529
65.3	435	26.44592458	34.5009344	9.583592889	4.073026978	1.677128756	0.239589822	11511.9	27.6	0		29.46954813	70.53045187
73.3	502	27.58885982	34.00523157	10.40160025	4.800738575	2.800430836	0	9993.3	159.9	0		30.00461609	69.99538391
81.3	569	24.32432432	40.04914005	9.582309582	6.87960688	2.211302211	0.491400491	10593	78.1	78.1		23.58722359	76.41277641
89.3	638	19.65886901	47.34388076	6.45598374	4.662654924	1.434663053	0.717331527	22940.2	329.1	0		23.31327462	76.68672538
97.3	709	25.67157206	45.98094941	8.481922708	3.348127385	4.240961354	0.223208492	19632.2	219.1	0		19.41913883	80.58086117
105.3	781	20.73011734	55.80182529	6.518904824	2.60756193	1.043024772	1.043024772	25351	528.8	0		17.47066493	82.52933507
113.3	854	24.42553191	50.04255319	3.404255319	3.914893617	3.404255319	0	16177.6	137.7	0		16.68085106	83.31914894
121.3	930	24.86338798	55.76806315	4.67516697	1.669702489	1.335761991	1.001821494	14734.7	442.8	0		14.69338191	85.30661809
129.3	1007	14.0325962	56.30170645	6.185613489	6.564324519	1.38860711	0	17787.3	5074.6	718.5		18.30436645	81.69563355
137.3	1087	9.398584353	67.80105939	6.600103127	3.900060938	0.900014063	0	14862.8	401.3	0		14.400225	85.599775
145.3	1168	13.39818011	65.57891434	3.608409162	3.451521807	1.882648259	0	14935.5	3248.8	0		14.43363665	85.56636335
153.3	1252	13.432079	56.11689351	10.44035228	3.480117427	1.740058714	0.217507339	6452.7	927.4	14		23.92580731	76.07419269
161.3	1338	7.803121248	43.93757503	12.00480192	10.32412965	3.601440576	0	3956.3	456	9.5		32.41296519	67.58703481
169.3	1426	11.00430892	46.73516738	11.43520053	2.983095791	3.480278422	0.994365264	3793.3	245.2	18.9		33.31123633	66.68876367
177.3	1518	6.39219935	50.48754063	13.43445287	5.200433369	4.767063922	0	4382.1	38	19		32.06933911	67.93066089
181.3	1565	9.681430799	52.60823876	13.96678905	1.86223854	3.957256898	0.465559635	4742.6	77.3	0		28.86469737	71.13530263
185.3	1612	14.76510067	46.6442953	12.75167785	2.684563758	2.684563758	0.33557047	2779.2	839.3	18.7		30.53691275	69.46308725
189.3	1661	10.45948111	54.73797759	13.85343877	3.716776256	2.027332503	2.027332503	5090.6	344	0		27.70687754	72.29312246
193.3	1710	9.348327333	48.49318393	12.6693904	7.426884026	5.024068606	0.218437765	5238.3	846.7	22.9		30.14441163	69.85558837
197.3	1761	14.87414188	41.4187643	14.87414188	2.745995423	3.432494279	1.372997712	8030.3	128.6	0		34.55377574	65.44622426
201.3	1811	24.72748782	42.52035039	8.906289609	4.596794637	4.309494972	0.287299665	4645.6	120.1	13.3		21.2601752	78.7398248
205.3	1863	14.03645097	44.65244419	11.5428087	4.252613733	5.771404352	0.911274371	9613.2	467.2	0		31.59084487	68.40915513
209.3	1916	10.79275676	50.72990218	8.598288505	9.673074568	3.654272615	0.644871638	7292.3	0	0		22.78546454	77.21453546
213.3	1970	22.33820459	53.23590814	7.306889353	2.087682672	3.549060543	0	8287	432.5	0		19.20668058	80.79331942
217.3	2025	43.85868182	37.51378404	2.845873272	6.985325303	1.811010264	0.258715752	10206.9	316.9	105.6		9.831198575	90.16880143
221.3	2082	34.49575872	48.30348728	5.89066918	3.063147974	1.64938737	0	20861.9	786.5	0		10.83883129	89.16116871
225.3	2139	28.44187964	47.48557296	7.089859852	4.286892003	3.462489695	0.164880462	16423.3	270.8	0		16.48804617	83.51195383
229.3	2198	32.60153677	50.49396268	3.951701427	2.195389682	1.756311745	0	25786.4	1754.9	0		10.75740944	89.24259056
233.3	2258	35.0624163	45.35841273	6.200070805	5.710591531	1.468437822	0.163159758	10032.8	212.8	0		11.2580233	88.7419767
237.3	2320	33.31310219	50.98247477	4.77960701	1.365602003	0.682801001	0	14730.9	1240.5	0		12.06281769	87.93718231
241.3	2383	30.85714286	44.19047619	4.761904762	6.857142857	1.904761905	0	8771.2	1036.5	16.7		14.85714286	85.14285714
245.3	2447	31.81140823	46.86646246	9.288848415	1.68888153	0.211110191	0.422220382	13405.4	1160.3	0		16.8888153	83.1111847
249.3	2514	40.50611121	38.73300052	5.887416078	2.478912033	4.338096058	0	4846.9	120.2	0		15.49320021	84.50679979
253.3	2582	34.05992495	46.32964381	7.108781325	0.245130391	0.245130391	0.735391172	4358.5	384.6	0	500	17.15912734	82.84087266
257.3	2652	40.31947937	44.81585564	2.218606715	2.884188729	1.109303357	0.221860671	5082.5	0	0		9.983730217	90.01626978
261.3	2724	36.91775353	44.98269896	6.654245409	0.798509449	0.532339633	1.064679265	8549.1	455.1	0		16.50252861	83.49747139
265.3	2798	40.79639369	43.72652141	1.352366642	5.259203606	1.202103681	0	8476	25.5	0		7.062359128	92.93764087
269.3	2875	41.01662404	47.71419437	2.877237852	1.918158568	0.719309463	0	11372.8	709	54.5		8.152173913	91.84782609
273.3	2954	32.00498132	50.68493151	2.241594022	6.724782067	0.99626401	0	6244.4	7.8	7.8		8.468244085	91.53175592
277.3	3035	30.5019305	55.5984556	4.826254826	1.351351351	0	0.386100386	10530	792.8	0		10.03861004	89.96138996
280.9	3111	39.79559544	49.14645271	2.252545749	2.866876408	0.409553773	0	10863.1	1357	89		6.962414133	93.03758587
284.9	3199	30.81203494	56.73891944	2.872856681	1.197023617	0.239404723	0.239404723	12258.7	1106.4	85.1		8.379165319	91.62083468
286.9	3244	28.43721265	53.17235038	4.797505297	6.196777676	0.799584216	0	13726.5	274.4	27.4		10.79438692	89.20561308
290.9	3337	36.69542137	44.79097545	2.687458527	7.465162575	0.597213006	0	7997.3	0	0		8.659588587	91.34041141
294.9	3433	30.35601227	45.80431501	4.017922369	3.750060878	0.535722983	0.267861491	9551.2	102.3	0		18.21458141	81.78541859
298.9	3534	35.02538071	56.85279188	1.776649746	1.776649746	0	0	8245.5	502.3	20.9		5.329949239	94.67005076
302.9	3640	24.64358452	62.45756959	4.073319756	2.26295542	0.452591084	0.226295542	7221.2	626.4	54.5		8.599230595	91.4007694
306.9	3751	36.01570167	52.99313052	1.177625123	0.785083415	0.196270854	0	7059	429.5	41.6		8.047105005	91.952895
310.9	3868	29.66002345	58.38218054	4.454865182	1.406799531	0.234466589	0	8203.5	1461.8	38.5		8.206330598	91.7936694
314.9	3991	35.33727473	55.21760809	1.695277441	1.695277441	0	0	7553.6	347.6	18.3		6.538927274	93.46107273
318.9	4121	23.82147338	62.28714823	4.481089801	0.67216347	0	0.44810898	11931.6	1042.6	0		10.08245205	89.91754795
322.9	4260	24.3940371	63.58912112	5.841520313	1.168304063	0.667602321	0	11650.7	233.3	38.9		8.011227857	91.98877214

Appendix

Depth (cm)	Age cal yrs BP	conifer	deciduous	poaceae	mediterranean	cultivated	ruderals	tot pollen	charcoal 10-50	charcoal 50-125	charcoal >125	NAP	AP
326.9	4408	24.5398773	59.30470348	6.748466258	0.81799591	1.022494888	0.204498978	12622.7	697	51.6		11.04294479	88.95705521
330.9	4566	24.78386167	57.34870317	8.357348703	3.458213256	0.864553314	0	10433.4	210.5	60.1		10.37463977	89.62536023
332.9	4650	23.12849162	59.66480447	5.586592179	1.340782123	0.670391061	0.670391061	11882.4	185.9	0		12.29050279	87.70949721
334.9	4736	24.1958042	58.74125874	5.034965035	2.517482517	1.398601399	0	11383.3	605	0		10.90909091	89.09090909
336.9	4826	19.21568627	71.76470588	3.921568627	0	0.980392157	0.392156863	10789	63.5	21.2		6.078431373	93.92156863
338.9	4919	29.54990215	50.09784736	5.479452055	5.088062622	0.782778865	0	8323.4	0	0		11.35029354	88.64970646
340.9	5016	21.05263158	61.96172249	7.416267943	0.23923445	0.956937799	0	9198.1	154	0		13.15789474	86.84210526
342.9	5117	18.08383234	63.23353293	6.467065868	0.958083832	0.239520958	0	10292.1	468.4	0		13.89221557	86.10778443
344.9	5222	24.10714286	67.1875	2.232142857	0.446428571	0.892857143	0.223214286	9268.1	165.5	0		6.25	93.75
346.9	5331	23.26139089	58.27338129	6.474820144	2.158273381	0.479616307	0.959232614	7992.9	76.7	0		11.75059952	88.24940048
348.9	5443	21.27139364	64.05867971	6.601466993	0.97799511	0.488997555	0.244498778	11574.2	226.4	0		11.73594132	88.26405868
350.9	5560	20.0622084	64.38569207	5.287713841	4.976671851	0.311041991	0	11690.9	109.1	36.4		8.709175739	91.29082426
352.9	5680	24.66907341	66.18531889	3.85078219	0.240673887	0.240673887	0.240673887	7795.9	56.3	0		7.220216606	92.77978339
354.9	5804	22.78876171	55.77523413	8.740894901	2.081165453	0.832466181	0	7425.2	154.5	0		15.60874089	84.39125911
356.9	5930	22.61072261	59.20745921	6.060606061	0.699300699	0.233100233	0	4828.8	0	0		15.15151515	84.84848485
358.9	6059	27.44860943	61.66868198	3.38573156	2.902055623	0.725513906	0.241837969	4887.2	23.6	59.1		6.287787183	93.71221282
360.9	6189	24.85136742	60.40428062	4.994054697	1.426872771	0.713436385	0.475624257	7242.9	241.1	17.2		9.274673008	90.72532699
362.9	6320	27.84222738	55.45243619	4.64037123	0.928074246	0.232018561	0	5902.1	232.8	27.4		11.83294664	88.16705336
364.9	6450	21.94543298	64.0569395	4.744958482	0.474495848	0.474495848	0.711743772	5658.9	120.8	13.4		9.015421115	90.98457888
366.9	6579	23.01740812	61.12185687	4.255319149	0.773694391	1.547388781	0	7790.4	60.3	0		11.21856867	88.78143133
368.9	6706	35.66739606	50.98468271	4.814004376	1.094091904	0.656455142	0.437636761	5880	257.3	0		9.628008753	90.37199125
370.9	6830	30.51948052	50.64935065	5.411255411	1.731601732	0.432900433	0.216450216	7559.7	801.8	49.1		13.85281385	86.14718615
372.9	6951	24.48233861	62.60657734	4.141291108	1.461632156	0.730816078	0	5866	285.8	0		8.038976857	91.96102314
374.9	7068	21.2863706	62.48085758	5.819295559	2.450229709	0.306278714	0.306278714	3481.1	170.6	0		12.55742726	87.44257274
376.9	7182	25.31277277	57.62292697	4.698865289	1.236543497	0.494617399	0	4538.9	190.8	11.2		11.87081757	88.12918243
378.9	7291	22.92917167	57.38295318	6.00240096	4.321728691	0	0.240096038	6007.7	389.5	14.4		12.96518607	87.03481393
380.9	7397	24.48733414	59.34861279	3.136308806	2.653799759	0.965018094	0	5510.2	132.9	0		7.961399276	92.03860072
382.9	7498	26.1125105	54.57598657	8.396305626	2.183039463	1.175482788	0	7112.2	0	0		15.11335013	84.88664987
384.9	7596	24.66257669	59.14110429	2.944785276	1.963190184	0.736196319	0	4821.9	260.3	0		8.588957055	91.41104294
386.9	7690	16.57271702	62.90868095	5.636978579	2.705749718	0.450958286	0	4938.4	556.8	11.1		10.14656144	89.85343856
388.9	7781	22.08436725	58.06451613	4.962779156	2.977667494	0.496277916	0	4020.6	209.5	0		8.933002481	91.06699752
390.9	7868	11.8694362	70.02967359	3.264094955	2.077151335	0.59347181	0	4532.1	201.7	26.9	500	10.68249258	89.31750742
392.9	7952	21.32873069	60.845453	2.376775508	4.753551016	0.237677551	0.237677551	4374	0	0		8.794069379	91.20593062
394.9	8033	14.6039604	65.34653465	1.732673267	1.237623762	0.99009901	0	6648.6	576	0	500	10.89108911	89.10891089
396.9	8112	19.60049938	59.67540574	2.996254682	3.995006242	0.49937578	1.248439451	5705.1	28.5	0	500	12.48439451	87.51560549
398.9	8187	17.32486897	64.4866022	1.653502621	4.251863881	0.47242932	0.70864398	3712.4	8.8	0		7.322654462	92.67734554
400.9	8260	21.3986014	60.27972028	3.916083916	4.755244755	0.559440559	0	4195.8	0	0		7.132867133	92.86713287
402.9	8331	19.17475728	59.46601942	4.368932039	0.970873786	0.485436893	1.213592233	5885.9	171.4	0		11.40776699	88.59223301
406.9	8467	13.43839491	60.98139461	6.395052619	2.5123421	0.913578946	0	3886.5	426.2	13.7	500	14.84565786	85.15434214
412.9	8655	12.28070175	61.75438596	9.473684211	0.701754386	0.350877193	0	9240.4	421.5	32.4		18.24561404	81.75438596
414.9	8714	14.93506494	59.09090909	4.761904762	3.246753247	0	0	6342.5	315.8	13.7		14.5021645	85.4978355
418.9	8829	11.70538582	60.28236349	5.154254127	2.01688205	0.448196011	0	8992	423.2	20.2		17.47964443	82.52035557
422.9	8937	10.86350975	50.69637883	7.242339833	6.685236769	0.278551532	0	10960.3	61.1	0		21.7270195	78.2729805
426.9	9041	6.666666667	58.90909091	9.212121212	2.424242424	0	0	13493.4	914.3	0		24.24242424	75.75757576
430.9	9140	8.789808917	66.75159236	7.898089172	2.547770701	0.25477707	0	8925.3	386.6	22.7		16.81528662	83.18471338
434.9	9235	9.239766082	60.11695906	4.678362573	2.807017544	0.701754386	0	7525.6	440.1	35.2		19.41520468	80.58479532
438.9	9327	6.053268765	67.55447942	8.232445521	1.937046005	0.726392252	0	8405.3	793.7	40.7		20.0968523	79.9031477
442.9	9414	12.1619922	48.67312288	10.86655767	1.811092944	0.226386618	0	11627.1	368.5	79		29.43026034	70.56973966
446.9	9499	6.728538283	51.74013921	13.225058	2.088167053	0.696055684	0.232018561	5993.6	111.3	13.9		31.78654292	68.21345708
450.9	9581	8.492569002	43.31210191	16.34819533	1.27388535	0.8492569	0.42462845	8213.5	560.3	0		37.36730361	62.63269639
454.9	9660	11.94444444	52.22222222	11.66666667	2.222222222	0.277777778	0	3284.5	319.3	9.1		27.22222222	72.77777778
458.9	9736	8.59030837	40.30837004	14.97797357	2.863436123	0.440528634	0.660792952	3694	219.7	16.3	500	37.66519824	62.33480176
462.9	9811	13.96508728	43.14214464	12.21945137	2.992518703	0.748129676	0.249376559	3167.8	126.4	0	500	33.16708229	66.83291771
466.9	9883	9.9756691	48.41849148	8.759124088	2.676399027	0.729927007	0	3936.7	162.8	9.6		31.87347932	68.12652068
470.9	9953	15.4855643	54.06824147	5.249343832	1.837270341	0	0	5897.4	1331.2	61.9		23.62204724	76.37795276
474.9	10021	15.76470588	40	13.64705882	0.705882353	0.941176471	0.235294118	5082.8	191.4	0		35.05882353	64.94117647
478.9	10087	9.489051095	52.55474453	14.30656934	4.96350365	0.583941606	0.583941606	4158.1	254.9	0		30.0729927	69.9270073
482.9	10152	13.15136476	44.41687345	10.42183623	5.210918114	0.248138958	1.240694789	4833.8	60	24		32.25806452	67.74193548
486.9	10215	12.67332013	41.66730154	13.72276398	2.994057596	0.748514399	0.499009599	4684.2	151.9	0		33.43364315	66.56635685

Appendix

Depth (cm)	Age cal yrs BP	conifer	deciduous	poaceae	mediterranean	cultivated	ruderals	tot pollen	charcoal 10-50	charcoal 50-125	charcoal >125	NAP	AP
492.9	10307	17.34390486	34.48959366	11.10009911	0.396432111	0.594648167	0.198216056	4001.8	198.3	0		36.47175421	63.52824579
500.9	10424	11.64462764	33.98283552	14.23031237	2.548712664	0.637178166	0.212392722	5858.7	326.6	0		42.90332985	57.09667015
508.9	10537	17.70114943	27.12643678	17.24137931	1.149425287	0.229885057	0.229885057	3423.9	110.2	0		46.89655172	53.10344828
516.9	10645	11.75757576	27.15151515	24	2.424242424	0.96969697	0.727272727	4074.7	148.2	29.6		51.63636364	48.36363636
524.9	10749	14.33172303	20.93397746	17.71336554	0.966183575	0	0	3095.6	129.6	0		56.36070853	43.63929147
532.9	10849	11.44278607	16.91542289	22.13930348	1.243781095	0.248756219	0.497512438	3906.3	602.5	9.7		63.93034826	36.06965174
540.9	10946	13.07550645	18.41620626	16.94290976	2.209944751	0	1.104972376	2563.7	103.9	9.4		61.51012891	38.48987109
550.9	11063	14.4	20	17.2	2.4	0.8	0	2990.8	346.9	107.7		58.8	41.2
562.9	11197	13.4872418	20.17010936	14.82381531	0.972053463	0.729040097	1.458080194	3145.8	259.9	0	500	58.32320778	41.67679222
574.9	11325	10.45751634	25.81699346	17.64705882	1.633986928	0.326797386	0.653594771	3538.1	312.2	11.6	500	56.53594771	43.46405229
580.9	11387	14.87603306	17.3553719	19.4214876	2.066115702	0	0.826446281	3529.3	218.8	14.6		58.67768595	41.32231405
586.9	11448	15.2861757	21.67097831	24.7355611	1.094493854	0.218898771	0.218898771	5297.9	777	92.8		55.38138901	44.61861099
592.9	11508	11.38014528	13.55932203	21.0653753	0.242130751	0	0.726392252	2550.7	636.1	18.5		68.76513317	31.23486683
598.9	11566	4.922644163	6.4697609	10.97046414	0.843881857	0	0.562587904	3444.4	1056.1	19.4		82.70042194	17.29957806
604.9	11624	5.83501006	4.828973843	15.69416499	0	0	0	3068.3	679.1	12.3	500	86.1167002	13.8832998

Erklärung (Explanation in German)

Ich versichere, dass ich die von mir vorgelegte Dissertation selbständig angefertigt, die benutzten Quellen und Hilfsmittel vollständig angegeben und die Stellen der Arbeit – einschließlich Tabellen, Karten, und Abbildungen -, die anderen Werken im Wortlaut oder dem Sinn nach entnommen sind, in jedem Einzelfall als Entlehnung kenntlich gemacht habe; dass diese Dissertation noch keiner anderen Fakultät oder Universität zur Prüfung vorgelegen hat; dass sie – abgesehen von unten angegebenen Teilpublikationen – noch nicht veröffentlicht worden ist, sowie, dass ich eine solche Veröffentlichung vor Abschluss des Promotionsverfahrens nicht vornehmen werde. Die Bestimmungen der Promotionsordnung sind mir bekannt. Die von mir vorgelegte Dissertation ist von Prof. Dr. Janet Rethemeyer betreut worden.

Nachfolgend genannte Teilpublikationen liegen vor:

Thienemann M, Masi A, Kusch S, et al. (2017) Organic geochemical and palynological evidence for Holocene natural and anthropogenic environmental change at Lake Dojran (Macedonia/Greece). *The Holocene* 27: 1103-1114.

Köln, 16.10.2017

Matthias Thienemann